Novel materials for direct Li extraction from geothermal brine

Zur Erlangung des akademischen Grades einer

DOKTORIN DER NATURWISSENSCHAFTEN

(Dr. rer. nat.)

von der KIT Fakultät für

Bauingenieur-, Geo- und Umweltwissenschaften

des Karlsruher Instituts für Technologie (KIT)

genehmigte

DISSERTATION

von

M.Sc. Rebekka Sophie Reich

aus Schwäbisch Gmünd

Tag der mündlichen Prüfung: 15.07.2024

Referent: Prof. Dr. Jochen Kolb

Korreferent: Dr. Holger Paulick

Karlsruhe (2024)

Abstract

Lithium is a valuable critical raw material in the modern society. Currently, it is mainly used in Li-ion batteries of cars and portable electronics but is also needed in the ceramics and glass industry, in lubricating greases, fluxes, polymers, air treatment and in medicals. The progressing energy transition increases the global Li demand and models predict a demand of up to 560 kt Li metal in 2030, i.e. an increase by 760% compared to 2020, thus leading to the fear of supply threats since only 130 kt Li metal was globally produced in 2022.

To cover the global Li demand, novel technologies for Li extraction from unconventional resources, like geothermal brines, can contribute to the supply and improve Europe's independence from the global Li market. Geothermal brines in Germany reach a concentration of up to 240 mg/L. Examining the potential applicability of different direct Li extraction (DLE) technologies, sorption and ion exchange is regarded as one of the most appropriate techniques for operating geothermal power plants. In sorption and ion exchange technology, many different materials can be used that have different advantages and disadvantages for the DLE process. Important parameters are the kinetics of Li extraction, Li selectivity, chemical stability and sorption capacity under ambient physicochemical conditions. Lithium-manganese oxide (LMO), lithium-titanium oxide (LTO) and lithium-aluminum hydroxide (often LADH) have been intensely investigated, recently. But other materials, like iron phosphate, clay minerals, zeolite group minerals and many more are generally able to sorb Li. Based on literature data, iron phosphate and zeolite are regarded to be promising novel sorbents to be investigated.

Synthetic zeolite 13X exchanges Na^+ ions by Li^+ during extraction, but also ion exchange of H^+ with Li^+ and physisorption may be important processes. Zeolite 13X has a high Li-sorption capacity and fast kinetics, but the DLE performance is significantly reduced when the powder is formulated to beads of larger grain size or when the pH is decreased to 5 – 6, which reflects geothermal brine pH. The complex geochemical composition of the geothermal brines is a severe challenge for the poor

Li-selectivity of zeolite 13X, limiting its application to less complex chemical compositions. Zeolite 13X may thus be used for DLE from different unconventional resources, like battery recycling, battery manufacturing wastewaters or low saline mine waters.

The iron phosphate mineral heterosite intercalates Li during phase transition to the lithium-iron-phosphate mineral triphylite, commonly used as cathode material in LFP batteries. The phase transition is a fully reversible process and the sorbent is highly selective for Li, making it suitable for application in geothermal brines. In LFP batteries, the phase transition is achieved electrochemically, steering the redox state of Fe. In a purely chemical approach, challenges regarding the use of an additive, i.e. a reducing agent for the reduction of iron, required for the intercalation of Li, need to be overcome. However, by adjusting the optimal extraction parameters, LFP is applicable in different geothermal brines, reaching high recovery rates of > 99% in laboratory experiments.

Although some challenges must be overcome, novel sorbents may be a game-changer in DLE technology, making Li-mining more sustainable in the future. Compared to LMO, LTO and LADH, commercially available novel sorbents provide a good alternative in DLE from geothermal brine because of higher chemical stability and a more appropriate operating pH than e.g. $Li^+ – H^+$ exchanging sorbents that need alkaline pH to achieve high Li recovery. Furthermore, the formulation of any powdery material to be used in geothermal power plants is still not technically approved, widening the research portfolio for technology development in the future.

Zusammenfassung

Lithium ist ein wertvoller kritischer Rohstoff der modernen Gesellschaft. Derzeit wird es hauptsächlich in Lithium-Ionen-Batterien (LIB) von Autos und mobilen elektronischen Geräten eingesetzt. Daneben wird es aber auch in der Keramik- und Glasindustrie, in Schiermitteln, in der Flussmittel- und Polymerindustrie sowie in der Luftaufbereitung und in Medikamenten benötigt. Die voranschreitende Energiewende erhöht die globale Lithiumnachfrage, die auf bis zu 560 kt Li Metall im Jahr 2030, d.h. 760% höher als im Jahr 2020, prognostiziert wird. Dies führt zur Sorge von Versorgungsengpässen, da die globale Lithiumproduktion im Jahr 2022 nur 130 kt Li Metall erreichte.

Um den globalen Lithiumbedarf decken zu können, werden neuartige Technologien für die direkte Lithiumextraktion (DLE) aus unkonventionellen Ressourcen benötigt. Die Lithiumgewinnung aus solchen Quellen würde zur globalen Lithiumproduktion beitragen und Europas Unabhängigkeit vom globalen Markt stärken. Geothermalwässer, die in Deutschland vorkommen, besitzen Lithiumgehalte von bis zu 240 mg/L. Im Vergleich zu anderen direkten Lithiumextraktionsverfahren (DLE), stellt Sorption und Ionenaustausch eine der vielversprechendsten, einsetzbaren Technologien dar, um Lithium in laufenden Geothermiekraftwerken zu gewinnen. Bei Sorption und Ionenaustausch können jedoch viele unterschiedliche Materialien eingesetzt werden, die unterschiedliche Vor- und Nachteile für die DLE aus Geothermalwasser mit sich bringen. Wichtige Parameter sind die Kinetik der Lithiumextraktion, die Li-Selektivität, chemische Stabilität und die Sorptionskapazität unter den gegebenen physikochemischen Bedingungen. Lithium-Mangan-Oxid (LMO), Lithium-Titan-Oxid (LTO) und Aluminium-Hydroxid (häufig LADH) sind intensiv erforscht. Andere Materialien, wie Eisenphosphat, Tonminerale, Zeolith-Gruppen Minerale und viele weitere können Li sorbieren. Basierend auf Literaturdaten werden Eisenphosphat und Zeolith als vielversprechende neuartige Sorbenzien erachtet.

Synthetischer Zeolith 13X ist in der Lage, während der Extraktion Na^+ gegen Li^+ auszutauschen, der $H^+ – Li^+$ Austausch und Physisorption scheinen daneben ebenfalls wichtige Prozesse zu sein. Zeolith 13X besitzt eine hohe Li-Sorptionskapazität und zeigt

eine schnelle Kinetik. Die DLE Leistung nimmt aber extrem ab, wenn das Pulver in Form von Kügelchen größerer Korngröße vorliegt oder wenn der pH-Wert auf 5 – 6 abgesenkt wird, was repräsentativ für den pH-Wert von Geothermalwasser ist. Die komplexe geochemische Zusammensetzung von Geothermalwasser ist eine große Herausforderung für Zeolith 13X, der eine niedrige Li-Selektivität zeigt. Daher ist die Verwendung von Zeolith 13X zur DLE auf Fluide weniger komplexer Zusammensetzung beschränkt. Zeolith 13X könnte beispielsweise zur Li-Gewinnung im Batterierecycling, aus Produktionswässern der Batterieindustrie oder in niedrig salinaren Bergbaufluiden eingesetzt werden.

Eisenphosphat Heterosit kann Li im Zuge der Phasenumwandlung zu Lithium-Eisenphosphat Triphylit in sein Gerüst einbauen. Triphylit kommt normalerweise als Kathodenmaterial in LFP Batterien zum Einsatz. Die Phasenumwandlung ist vollständig reversibel und es handelt sich um ein Material mit hoher Li-Selektivität, wodurch es sich für die Anwendung in Geothermalwasser eignet. In LFP Batterien wird die Phasentransformation, bzw. der Oxidationszustand von Fe elektrochemisch kontrolliert. In einem rein chemischen Ansatz ist die Verwendung eines Additivs, einem Reduktionsmittel, das für die Reduktion von Fe und damit für den Li-Einbau benötigt wird, herausfordernd. Wenn die Extraktion jedoch auf die optimalen Parameter eingestellt wird, ist LFP in unterschiedlichen Geothermalwässern einsetzbar, wobei eine Ausbringung von > 99% erreicht wird.

Obwohl noch Herausforderungen zu bewältigen sind, können neuartige Sorbenzien die DLE-Technologie entscheidend verändern und zu einem nachhaltigeren Li-Bergbau beitragen. Verglichen mit LMO, LTO und LADH sind kommerziell verfügbare, neuartige Sorbenzien eine vielversprechende Alternative für die DLE aus Geothermalwasser, weil sie eine höhere chemische Stabilität zeigen und im Vergleich zu $Li^+ – H^+$ austauschenden Sorbenzien in einem für Geothermalwasser optimaleren pH Bereich wirksam sind. Die Formulierung von Pulvern für diese Anwendung ist allerdings noch nicht ausreichend entwickelt, was das Forschungsfeld für die Technologieentwicklung in der Zukunft erweitert.

Danksagung

Liebe Mama, lieber Papa, danke. Danke, dass ihr mir ermöglicht habt zu studieren. Danke, dass ihr immer an mich geglaubt habt und mich bei allen Entscheidungen, die ich in meinem bisherigen Leben getroffen habe, unterstützt habt. Ihr habt euch immer mit mir gefreut, wenn ich Ziele erreicht und erfolgreiche Momente hatte und ihr habt mich getröstet, wenn ich traurig und gestresst war oder nicht mehr weiterwusste. Danke Thomas, dass du die letzten Jahre immer an meiner Seite warst. Danke, dass du mit mir lachst, dich mit mir über Dinge ärgerst, dass du Verständnis zeigst, immer an mich glaubst und mich unterstützt. Danke Steffen und Christoph, dass ihr tolle große Brüder seid, mir zuhört und mich unterstützt. Danke Steffen, dass du alle Phasen der Promotion nachempfinden konntest, die ich gerade durchlebt hatte und dass du immer einen guten fachlichen, strategischen und zwischenmenschlichen Rat parat hast.

Bei Prof. Dr. Kolb und PD Dr. Elisabeth Eiche möchte ich mich für die Möglichkeit der Promotion bedanken. Ich danke euch für die Vergabe meines Promotionsthemas und die Betreuung während meiner Promotion. Ich möchte mich vor allem dafür bedanken, dass ihr immer Zeit für mich und meine Anliegen gefunden habt. Außerdem möchte ich mich für eure Anregungen und Ideen bedanken, die in meine Promotion eingeflossen sind, aber auch dafür, dass ihr immer ein Gespür dafür hattet, wann ich Hilfe benötigte und wann ich einfach frei arbeiten wollte.

Bei Prof. Dr. Kirsten Drüppel möchte ich mich für ihre schnelle und unkomplizierte Hilfe bei Fragen rund um die XRD Analytik und Kristallographie bedanken. Ich bedanke mich außerdem bei allen Projektpartnern, Kollegen und bei den Co-Autoren meiner Publikationen, insbesondere PD Dr. Benjamin Walter, Dr. Tobias Kluge, PD Dr. Elisabeth Eiche, Prof. Dr. Jochen Kolb, Klemens Slunitschek, Rosa Micaela Danisi und Laura Spitzmüller.

Für die herausragende Hilfe bei sämtlichen analytischen Untersuchungen möchte ich mich herzlich bei Janine Wagner, Nadine Hüll, Maya Denker, Claudia Mößner, Beate Oetzel, Maria Maravillas Prieto Sevilla und Gesine Preuß bedanken. Bei Kristian Nikoloski bedanke ich mich für seine Hilfe bei der Probenpräparation. Kevin

Altinger und Ralf Wachter danke ich für ihre schnelle und unkomplizierte Hilfe bei technischen Arbeiten und der Anlagenbetreuung während der Projektarbeiten. Ralf Wachter danke ich außerdem für das jederzeit für meine Anliegen offene Ohr und natürlich der häufigen und schnellen Reparatur der Kaffeemaschine. Chantal Kotschenreuther danke ich herzlichst für die wahnsinnig große Hilfe bei den ICP-OES Analysen. Danke, dass du mich so gut in dieses Gerät eingearbeitet hast. Liebe Chantal und lieber Ralf, danke, dass ihr immer gut gelaunt und für einen Spaß zu haben seid. Ich hatte immer viel Freude, wenn ich mit euch arbeiten durfte!

Ich danke euch, Michèle Jungmann, Dr. Tatjana Epp, Patricia Marks und Sandra Schraml. Liebe Michèle, ich danke dir, dass du mir anfangs geduldig gezeigt hast, wie ich eine Lösung bestimmter Salzkonzentration herstelle, was MilliQ-Wasser überhaupt ist und wie ich mich generell im Chemielabor zu verhalten habe. Ich danke dir, dass du immer meine kleinen Fragen „Kannst du das bitte nochmal nachrechnen?“ und „Wie würdest du das zitieren?“ oder „Was hältst du denn davon?“ beantwortet hast, dass du meine Interpretationsideen und Erklärungsansätze angehört und immer mitdiskutiert hast. Liebe Tati, danke, dass du mir immer zuhörst und mir ehrliche Ratschläge gibst. Danke, dass du hast mir gezeigt, wie man schöne Grafiken macht, Paper einreicht und den Promotionsalltag übersteht. Liebe Paddy, danke für die gemeinsame Zeit im Studium und den Austausch während unserer Promotionen und dafür, dass wir immer eine lustige Zeit miteinander haben. Danke Sandra, dass du mich während meiner Promotion begleitet hast und immer geholfen hast, wo du nur konntest, meine kreativen Denkpausen beim Spazieren gefördert hast und für mich da bist.

„Neue Wege entstehen, indem wir sie gehen“

Friedrich Wilhelm Nietzsche (1844 – 1900)

Table of content

1. Introduction

Lithium (Li) is an alkali metal and the lightest metal on Earth. Since 2020, it has been classified as a critical raw material by the European Union (European Commission, 2020). Due to its high energy density, it is used in Li-ion batteries (LIB) among ceramics and glass, lubricating greases, fluxes and polymers, in air treatment and medicals (Perez, 2023; US Geological Survey, 2023). In 2015, 37% of the global Li supply was used in LIBs and the share progressively increased to 80% in 2022 (Figure 1; US Geological Survey, 2020, 2023). With the progressing energy transition, the demand for Li rises as long as Li cannot be substituted at a significant share in batteries (Zhao et al., 2021) and models predict a global Li metal demand of 316.3 – 558.8 kt per year in 2030 (Schmidt, 2023). This would be an increase in Li demand by 430 – 760% compared to 73.6 kt Li metal in 2020 (Schmidt, 2023).

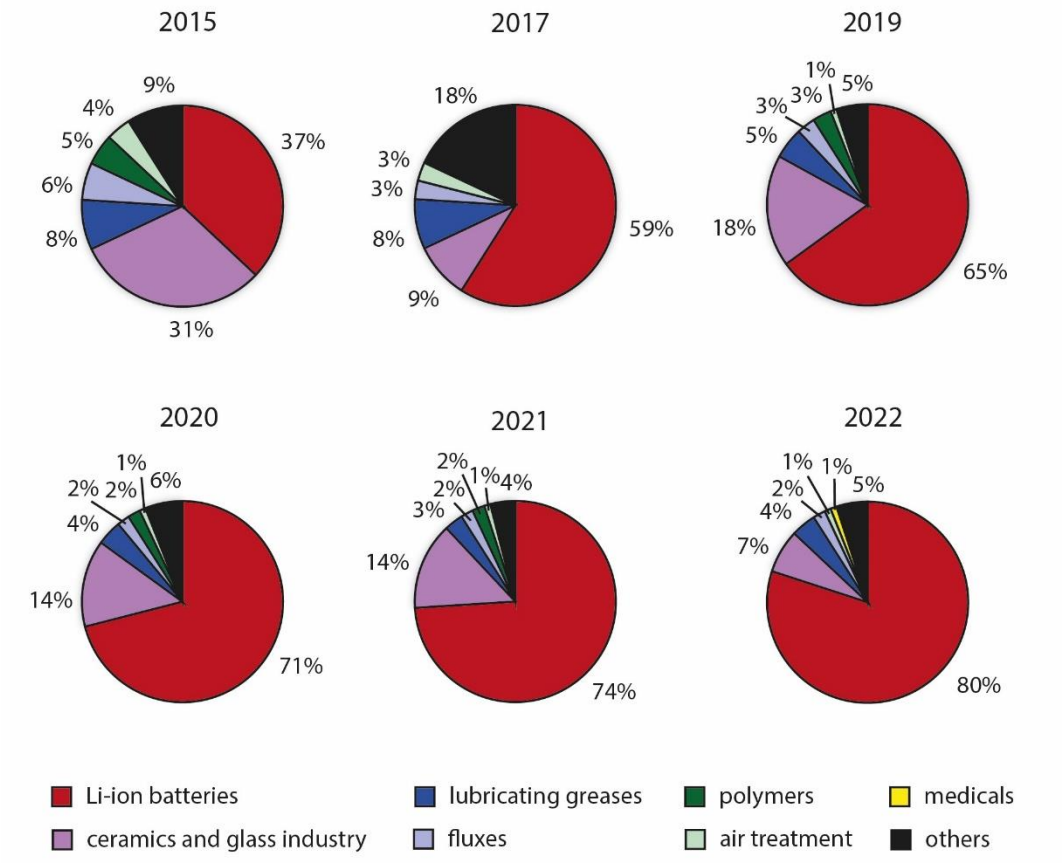

Figure 1. End-user market development of Li between 2015 and 2022. Data compiled from the US Geological Survey (2020, 2023).

Since Li is used in different applications, Li products are variable in composition and purity. Lithium carbonate (Li_2CO_3) is available in battery and industrial or technical grade, i.e. a purity higher than 99.5% and 99 – 99.5%, respectively (Schmidt, 2023). An alternative to Li_2CO_3 is lithium hydroxide monohydrate ($LiOH \cdot H_2O$), which is the preferred product for cathode producers since its use results in better product properties and it can be transferred more easily compared to Li_2CO_3 (Dahlkamp et al., 2023; Liebetreu, 2022). Battery grade $LiOH \cdot H_2O$ usually has a purity of 56.5 – 57.5% (Schmidt, 2023). When Li has to be shipped over large distances, Li_2CO_3 is the preferred product because of its higher stability compared to LiOH, which reacts with CO_2 to Li_2CO_3 (Dahlkamp et al., 2023). The cheapest Li product is a spodumene concentrate, which usually has a minimum Li_2O content of 5 – 6% (Schmidt, 2023). The concentrate can be further processed into Li_2CO_3 and $LiOH \cdot H_2O$ (Chordia et al., 2022).

During the 1990s, the Li price was stable and low (Figure 2). Due to stable supply and low demand, one ton of battery grade Li_2CO_3 cost 4,200 – 4,500 US$ (US Geological Survey, 1996, 2000). During the 2000s, increasing Li supply, economic crises and increasing Li demand for electronics led to price fluctuations (Bowell et al., 2020). In 2016, the prices for battery grade Li products significantly increased to a maximum of almost 27,000 US$/t $LiOH \cdot H_2O$ (Figure 2a, Australian Government, 2020). The rising demand was followed by an increase in global Li production (Figure 2b). The COVID-19 crisis, however, significantly decreased the demand and the resulting oversupply of Li on the market decreased its costs (US Geological Survey, 2021). As a result, the mines decreased production and when the pandemic ended, the demand rose again and a supply shortage increased the Li prices to a maximum of 70,000 US$/t for battery grade Li_2CO_3 (Figure 2a, Australian Government, 2023). The global Li production in 2022 reached 130 kt Li metal, i.e. production increased by +157% compared to 2020, reducing the price to approximately 36,000 US$/t battery grade Li_2CO_3 (US Geological Survey, 2022, 2023). This reflects the high volatility of Li market, recently.

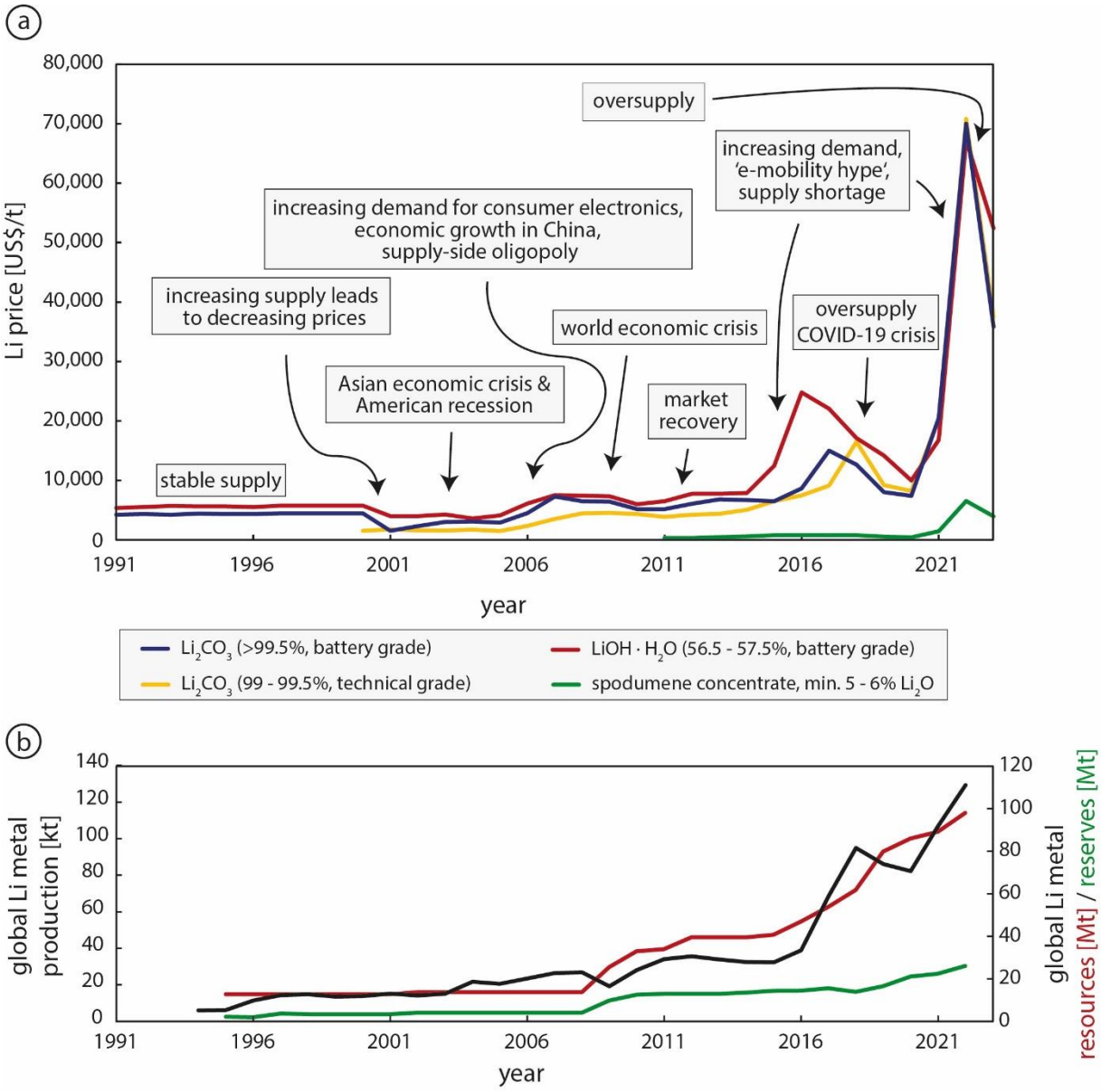

Figure 2. a) Li price development between 1991 and 2023 for battery and technical grade Li_2CO_3, battery grade $LiOH{\cdot}H_2O$ and spodumene concentrate. b) Global Li production from 1994 – 2022, and resource and reserve estimations between 1995 – 2022. Data compiled from Australian Government (2020, 2023); DERA (2019, 2023, 2024); Piedmont Lithium Limited (2020); London Metal Exchange (2021); Martin et al. (2017); Schmidt (2017); Statista (2021); US Geological Survey (1996-2023).

1.1 Global Li occurrences

Lithium deposits can be distinguished into hard rock deposits and brine deposits (Bowell et al., 2020). Both types comprise significant resources and reserves and contribute to the global annual Li production. The global Li resources are 97 Mt Li metal, but only 25 Mt Li metal are classified as reserves (US Geological Survey, 2023).

The major Li-producing countries are Chile, Argentina, Australia and China (US Geological Survey, 2023). Chile and Argentina host 9.3 Mt and 2.7 Mt Li metal reserves in brines, respectively, whereas Australia's Li reserves of 6.2 Mt Li metal are hosted in hard rock deposits (Figure 3; US Geological Survey, 2023). Spodumene concentrate produced in Australia is shipped to and refined in China. China additionally has Li reserves of 2 Mt Li metal (Figure 3; US Geological Survey, 2023). As of 2023, the USA, Canada, Zimbabwe, Brazil and Portugal have Li metal reserves of 1 000 kt, 0.93 kt, 310 kt, 250 kt and 60 kt, respectively (Figure 3). Minor Li reserves are found in, among others, Austria, Finland, Kazakhstan and Namibia and sum up to 3.3 Mt Li metal (US Geological Survey, 2023).

The largest Li resources are found in Bolivia, comprising 21 Mt Li metal in brines (Figure 3; US Geological Survey, 2023). In Bolivia, although technical possibilities exist, Li is not mined due to land-use conflicts and political reasons, e.g. the natural resource ownership by the state (Barandiarán, 2019). As of 2023, Germany increased its estimated Li resources to 3.2 Mt Li metal, hosted in hard rock and geothermal brine deposits, representing the 7th largest resource worldwide (Figure 3; US Geological Survey, 2023). Lithium is also found in the Democratic Republic of Congo, Canada, Mexico, the Czech Republic, Serbia, Peru, Mali, Spain, Ghana and Russia. The Li metal resources in these countries cumulate to 13.3 Mt (Figure 3; US Geological Survey, 2023). Another large Li resource is seawater. According to estimations, the resource is of low concentration (0.17 mg/L average Li concentration), but giant, comprising 230 Gt Li metal (Fasel and Tran, 2005; Kudryavtsev, 2016).

Examples for hard rock deposits are Greenbushes in Australia, the Kings Mountain Belt in the USA and Zinnwald in Germany (Ambrose and Kendall, 2020; Bowell et al., 2020). The geology of hard rock Li deposits mainly comprises pegmatite, greisen and alkaline granite deposits, but also volcano-sedimentary and clay deposits (Bowell et al., 2020; Gourcerol et al., 2019). The major Li-bearing minerals are spodumene ($LiAlSi_2O_6$), petalite ($LiAlSi_4O_{10}$), lepidolite ($K[Li,Al]_3[Al,Si]_4O_{10}[OH,F]_2$), zinnwaldite ($K[Li,Al,Fe]_3[Al,Si]_4O_{10}[OH,F]_2$), amblygonite ($[Li,Na]Al[OH,F]PO_4$),

montebrasite ($LiAl[PO_4][OH]$), eucryptite ($LiAlSiO_4$), triphylite ($Li[Fe,Mn]PO_4$), jadarite ($LiNaSiB_3O_7[OH]$) and hectorite ($Na_{0.3}[Mg,Li]_3[Si_4O_{10}][F,OH]_2 \cdot nH_2O$) (Bowell et al., 2020). These minerals usually contain 1.0 – 9.7 wt% Li_2O, highly enriched compared to the Clarke value of ~0.007% (Bowell et al., 2020; Swain, 2017).

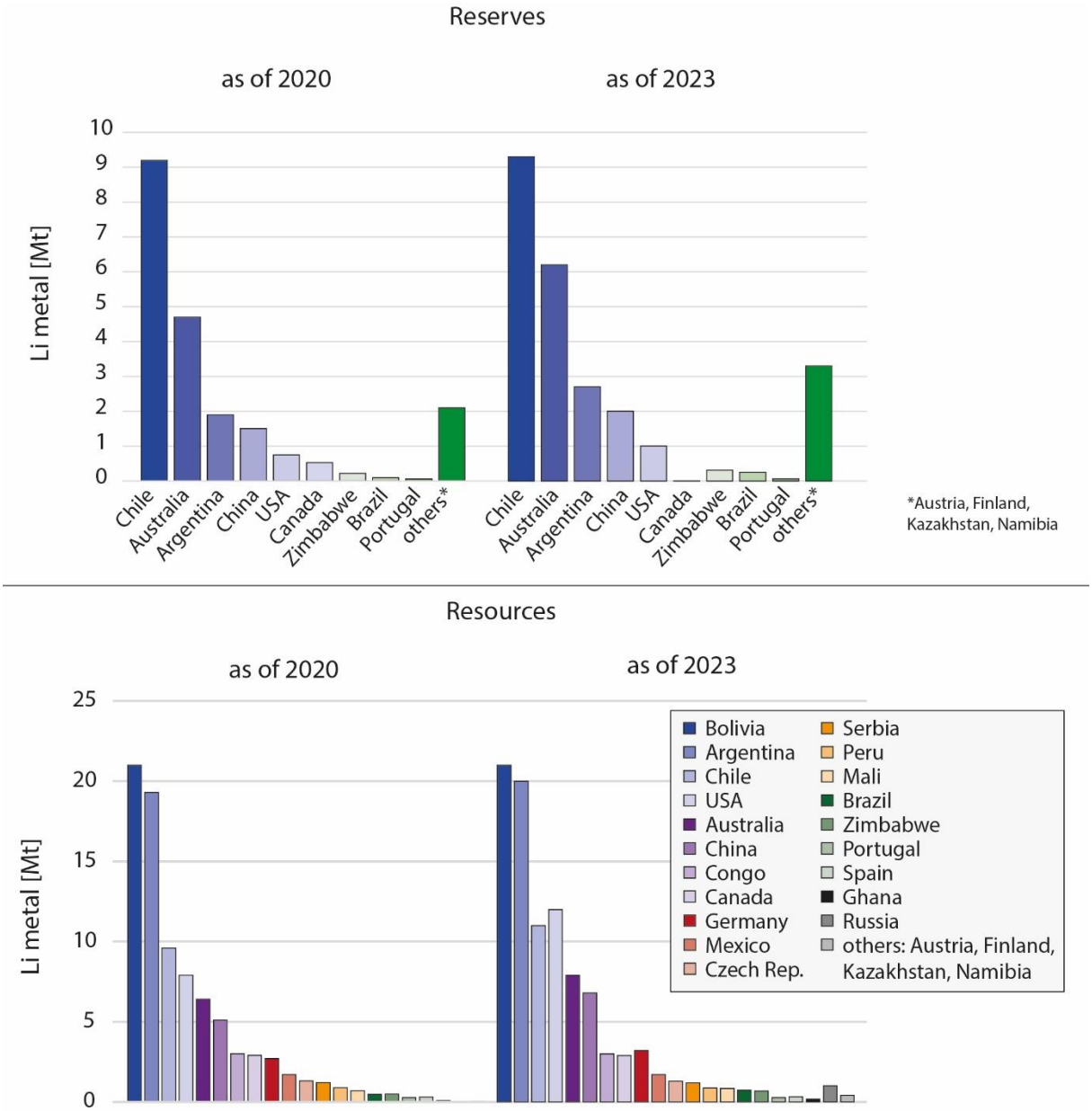

Figure 3. Global Li reserves and resources from hard rock and brine deposits by country, as of 2020 and 2023. Data compiled from US Geological Survey (2020, 2023).

Brine deposits include lakes, salars, oilfield brines and geothermal brines (Bowell et al., 2020; Murodjon et al., 2020). Prominent examples of commercially mined salars are the Salar de Atacama in Chile, mined by SQM and Albemarle and the Salar del Hombre

Muerto in Argentina, mainly mined by Livent (Schmidt, 2023). Brines usually have a high salinity with total dissolved solids (TDS) of 100 – 330 g/L and a Li concentration of 10 mg/L – 1.84 g/L (An et al., 2012; Bowell et al., 2020; Reich et al., 2022).

1.2 Li metallurgy

1.2.1 Hard rock ores

Lithium is usually recovered hydro- or pyrometallurgically from hard rock ores (Figure 4). The Li-rich ore (e.g., spodumene) is separated and concentrated by crushing, grinding, sieving, gravity and magnetic separation as well as flotation (Banks, 1953; Peerawattuk and Bobicki, 2018). After the separation and concentration, the ore is usually calcined at ~1100°C to convert α-spodumene into β-spodumene for further processing (Choubey et al., 2016). In the acid process (Figure 4a), the calcined ore is mixed with hot H_2SO_4 and a Li_2SO_4 solution is recovered (Meng et al., 2021; Peerawattuk and Bobicki, 2018; Swain, 2017). The addition of sulfuric acid, however, leaches Mg and Ca simultaneously, diluting the Li-concentrate (Peerawattuk and Bobicki, 2018). The water leached solution undergoes several additional precipitation, filtration and purification steps before Li_2CO_3 is produced by Na_2CO_3 addition reaching 85% Li recovery (Choubey et al., 2016; Meng et al., 2021; Swain, 2017). In the alkaline processing (Figure 4b), either $CaCO_3$ or Na_2CO_3 are mixed with the calcined ore (Meng et al., 2021). Due to reaction with CO_2, soluble $LiHCO_3$ is produced. From the $LiHCO_3$ solution, Li_2CO_3 or $LiOH{\cdot}H_2O$ are produced by evaporation and/or crystallization (Choubey et al., 2016; Meng et al., 2021). To chlorinate the ore (Figure 4c), HCl, NaCl, $CaCl_2$ or Cl_2 gas are added before chlorination at 800 – 1100°C (Meng et al., 2021; Meshram et al., 2014). By water leaching, a LiCl solution is produced that can be processed into different products, like LiCl, Li_2CO_3 or via electrodialysis into $LiOH{\cdot}H_2O$ (Meng et al., 2021; Meshram et al., 2014).

In pressure leaching, the pre-concentrated ore is mixed with lime and water. Then, the mixture is heated to 205°C and approximately 17 bar (Gabra et al., 1975; Meng et al., 2021), reaching a Li recovery of up to 90%. The efficiency of pressure

leaching is influenced by the addition of variable concentrations of sodium chloride, sodium carbonate, sodium sulfate, sodium hydroxide and calcium hydroxide as well as variable leaching durations, particle sizes and temperatures (Gabra et al., 1975; Meng et al., 2021, and references therein; Swain, 2017). The ore pre-treatment for hydro-, pyrometallurgy and pressure leaching is simple and the processes are easily scaled up to be used commercially, producing high-purity products (Meng et al., 2021).

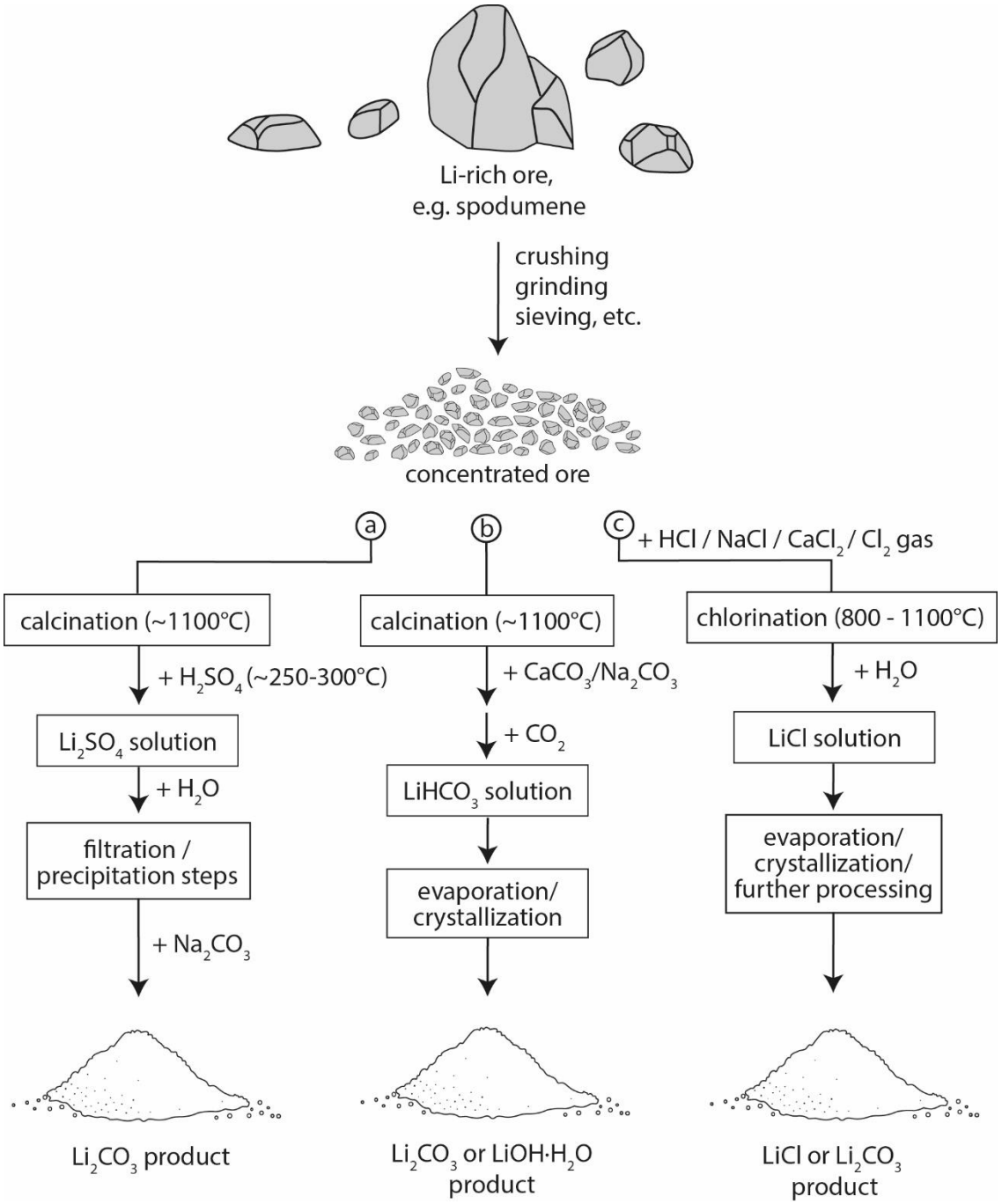

Figure 4. Schematic illustration of hydro- and pyrometallurgical processing for Li recovery from hard rock ores, e.g. spodumene. a) acid process, b) alkaline process and c) chlorination process.

In bioleaching, also called bio-hydrometallurgy, bacteria are used for metal extraction. End-of-life LIBs or tailings are the Li sources (Liu et al., 2007; Niu et al., 2014). Roy et al. (2021) performed bioleaching experiments where they shredded spent LIBs. They sieved the product to receive a powder of 100 µm grain size that is washed, dried and autoclaved after sieving. The powder is then mixed with *Acidithiobacillus ferrooxidans* to leach Li and Co by a series of biochemical reactions. Bioleaching is a cheap process to recover Li from low-grade deposits and it is environmentally friendly and sustainable, highly efficient at low temperatures and does not need high-performance industrial techniques (Meng et al., 2021; Niu et al., 2014; Roy et al., 2021). On the other hand, the process is time-consuming due to slow kinetics and the microorganisms can be sensitive to the presence of other metals, which limits their application to non-polymetallic compositions (Meng et al., 2021; Roy et al., 2021; Swain, 2017).

1.2.2 Brines

Brine and seawater evaporation is to date the commercial technique for Li recovery from aqueous solutions (Peerawattuk and Bobicki, 2018). The fluid is pumped from its reservoir into large evaporation ponds where less soluble salts, e.g. halite, gypsum, carbonates, sylvite, sylvinite, carnallite or bishoffite, are precipitated to remove undesired cations like K^+, Mg^{2+} and Ca^{2+} (An et al., 2012; Meshram et al., 2014; Peerawattuk and Bobicki, 2018; Tran and Luong, 2015; Ventura et al., 2016). Proceeding precipitation increases the Li content to ~ 6%, needed for further processing (Chordia et al., 2022; Peerawattuk and Bobicki, 2018). The concentrated brine is processed by addition of Na_2CO_3 in shallow PVC ponds or in a refining plant (Agusdinata et al., 2018; Vera et al., 2023). Due to prior Li-carnallite ($LiCl{\cdot}MgCl_2{\cdot}6H_2O$) precipitation, however, the Li recovery from evaporation is limited (i.e., max ~ 50 – 80%), compared to other extraction methods (An et al., 2012; Liu et al., 2023; Meshram et al., 2014; Ventura et al., 2016). Moreover, this conventionally used methodology is challenging to be applied for Mg and sulfate-rich brines (Aljarrah et al., 2023; Jin et al., 2023).

1.2.3 Socio-environmental considerations

Lithium mining, in general, increases the profit for the state and operating companies, but it also leads to socio-environmental problems, like groundwater consumption and land-use conflicts in protected areas (Agusdinata et al., 2018; Vivoda et al., 2024). Mining can strengthen a country's independence from third states, improving the development of novel technologies, innovations, the citizens' living standard, diversity and sustainability (Vivoda et al., 2024). It can be challenging to establish reliable and sustainable supply chains from countries like Mexico and Bolivia, due to a leading progressive regime, making the country unattractive for companies and stakeholders, or organized criminality, impeding mine development (Barandiarán, 2019; Vivoda et al., 2024). In these countries, environmental and social protection regulations are often insufficient (Vivoda et al., 2024).

The environmental impact of Li mining from spodumene is often calculated for Australian concentrates, refined in China (Kelly et al., 2021). Lithium mining from hard rock ores is energy-consuming and during the pyrometallurgical treatment, potentially toxic gases and Li are to some part volatilized (Liu et al., 2017; Meng et al., 2021; Peerawattuk and Bobicki, 2018; Swain, 2017). The use of acids and other additives, such as lime and gypsum, can be problematic (Swain, 2017). Per ton of spodumene concentrate, 0.03 – 1.25 MWh electricity, 120 MJ heat and 0.4 – 3.0 m^3 fresh water are needed to produce a concentrate of 2.0 – 2.3% Li (Chordia et al., 2022; Kelly et al., 2021). After shipment of the spodumene concentrate, 6 – 14 t spodumene concentrate and 3.5 – 6.6 MWh electricity, 71 – 136 GJ heat, 3 – 12 t of chemicals and 11 – 77 m^3 of fresh water are consumed to produce one ton Li_2CO_3 or $LiOH{\cdot}H_2O$ (Chordia et al., 2022; Kelly et al., 2021). In comparison, the per capita municipal water consumption in developed countries varies between 74 – 231 m^3 per year (Song and Jia, 2023).

As the Li mining from salars is mainly conducted in the south American Li triangle, most studies that focus on the socio-environmental impact consider the Li mining from salars in Argentina and Chile (e.g., Chordia et al., 2022; Petavratzi et al., 2022). Mining from brines with low initial Li concentrations generally has a higher

environmental impact than mining from brines with higher Li concentrations (Chordia et al., 2022). Currently, the production of one ton of Li_2CO_3, consumes 4.0 – 4.2 t of concentrated brine, 0.4 – 0.6 MWh electricity, 3.0 – 3.2 GJ heat and 2 – 8 t of chemicals (Chordia et al., 2022; Kelly et al., 2021). For the $LiOH \cdot H_2O$ production from Li_2CO_3, 0.7 – 1.4 MWh electricity, 3.8 – 24 GJ heat, 1.2 – 1.6 t of chemicals and 0.5 – 29 m^3 fresh water are consumed, additionally (Chordia et al., 2022; Kelly et al., 2021).

Different studies compare and assess the environmental footprint of Li mining from salars and hard rock ores (Chordia et al., 2022; Flexer et al., 2018; Kelly et al., 2021). Although Li mining from brines seems to have a smaller environmental footprint than Li mining from pegmatites, mainly regarding emissions and material consumption, the prognoses for the future are slightly different. Due to the increasing Li demand and proceeding mining activities, it is expected that Li mining in South America will shift towards, on average, lower Li concentrations leading to higher emissions (Chordia et al., 2022). This trend, however, could profit from the development of novel, low CO_2 emitting and low energy, chemical and water consuming techniques, different from evaporation and precipitation (Chordia et al., 2022; Flexer et al., 2018). The Li mining from hard rock sources can be significantly improved if green energy is used in the mines of Australia and during refinement in China, rather than burning coal or diesel, rendering deposits with lower Li grades, like in Finland or Canada, more eco-friendly (Chordia et al., 2022).

The increasing water scarcity in the anyways dry region of the Atacama desert forces people to migrate (Agusdinata et al., 2018). The unique flora and fauna in the region is sensitive to minor changes in the water supply, e.g. the decrease of the threatened flamingo population by 10 – 12% within 11 years is related to Li mining in the Salar de Atacama and the salars in South America. Moreover, the salars are a sightseeing for tourists that additionally use the sparse fresh water (Agusdinata et al., 2018; Gutiérrez et al., 2022; Petavratzi et al., 2022). It is estimated that approximately one to five million liters of raw brine are needed to produce one ton of Li metal (Agusdinata et al., 2018; Chordia et al., 2022; Kelly et al., 2021). The brine is, however,

of high salinity and cannot directly be used for agriculture or as drinking water (Kelly et al., 2021). But the lack of reinjection of the large volume of brine that is pumped into evaporation ponds impacts the hydrology of the area, e.g. leads to a decreasing aquifer height, dilution of brine by groundwater mixture, which reduces its availability for other purposes, like drinking water or agriculture (Chordia et al., 2022; Kesler et al., 2012). Occasional leakage in the PVC ponds during evaporation bears the risk of contaminating the subsurface with chemicals, used for the precipitation during the extraction step (Agusdinata et al., 2018; Vivoda et al., 2024). For sustainable Li mining in the future, further detailed scientific studies on the socio-environmental impact are indispensable and the data should contribute to and strengthen the dialogue between residents, governments, acting companies and stakeholders (Petavratzi et al., 2022).

1.3 Geothermal brines

A valuable resource for Li is hosted in geothermal brines. The brines are produced in geothermal power plants that are usually used for heat and energy production. The geochemical composition of geothermal brines is highly variable and is determined by its source and its pathway. The main parameters controlling the physicochemical character of a brine are (1) the geology of the reservoir, (2) the reservoir temperature, (3) the brine pressure and (4) water-rock interaction (e.g., Drüppel et al., 2020). The geothermal brines in Germany are produced in the Ruhr District, Molasse Basin, the Upper Rhine Valley, e.g. in Bruchsal, Landau, Insheim, and the North German Basin, e.g. in Neustadt-Glewe, Neubrandenburg and Waren (Figure 5). In the Ruhr District, the brines occur in flooded parts where coal mining activities have ceased (Kranz and Dillenardt, 2010). The brines are a mixture of mine water, formation water, leachate and process water (Kessler et al., 2020). The geothermal brines in the Molasse Basin derive from Triassic – Jurassic sediments and a deeper Triassic Muschelkalk aquifer. Calcareous reservoirs are expected to lack high Li concentrations but in the Molasse Basin, the deep brines are NaCl dominated, have a TDS content of 10 – 75 g/L and locally reach Li concentrations of up to 162 mg/L (Stober et al., 2023).

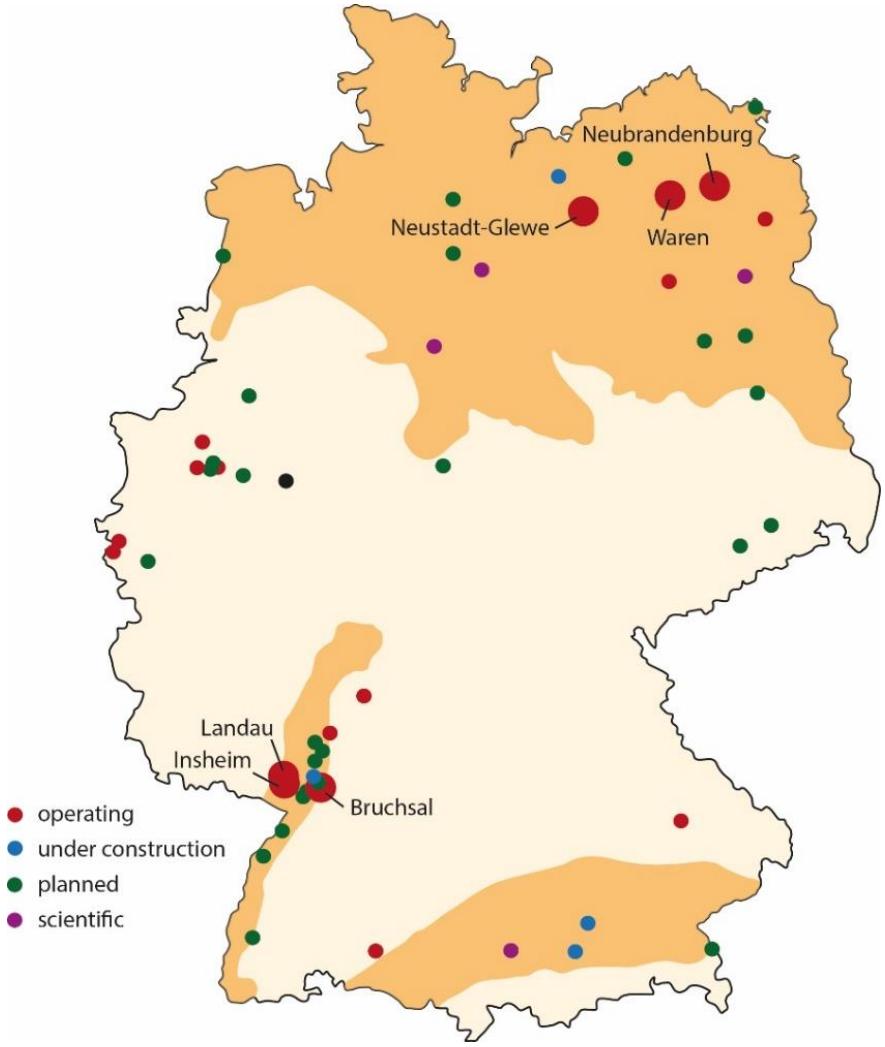

Figure 5. Overview on geothermal projects in Germany, modified after Bundesverband Geothermie (2021).

The reservoir geology in the Upper Rhine Valley and the North German Basin is dominated by Carboniferous gneiss, granite and Permian – Triassic sandstone (Regenspurg et al., 2016; Sanjuan et al., 2016). The geothermal brines in the Upper Rhine Valley have a TDS content of 106 – 125 g/L and a near-neutral to acidic pH (Sanjuan et al., 2016; Stober et al., 2014). Major constituents are Na^+ (28 – 38 g/L), K^+ (2.2 – 4.0 g/L), Ca^{2+} (7.3 – 7.7 g/L), Mg^{2+} (80 – 430 mg/L), SiO_2 (40 – 170 mg/L), Cl^- (64 – 75 g/L) and SO_4^{2-} (130 – 390 mg/L). The trace elements are dominated by Br, B, Sr, Ba, Mn, Fe, As, Rb, Cs, Zn and Pb. The Li concentrations in these brines are 160 – 180 mg/L (Sanjuan et al., 2016). In the North German Basin, the geothermal

brines have a TDS content of typically > 150 g/L (Stober et al., 2014). Major components are $Na^+ + K^+$ (54 – 81 g/L), Ca^{2+} (2.8 – 42.3 g/L), Mg^{2+} (0.9 – 2.3 g/L) and Cl^- (92 – 176 g/L) (Stober et al., 2014). Trace constituents are Fe, Mn, Ba, Sr, Li, Br, SiO_2, HCO_3^- (0.1 – 0.6 g/L) and SO_4^{2-} (0.3 – 2.4 g/L) (Stober et al., 2014). The gas content of geothermal brines is locally high, with gas/fluid ratios varying between 0.1 – 2.3 (Sanjuan et al., 2016; Stober et al., 2014). The gas phase in the Upper Rhine Valley is dominated by CO_2, with minor N_2, CH_4 and traces of He, O_2, H_2 and Ar (Sanjuan et al., 2016). In the North German Basin, the gas phase mainly comprises CO_2 with minor N_2 and CH_4 (Stober et al., 2014). Due to the complex chemistry of geothermal brines, the precipitation of minerals like calcite, gypsum, silica or barite, known as scaling, is a major challenge. Scaling may occur in the reservoir, boreholes or heat exchangers. The scaling, however, is avoided by keeping the brine's physicochemical properties constant at near-natural conditions or by adding inhibitors (Haklıdır and Balaban, 2019; Mundhenk, 2013; Wisotzky, 2019).

1.4 Direct Li extraction (DLE) state of the art

Direct Li extraction (DLE) comprises different techniques, such as direct precipitation, solvent extraction, membrane-based technologies and sorption (Choubey et al., 2017; Meng et al., 2021; Stringfellow and Dobson, 2021; Swain, 2017). All techniques aim at selectively recovering Li over competing ions in a minimal-invasive way. Currently, DLE undergoes intensive scientific investigation and some techniques, like electrochemical extraction, electrodialysis and sorption are already being tested at pilot-plant stage (Joo et al., 2020; Melnikov et al., 2017; Warren, 2021). Direct Li extraction techniques are considered for Li extraction from salars, seawater, geothermal brines and oilfield brines (Aljarrah et al., 2023; Joo et al., 2020; Kölbel et al., 2023; Li et al., 2021; Warren, 2021). This chapter aims at illustrating recent scientific advances in different DLE technologies, not included in Study I.

Evaporation, the currently used process to recover Li from salars at industrial scale (chapter 1.2.2), includes the controlled precipitation of mineral phases, like Li_2CO_3

by addition of Na_2CO_3 (Jin et al., 2023). Impurities in produced Li salt can be reduced by controlled crystallization. The crystallization of high purity $Li_2SO_4 \cdot H_2O$, for example, can be achieved by evaporation of a Li-rich H_2SO_4 solution. By ethanol addition, the yield increases but the product purity decreases due to co-precipitation of other phases. This method is, however, limited to a H_2SO_4 matrix (Ooi et al., 2017) and is thus not applicable for direct Li_2CO_3 crystallization from brines. Recent investigations show that by improved evaporation under low pressure, followed by precipitation, Li_2CO_3 of 95.8% purity is produced. The evaporation process is faster than the commercially established process, i.e. one ton Li_2CO_3 is produced within 1.84 days at a precipitation rate of 99.6% lithium salt (Aljarrah et al., 2023; Yi et al., 2018).

Organic chemicals that are insoluble in water are used in solvent extraction by mixing with a Li-bearing fluid leading to Li separation into the organic solvent (Shi et al., 2017). Due to the immiscibility of the two fluids, they separate by settlement for some time (Su et al., 2020). The acidic pH during the process is challenging and requires the use of highly resistant materials (Aljarrah et al., 2023). Using special mixtures of organic solvents as extractants, a recovery of 86% – >99% is achieved (Li et al., 2023; Su et al., 2020). However, organic solvents used for DLE, like tributyl phosphate, are often toxic or carcinogenic (Joshi and Adhikari, 2019; Zhang et al., 2021). The mixing with natural brine that is disposed or re-injected into the environment or reservoir, should thus be handled carefully.

The DLE from seawater and the brines produced by seawater desalination may contribute to 27 – 33% of the global Li demand in 2050 (Lundaev et al., 2022). In a three-step process (Li extraction, rinsing and recovery) Li is recovered from a desalination concentrate. A Li recovery of 88% (enrichment by a factor 1800) is achieved in electrochemical pilot plant experiments using λ-MnO_2/Ag electrodes after five cycles (Joo et al., 2020). The use of Ag electrodes, however, is challenging due to Ag availability and cost (Lundaev et al., 2022). By electrodialysis with ion-exchange membranes, 90.5% Li can be recovered from brines, tested for the East-Taijiner salt lake. The samples were, however, diluted before DLE (Nie et al., 2017).

In DLE using sorption and ion exchange, the sorbents are mixed with the Li-bearing brine (Chitrakar et al., 2012). After separation, the Li-depleted brine is treated accordingly, e.g. reinjected to its reservoir, and Li is recovered from the sorbent using a specific desorption solution (Chitrakar et al., 2012; Kölbel et al., 2023). From the solution, a Li product, like Li_2CO_3, can be precipitated (Kölbel et al., 2023). Lithium-aluminium hydroxide (often layered double Li-Al-hydroxide; LADH), lithium-titanium oxide (LTO) and lithium-manganese oxide (LMO) are the most studied sorbents for DLE (Kölbel et al., 2023; Orooji et al., 2022; Safari et al., 2020). These groups, only considering the chemical composition, comprise multiple different minerals with different properties in e.g. maximum Li capacity, selectivity, stability and kinetics (Bajestani et al., 2019; Isupov et al., 1999; Orooji et al., 2022; Safari et al., 2020). LADH are generally considered to achieve low Li sorption capacities of a few mg/g (e.g. 8 – 13.4 mg/g), but polymeric $Al(OH)_3$ has a sorption capacity of 123 mg/g (Hawash et al., 2010; Isupov et al., 1999; Zhang et al., 2023). Lithium-titanium oxide ion sieves have a maximum Li sorption capacity of 94.5 mg/g, whereas Mo-doped LTO achieves 78 mg/g, both tested in LiOH solutions (Lawagon et al., 2016; Orooji et al., 2022). LTO may overcome the challenge of limited chemical stability which is often a crucial issue for DLE (Orooji et al., 2022).

1.5 Sorption processes

Sorption processes comprise adsorption, absorption, ion exchange and surface precipitation. Adsorption is a term, established for the attraction of Li to typically Al-based sorbents (Farahbakhsh et al., 2023; Tran et al., 2017). It is defined as the accumulation of a solute at the interface of a sorbent and a fluid in a monolayer due to short-range repulsive and electrostatic forces (Gregg and Sing, 1982; Li and Stanforth, 2000; Pourret et al., 2022). Adsorption is distinguished into physisorption and chemisorption. Physisorption is mainly based on van der Waals forces, whereas chemisorption involves the formation of chemical bonds (Everett, 1972). Surface precipitation may be regarded as a form of multilayer adsorption, i.e. the surface

complexation, forming a separate phase on the sorbent surface (Sposito, 1987). If surface precipitation occurs, it can, however, make adsorption sites inaccessible for the solute (Li and Stanforth, 2000). For adsorption, the charge and the (internal and external) surface area are fundamental properties that need to be determined for the adsorbent (Li and Stanforth, 2000; Tran et al., 2017). Absorption describes the diffusion of a solute into a sorbent, changing the sorbent's composition and structure (Everett, 1972; Sposito, 1987).

Considering these definitions, sorption processes, based on ion exchange and redox reactions, are a special variety of absorption. Ion exchange of Li with surface protons, might, however, also be regarded as adsorption, i.e. chemisorption. The terms are often mixed up and used misleadingly in the existing literature, e.g. the term adsorption is often used when ion exchange is the described sorption process and changes in the crystal lattice parameters are identified (Farahbakhsh et al., 2023; Pourret et al., 2022). Moreover, LMO sorbents are known to undergo a redox reaction simultaneous to Li (de-)sorption (e.g., Seip et al., 2021), which should thus be regarded as absorption. The broader term sorption includes adsorption and absorption to or in a particle, respectively (Pourret et al., 2022). If the underlying sorption process cannot be specified or if multiple sorption processes are identified, which is often the case, the process should be referred to as sorption (Everett, 1972; Pourret et al., 2022; Sposito, 1984).

To investigate the sorption behavior of a solute to a mineral, sorption isotherms are experimentally obtained at constant physicochemical conditions, like temperature or reaction time (Limousin et al., 2007). Sorption isotherms are usually kinetically controlled. The reaction time for reaching equilibrium must thus be determined before sorption isotherms are conducted, otherwise, the sorption capacity of a sorbent may be underestimated by not reaching equilibrium (Limousin et al., 2007). Furthermore, (de-)sorption isotherms can either show the extraction of a solute from a mobile phase (i.e., liquid or gas), or the release of a solute into a mobile phase (Limousin et al., 2007). Kinetics are illustrated by plotting the amount of solute that is sorbed to a solid

(sorbent) versus the reaction time. Sorption isotherms, in contrast, illustrate the relation between residual solute concentration in the liquid/gas after the reaction and the amount of solute, sorbed to the sorbent (Limousin et al., 2007; Tran et al., 2017). The sorption and desorption processes are often not thermodynamically equal, i.e. sorption and desorption kinetics are different, resulting in a hysteresis, apparently indicating an irreversible process, which, however, is only an effect of kinetics rather than reflecting an incomplete process (Everett, 1972; Limousin et al., 2007).

Isotherms are described by their shape (Figure 6). The C isotherm, for instance, shows a proportional behavior between solute in a solution and sorbed to a sorbent. This isotherm is limited to low solute concentrations or implies that a sorbent has an infinite number of sorption sites that can be occupied by the solute. This sorption isotherm is also referred to in the Freundlich model (Limousin et al., 2007). The L isotherm often is the most suitable for the sorption of solutes to minerals. It reaches a plateau at high sorption capacities, indicating a progressive saturation of the limited number of sorption sites that can be occupied in a sorbent (Limousin et al., 2007). The H isotherm is a variety of an L isotherm with a very steep initial slope, indicating a high affinity of the solute for the sorbent (Limousin et al., 2007).

Assuming that all sorption sites are identical, can be occupied by one solute and are independent of one another, the Langmuir model is valid. The L and H isotherms, however, can be applied to many different models, like Freundlich, Rothmund-Kornfeld (for ion exchange), Redlich-Peterson, etc., which have to be considered for the specific case (Limousin et al., 2007). The S isotherm is a special isotherm, where the first sorption mechanism reflects the complexation of a mineral. After reaching the point of inflection, a 'normal' sorption of the solute takes place which can be modeled by a Sigmoidal Langmuir model (Limousin et al., 2007). The models are, however, mostly applicable to solute concentrations < 1 000 mg/L, i.e. limited to trace elements (Limousin et al., 2007).

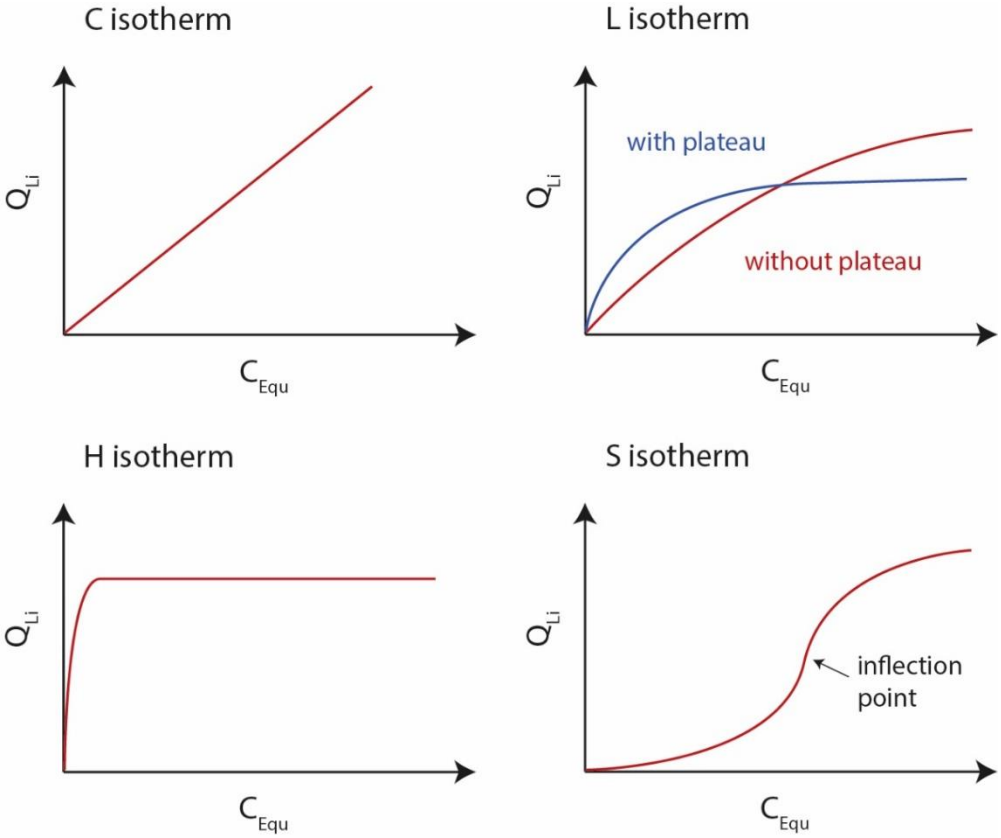

Figure 6. Overview of different sorption isotherms, modified after Limousin et al. (2007).

1.6 Objectives

The present thesis aims at identifying and testing potential novel materials that can be used to directly extract Li from high saline geothermal brines at elevated temperature. Mainly minerals that are already used in related applications, like wastewater treatment or the battery industry, and commercially available materials, are taken into consideration. The following tasks, objectives and research questions are addressed in this thesis:

(1) Sorbents that are used and/or tested at laboratory-scale for DLE are evaluated regarding Li sorption capacity, equilibration time and selectivity. Based on the assessment, novel minerals have been identified that may be applied in DLE. The results have been summarized in a literature review on DLE techniques from brines (Study I).
    - Which minerals can sorb Li and to which extend?
    - What are the underlying (de-)sorption processes and are they applicable in operating geothermal power plants?
    - What are the technical limitations, disadvantages and advantages of each sorbent?

(2) Preliminary Li extraction experiments with multiple sorbents that are regarded to have a high potential for DLE have been performed.
    - Which sorbents achieve the highest Li sorption capacity at fast kinetics in laboratory experiments under the same and required operating conditions, regarding Li concentration and pH?

(3) Identification of 1 – 2 sorbents that should be intensely tested in laboratory studies. Therefore, different systematic laboratory experiments had to be conducted with synthetic solutions, geothermal brine from Bruchsal, Germany and geothermal brine from the North German Basin, e.g. Neustadt-Glewe, Germany.

(4) The effects of different influencing parameters are evaluated regarding important physicochemical parameters.

- What is the maximum sorption capacity of the specific sorbent and under which conditions is it achieved?
- Which influence do variable pH and T have on the sorption process?
- Which competing ions influence the Li sorption? Does Li always have the same competing ions, universally transferable to every sorbent? What controls the Li selectivity? Can the Li selectivity be quantified for each sorbent?
- Which desorption solution is needed for the specific sorbent?
- What influences the sorption and desorption kinetics and how can the processes be characterized?
- What controls the chemical stability of the sorbent during sorption and desorption?
- Are the results obtained from experiments with synthetic solutions transferable to different geothermal brines?

(5) The sorbents are carefully characterized geochemically and mineralogically before and after the experiments to identify changes in the crystal lattice and prove the successful sorption and desorption of Li.

- Has Li sorption an effect on the sorbent crystal structure?
- Are desorption and sorption fully reversible processes?
- Can sorbent instability be specified at a crystallographic or microscopic scale?

2. Materials and Methods

2.1 Design of sorption experiments

Direct Li extraction (DLE) is generally conducted in 4 steps: (1) A high saline natural or artificial brine is mixed with a Li-ion sieve (LIS) for a defined amount of time and solid/liquid ratio. (2) After the reaction takes place, the sorbent is physically separated from the brine and the brine is disposed or treated appropriately. (3) The sorbent is mixed with a desorption solution where the sorbent is recycled and a Li-rich recovery solution is produced. (4) After physical separation of the desorption solution and the sorbent, the Li-enriched desorption solution is ready for further processing of a Li product and the sorbent is used for the repetition of steps (1 – 4; Figure 7). When DLE experiments are conducted in the laboratory, different issues have to be addressed and considered in the planning and performance.

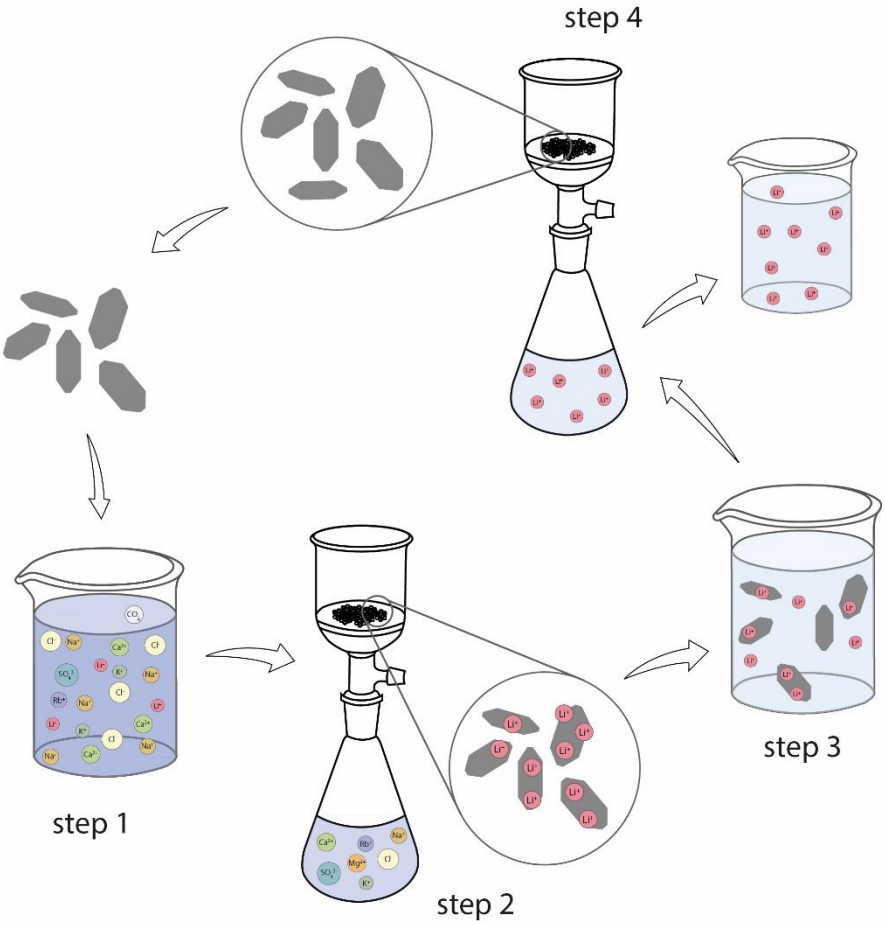

Figure 7. Schematic illustration of DLE experiments conducted in this thesis.

- The used sample and experimental vessels have to be rinsed and cleaned properly before the experiment. For this, high-purity millipore water and/or 1 – 2% HNO_3 should be used.
- The experiments should be planned according to the objective. Reaction time, temperature, stirring speed/shaking intensity, pH, sorbent/fluid ratio and element concentrations have to be defined.
- Ideally, only one parameter per experiment is variable to exclude the influence of multiple variable parameters. This ensures robust scientific results.
- For the kinetic experiments, the reaction time for each experiment in the isotherm has to be planned according to the used sorbent. If the equilibrium time is unknown, a large time interval should be covered by one experimental batch, e.g. experiments between one minute and several days should be conducted.
- For the isotherm experiments, the required sorbent/fluid ratios need to be defined. Alternatively, the sorbent mass/fluid ratio can be fixed while initial Li concentrations are variable.
- For experiments using natural geothermal brine, the brine should be filtered before the experiment to ensure that pre-precipitated crystals are removed and do not influence the experiments, i.e. pre-precipitated phases may represent nuclei where ions can adsorb or lead to the precipitation of secondary phases.
- The solutions should be prepared and equilibrated with the experimental vessel at the needed temperature.
- Before each experiment, a sample for ICP-OES and/or ICP-MS analysis should be taken. Additionally, the millipore water, used for rinsing of the material after DLE, should be sampled. A small amount of each sample should be used for the determination of temperature and pH before the experiment.

- Directly after sampling, the sorbent must be added, the vessel must be properly closed and the experiment starts.
- After the experiment, the samples are filtered immediately. Thereafter, a sample of the solution must be taken for chemical analysis. A small volume of the sample should be separated for pH and temperature determination.
- The instruments should be rinsed with millipore water, e.g. the feeding bottle of the vacuum filtration instrument. Thereafter, the filter cake (with the sorbent) is rinsed with a defined volume of millipore water to remove the remaining interparticle fluid.
- The sorbent is rinsed from the filter and dried in an oven at 60°C (40°C for the experiments with clay minerals) for a minimum of 24 h or absolute dryness.
- In sum, fluid samples are taken of at least the initial solution before each experiment and the solution after the experiment. Additional samples of the rinsing fluid can be added for quality control. Temperature and pH must be measured. The samples for the cation analyses by ICP-OES and ICP-MS are conserved by the addition of 1 µL 65% (subboiled) HNO_3 per mL sample. Afterward, the samples are stored in the fridge to avoid occasional microbial activity.

2.2 Preliminary sorption experiments

Different potentially promising novel minerals for DLE from geothermal brines have been identified by an intense literature review (Study I). In preliminary sorption experiments, a clay mineral mixture mainly comprising montmorillonite (Alfa Aesar, Montmorillonite K10, CAS: 1318-93-0, LOT: 10230622), a natural zeolite clinoptilolite (Cellavita, micronized 1 – 40 µm, LOT: ZW-5-9-11), a synthetic zeolite 13X (Alfa Aesar, powder, CAS: 63231-69-6, LOT: 10229992) and iron phosphate tetrahydrate (Sigma Aldrich, CAS: 31096-47-6, LOT: BCBW9874), have been tested. The aim of the experiments was a first qualitative estimation of the Li sorption ability of the minerals.

Before the experiments, clinoptilolite and zeolite 13X were calcined at 400°C for 3 h in an oven for material activation and crystal stabilization. The chemical composition of the starting materials was determined by X-ray fluorescence (XRF) in wavelength dispersive mode of fused beads, except for Fe-phosphate tetrahydrate which has been digested in aqua regia and analyzed by ICP-OES due to its low melting point at ~ 550°C. The XRF results have been corrected for the loss of ignition (LOI) and the results are presented in Table 1. The batch experiments have been conducted in HDPE vessels. In all experiments, 200 mL of a synthetic LiCl solution was mixed with 1 g sorbent material. All solutions have been buffered using KH_2PO_4. The pH was adjusted to pH = 5 – 6 using NaOH. The mixtures were stirred for 1, 5, 15, 30, 45, 60, 120, 180, 540 and 1440 min at a constant stirring rate of approximately 300 rpm. After vacuum filtration, the filter cake was rinsed with 100 mL millipore water and afterward dried at 60°C (40°C for the clay minerals) in an oven for 24 h. The synthetic LiCl solutions before and after the experiments were analyzed by ICP-OES.

Clay minerals are known to adsorb cations, like Li, to their negatively charged phyllosilicate surface (Williams and Hervig, 2005). Lithium can additionally substitute octahedrally coordinated cations in the clay mineral lattice or protons at the crystal edges (Eckstein et al., 1970; Williams and Hervig, 2005). The reason why montmorillonite was chosen for preliminary experiments is that Li is often found in montmorillonite in nature (Amer, 2008). Furthermore, smectite-group minerals, which montmorillonite belongs to, are typically associated with sedimentary Li deposits or occur in alteration zones of pegmatites and granites (Dill, 2020). The montmorillonite sample used for preliminary kinetic experiments consists of Si (311 mg/g), Al (35 mg/g), K and Fe (8 mg/g), Mg (6 mg/g), Ti (3 mg/g), Ca (2 mg/g), Na (1 mg/g) and minor Mn (0.1 mg/g) (Table 1).

Zeolite group minerals have a microporous framework and their negative lattice charge increases with decreasing Si/Al ratio (Luan et al., 1999; No et al., 1981), advantageous for the sorption of cations, like Li^+, to achieve charge balance. The zeolite 13X powder has a Si/Al ratio of 1.2, whereas the Si/Al ratio of natural clinoptilolite is

4.8. The clinoptilolite sample has a high content of Ca and K at 22 mg/g and 14 mg/g, respectively. The zeolite 13X is mainly of Na endmember composition (61 mg/g Na). Minor and trace elements are Mg, P, Ti, Mn and Fe (Table 1). For zeolites, literature data on the extraction of Li from geothermal brines is available (Lemaire et al., 2014; Wiśniewska et al., 2018). Zeolite 13X reached a sorption capacity of ~ 12 mg/g using LiCl solutions (Lemaire et al., 2014). In another study, a natural clinoptilolite and a synthetic zeolite Na-X were compared for DLE and the achieved Li sorption capacity for both zeolites was rather low at < 0.5 mg/g (Wiśniewska et al., 2018). The two zeolites were chosen to test if these results can be reproduced or if higher sorption capacities may be achieved with a different fluid composition.

Iron phosphate is known to be able to intercalate Li, with a rather high selectivity (Intaranont et al., 2014). Literature data is available for the Li intercalation in heterosite and deintercalation from triphylite (Intaranont et al., 2014; Kuss et al., 2014). A high Li sorption capacity of > 40 mg/g is indicated and competing ions are extracted at < 3 mg/g (Intaranont et al., 2014). Due to the promising results, a Fe-phosphate was additionally tested. The sample for the preliminary experiments is of high purity, but analyses show a Na content of 12 mg/g (Table 1).

Table 1. Chemical composition of starting materials for preliminary sorption experiments.

		montmorillonite	zeolite clinoptilolite	zeolite 13X	iron phosphate tetrahydrate
method		XRF	XRF	XRF	ICP-OES
LOI	wt%	12.92	10.14	11.10	-
total	wt%	86.40	89.48	88.38	-
corrected total	wt%	98.73	99.28	99.02	-
Li	mg/g	-	-	-	<0.0008
Na	mg/g	1	2	61	12
Mg	mg/g	6	3	2	0.02
Al	mg/g	35	32	78	0.06
Si	mg/g	311	317	192	<0.02
P	mg/g	0.1	0.04	0.01	139
K	mg/g	8	14	1	0.1
Ca	mg/g	2	22	2	0.1
Ti	mg/g	3	1	0.1	-
Mn	mg/g	0.1	0.2	-	-
Fe	mg/g	8	5	1	240

The results of preliminary kinetic experiments confirm that all tested minerals may be able to sorb Li, generally (Figure 8). The results from blank experiments, however, indicate that the apparent sorption capacity for montmorillonite and zeolite clinoptilolite might be extremely low (< 1.5 mg/g) or neglectable due to analytical uncertainties and the high blank values (Figure 8a, b). In experiments with montmorillonite, the vacuum filtration was much slower, e.g. 30 min – 1 h. Furthermore, due to the long filtration, the laboratory pumps overheated and filtration occasionally had to be stopped. Due to the platy phyllosilicate habitus and dispersion behavior of clay minerals, they are not recommended to be used for DLE, neither in laboratory experiments nor at industrial scale. The filtration time for zeolite clinoptilolite was comparably long, with a duration of 20 min per sample, indicating that the sample clogged the filter, disadvantageous for DLE. Furthermore, the blank experiment that was stirred for more than 14 h indicates a higher Li sorption capacity than all experiments where clinoptilolite was included, confirming that the Li sorption capacity of clinoptilolite is neglectable.

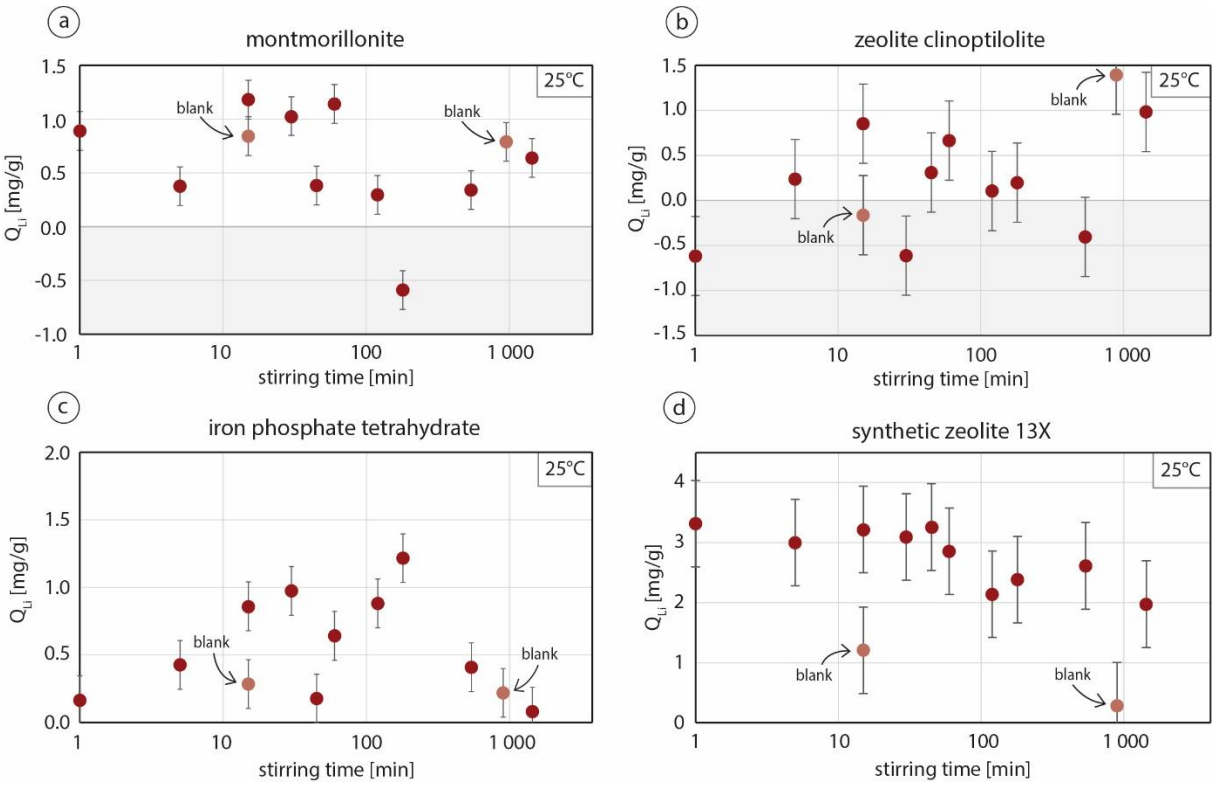

Figure 8. Preliminary kinetic sorption experiments of montmorillonite, iron phosphate tetrahydrate, zeolite clinoptilolite and zeolite 13X at 25 °C, plotted as Q_{Li} [mg/g] versus stirring time [min].

The iron phosphate tetrahydrate sample indicates a higher sorption capacity for Li than observed in the specific blank experiments (Figure 8c). However, the achieved 1.2 mg/g after 3 h reaction time is low (Figure 8c). The Fe-phosphate tetrahydrate is amorphous and does not reflect the crystal properties needed for Li intercalation (Intaranont et al., 2014; Kuss et al., 2014).

The synthetic zeolite 13X achieved a Li sorption capacity of 3.3 mg/g within the first minute of the reaction (Figure 8d). The sorption capacity is significant compared with the blank experiments (max. 1.2 mg/g). Therefore, synthetic zeolite 13X was considered most promising for a detailed investigation for DLE.

3 List of publications

Study I

Rebekka Reich, Klemens Slunitschek, Rosa Micaela Danisi, Elisabeth Eiche & Jochen Kolb (2022): Lithium Extraction Techniques and the Application Potential of Different Sorbents for Lithium Recovery from Brines, Mineral Processing and Extractive Metallurgy Review, DOI: 10.1080/08827508.2022.2047041

Study II

Rebekka Reich, Rosa Micaela Danisi, Tobias Kluge, Elisabeth Eiche & Jochen Kolb (2023): Structural and compositional variation of zeolite 13X in lithium sorption experiments using synthetic solutions and geothermal brine, Microporous and Mesoporous Materials, DOI: 10.1016/j.micromeso.2023.112623

Study III

Rebekka Reich, Elisabeth Eiche & Jochen Kolb (2024): Delithiation and lithiation of $LiFePO_4$: Implications for direct Li extraction from synthetic solutions and geothermal brines, Desalination, DOI: 10.1016/j.desal.2024.117883

Other publications, related to but not included in this thesis

Katharina Steiger, Rebekka Reich, Klemens Slunitschek, Klaus Steinmüller, Christian Bergemann, Christoph Hilgers, Jochen Kolb (2022): Lithium in Europa, In: Katharina Steiger, Christoph Hilgers, Jochen Kolb (Eds.), THINKTANK für Industrielle Ressourcenstrategien, 101 S., Karlsruhe, DOI: 10.5445/IR/1000154047

Lena Kölbel, Klemens Slunitschek, Elif Kaymakci, Thomas Kölbel, Rebekka Reich, Jochen Schneider (2024): Lithium recovery from geothermal brines: An investigation into radioactive nuclide uptake on lithium-manganese-oxide (LMO) granules, Hydrometallurgy, DOI: 10.1016/j.hydromet.2024.106266

4. Personal contribution

The contributions of each author for Studies I – III, included in this thesis, are listed in the tables below. The contribution percentages for the categories *scientific ideas*, *data generation*, *analysis and interpretation* and *paper writing* are approximate estimations and do not result from a calculation based on a numerical dataset.

Author	Author position	Scientific ideas [%]	Data generation [%]	Analysis and interpretation [%]	Paper writing [%]
Reich, R	**1**	**45**	**65**	**55**	**50**
Slunitschek, K	2	5	15	15	5
Danisi, RM	3	5	5	5	15
Eiche, E	4	15	5	5	10
Kolb, J	5	30	10	20	20
Study I	Lithium Extraction Techniques and the Application Potential of Different Sorbents for Lithium Recovery from Brines				
Status	Accepted and published				

Author	Author position	Scientific ideas [%]	Data generation [%]	Analysis and interpretation [%]	Paper writing [%]
Reich, R	**1**	**40**	**95**	**55**	**60**
Danisi, RM	2	20	0	20	15
Kluge, T	3	10	0	10	10
Eiche, E	4	10	5	5	5
Kolb, J	5	20	0	10	10
Study II	Structural and compositional variation of zeolite 13X in lithium sorption experiments using synthetic solutions and geothermal brine				
Status	Accepted and published				

Author	Author position	Scientific ideas [%]	Data generation [%]	Analysis and interpretation [%]	Paper writing [%]
Reich, R	**1**	**80**	**95**	**70**	**70**
Eiche, E	2	10	5	15	15
Kolb, J	3	10	0	15	15
Study III	Delithiation and lithiation of $LiFePO_4$: Implications for direct Li extraction from synthetic solutions and geothermal brines				
Status	Accepted and published				

For the publications that are related to, but not included in this thesis, no numerical estimation of the contributions can be given. Therefore, my contributions to these studies are described in the following.

"Lithium in Europa" was published by the THINKTANK für Industrielle Ressourcenstrategien, Karlsruhe in 2022 (Steiger et al., 2022). The study provides an overview of the global Li market and mine production. Furthermore, it summarizes different Li projects that are currently under development. As the second author of this study, I contributed with a database on global Li occurrences, market prices and global production data. Furthermore, I have written and/or contributed to the introduction, the chapters about global Li occurrences and production, global market, mining, refinement and metallurgy, projects related to magmatic hard rock deposits, sedimentary deposits and fundamentals of Li extraction methods. In addition, I have read and revised the full publication together with the other authors. Parts of the publication that were delivered by myself, are included in chapter 1 of this thesis.

The publication "Lithium recovery from geothermal brines: An investigation into radioactive nuclide uptake on lithium-manganese-oxide (LMO) granules" was published in the journal Hydrometallurgy in 2024 (Kölbel et al., 2024). I have been involved in conducting the experiments and the sampling on-site. I also contributed by writing and editing during the review process of the publication.

5. Scientific investigations

3.1 Study I: *Lithium Extraction Techniques and the Application Potential of Different Sorbents for Lithium Recovery from Brines*

Large Li resources are hosted in brine deposits around the globe. The study represents a comprehensive review of different direct Li extraction (DLE) techniques from aqueous resources, including evaporation, direct precipitation, membrane processes, solvent extraction and ion exchange and sorption.

Based on literature data, different sorbents and Li-ion sieves (LIS) are assessed for their potential application in DLE from geothermal brines. An evaluation of advantages and disadvantages of Li-Mn-oxides (LMO), Ti-oxides (LTO), Al-hydroxides, Fe-oxy-hydroxides, Li-Fe-phosphates (LFP), clay minerals and zeolite group minerals in operating geothermal power plants is a focus in this study. Additionally, research questions that should be addressed in the future are raised and minerals, potentially interesting for an industrial application in DLE are identified.

3.2 Study II: *Structural and compositional variation of zeolite 13X in lithium sorption experiments using synthetic solutions and geothermal brine*

Zeolite group minerals have been identified as promising novel sorbents for DLE from geothermal brines. This study investigates synthetic zeolite 13X powder and compares zeolite 13X powder with beads in DLE performance in laboratory experiments. Both materials are characterized structurally and chemically. The underlying sorption processes are investigated for synthetic solutions. The results have been adapted in experiments with geothermal brine, considering the optimal conditions for the sorbent and the physicochemical conditions, like pH and temperature, ambient in operating geothermal power plants. It is concluded that commercially available zeolite 13X has many advantageous properties for DLE, but its limited Li selectivity makes an application in geothermal brines impossible.

3.3 Study III: *Delithiation and lithiation of $LiFePO_4$: Implications for direct Li extraction from synthetic solutions and geothermal brines*

Since zeolite 13X has been identified as not being appropriate for DLE application in geothermal power plants, Li-Fe-phosphate (LFP) cathode material, representing a highly Li-selective material, is investigated for its applicability in DLE from geothermal brines. The study investigates the optimal delithiation and lithiation conditions of LFP in a purely chemical redox process. The high Li selectivity of the material is confirmed but other limitations are identified, like the use of a problematic additive, lacking material formulation of nanoparticles and co-precipitation of undesired phases. Nevertheless, this novel sorbent has a promising DLE performance, applicable to different brine compositions.

Study I

Lithium Extraction Techniques and the Application Potential of Different Sorbents for Lithium Recovery from Brines

Rebekka Reich, Klemens Slunitschek, Rosa Micaela Danisi, Elisabeth Eiche & Jochen Kolb

This work has been published in Mineral Processing and Extractive Metallurgy Review

published online: 08 Mar 2022

available online:

https://www.tandfonline.com/doi/full/10.1080/08827508.2022.2047041

DOI: 10.1080/08827508.2022.2047041

MINERAL PROCESSING AND EXTRACTIVE METALLURGY REVIEW
https://doi.org/10.1080/08827508.2022.2047041

Taylor & Francis
Taylor & Francis Group

Lithium Extraction Techniques and the Application Potential of Different Sorbents for Lithium Recovery from Brines

Rebekka Reich[a], Klemens Slunitschek[a], Rosa Micaela Danisi[b], Elisabeth Eiche[a], and Jochen Kolb[a]

[a]Chair of Geochemistry and Economic Geology, Institute of Applied Geosciences, Karlsruhe Institute of Technology, Karlsruhe, Germany; [b]Chair of Technical Petrophysics, Institute of Applied Geosciences, Karlsruhe Institute of Technology, Karlsruhe, Germany

ABSTRACT

Geothermal power plants produce large amounts of high-temperature fluids from variable depths. These fluids can be enriched in lithium to up to 240 mg/L, rendering them an exploitable resource, not yet processed at industrial scale. The pressure on Li demand is expected to increase in the future, making the technical degradability of new Li resources indispensable. We examine Li-extraction methods from aqueous solutions systematically, dealing with evaporation, direct precipitation, membrane-related processes, solvent extraction, sorption, and ion exchange. Sorption and ion-exchange techniques are regarded to be the most promising methods with a high potential for the feasible lithium extraction. Therefore, Li sorption on different inorganic sorbents, in particular for the implementation into operating geothermal power plants, is evaluated. Inorganic sorbents, such as lithium–manganese oxide, titanium oxide, aluminum hydroxide, iron phosphate, clay minerals, and zeolite group minerals besides other sorbents, e.g. zirconium phosphate, tin antimonate, antimony oxide, tantalum oxide, and niobium oxide, are regarded. Promising inorganic sorbents for an environmentally friendly, efficient, and selective Li extraction are lithium–manganese oxide, iron phosphate, or zeolite. To evaluate the effectiveness of these sorbents to large-scale industrial Li_2CO_3 (or LiOH) production, we highlight their potential advantages and disadvantages in the application under geothermal operating conditions.

KEYWORDS

Sorption; ion-exchange; inorganic sorbents; geothermal; direct lithium extraction (DLE)

Introduction

Lithium is an important component in several industrial applications and is used in lithium–ion batteries (LIBs), ceramics, glass, cement, special alloys, lubricants, air conditioners, polymers, chemicals, and nuclear power plant industry as well as psycho-medical pharmacy (Gruber et al. 2011; Kudryavtsev 2016; Meng et al. 2021; Nie et al. 2017; Peerawattuk and Bobicki 2018; Swain 2017). It is lithophile, the lightest solid alkali earth element and highly mobile in fluidal systems due to its incompatibility in most silicates (Benson et al. 2017; Gruber et al. 2011; Mohr, Mudd and Giurco 2012). It mainly occurs as monovalent cation in solution and is characterized by a small dehydrated and hydrated ionic radius of 0.6 and 3.4 Å, respectively (Helmke and Sparks 1996). Its small ionic radius is similar to that of Mg^{2+} and Na^{+} (0.72 and 1.02 Å, respectively), which makes Li separation from these elements in solution difficult (e.g. Song et al. 2017; Wei et al. 2020). Lithium occurs in several species, e.g. $Li^{+}_{(aq)}$, $LiOH_{(aq,s)}$, $Li_{(s)}$, $LiH_{(s)}$, $LiSO_4^{-}$, $Li_2O_{(s)}$ and $Li_2O_{2(s)}$ (Blanc et al. 2012; Takeno 2005) and the oxygen coordination of Li is mostly tetrahedral or distorted octahedral (Tadesse et al. 2019; Wenger and Armbruster 1991). The dominant Li species in aqueous solutions is Li^{+}, which is assumed to occur in four-fold $[Li(H_2O)_4]^{+}$ clusters at T = 25–100°C, P = 1 bar, pH < 13.5, Eh = −0.8–1.2 V, total dissolved solids (TDS) = 100 g/L (Blanc et al. 2012; Bowell et al. 2020; Sanjuan et al. 2016; Sverjensky, Shock and Helgeson 1997; Takeno 2005; Wunder et al. 2007).

Major Li deposits are igneous rocks, sedimentary rocks, and brines comprising 25–35%, 8–13%, and 52–66% of the world's Li resources in 2019, respectively (Figure 1; Gruber et al. 2011; Mohr, Mudd and Giurco 2012; Sykes 2019). Ambrose and Kendall (2020a) estimate the total global Li resource at 55–99 Mt Li. Bolivia, Argentina, Chile, USA, and Australia have the largest resources world-wide, owning 21 Mt, 19.3 Mt, 9.6 Mt, 7.9 Mt, and 6.4 Mt Li, respectively (Figure 1; Schmidt 2017; US Geological Survey 2021). Currently, the world's major Li producers are Australia, Chile, Argentina, and China (Schmidt 2017; US Geological Survey 2021). An additional theoretical resource is seawater, comprising 230 Gt Li (Fasel and Tran 2005).

The future demand of Li is expected to grow rapidly. The global annual Li demand is estimated to increase by factors of 27–37 from 32,000 t annual production in 2012 to 850,000 – 1,200,000 t Li in 2050 (Xu et al. 2020; Ziemann et al. 2018). Considering 90% recycling rate and an increase in the annual gross domestic product of 2–3%, 12–20 Mt Li would be required globally between 2010 and 2100 (Gruber et al. 2011). However, recycling is not expected to significantly reduce the global Li demand by 2050 since most recycling technologies are currently under investigation only at lab-scale (Ambrose and Kendall 2020a; Asadi Dalini et al. 2021; Moazzam et al. 2021; Xu et al. 2020). It remains uncertain whether recycling can reduce the demand for battery-grade Li since current recycling technologies produce Li with insufficient purity (e.g. Qiao et al. 2021; Ziemann et al. 2018).

CONTACT Rebekka Reich rebekka.reich@kit.edu Chair of Geochemistry and Economic Geology, Institute of Applied Geosciences, Karlsruhe Institute of Technology, Campus Süd, Adenauerring 20b, Gebäude 50.40, Karlsruhe 76131, Germany

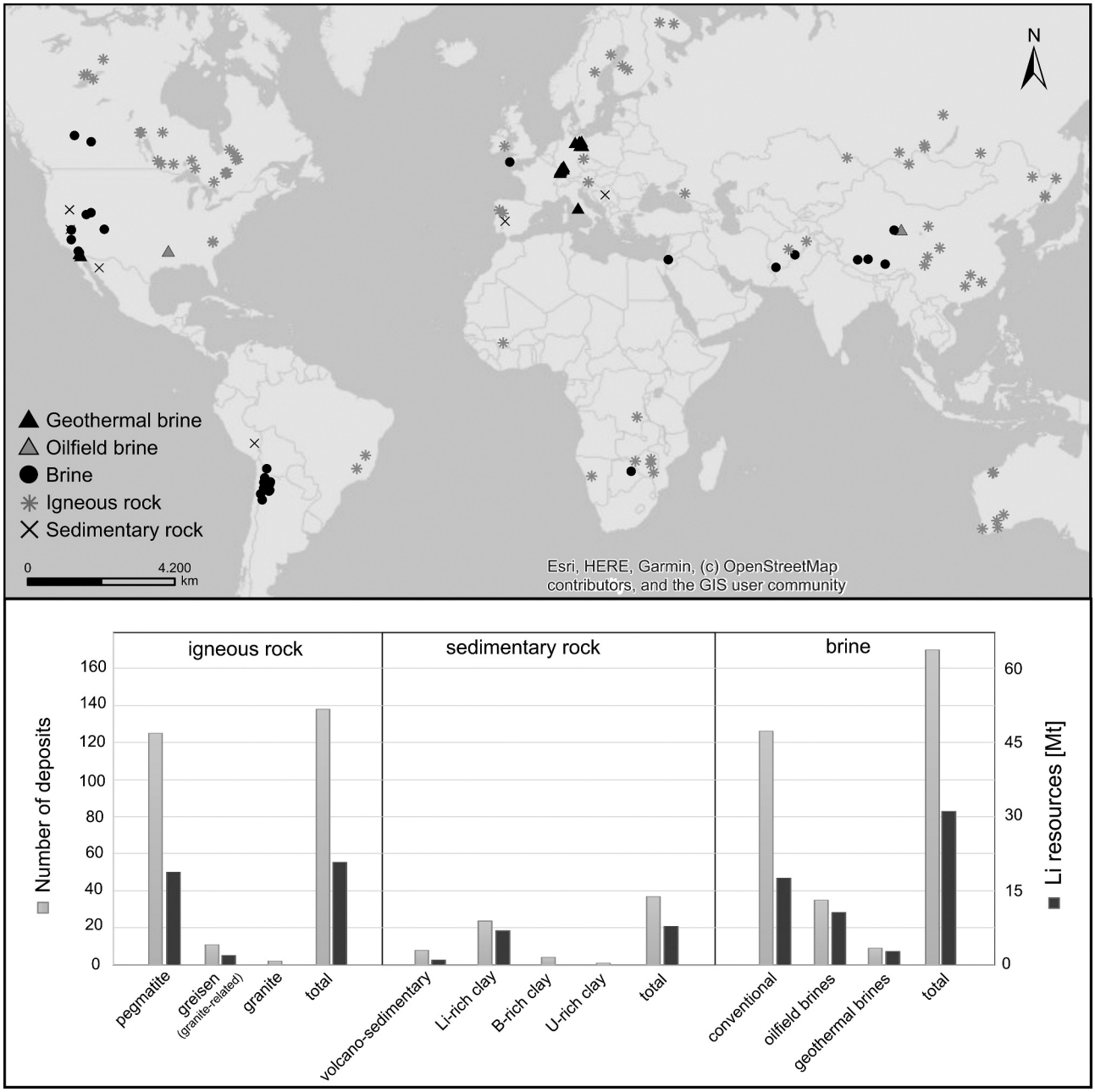

Figure 1. Global Li deposits and resource distribution between different deposit types. Data from Pauwels et al. (1993), Houston (2010), Savannah Resources Plc (2010-2021), Kesler et al. (2012), Schmidt (2017), Sykes (2019), The Mineral Corporation (2019), Bowell et al. (2020), Bundesanstalt für Geowissenschaften and Rohstoffe (2020), Rio Tinto (2020), Mining Data Online (2021). Basemap from ArcGIS (2020).

With the resources currently available, the demand can be met, but new methods for Li extraction from aqueous solutions will become more important in the future (Kawamoto and Tamaki 2011; Liu et al. 2014; Peerawattuk and Bobicki 2018; Yaksic and Tilton 2009). An alternative source may be geothermal brines. The geochemistry of the brines is variable (Table 1) and differs between the various localities, but can also change over time at one location, reflecting water–rock interaction processes. Lithium-bearing, conventionally mined brines and typical geothermal brines are similarly characterized by TDS ~100–330 g/L, slightly acidic to slightly alkaline pH and high concentrations of major cations (e.g. 47–135 g/L Na^+, 2–27 g/L K^+) and anions (e.g. 50–190 g/L Cl^-, 1.5–470 g/L SO_4^{2-}) (Table 1; Pauwels, Brach and Fouillac 1993, Aquilina et al. 1997, Pueyo, Chong and Ayora 2017, Reidel and Ehren 2018, Garcia et al. 2020). Lithium concentrations in most brines vary between 20 and 1750 mg/L (Table 1), which is considerably higher than Li concentrations in Earth's major lakes, oceans (0.17 mg/L Li^+) and freshwater (Ambrose and Kendall 2020a; Dodbiba et al. 2014; Hoyer, Kummer and Merkel 2015; Kudryavtsev 2016; Meng et al. 2021). Besides geothermal brines, oilfield brines, which are similar to geothermal brines regarding temperature, pressure, and flow rate, are reported to comprise Li and can significantly increase the global Li resources (e.g. 750,000 t Li in the Smackover Formation, USA) (Collins and Vine 1976; Evans 2008). However, reliable resource estimations for brine systems are complicated since climatic effects, precipitation of salts with time and fluid flux have to be taken into consideration (Border and Sawyer 2014).

Table 1. Comparison of chemical composition and average pH values in geothermal brines (Germany), conventionally mined brines and common fluids, sediments, soils, and Earth's crust.

	Li^+[mg/L]	Na^+[g/L]	K^+[g/L]	Ca^{2+} [g/L]	Mg^{2+} [g/L]	Cl^- [g/L]	SO_4^{2-} [g/L]	TDS [g/L]	pH
Geothermal brines	150–240	60–135	4–27	1–16	2–17	120–180	1.5–62	100–300	~5
Conventionally mined brines	18–1750	47–110	2–25	0.02–36	0.030–34	50–190	3.5–470	170–330	~8
Earth's major lakes and oceans	0.1–14	30	5	15	30	160	0.5	0.5–30	~8
Freshwater	0.0007–0.04	0.005–0.013	0.0002–0.0008	0.0008–0.009	0.0005–0.002	0.007–0.024	0.003–0.008	<0.5	6–7
Seawater	0.17	10	0.4	0.4	1	20	3	30–40	~8
	Li [mg/kg]	Na [g/kg]	K [g/kg]	Ca [g/kg]	Mg [g/kg]	Cl [g/kg]	S [g/kg]		
Sediment	56	4–12	4–12	7–54	9–18	-	-	-	6–7.5
Soil	3–350	0.001–7	0.0007–10	0.001–10	0.00005–6	0.001–0.1	0.001–0.5	-	4–11
Earth's crust	20–60	12–25	12–30	25–50	15–30	0.3–0.6	9–20	-	-

Data from Banks (1953), Gorham (1956), Morcos (1970), Butterman (1988), Bukowsky and Uhlemann (1993), Condie (1993), Wedepohl (1995), Bohn, Myer and O'Connor (2002), Banks et al. (2004), Zhu et al. (2006), Blackford and Gilbert (2007), Ferreira et al. (2007), Aral and Vecchio-Sadus (2008), McCauley, Jones and Jacobsen (2009), Marion et al. (2011), An et al. (2012), Dodbiba et al. (2014), Hoyer, Kummer and Merkel (2015), Choubey et al. (2017), Flexer, Baspineiro and Galli (2018), Moran (2018), Mimura et al. (2019)

Direct Li extraction (DLE) from geothermal brines is accompanied by major challenges. The process has to be stable in order to resist high pressure (~20 bars), high temperature (~60–80°C), and needs to operate at specific pH due to the danger of scaling at high pH, depending on the solubility of the respective mineral phase (Haklıdır and Balaban 2019). As the flow rate in geothermal power plants is continuously high with up to 90 L/s (Stober and Bucher 2012), fast extraction kinetics are needed. Due to the high TDS of up to 300 g/L (Table 1), the DLE must have a high Li selectivity to prevent extraction of undesired components and thus, reduce purification efforts in previous or following processing steps. Additionally, a high Li recovery rate is needed to minimize Li reinjection into the ground and to increase the efficiency of the DLE process (Warren 2021).

Review articles about different Li extraction methods from minerals (e.g. Cisternas et al. 2021; Gourcerol et al. 2019; Salakjani, Singh and Nikoloski 2021; Tadesse et al. 2019), aqueous solutions (e.g. Meng et al. 2021; Meshram and Pandey 2018; Stringfellow and Dobson 2021; Swain 2016; Zhang et al. 2019) and different sorbents are available (e.g. Choubey et al. 2017, 2016; Safari, Lottermoser and Alessi 2020). However, sparse work has been done in specifically addressing the technical challenges and practicability of Li recovery from geothermal brines. Therefore, this article aims at examining the potential application of different extraction techniques for future implementation into geothermal power plants.

Extraction techniques for brines

Evaporation

Evaporation is one of the most popular techniques for Li recovery from salt lake brines and is also considered for seawater (e.g. An et al. 2012; Epstein et al. 1981). The liquid is pumped into large evaporation ponds where the concentration of Li and other dissolved elements becomes relatively enriched during evaporation (Figure 2)). With increasing concentration, precipitation of less soluble salts, e.g. halite (NaCl), gypsum ($CaSO_4 \cdot 2\ H_2O$), carbonates ($(Ca, Mg, Fe)CO_3$), carnallite ($KCl{\cdot}MgCl_2 \cdot 6H_2O$), or bischofite ($MgCl_2 \cdot 6H_2O$) at ~4.4 wt.% Li proceeds (Figure 2); An et al. 2012; Ventura et al. 2016). Lithium concentration is increased to ~6 wt.% before further processing (Peerawattuk and Bobicki 2018). Ions such as Mg^{2+}, Ca^{2+}, and BO_3^{3-} are removed by addition of precipitants to increase the purity of Li-concentrates (An et al. 2012; Peerawattuk and Bobicki 2018). Finally, the addition of Na_2CO_3 induces precipitation of Li_2CO_3 at high purity (99.5–99.9% Li_2CO_3) (An et al. 2012; Peerawattuk and Bobicki 2018).

Due to Li-carnallite precipitation, Li recovery only reaches ~50–80% (Table 2; An et al. 2012, Ventura et al. 2016). This effect is minimized by attentive control of the evaporated volume, since Li recovery is increased by ~50%, with the Li concentration not exceeding 1500 mg/L and the solution level in the ponds kept above 0.32 m (Valdez, Flores and Orce 2016). Lithium recovery is additionally dependent on the brine chemistry: Li_2SO_4 precipitation occurs after 31 days of evaporation at the Salar de Uyuni, whereas Li is progressively enriched in the Salar de Atacama due to preferred Na and K precipitation (Ogawa et al. 2014).

Evaporation is simple and cheap, with total production costs of 2,000–5,700 US$/t lithium carbonate equivalent (LCE) (Ambrose and Kendall 2020a; Gaikwad, Misal and Gupta 2011). The evaporation process, however, is time consuming (i.e. several months or years) and only works in areas where the ponds are exposed to the sun with high evaporation and low precipitation rates (Gaikwad, Misal and Gupta 2011; Safari, Lottermoser and Alessi 2020; Wiśniewska et al. 2018). Significant amounts of freshwater (5–50 m^3 freshwater/t LCE) are consumed, which is of concern regarding the aridity of most areas with processing facilities (Flexer, Baspineiro and Galli 2018) and large areas for the evaporation ponds (80.53 km^2 in the Salar the Atacama in 2017, Liu, Agusdinata and Myint (2019d)) are needed. Scientific studies concerning the environmental effects of water consumption and land-use change for Li extraction are sparse (Flexer, Baspineiro and Galli 2018; Kaunda 2020; Kelly et al. 2021; Marazuela et al. 2020). Evaporation can be optimized by manual induction of energy, rendering the method more efficient although higher energy consumption increases the environmental impact and the cost (Gaikwad, Misal and Gupta 2011). Although suitable

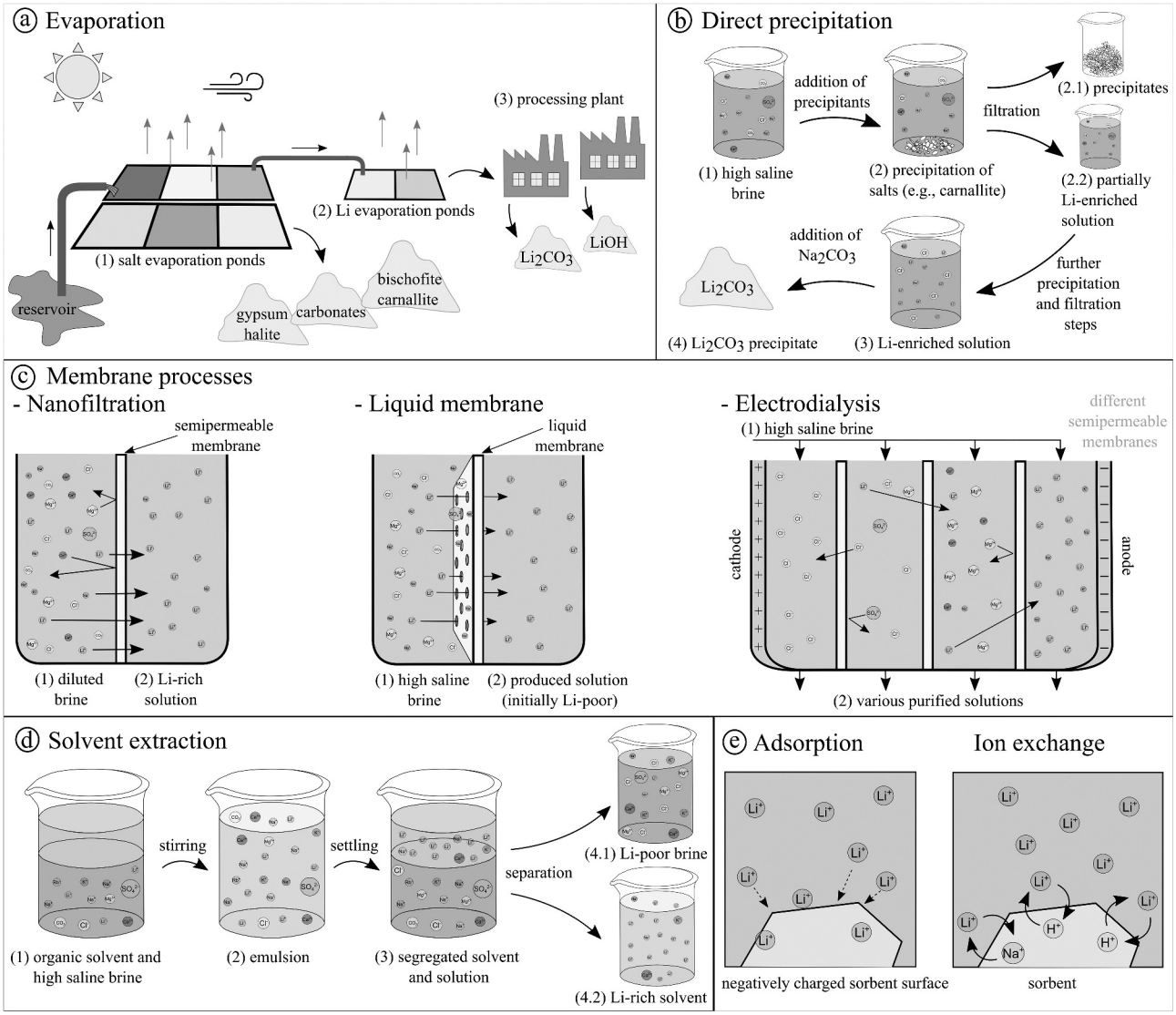

Figure 2. Sketch of different extraction technologies for Li from aqueous solutions. (a) Evaporation process of conventionally mined brines in Bolivia, Chile and Argentina; (b) Direct precipitation from brines including the precipitation of e.g. carnallite and optional further purification steps prior to Li precipitation; (c) Different membrane processes, e.g. nanofiltration (selectivity based on ion charge), liquid membrane (selectivity based on ionic radius and complexation) and electrodialysis (combination of electric current and different semipermeable membranes); (d) Solvent extraction using organic solvents for Li extraction; and (e) Adsorption, where a negatively charged surface causes van der Waals bonding with a positively charged Li ion and Ion exchange, where Li ions substitute monovalent cations in the sorbent.

for Li processing from salars, evaporation for processing geothermal brines is not generally applicable globally because of long evaporation times needed, the land use of evaporation ponds, and the required climatic conditions (Flexer, Baspineiro and Galli 2018; Gaikwad, Misal and Gupta 2011; Liu, Agusdinata and Myint 2019d).

Direct precipitation

Direct extraction by precipitation is based on the formation of chemical compounds by reducing the solubility of dissolved species. Precipitation is influenced by variation in pH, temperature, redox, impurities, and concentration of precipitant (Figure 2); Zhang et al. 2019). For natural brine systems, numerous precipitation methods exist, e.g. carbonate and aluminate precipitation, and borate and phosphate co-precipitation (Zhang et al. 2019). The method used depends on the specific brine composition, especially on the Mg/Li ratio, as Mg and Li have similar ionic properties and are therefore difficult to separate (Table 2; Nie et al. 2017). With increasing Mg/Li ratio, Mg has to be pre-precipitated to recover Li (Figure 2)). Thereby, 20–30% of the Li are lost (Zhang et al. 2019), presumably due to Li-carnallite precipitation (An et al. 2012). By-products and interfering elements (e.g. B, Mg, Fe, Ca) are precipitated by addition of different reagents (e.g. CaO, NaOH, $C_2H_2O_4$, $AlCl_3{\cdot}H_2O$) prior to the extraction of the desired element (Table 2; An et al. 2012, Zhang et al. 2019, Ambrose and Kendall 2020a). At the last stage, Li_2CO_3 precipitation is induced by Na_2CO_3 addition (Figure 2); Zhang et al. 2019). To increase the Li recovery to up to 98–99%, aluminum salts (i.e. $NaAlO_2$ or $AlCl_3$) are the most suitable co-precipitants for Li at pH of 10–13 (Table 2; Yoshinaga, Kawano and Imoto 1986). Precipitation of solutes from geothermal brines is currently investigated in pilot-scale projects (Borrmann, Schweig and Johnston 2019; Goldberg et al.

Table 2. Overview of commonly used and recently studied lithium extraction methods.

Method	Time	Technical effort	Industrial scale	Energy consumption	CO_2	Applicable to (medium)	Resources [Mt Li]*	Chemicals/ hazards	Li recovery [%]	Cost	Source
Evaporation	+	-	Yes	-	o	Brine	31–67	NaOH, $C_2H_2O_4$, $AlCl_3{\cdot}H_2O$, CaO, $NaAlO_2$, Na_2CO_3	~50–80	o	Gaikwad, Misal and Gupta (2011), Ambrose and Kendall (2020a), Kelly et al. (2021)
Precipitation	-	-	Yes	-	o	(Low Mg/Li-) brine	31–38	Seawater evaporation	98–99	o	Yoshinaga, Kawano and Imoto (1986), Liu et al. (2017), Nie et al. (2017), Zhang et al. (2019), Ambrose and Kendall (2020a), Ambrose and Kendall (2020b), Kelly et al. (2021)
Membrane processes	o	-	Pilot	-	-	Seawater, (low-Mg -B/"low"-Na) brine, LIBs	230,000 + 31–38 + ?	Organic membrane	5–22	o	Li et al. (1983), Sakamoto, Kimura and Shono (1987), Fasel and Tran (2005), Wen et al. (2006), Hoshino (2013), Somrani, Hamzaoui and Pontie (2013), Melnikov et al. (2017), Ambrose and Kendall (2020a)
Solvent extraction	o	o	Pilot	-	-	Brine, seawater, LIBs	31–67 + 230,000 + ?	TBP, TOPO, TTA, HDBM, kerosene/ methyl isobutyl ketone, isoamyl alcohol, 2-Ethyl-1,3-hexanediol, diisopropyl ether, diethyl ether, $FeCl_4^-$, ClO_4^-, $B(C_6H_5)_4^-$, acidic wastewater	65–96	-	Epstein et al. (1981), Bukowsky and Uhlemann (1993), Nan, Han and Zuo (2005), Kawamoto and Tamaki (2011), Harvianto, Kim and Ju (2016), Xiang et al. (2016), Liu et al. (2017), Shi et al. (2017), Ambrose and Kendall (2020a), Millennial Lithium Corp (2020), Warren (2021)
Sorption and ion exchange	-	o	Pilot	-	-	Brine, LIBs	31–67 + ?	Desorption/ leaching solution (see Table 3)	95	-	Pauwels, Brach and Fouillac (1990), Tian, Ma and Han (2010), Ambrose and Kendall (2020a)

- Minor/less.
o Neutral/none/average.
+ Yes/high/much.
? No literature data.
* Estimated resource to which the method is applicable.

Table 3. Overview of different mineral sorbents studied for selective Li-extraction from geothermal brines.

Sorbent	t_{Equ}	Ideal pH	Ideal temperature [°C]	Type of sorption	Q_{max} [mg/ g]	Chemicals/ hazards	Industrial scale	Source
Mn-oxides	24 h	Alkaline	>30	$H^+ \leftrightarrow Li^+$ ion exchange	53.5	HCl, HNO_3	Pilot	Wang et al. (2008), Tian, Ma and Han (2010), Xiao et al. (2012), Liu et al. (2015), Bajestani, Moheb and Masigol (2019), Qian et al. (2019), Ventura et al. (2020), Warren (2021)
Ti-oxides	10–192 h	Alkaline	60	$H^+ \leftrightarrow Li^+$ ion exchange	94.5	HCl, HNO_3	Pilot	Chitrakar and Abe (1988), Shi et al. (2013), Moazeni et al. (2015), Lawagon et al. (2016), Wang et al. (2016), Wei et al. (2020), Li et al. (2021), Marthi et al. (2021)
Al-hydroxides	5 min–24 h	7–9	30–80	Physisorption & $H^+ \leftrightarrow Li^+$ ion exchange	123.5	CH_3COONH_4, H_2SO_4, HF	Pilot	Pauwels, Brach and Fouillac (1990), Hawash, Abd El Kader and El Diwani (2010), Prodromou (2016), Heidari and Momeni (2017), Fukuda (2019)
Fe-oxy-hydroxides	?	Alkaline	?	Physisorption & $H^+ \leftrightarrow Li^+$ ion exchange	3.5	?	No	Nielsen et al. (2005), Kim, Nielsen and Grey (2008), Heidary, Khodabakhshi and Kharat (2016)
$FePO_4$	1.5–3 h	7	25–65	$Na^+ \leftrightarrow Li^+$ ion exchange/redox reaction	46.4	$K_2S_2O_8$, NaCl	No	Intaranont et al. (2014), Fukuda (2019), Liu et al. (2019c), Sun et al. (2020)
Clay minerals	?	Alkaline?	<50	Physisorption & $H^+ \leftrightarrow Li^+$ ion exchange	0.9	$Ca(CH_3COO)_2$	No	Greene-Kelly (1955), Eckstein, Yaalon and Yariv (1970), Gaskova and Bukaty (2008), Meroufel et al. (2013)
Zeolites	15–30 min	Alkaline	40– ?	$Na^+ \leftrightarrow Li^+$ ion exchange	25.0	HCl	No	Navarrete-Casas et al. (2007), Lemaire et al. (2014), Wiśniewska et al. (2018)

? No literature data.

2021) and thus needs more research and development for upscaling. The major challenge in applying direct precipitation is related to the complexity of controlling coprecipitation effects to maximize the Li recovery rate.

Membrane processes

Selective extraction using membranes gains increasing interest for Li extraction from brines (Somrani, Hamzaoui and Pontie 2013; Song et al. 2017). Membrane processes, also referred to as reverse osmosis, include the technologies of nanofiltration, liquid-membrane, and electrodialysis (Gaikwad, Misal and Gupta 2011; Wiśniewska et al. 2018). The membranes are selective for Li rather than other ions due to differences in ion charge, ionic radius or diffusive properties (Sun et al. 2015).

Nanofiltration describes ion filtration through membranes with different selectivity for mono- and divalent ions (Figure 2)), which is often also called "near reverse osmosis" or "near ultrafiltration" (Gaikwad, Misal and Gupta 2011; Van der Bruggen 2013). The membranes can be made of polymers, ceramics, or polymeric-ceramic combinations (Van der Bruggen 2013). To reduce the osmotic pressure on the membranes prior to the separation of monovalent Li^+ from divalent ions, such as Mg^{2+} or Ca^{2+}, the brine must be diluted (Figure 2); Somrani, Hamzaoui and Pontie 2013; Song et al. 2017; Sun et al. 2015; Wen et al. 2006). Furthermore, Sun et al. (2015) found that an increase in temperature to >18–20°C negatively affects the selectivity of the membrane due to an increased osmotic pressure, decreasing viscosity of the solution and a change in the membrane pore size. Wen et al. (2006) and Somrani, Hamzaoui and Pontie (2013) show that nanofiltration is not applicable for Li separation of high Mg- and B-brines and it also fails to separate Li^+ from Na^+ (Figure 2)).

Liquid membranes separate a large volume of Li-rich solution from a smaller volume of Li-poor solution. Lithium is thereby efficiently transported against the osmotic gradient from the Li-rich into the Li-poor solution (Figure 2); Sakamoto, Kimura and Shono 1987). Most liquid membranes reported in literature are organic compounds, e.g. nitrophenols, polyether amide derivatives, or crown ether derivatives (Sakamoto, Kimura and Shono 1987; Warnock et al. 2021). High selectivity for Li^+ compared to Na^+ in a chloride matrix was found since Na^+ dehydrates more easily than Li^+ forming complexes with the studied membrane (Figure 2)). Hoshino (2013) coupled an organic liquid membrane with electrodialysis to selectively recover Li^+ over Na^+ from seawater with Li recoveries between only 5–22% (Table 2).

Electrodialysis is based on different diffusion rates for monovalent and divalent cations in an electric current (Figure 2)). For electrodialysis application, a cathode, an anode, and an electrolyte medium are needed (Figure 2); Peerawattuk and Bobicki 2018). The electric current applied induces redox reactions in the electrodes by incorporation of Li^+ where the anode recovers Li from the aqueous solution, which is very similar to electrolysis (Song et al. 2017). However, semipermeable membranes are used in electrodialysis to successively separate the ions and thereby purify the recovered solution (Figure 2); Melnikov et al. 2017). For cathodes and anodes, different materials are used, e.g. $FePO_4/LiFePO_4$, $Ag/Na_2S_2O_3$ and λ-MnO_2/Ag (Peerawattuk and Bobicki 2018; Song et al. 2017). Due to their high salinities, brines or spent LIBs can be used as the electrolyte and the Li source. Also, brines with complex chemical composition, e.g. those with high Mg/Li ratios can be treated, as Li and Mg are separated by the semipermeable membrane (Figure 2); Song et al. 2017). The presence of sulfate ions improves Li recovery (Nie et al. 2017). The voltage has to be carefully controlled, as deposition of contaminants, e.g. Na^+, Mg^{2+}, on the electrodes may be caused (Zhao et al. 2013).

Operational costs for membrane processing of Li from brines are estimated at ~3.000 $/t LCE (Song et al. 2017; Warren 2021). Direct lithium extraction techniques based on membrane processes combined with organic ion-exchange resins are already tested at pilot scale (Melnikov et al. 2017). Reaction times of 8 h were applied for 77 cycles over a total test time of 770 h (Melnikov et al. 2017). This is however much longer compared to ~10 min for >85% extraction of Cu (Li et al. 1983; Melnikov et al. 2017). Membrane processes are easy to control and require little energy because only low electrical currents of 1–18 V are applied (Song et al. 2017). The main problem by applying Li selective membranes is that poorly soluble phases, e.g. $CaSO_4$, become enriched in the brine (Gaikwad, Misal and Gupta 2011). The application of membrane technologies for processing Li from geothermal brines is challenging because cooling of the brine is critical and their efficiency is limited to specific brine compositions and long reaction times in a regime with high flow rates (Melnikov et al. 2017; Somrani, Hamzaoui and Pontie 2013; Sun et al. 2015; Wen et al. 2006).

Solvent extraction (or liquid–liquid extraction)

The solvent extraction method, also called liquid–liquid extraction, is based on the distribution of a solute, e.g. Li, in two immiscible liquid phases of different densities physically separated in a vessel (Figure 2); Rydberg 2004). One phase contains the solute (e.g. Li in the brine or seawater), while the other one acts as solvent (commonly an organic compound) into which the solute diffuses after mixing (Figure 2)). The extraction efficiency is given by the ratio of solute concentration in both phases. It increases with increasing solvent volume and simultaneously decreases with equilibrium extraction time (Harvianto, Kim and Ju 2016; Rydberg 2004). Known solvents for Li extraction are listed in Table 2 (Harvianto, Kim and Ju 2016; Lee et al. 1968; Shi et al. 2017; Xiang et al. 2016). However, there is only a limited selectivity for Li^+ compared to Na^+, K^+, Ca^{2+}, and Mg^{2+} (Figure 2); Harvianto, Kim and Ju 2016). Seawater, for example, needs to be pretreated: Mg is removed by precipitation and the pH must be increased to 10.6–11.0 before Li extraction (Harvianto, Kim and Ju 2016; Warren 2021). In contrast, Bukowsky and Uhlemann (1993) found increasing extraction efficiency for LiCl with decreasing pH (<6) using an isoamyl alcohol and 2-ethyl-1,3-hexanediol solvent. Solvent extraction is also used to recycle spent LIBs (Asadi Dalini et al. 2021; Nan, Han and Zuo 2005). The LIBs have to be dismantled before leaching the metals by alkalis,

dissolution with H_2SO_4 and filtration, before the actual solvent extraction of Co, Cu, as well as Li_2CO_3 precipitation can be performed (Asadi Dalini et al. 2021; Nan, Han and Zuo 2005).

The solvent extraction method has to be used in combination with other extraction techniques due to limited selectivity (Table 2; compare Nan, Han and Zuo 2005, Harvianto, Kim and Ju 2016). A Li recovery between 65% and 96% is reached and it is an inexpensive technology (~2,800 US$/t LCE from the Dead Sea) but produces large amounts of acidic wastewater and toxic organic solvent waste (Table 2; Epstein et al. 1981, Kawamoto and Tamaki 2011, Harvianto, Kim and Ju 2016, Liu et al. 2017, Shi et al. 2017, Joshi and Adhikari 2019, Su et al. 2020). The method is already part of pilot-scale tests, e.g. in Salta, Argentina (Millennial Lithium Corp., 2020). The application of solvent extraction for DLE from geothermal water is regarded to be critical since the fluid's physicochemical properties have to be changed and competitive elements need to be removed (Harvianto, Kim and Ju 2016).

Sorption and ion exchange

Inorganic sorbents are intensively studied regarding their implementation into new technologies for Li recovery from (geothermal) brines (e.g. Guneysu 2020; Taghvaei, Taghvaei and Askari 2020; Weng et al. 2020; Xue et al. 2020). Sorption is defined as a reaction between a solute and an insoluble phase that removes the solute from the solution (Figure 2); Barrow 2008). Sorption of a solute on a sorbent can occur in different ways: (1) hydrated ionic species can form outer-sphere complexes on the sorbent surface, (2) dehydrated ions can form inner-sphere complexes, or (3) the ion can be more strongly bound to the crystal structure of the sorbent (Limousin et al. 2007).

Because sorption is a kinetically, and sometimes also physically, controlled process, adsorption and desorption durations can be extremely variable and thermodynamic equilibrium is often not reached (Limousin et al. 2007). To describe a sorption process, it is crucial to characterize the retention (i.e. adsorption) and release (i.e. desorption) of a solute, by sorption isotherms (Limousin et al. 2007).

In ion-exchange processes, an insoluble solid phase, comprising exchangeable cations or anions, interacts with the compounds in a liquid phase (Helfferich 1995). An equal amount of exchangeable cations from the exchanger can be substituted by cations from the solution (Figure 2); Bruggenwert and Kamphorst 1979; Helfferich 1995). All ion-exchange processes (independent of the selected exchanger) depend on pH, temperature, ion concentration in the solution, the structure and specific kinetics of the exchanger and its cation exchange capacity (CEC), the use of additives, contact time, and the stirring rate (e.g. Bouguerra et al. 2007; Eckstein, Yaalon and Yariv 1970; Hawash, Abd El Kader and El Diwani 2010; Lemaire et al. 2014; Navarrete-Casas et al. 2007; Ooi et al. 2016; Prodromou 2016; Sullivan et al. 2003; Sun et al. 2020; Wiśniewska et al. 2018). The most common ion-exchange process for systems containing Li can be described as: $Li^+_{(aq)} + Cl^-_{(aq)} + (Na,H)X \leftrightarrow (Na,H)^+_{(aq)} + Cl^-_{(aq)} + LiX$ where X denotes the ion exchanger (Figure 2); e.g. Gast and Klobe 1971; Kim and Grey 2010; Marthi et al. 2021; Navarrete-Casas et al. 2007; Ooi et al. 2016).

Inorganic sorbents

Li-Mn-oxides

Lithium manganese oxide sorbents (LMO) are a group of synthetical sorbents with a Mn-O framework and various crystal structures, e.g. orthorhombic ramsdellite-type (e.g. Zhang et al. 2007), tetragonal hollandite-type (e.g. Feng et al. 1995b) or cubic spinel-type (e.g. Chitrakar et al. 2000). Spinel-type sorbents, e.g. $Li_{1+x}Mn_{2-x}O_4$, $Li_{1.6}Mn_{1.6}O_4$ and λ-type MnO_2, are of particular interest as they reach Li sorption capacities of up to 53.5 mg/g (Figure 3, Table 3) after 24 h equilibration time (e.g. Bajestani, Moheb and Masigol 2019; Ohashi and Tai 2019; Slunitschek, Kolb and Eiche 2021; Yoshizuka et al. 2021). Additionally, spinel-type LMO have high Li selectivity (sorption of <5 mg/g competing ions) and stability (Bajestani, Moheb and Masigol 2019; Kawamoto and Tamaki 2011; Ohashi and Tai 2019; Ooi, Miyai and Katoh 1987; Ryu et al. 2015). The sorption capacity increases with increasing temperature during the experiments and T > 30°C increases the Li uptake (Qian et al. 2019; Wang et al. 2008). Lithium is de-/intercalated in LMO by Li^+ $^-$ H^+ -ion exchange and a redox reaction, whereas the share of each process on total Li sorption depends on the LMO chemistry (Feng et al. 1992; Gao et al. 2019; Ooi, Miyai and Sakakihara 1991; Xu et al. 2016; Yoshizuka et al. 2021). While desorption of redox-intercalated Li leads to LMO degradation caused by the disproportionation of $Mn(III)_{(s)}$ to $Mn(IV)_{(s)}$ and $Mn(II)_{(aq)}$, ion-exchange-intercalated Li has no effect on the chemical stability of the material (Feng et al. 1992; Gao et al. 2019; Hunter 1981; Ooi, Miyai and Sakakihara 1991). Commonly used desorption solutions (Table 3) are diluted acids, such as HCl (Xiao et al. 2015b, 2012; Yoshizuka et al. 2021; Zhu et al. 2014) or HNO_3 (Feng et al. 1995a; Ooi et al. 1989; Sato et al. 1997). During Li^+ elution using HCl, Mn dissolution of up to 60% with 3 mol/L HCl occurs but can be reduced significantly by using less concentrated (<2 mol/L) HCl (Yoshizuka et al. 2021). Ventura et al. (2020) tested Li desorption using CO_2 gas without affecting the chemical stability of the sorbent. To increase the chemical stability, transition metals (e.g. Sb, Ce, Cr, Cu, Co, Ni, Fe) can be incorporated into the framework during synthesis (Bajestani, Moheb and Masigol 2019; Cao et al. 2019; Chitrakar et al. 2014; Li et al. 2014; Liu, Sun and Yu 2019a; Zhao et al. 2018).

The high Li selectivity of spinel-type LMO results from tunnels in the Mn-O structure that forms a Li-selective ion-sieve (e.g. Bajestani, Moheb and Masigol 2019; Cao et al. 2019; Chitrakar et al. 2014; Han, Kim and Park 2012; Hong et al. 2018; Li et al. 2014; Liu, Sun and Yu 2019a; Yoshizuka et al. 2021). Lithium is sorbed inside the structure and on the surface while sorption of competing ions is restricted to the sorbent surface (Miyai, Ooi and Katoh 1988; Slunitschek, Kolb and Eiche 2021; Zhang et al. 2010b). To improve the sorption performance and chemical stability of LMO-type sorbents, the parameters during synthesis are modified. The framework

structure of spinel-type Mg-doped LMO is achieved by focusing on the structural properties during synthesis (Chitrakar et al. 2013). The combination with $Al(OH)_3$ or with electrochemical techniques improves the LMO sorption properties as well (Tian, Ma and Han 2010, Han, Kim and Park 2012; Chitrakar et al. 2014; Li et al. 2014; Hong et al. 2018; Bajestani, Moheb and Masigol 2019; Cao et al. 2019; Liu, Sun and Yu 2019a).

The selectivity order is $Na^+ < K^+ < Rb^+ < Cs^+ \sim Mg^{2+} < Ca^{2+} < Li^+$ (Figure 3; Ooi, Miyai and Katoh 1987; Zandvakili and Ranjbar 2018; Zhang et al. 2007), but strongly depends on the chemical composition of the solution (Chitrakar et al. 2000; Miyai, Ooi and Katoh 1988; Zhang et al. 2010b). The Li^+ sorption capacity generally increases with increasing pH (optimum at pH 12) and Li^+ concentration (200 mg/L) up to 37.4 mg/g, reaching recoveries up to 95% after four adsorption/desorption cycles (Tian, Ma and Han 2010). Chitrakar et al. (2014) extracted Li^+ from unbuffered and buffered brines of the Salar de Uyuni (Bolivia) using Fe-doped LMO reaching Li^+ uptake capacities of 18 mg/g at pH = 2 and 28 mg/g at pH = 7.2. Chromium-doped LMO reach sorption capacities of 31.7 mg/g but show Mn loss of 0.35–3.5% within the first 20 adsorption/desorption cycles, resulting in decreasing sorption capacities of 2.5–19.5% (Bajestani, Moheb and Masigol 2019; Cao et al. 2019, and references therein; Ohashi and Tai 2019). The kinetics and chemical stability of λ-MnO_2 are improved by coating with CeO_2 (Li et al. 2014).

Ryu et al. (2013) improve Li selectivity of $Li_xMn_{2-x}O_4$ by 3 times by applying an electric voltage. Moreover, they reduce the use of acids for Li desorption and improve the lifetime of the sorbents. The combination of LMO-type sorbents with electrochemical techniques in a flow-through reactor produces a Li-solution of 94% purity after 9 sorption cycles (Palagonia, Brogioli and La Mantia 2020). The application of 0.5 mA induces the reduction of LMO and simultaneously oxidizes NiHCF in a brine containing 1 mM LiCl and 100 mM NaCl. This represents a coupled process where Li^+ is de-/intercalated to LMO by redox reactions and a $Na^+ \leftrightarrow K^+$ exchange takes place in NiHCF (Palagonia, Brogioli and La Mantia 2020).

With the aim of making DLE from seawater industrially applicable, Han, Kim and Park (2012) synthesized a spherical mm-sized ion-sieve foams (SIFs) from spinel-type LMO. Using the SIFs, Li^+ adsorption capacity reaches 3.4 mg/g, which remains constant over five adsorption/desorption cycles. The desorption rate is 86%. Yoshizuka et al. (2021) synthesized $Li_{1.6}Mn_{1.6}O_4$ hydrothermally and reached sorption capacities of 36 mg Li^+/g from seawater at pH = 8.1. Hong et al. (2018) investigate composites consisting of 75% LMO and 25% Al_2O_3 and find a Li^+ adsorption capacity of 9 mg/g and <1% Mn loss after five adsorption/desorption cycles.

The application of LMO-type sorbents for DLE from geothermal water remains challenging due to high cost of the raw material, the use of acids for desorption (e.g. Ventura et al. 2020; Xiao et al. 2015a), its redox-sensitivity (e.g. Ariza et al. 2006; Park, Singhal and Jho 2015) and possibly time-consuming synthesis of the sorbent (Zhang et al. 2010b). Nevertheless, LMO are already intensively studied and regarded as potentially feasibly applicable and are therefore tested in pilot-scale projects for DLE from geothermal brines and seawater Li extraction (Liu et al. 2015; Ventura et al. 2020; Warren 2021).

Ti-oxides

Titanium nanoribbons, $H_2Ti_3O_7$, $H_4Ti_5O_{12}$, H_2TiO_3 and Ti-Sb-sorbents have been studied for their Li sorption behavior (Safari, Lottermoser and Alessi 2020; Wei et al. 2020; Wiśniewska et al. 2018; Zhang et al. 2010c). These phases can be hydrothermally and/or thermally synthesized from TiO_2 (anatase or rutile) (e.g. Chaban et al. 2019; Gentili et al. 2012; Li et al. 2020; Moazeni et al. 2015; Olson, Nelson and Islam 2006; Taghvaei, Taghvaei and Askari 2020), but the synthesis is complicated and time-consuming (e.g. Zhang et al. 2010c; Safari, Lottermoser and Alessi 2020 and references therein).

Ji et al. (2017) synthesized a H_2TiO_3 Li sorbent from Li_2CO_3 and TiO_2 within 5 h. Sorption capacities for an equilibrium time of 60 min decreased from ~27–24 to ~19–17 mg/g Li^+ after three sorption/desorption cycles. Synthetic porous spinel $H_4Ti_5O_{12}$ nanofibers are highly Li^+ selective ($K_d(Li^+)$ = 232 mL/g, K_d (Na^+, K^+, Mg^{2+}, Ca^{2+}) <1.5 mL/g) and reach a high sorption capacity of ~60 mg/g, which decreases after 6 adsorption/desorption cycles to 86.5% of the initial value (Wei et al. 2020). Molybdenum-doped Ti-oxide is highly selective for Li (i.e. ~93% Li^+, ~7% competing ions of total ions adsorbed) and adsorbs up to 78 mg/g Li^+ (Table 3; Wang et al. 2019).

The sorption kinetics of Ti-oxide sorbents are relatively slow, but increase with increasing temperature (Table 3; Zhang et al. 2010c, Moazeni et al. 2015, Lawagon et al. 2016, Wei et al. 2020, Marthi et al. 2021). Equilibrium times vary between 10 and 192 h (Table 3) for hydrothermal waters and synthetic LiCl and LiOH solutions, with sorption capacities between <1 and 94.5 mg/g Li^+ at alkaline pH, respectively (Figure 3; Zhang et al. 2010c; Shi et al. 2013; Lawagon et al. 2016; Choubey et al. 2017, and references therein). The ad-/desorption process is a Li^+ – H^+-ion exchange (Marthi et al. 2021; Moazeni et al. 2015; Wei et al. 2020). Titanium loss (0.06–2.50% Ti^{4+}) during desorption with HCl or HNO_3 results in a progressive decrease in sorption capacity within five cycles (Gu et al. 2018; Kamran and Park 2020; Lawagon et al. 2016).

Titanium oxides are promising for an industrial-scale application in geothermal power plants regarding implementation possibilities (e.g. as nanoribbons) and high sorption capacities. The long equilibration times needed and limited chemical stability of the sorbent are challenging, but Ti-oxides are already tested regarding Li extraction from geothermal brines and seawater at pilot scale (Li et al. 2021).

Al-hydroxides

Amorphous, polymeric, and crystalline $Al(OH)_3$ as well as hexagonal $LiAl_2(OH)_6$ are used as selective adsorbents for DLE from brines (Bouguerra et al. 2007; Hawash, Abd El Kader and El Diwani 2010; Prodromou 2016). Variable Li^+ sorption capacities of up to 123 mg/g at alkaline pH (Hawash, Abd El Kader and El Diwani 2010) or only ~0.6–22.9 mg/g in flow through and batch sorption experiments are reached (Jiang et al. 2020a; Jiang, Yang and Yu 2020b; Xue et al. 2020). Sorption temperature >30°C has negligible effects on the Li^+ sorption capacity (Figure 3; Hawash, Abd El Kader and El

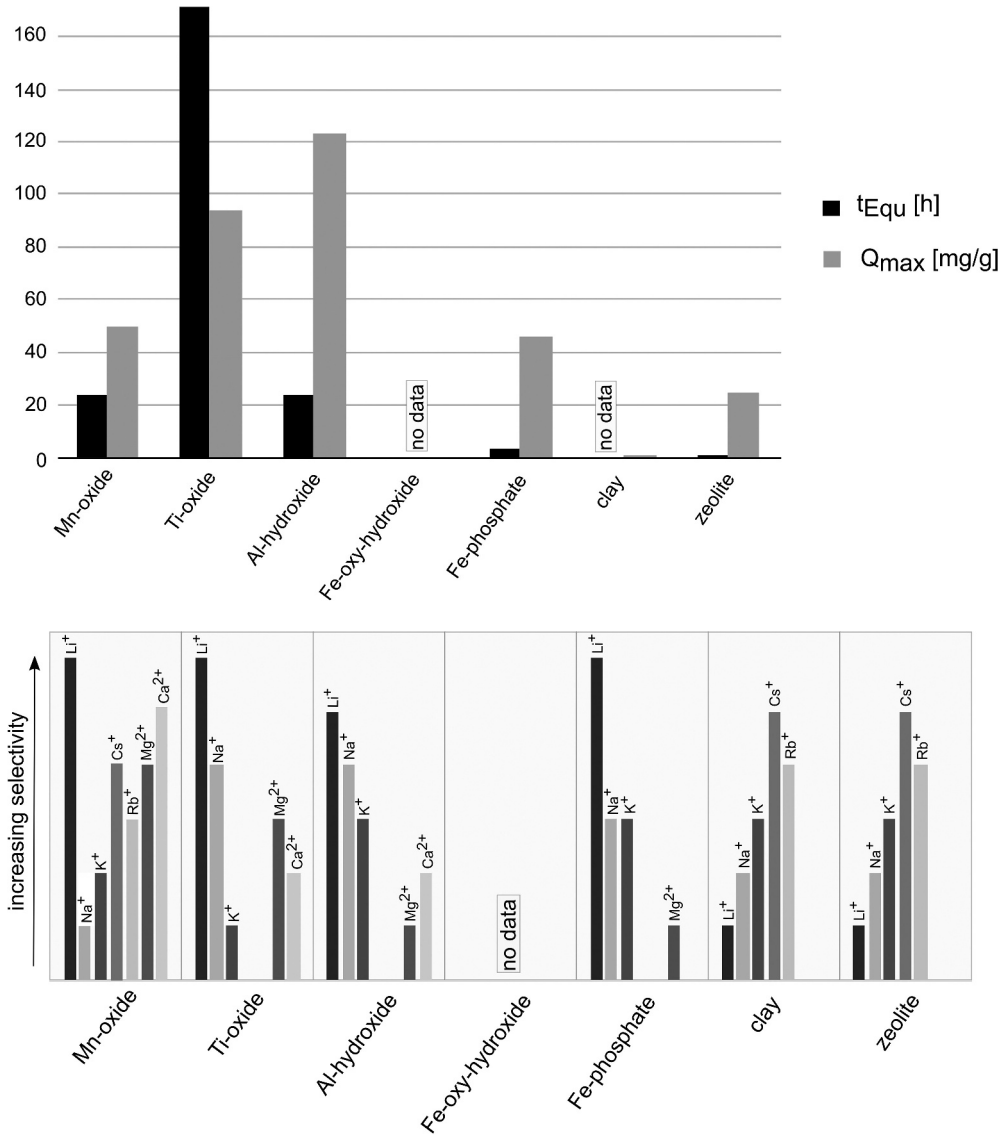

Figure 3. Comparison between sorbents according to equilibrium time (t_{Equ} [h]), maximum sorption capacity (Q_{max} [mg/g]) (top) and relative qualitative selectivity of different ions (bottom) (Bajestani et al. 2019; Chitrakar et al. 2000; Choubey et al. 2017; Colella 1996; Greene-Kelly 1955; Han et al. 2012; Hawash et al. 2010; Heidari and Momeni 2017; Hoyer et al. 2015; Intaranont et al. 2014; Jiang et al. 2020a; Lawagon et al. 2016; Lemaire et al. 2014; Prodromou 2016; Shi et al. 2013; Wisniewska et al. 2018; Zhang et al. 2010a; Zhang et al. 2010b).

Diwani 2010; Heidari and Momeni 2017). Equilibrium times vary significantly between 5 min and >24 h (Pauwels, Brach and Fouillac 1990; Prodromou 2016; Xue et al. 2020).

Pauwels, Brach and Fouillac (1990) investigated Li sorption from natural geothermal waters on amorphous Al-hydroxide. Optimum sorption conditions occur at 80°C, at pH >5 and an Al/Li ratio ~3.5, reaching Li-recovery >90%. Experiments with polymeric $Al(OH)_3$ combined with ion-exchange resins at varying Li concentrations (5.5–1000 mg/L in brines and synthetic solutions, respectively) show that Li-uptake correlates positively with initial Li concentration and increasing pH in 70 experimental runs (Hawash, Abd El Kader and El Diwani 2010). This indicates that $Li^+ - H^+$ substitution is the main Li-uptake process, whereas only ~10% of total amount of Li^+ adsorbed can be attributed to physisorption (Prodromou 2016, compare Heidari and Momeni 2017). In contrast, Heidari and Momeni (2017) concluded that optimal conditions were reached at pH ~7.

To investigate the applicability of Al-hydroxides in geothermal plants, flow tests have been performed. Thereby, the Li uptake is positively influenced by decreasing bed height and increasing flow rate (Jiang, Yang and Yu 2020b). Besides CH_3COONH_4, acids, such as H_2SO_4 or HF, are used for desorption (Hawash, Abd El Kader and El Diwani 2010; Heidari and Momeni 2017; Prodromou 2016). To apply Al-hydroxides for DLE from geothermal brines, further research is needed concerning desorption with non-problematic acids for technical application. However, they are recently tested in pilot-scale projects (Fukuda 2019).

Fe-oxy-hydroxides

Iron-oxy-hydroxides are widespread in soils world-wide and known to adsorb cations (e.g. Li^+, Mg^{2+}, Ni^{2+}, Zn^{2+}, Cu^{2+}, Cd^{2+}) due to their negatively charged surface at alkaline pH (Nielsen et al. 2005). Synthetic akageneite ($FeO_{0.833}(OH)_{1.167}Cl_{0.167}$ or β-FeOOH), for instance, has a large surface area of

up to 280 m^2/g which is generally advantageous for adsorption (Kim and Grey 2010). Natural Fe-oxy-hydroxides, e.g. goethite (α-FeOOH) and lepidocrocite (γ-FeOOH), have similarly large surface areas of up to 260 m^2/g (Kim, Nielsen and Grey 2008). The crystal structure of lepidocrocite is not affected by Li adsorption (Kim, Nielsen and Grey 2008). In goethite, Li^+ occupies octahedral and tetrahedral sites in the tunnels (Nielsen et al. 2005). At pH > 7.1, Li^+ is more strongly attached to the sorbent surface and OH^- groups are deprotonated, indicating that the substitution of H^+ by Li^+ is the main process of Li^+ uptake (Kim, Nielsen and Grey 2008). Sorption experiments with Fe-oxy-hydroxides were run for 24 h–7 days, but no information on equilibrium times, optimal temperatures or eluting solutions are available (Table 3; Nielsen et al. 2005, Kim, Nielsen and Grey 2008, Kim and Grey 2010).

Iron-oxy-hydroxides are cheap but have relatively low adsorption capacities of 0.2–0.5 meq/g corresponding to 3.5 mg/g Li^+ (Table 3; reported for membranes with in-situ formed FeOOH nanoparticles) (Heidary, Khodabakhshi and Kharat 2016; Kim and Grey 2010). Their application for Li extraction from geothermal brines is critical as they are not selective for Li compared to toxic metals and radioactive ions, such as Pb^{2+}, Cd^{2+}, Cr^{6+}, and As^{3+} (Cole et al. 2004; Kim and Grey 2010).

(Li)$FePO_4$

Lithium–iron-phosphates are synthetic sorbents characterized by an iron phosphate framework with the ability to reversibly incorporate monovalent cations, such as Li^+ (Dodd, Fultz and Yazami 2006). Iron–phosphate is used as a sorbent for selective Li^+ recovery from high saline solutions (Intaranont et al. 2014). $LiFePO_4$ (triphylite) and $FePO_4$ (heterosite) are commonly used as electrodes in LIBs (Arnold et al. 2003; Liu et al. 2014).

In batch experiments, 0.3 and 0.7 M sodium thiosulfate ($Na_2S_2O_3$) is added to the Li-bearing solution and $FePO_4$ sorbent at Na^+/Li^+ ratios of 10/1 to 100/1. After 24 h, Li is eluted from $LiFePO_4$ by oxidation with potassium persulfate ($K_2S_2O_8$) and thereby a Li-sulfate ($Li_2SO_{4(aq)}$) – K-sulfate ($K_2SO_{4(aq)}$) solution and the delithiated sorbent are recovered (Intaranont et al. 2014). The use of an oxidizing agent is needed since the sorption process is mainly controlled by the redox-reaction $Fe^{+III}PO_4 + e^- + Li^+ \rightarrow LiFe^{+II}PO_4$ (Fukuda 2019; Intaranont et al. 2014). Sorption capacity increases with temperature between 25°C and 65°C and it is optimal at pH = 7 (Fukuda 2019). Up to 46 mg Li^+/g are incorporated at 65°C when reaching equilibrium (Table 3; Intaranont et al. 2014, Fukuda 2019), exceeding the theoretically possible maximum adsorption capacity of 44 mg/g reported by Zhao et al. (2013) within analytical error.

The sorption of competing ions, such as Na^+, K^+ and Mg^{2+}, is <3 mg/g, indicating high Li selectivity (i.e. $Li^+/Na^+_{(s)}$ of 390–4000 at $Li^+/Na^+_{(aq)}$ of 10–100, respectively, Figure 3) (Intaranont et al. 2014). Equilibrium times vary between 1.5 and 3 h (Figure 3; Intaranont et al. 2014; Sun et al. 2020). For high Mg/Li brines, Li^+ can be successively separated from Mg^{2+} by controlling the applied voltage precisely (Zhao et al. 2013). Up to 41.3 mg/g Li^+ can be incorporated during the electrochemically induced redox reaction at an applied current of less than 1 V (Zhao et al. 2013). Geothermal water with a composition of 2.5 g/L TDS and a Li^+ concentration of 25.8 mg/L at pH 8.8 is processed by a $LiFePO_4$-$FePO_4$-Ag/AgCl electrode combined with a semipermeable, Cl^-–selective membrane (Sun et al. 2020). By applying 1 V, 97.8% (~10 mg/g) Li^+ are recovered from the initial solution. The adsorption capacity is increased by ~27–36% when using additives, such as NH_4HCO_3 or PEG-6000 (i.e. a water-soluble polymer), in the electrode (Sun et al. 2020). To avoid redox-reactions, NaCl is an ideal reagent to recover LiCl and $NaFePO_4$ and finally to precipitate Li_2CO_3 in an acid-free procedure (Liu et al. 2019c). Thereby, the isomorphic substitution of Li^+ by Na^+ in $LiFePO_4$ yields a Li-recovery of 27%. Another approach for the recovery of Li^+ from $LiFePO_4$ by leaching, using a mixture of H_2O_2 and CH_3COOH that only reacts with Li^+ rather than with $FePO_4$ (Yang et al. 2018). Thereby, less acid is consumed to extract 95.0% of Li^+ with high purity (i.e. 99.95 wt.%). Further research concerning technical implementation is needed to evaluate the applicability of $FePO_4$ for DLE from geothermal water at industrial scale, although the available data on chemical stability, selectivity, and sorption capacity are promising.

Clay minerals

Clay minerals are phyllosilicates comprising alternating layers of $(Si,Al,Fe)O_4$ tetrahedra (T) and $(Al,Mg,Fe)(OOH)_6$ octahedra (O) (Kloprogge, Komarneni and Amonette 1999; Zhang et al. 2010a). Lithium can adsorb onto negatively charged surfaces of clay minerals or substitute octahedrally bound elements in the clay mineral lattice (Gaskova and Bukaty 2008; Odom 1984; Williams and Hervig 2005). Most likely, Li forms hydrated inner-sphere and outer-sphere complexes onto the clay mineral surface or in the interlayers but can also be octahedrally or tetrahedrally coordinated by exchange with H^+ (Eckstein, Yaalon and Yariv 1970; Greene-Kelly 1955; Li and Liu 2020; Odom 1984). This indicates pH reduction during adsorption and better performance at higher pH, which has been proven for Zn^{2+} sorption on kaolinite (Meroufel et al. 2013). Chemisorption is the dominating process at high pH, whereas both physisorption and chemisorption are of importance at lower pH (Li and Liu 2020). Lithium is preferentially strongly bound in hectorite ($Na_{0.33}(Mg,Li)_3Si_4O_{10}(OH,F)_2$) and Li-bearing montmorillonite ($Li_x(Al_{4-x}Mg_x)Si_8O_{20}(OH)_4{\cdot}nH_2O$) among Li-free montmorillonite, kaolinite ($Al_4Si_4O_{10}(OH)_8$) and vermiculite ($(Mg,Ca)_{x/2}^{2+}(Al_{4-x}Mg_x)Si_8O_{20}(OH)_4 \cdot 8H_2O$), where it can only be adsorbed (Amer 2008; Chang, Skipper and Sposito 1997; Eckstein, Yaalon and Yariv 1970; Greene-Kelly 1955; Kloprogge, Komarneni and Amonette 1999; Nir et al. 1986).

The maximum adsorption capacity for Li on clay minerals varies between 0.02 and 0.90 mg/g Li^+ and 0.5–0.6 mg/g Li^+ for kaolinite and montmorillonite, respectively (Figure 3; Eckstein, Yaalon and Yariv 1970; Greene-Kelly 1955). Increasing temperature leads to decreasing adsorption capacity as well as decreasing selectivity for Li (Gast and Klobe 1971). Vermiculite, opposed to montmorillonite, preferentially adsorbs Na^+ over Li^+ (Gast and Klobe 1971). The few studies that report sorption data from an experimental approach used stirring times of 24 h and desorbed afterward using calcium

acetate (Table 3; Eckstein, Yaalon and Yariv 1970, Hoyer, Kummer and Merkel 2015). No data on equilibration times and kinetics are available (Figure 3; Table 3), revealing the necessity for further research on Li sorption to clay minerals. The technical applicability of clay minerals for the DLE is critical due to limited temperature stability, low Li sorption capacity, as well as their coagulation and decomposition behavior.

Zeolites

Zeolite group minerals are hydrous framework aluminosilicates that consist of interconnected SiO_4 – AlO_4 tetrahedra resulting in a network of micropores and channel systems (e.g. Navarrete-Casas et al. 2007; Obaid et al. 2018; Rao et al. 2006; Zhou et al. 2013). Due to the substitution of Si^{4+} by Al^{3+}, a negatively charged surface develops, which enables cation sorption (Belova 2019; Erdem, Karapinar and Donat 2004; Gaikwad, Misal and Gupta 2011; Obaid et al. 2018; Rao et al. 2006).

Zeolites possess a large and well-developed surface area (up to 726 m^2/g, Zhou et al. (2013)), high ion exchange and adsorption capacity, as well as fast kinetics enabling it to perform as ion-sieve (Figure 3; Corma 2003; Danisi and Schilling 2021; Wiśniewska et al. 2018). They are nontoxic, cheap, widely available in different grain size, shape, and composition and are reusable over several adsorption–desorption cycles that renders them rather environmentally friendly (Akgül et al. 2006; Belova 2010; Wiśniewska et al. 2018; Zhou et al. 2013).

Zeolites can be easily modified to tune their physicochemical properties (Beyaz Kayiran and Lamari Darkrim 2002). Pretreatment and post-synthetic modifications increase the sorption capacity and allow desorption with NaCl instead of acids (Athanasiadis and Helmreich 2005; Carland and Aplan 1995; Navarrete-Casas et al. 2007; Zamzow et al. 1990; Zamzow and Murphy 1992). The chemical stability of zeolite is limited to moderate pH values (Hoyer, Kummer and Merkel 2015), although some authors state that zeolitic materials would be alkali and acid resistant (Belova 2019; Zhou et al. 2013).

Lithium sorption on zeolite depends on pH, temperature, Li concentration, and competing ions, channel diameter and surface area (Colella 1996; Hoyer, Kummer and Merkel 2015; Inglezakis et al. 2005; Lemaire et al. 2014; Navarrete-Casas et al. 2007; Sullivan et al. 2003; Wiśniewska et al. 2018). Lithium is extracted from geothermal brines and synthetic LiCl solution by natural clinoptilolite and synthetic zeolite Na-X using polyacrylic acid (PAA) as additive to prevent precipitation of hydroxides and improve Li selectivity (Wiśniewska et al. 2018). The amount of 50% Li was recovered with clinoptilolite at naturally relevant pH of 5.5. Under laboratory conditions, 100% Li was extracted from synthetic LiCl solutions at pH = 9 with zeolite Na-X and PAA. In contrast, Belova (2010) and Belova (2017) improve zeolite selectivity for Li by modifying the precursor zeolite Si/Al ratio with $Al(OH)_3$ without the use of additives. A sorption capacity for Li^+ of 1.6 mg/g is reached at an initial Li-concentration of 40 mg/L at pH = 8.5 (Belova 2017). Approximately 83% Li^+ is recovered from a synthetic solution with a Li-concentration of 3 mg/L after 2 h (Belova 2017).

Zeolites are promising sorbents for DLE from geothermal brines concerning kinetics and sorption capacity. They are thermally stable within the temperature ranges of thermal waters, which is beneficial for their application in geothermal brines (Zhou et al. 2013), but data on sorption characteristics at T > 40°C are lacking and need further research.

Other sorbents

Other sorbents, such as Zr-phosphate, Sn-antimonates, Sb-oxides, Ta-oxides, and $H_8Nb_{22}O_{59} \cdot 8H_2O$ have been studied for their selective Li uptake behavior. Zirconium phosphate reaches 48.9 mg/g adsorption capacity at equilibration times of 48 h and its selectivity is dependent on the total amount of ions that are adsorbed and is represented by $Cs^+ \sim Na^+ < Li^+$ for high and $Li^+ < Na^+ < Cs^+$ for low loadings (Clearfield and Troup 1970; Clearfield and Tuhtar 1976). Lithium substitutes H^+ sites during adsorption, resulting in a $Zr(LiPO_4)_2 \cdot 4H_2O$ phase after 80% exchange. By acid treatment with HCl, only 5% of the exchanged Li is recovered (Clearfield and Troup 1970). The incorporation of H^+ during desorption, however, is accompanied by a structural change indicated by the resulting gel-like structure of Zr-phosphate sorbent (Clearfield and Troup 1970).

Synthetic Sn-antimonates are highly Li-selective sorbents represented by the sequences $Na^+ < K^+ < Rb^+ < Cs^+ \ll Li^+$ and $Cs^+ < Rb^+ < K^+ < Na^+ < Li^+$ for Li^+/H^+ equivalent fractions in the sorbent between 0–0.04 and >0.14, respectively (Abe and Furuki 1986; Abe and Tsuji 1983). Isotherm batch experiments have been performed in the temperature range between 30°C and 60°C. The ion-exchange reaction is represented by $Li^+ – H^+$ substitution (Abe and Furuki 1986). Information on the maximum adsorption capacity is lacking, but slow kinetics for Li^+ (~10 days) compared to the other alkali ions (~24 h) have been reported (Abe and Furuki 1986).

For Sb-oxides, the maximum sorption capacity for Li^+ reaches ~22 mg/g (Chitrakar and Abe 1988). The selectivity sequences are determined to be Li < Na < K < Rb < Cs and Li ≪ K < Cs < Rb ≪ Na for amorphous and crystalline sorbents in acid media, respectively (Chitrakar and Abe 1988, 1989). Monoclinic $LiSbO_3$ sorbs up to 39.8 mg Li^+/g from a buffered LiOH solution at 90°C and pH = 9.2 (Oi et al. 2000). The Li uptake is almost twice as much for LiOH compared to LiCl solutions at 90°C. The sorbent undergoes an irreversible phase transition from monoclinic to cubic during incorporation of Na rather than reversibly from monoclinic to orthorhombic by exchange of Li^+ with H^+. For desorption of Li^+, the loaded sorbent $LiSbO_3$ is treated with concentrated HNO_3 (Chitrakar and Abe 1988).

Lithium sorption on cubic $LiTaO_3$ reaches maximum sorption capacities of 16.7 mg/g at 60°C representing 56% of theoretically possible 29.9 mg/g exchangeable sites and increased

to 9.7 mg/g and 14.6 mg/g at 30°C and 45°C, respectively (Inoue and Abe 1996). The main sorption process is the exchange of H^+ and Li^+ (Inoue and Abe 1996).

Another Li-selective sorbent is hexagonal $H_8Nb_{22}O_{59} \cdot 8H_2O$. Its selective behavior is related to the ionic radii of different ions, i.e. $Cs^+ \ll Rb^+ < K^+, Na^+ < Li^+$ (Yang et al. 2005). Optimum pH values for selective Li adsorption are >11 as the ion-exchange process is the substitution of H^+ and Li^+ reaching up to 17.0–20.8 mg/g Li sorption capacities (Yang et al. 2005). Besides Li, Na and K are efficiently removed from the solution as well, reaching removal rates of up to 98–99.9% (Yang et al. 2005).

Discussion

The application of Li extraction from geothermal brines without disturbing the running operation of a power plant is a challenging task (Slunitschek, Kolb and Eiche 2021). The geochemistry of geothermal brines is similar to that from conventionally mined brines (Table 1), but the selected DLE technique implementable to geothermal power plants has to operate efficiently at 60–80°C and resist pressures and flow velocities of 20–50 bars and 30–90 L/s, respectively (Haklıdır and Balaban 2019; Stober and Bucher 2012).

Brine and seawater evaporation can be economically used for Li recovery, e.g. in the Salar de Atacama in Chile, the Salar de Hombre Muerto in Argentina or the Dead Sea in Israel (Bowell et al. 2020; Epstein et al. 1981). However, this technique is not applicable with respect to geothermal power plants as water flows continuously and is mostly reinjected into the deep reservoir, with few exceptions in Iceland, China, and Thailand, where the thermal water is discharged via surface waters (Kaya, Zarrouk and O'Sullivan 2011). The large areas and evaporation times of several months needed (Gaikwad, Misal and Gupta 2011) are not available in urban regions, limiting its feasibility. Additionally, arid climate conditions are not given in many places where geothermal plants are located.

High salinities and SiO_2 concentrations in brines (Table 1) circulating through geothermal power plants are critical. With decreasing temperature during processing, the formation of scales within the rods becomes more likely since SiO_2 solubility decreases with decreasing temperature and pH (Bouguerra et al. 2007; Palmer and Palmer 2003). Other phases, such as $(Ba,Sr,Ca)SO_4$, Pb-As-Sb-sulfides and carbonates, may precipitate depending on brine chemistry, which should always be prevented as they can cause corrosion or clogging and the accumulation of radionuclides (Goldberg et al. 2021; Haas-Nüesch et al. 2018; Haklıdır and Balaban 2019). In many geothermal power plants, therefore inhibiting chemicals, such as phosphate salts, phosphonic acid and polymers, are used (Haas-Nüesch et al. 2018; Haklıdır and Balaban 2019).

Direct precipitation is a cheap method for Li recovery, which is feasibly applicable and easy to set up (Zhang et al. 2019). Due to the complex chemical composition of many brines and their sensitivity on changes in geochemical conditions (i.e. changes in pH, major element chemistry, temperature, etc.), direct precipitation is regarded to be economically applicable but technically inappropriate for DLE in a running geothermal power plant as the risk of undesired scaling is too high.

The high flow rates in geothermal plants limit the feasibility of most membrane-related technologies since long reaction times of several hours for the Li extraction were needed in pilot tests with synthetic Li-solutions (Melnikov et al. 2017). The application of membranes is limited to low Na-Mg-B-brines, since they generally have a modest selectivity for Li compared to these ions (Somrani, Hamzaoui and Pontie 2013; Wen et al. 2006). By processing Ca^{2+}- and SO_4^{2-} -rich brines, $CaSO_4$ becomes progressively enriched in the residual brine and might precipitate, causing clogging of the pumping equipment (Gaikwad, Misal and Gupta 2011). Furthermore, Li recovery is <80% from brines with high Li concentrations when using membrane technologies (Safari, Lottermoser and Alessi 2020). The recovery decreases at temperatures >18–20°C, which contradicts the requirements of efficient and economic geothermal power plants (Sun et al. 2015). DLE using membranes is expensive and produces acidic wastewater, which is a main problem for its applicability in geothermal plants.

Solvent extraction is limited to specific hydrochemical compositions and is not applicable for high Mg/Li (mass ratio >6; Liu, Zhao and He 2020) fluids. Magnesium needs to be removed from the solution prior to increasing its pH to 10.6–11.0 necessary for the solvent extraction process (Harvianto, Kim and Ju 2016). The increase in pH toward more alkaline conditions could cause scaling (Harvianto, Kim and Ju 2016; Warren 2021) and the resulting precipitates must be extracted by membrane filtration (Harvianto, Kim and Ju 2016; Warren 2021).

In contrast, ion exchange and adsorption techniques can be highly efficient for fluids with different chemical compositions, reliable and environmentally friendly, depending on the type of exchanger, its selectivity and CEC for the solute, its commercial availability and its reusability and chemical stability concerning repeating loading/unloading cycles (Tables 2 and 3; Ambrose and Kendall 2020a; Liu et al. 2017; Tian, Ma and Han 2010). Compared to all the other extraction techniques described here, sorption and ion exchange in general are not restricted to specific brine composition (Table 2) and the different types of sorbents allow the applicability of one universal technique at several different locations for fluids differing in composition, temperature, pressure, and flow rate world-wide. For most studied sorbents except Mn-oxide and Al-hydroxide, lacking information on Li sorption at high temperature and pressure or on their stability over many sorption/desorption cycles make a reliable evaluation difficult.

Manganese-oxides are characterized by fast kinetics, high selectivity for Li (i.e. sorption of <5 mg/g competing ions) reaching high sorption capacity (up to 53.5 mg/g), which qualifies them for a potentially feasible DLE in geothermal power plants and the production of high-purity Li-products (Ariza et al. 2006; Bajestani, Moheb and Masigol 2019; Kawamoto and Tamaki 2011; Ohashi and Tai 2019; Ooi, Miyai and Katoh 1987; Ryu et al. 2015). However, the development of a large-scale synthesis process would be essential to supply sufficient amounts of LMO sorbent needed for industrial application. The redox sensitivity and pH treatment are challenging, since all sorbents that operate ideally at alkaline pH conditions require pH adjustment, whereas most natural brines are neutral or slightly acidic (Pirajno 2012).

Sorption of Li from geothermal brines on Al-hydroxides has been studied at temperatures up to 70°C and in 70 cycles (Hawash, Abd El Kader and El Diwani 2010). The sorbent proved a good stability, but (technically) problematic acids (e.g. HF or H_2SO_4, Table 3) are used for desorption, which cannot be implemented into a geothermal power plant (Hawash, Abd El Kader and El Diwani 2010; Heidari and Momeni 2017; Prodromou 2016). Data coverage on the chemical stability of Al-hydroxide-based sorbents against acids is low and needs further investigation.

Titanium-oxide-based sorbents reach rather high adsorption capacities and are highly selective for Li, but they also have to equilibrate up to 10–192 h, which is not viable in geothermal power plants (Lawagon et al. 2016; Shi et al. 2013; Taghvaei, Taghvaei and Askari 2020; Wei et al. 2020). Furthermore, the loss of Ti (e.g. 0.06–2.5% Ti^{4+} after five cycles) in repeating sorption/desorption cycles is significant causing a proceeding decrease in their sorption capacity (e.g. 13.5% after 6 cycles) over time and limits their feasibility (Gu et al. 2018; Kamran and Park 2020; Lawagon et al. 2016). The adsorption of toxic metals, radioactive ions and hazardous oxyanions are a criterion for exclusion of Fe-oxy-hydroxide as sorbents since these substances must not be accumulated at the surface and must not contaminate the Li-concentrate (Cole et al. 2004; Kim and Grey 2010).

Less investigated sorbents are $FePO_4$, clay minerals, and zeolite group minerals (Liu, Zhao and Ghahreman 2019b; Meng et al. 2021; Safari, Lottermoser and Alessi 2020; Stringfellow and Dobson 2021). High Li adsorption capacities (up to 46 mg Li^+/g, Figure 3) on $FePO_4$ are reached after equilibration for 24 h, which may be too long for an efficient implementation in a geothermal power plant with high flow rates. However, optimal adsorption conditions and equilibrium time for upscaling have to be determined. Intaranont et al. (2014), for example, identify a complete Li uptake in <3 h if Li^+ and $S_2O_3^{2-}$ concentrations exceed 0.7 M, which, however, exceed natural brine values by a factor of 3 to 48 (Table 1). Analogous to Mn-oxide ion sieves, redox-sensitivity of $LiFePO_4/FePO_4$ may limit its application in Li extraction from geothermal brines.

Clay minerals may be disadvantageous for applications in flow systems as the platy habitus could negatively influence the flow properties or clog the sorption unit. Coagulation of the particles due to sorbed cations (Lagaly and Ziesmer 2003) can lead to clumping and clogging and may reduce the adsorption capacity in terms of limited fluid-sorbent contact. Furthermore, clay minerals might partially or completely decompose at higher temperature or pH, lowering their adsorption capacities and selectivity for Li^+. So far, many studies focused on natural Li^+ adsorption on clay minerals in soil systems and alluvial plains rather than investigating their economic application potential in mineral processing (Figure 3; e.g. Chang, Skipper and Sposito 1997; Greene-Kelly 1955; Hoyer, Kummer and Merkel 2015; Li and Liu 2020; Odom 1984).

Zeolites successfully adsorb Li from synthetic solutions and geothermal waters (e.g. Navarrete-Casas et al. 2007; Wiśniewska et al. 2018). It was shown that the more negatively charged the zeolite surface, the higher the theoretical sorption capacity (Accardi and Lobo 2000; Barrer, Davies and Rees 1969). Therefore, zeolites with low Si/Al ratio are most suitable. Due to generally low Li selectivity (Figure 3), the use of additives may be necessary (Wiśniewska et al. 2018). However, sorption capacity and stability data for T > 40°C are lacking, which needs to be studied before their applicability for geothermal processes can be evaluated.

For all sorbents discussed in this article, the process of Li^+ intercalation and consequently, the change of the fluid hydrochemistry is a major issue that needs to be considered carefully. Redox-sensitive sorbents often have limited chemical stability since the redox-reactions during every sorption/desorption cycle lead to changes of crystal lattice parameters. This is in particular the case for LMO and $FePO_4$ although minor focus has been spent on $FePO_4$ stability without combination with electrochemical techniques (Cao et al. 2019; Gao et al. 2019; Hunter 1981; Intaranont et al. 2014; Kuss et al. 2014). If the underlying sorption process is an ion exchange, however, H^+ or alkalis (e.g. Na^+) are released to the brine, changing the pH (and requiring pH adjustment) or major fluid chemistry. However, Na^+-exchanged sorbents have never been sufficiently tested in high saline environments due to excess Na^+ in these fluids (Table 1). In this case, desorption by acid exchanges Li^+ by H^+ and not Na^+. This results in a different composition of the sorbent, which may have a negative effect on sorption capacity in the next cycle.

To improve the performance of sorbents, they can either be synthesized to target pure chemical compositions with controlled crystal structure or be combined with other sorbents. Composite materials have been suggested by Zandvakili and Ranjbar (2018) who mixed organic N-methyl-2-pyrrolidone and LMO in a 1:1 ratio. In contrast, Sullivan et al. (2003) show that the amount of clinoptilolite and smectite, as well as the bulk negatively charged surface area of a mixture correlate positively with Li^+ sorption proposing a mixture of clinoptilolite and smectite with a ratio of 1:0.5.

Conclusion

Increasing demand and pressure on the Li market is expected in the future. Widening the portfolio from primary Li deposits to geothermal brines may generate an alternative Li resource. The implementation of DLE into a geothermal power plant at industrial scale is subject of current research, due to the chemical variability of the brines and operating conditions (T = 60–80°C, P = 20–50 bars, flow-rates of 30–90 L/s).

Direct precipitation and evaporation are unlikely to be implemented into geothermal power plants due to the risk of scaling, land consumption, concurrent precipitation of undesired components and/or long evaporation times. Solvent extraction and membrane processes are only suitable for specific brine compositions and can thus only be applied to such brines or the necessity of further purification steps is indispensable. DLE by sorption and ion-exchange processes cannot be performed in a single-step procedure because sorption and desorption have to be temporally separated to prevent mixing of the geothermal brine with the desorption solution. Furthermore, depending on the selected sorbent/ion exchanger, the use of acids for desorption is indispensable. However, membrane-based techniques, sorption and ion exchange as

DLE are regarded most promising for implementation. Since the general DLE technology will be similar for all different materials for sorption and ion exchange, they have the potential to be universally applicable for different fluid compositions by choosing the most appropriate material for the local requirements at the lowest investment.

Sorbent-specific disadvantages are redox-sensitivity, pH adjustment, and the use of acids for desorption. Since operating conditions in geothermal power plants and brine composition vary largely between different sites, the Li-extraction process likely needs to be adjusted to the local context. Sorption using Fe-oxy-hydroxides is not applicable in the geothermal power plant due to adsorption of undesired ions. The phyllosilicate habitus of clay minerals that might cause clogging of the technical equipment are limiting their application. Titanium-oxide- and Al-hydroxide-based sorbents have been implemented in pilot plants, but long equilibration times, limited chemical stability, and problematic acids used for desorption are not appropriate for their application in a regime with high flow rates. Lithium–manganese oxides, in contrast, appear promising, due to fast kinetics and high selectivity for Li reaching high adsorption capacities although these sorbents are redox-sensitive. Other sorbents like $FePO_4$ and zeolite show fast kinetics, variably high sorption capacities, and excellent chemical stability under geothermal conditions, making them promising alternatives. Challenges for lithium–manganese oxide, $FePO_4$, and zeolite are the high flow-rates, high salinities of the brines and high pressures in the power plants, which need to be studied in detailed laboratory and pilot plant experiments to conclusively evaluate their potential for a feasible implementation into operating geothermal power plants for commercial Li-extraction.

Acknowledgments

Michèle Jungmann is acknowledged for many helpful discussions concerning lithium in hydrothermal systems. We especially thank Editor-in-Chief Dr. Kawatra as well as four anonymous reviewers for their comments and revisions that significantly improved the quality of this article. This research is part of the project “UnLimited” which is funded by the German Federal Ministry for Economic Affairs and Energy under Grant O3EE4023D.

Disclosure statement

No potential conflict of interest was reported by the author(s).

Funding

This work was supported by the German Federal Ministry for Economic Affairs and Energy [O3EE4023D].

References

Abe, M., and N. Furuki. 1986. Synthetic inorganic ion-exchange materials. XXXXI. Ion exchange equilibria of alkali metal ions/hydrogen ions on tin (IV) antimonate. *Solvent Extraction and Ion Exchange* 4:547–65.

Abe, M., and M. Tsuji. 1983. Synthesis of quadrivalent metal antimonates as ion exchangers and their selectivities for alkali metal ions. *Chemistry Letters* 12:1561–64.

Accardi, R. J., and R. F. Lobo. 2000. Accessibility of lithium cations in high-silica zeolites investigated using the NMR paramagnetic shift effect of adsorbed oxygen. *Microporous and Mesoporous Materials* 40:25–34.

Akgül, M., A. Karabakan, O. Acar, and Y. Yürüm. 2006. Removal of silver (I) from aqueous solutions with clinoptilolite. *Microporous and Mesoporous Materials* 94:99–104.

Ambrose, H., and A. Kendall. 2020a. Understanding the future of lithium: Part 1, resource model. *Journal of Industrial Ecology* 24:80–89.

Ambrose, H., and A. Kendall. 2020b. Understanding the future of lithium: Part 2, temporally and spatially resolved life-cycle assessment modeling. *Journal of Industrial Ecology* 24:90–100.

Amer, A. M. 2008. The hydrometallurgical extraction of lithium from Egyptian montmorillonite-type clay. *JOM* 60:55–57.

An, J. W., D. J. Kang, K. T. Tran, M. J. Kim, T. Lim, and T. Tran. 2012. Recovery of lithium from Uyuni salar brine. *Hydrometallurgy* 117:64–70.

Aquilina, L., H. Pauwels, A. Genter, and C. Fouillac. 1997. Water-rock interaction processes in the Triassic sandstone and the granitic basement of the Rhine Graben: Geochemical investigation of a geothermal reservoir. *Geochimica et cosmochimica acta* 61:4281–95.

Aral, H., and Vecchio-Sadus, A. 2008. Toxicity of lithium to humans and the environment - a literature review. *Ecotoxicology and Environmental Safety* 70:349–356.

ArcGIS. 2020. Hellgraue Hintergrundkarte. arcgis.com .

Ariza, M. J., D. J. Jones, J. Rozière, R. Chitrakar, and K. Ooi. 2006. Probing the local structure and the role of protons in lithium sorption processes of a new lithium-rich manganese oxide. *Chemistry of Materials* 18:1885–90.

Arnold, G., J. Garche, R. Hemmer, S. Ströbele, C. Vogler, and M. Wohlfahrt-Mehrens. 2003. Fine-particle lithium iron phosphate LiFePO4 synthesized by a new low-cost aqueous precipitation technique. *Journal of Power Sources* 119:247–51.

Asadi Dalini, E., G. Karimi, S. Zandevakili, and M. Goodarzi. 2021. A review on environmental, economic and hydrometallurgical processes of recycling spent lithium-ion batteries. *Mineral Processing and Extractive Metallurgy Review* 42:451–72.

Athanasiadis, K., and B. Helmreich. 2005. Influence of chemical conditioning on the ion exchange capacity and on kinetic of zinc uptake by clinoptilolite. *Water Research* 39:1527–32.

Bajestani, M. B., A. Moheb, and M. Masigol. 2019. Simultaneous optimization of adsorption capacity and stability of hydrothermally synthesized spinel ion sieve composite adsorbents for selective removal of lithium from aqueous solutions. *Industrial & Engineering Chemistry Research* 58:12207–15.

Banks, M. K. 1953. A Method For Concentration oi North Carolina Spodumene Ores.

Banks, D., Markland, H., Smith, P. V., Mendez, C., Rodriguez, J., Huerta, A., and Sæther, O. M. 2004. Distribution, salinity and pH dependence of elements in surface waters of the catchment areas of the Salars of Coipasa and Uyuni, Bolivian Altiplano. *Journal of Geochemical Exploration* 84:141–166.

Barrer, R. M., J. A. Davies, and L. V. C. Rees. 1969. Comparison of the ion exchange properties of zeolites X and Y. *Journal of Inorganic and Nuclear Chemistry* 31:2599–609.

Barrow, N. J. 2008. The description of sorption curves. *European Journal of Soil Science* 59:900–10.

Belova, T. P. 2010. The analysis of sorption extraction of boron and lithium from the geothermal heat-carriers. Proceedings of the World Geothermal Congress, Bali, Indonesia.

Belova, T. P. 2017. Experimental studies in the sorptive extraction of boron and lithium from thermal waters. *Journal of Volcanology and Seismology* 11:136–42.

Belova, T. P. 2019. Adsorption of heavy metal ions (Cu2+, Ni2+, Co2+ and Fe2+) from aqueous solutions by natural zeolite. *Heliyon* 5: e02320.

Benson, T. R., M. A. Coble, J. J. Rytuba, and G. A. Mahood. 2017. Lithium enrichment in intracontinental rhyolite magmas leads to Li deposits in caldera basins. *Nature Communications* 8:1–9.

Beyaz Kayiran, S., and F. Lamari Darkrim. 2002. Synthesis and ionic exchanges of zeolites for gas adsorption. *Surface and Interface Analysis: An International Journal Devoted to the Development and Application of Techniques for the Analysis of Surfaces, Interfaces and Thin Films* 34:100–04.

Blackford, J. C., and F. J. Gilbert. 2007. pH variability and CO2 induced acidification in the North Sea. *Journal of Marine Systems* 64:229–41.

Blanc, P., A. Lassin, P. Piantone, M. Azaroual, N. Jacquemet, A. Fabbri, and E. C. Gaucher. 2012. Thermoddem: A geochemical database focused on low temperature water/rock interactions and waste materials. *Applied Geochemistry* 27:2107–16.

Bohn, H. L., R. A. Myer, and G. A. O'Connor. 2002. *Soil chemistry*. New York, USA: John Wiley & Sons.

Border, S., and L. Sawyer. 2014. Evaporites and brines–geological, hydrological and chemical aspects of resource estimation. *Applied Earth Science* 123:95–106.

Borrmann, T., M. Schweig, and J. H. Johnston. 2019. Transforming silica into silicate–pilot scale removal of problematic silica from geothermal brine. *Chem NZ* 83:63–70 .

Bouguerra, W., M. B. S. Ali, B. Hamrouni, and M. Dhahbi. 2007. Equilibrium and kinetic studies of adsorption of silica onto activated alumina. *Desalination* 206:141–46.

Bowell, R. J., L. Lagos, C. R. de Los Hoyos, and J. Declercq. 2020. Classification and characteristics of natural lithium resources. *Elements: An International Magazine of Mineralogy, Geochemistry, and Petrology* 16:259–64.

Bruggenwert, M. G. M., and A. Kamphorst. 1979. Survey of experimental information on cation exchange in soil systems. In *Developments in Soil Science* 5 G.H. Bolt , 141–203. Amsterdam: Elsevier.

Bukowsky, H., and E. Uhlemann. 1993. Selective extraction of lithium chloride from brines. *Separation Science and Technology* 28:1357–60.

Bundesanstalt für Geowissenschaften und Rohstoffe. 2020. Lithium: Rohstoffwirtschaftliche Steckbriefe. 6.

Butterman, W. C.1988. Current status of the specialty metals. *Mineral Processing and Extractive Metallurgy Review* 3:69–86.

Cao, G., X. Yang, Z. Yin, Y. Lei, H. Wang, and J. Li. 2019. Synthesis, adsorption properties and stability of Cr-doped lithium ion sieve in salt lake brine. *Bulletin of the Chemical Society of Japan* 92:1205–10.

Carland, R. M., and F. F. Aplan. 1995. Improving the ion-exchange capacity and elution of Cu+ 2 from natural sedimentary zeolites. *Mining, Metallurgy & Exploration* 12:210–18.

Chaban, M. O., L. M. Rozhdestvenska, O. V. Palchyk, Y. S. Dzyazko, and O. G. Dzyazko. 2019. Structural characteristics and sorption properties of lithium-selective composite materials based on TiO 2 and MnO 2. *Applied Nanoscience* 9:1037–45.

Chang, F.-R. C., N. T. Skipper, and G. Sposito. 1997. Monte Carlo and molecular dynamics simulations of interfacial structure in lithium-montmorillonite hydrates. *Langmuir* 13:2074–82.

Chitrakar, R., and M. Abe. 1988. Synthetic inorganic ion exchange materials XLVII. Preparation of a new crystalline antimonic acid HSbO3. O. 12H2O. *Materials Research Bulletin* 23:1231–40.

Chitrakar, R., and M. Abe. 1989. Synthetic inorganic ion-exchange materials. XLVIII. ion-exchange reaction of alkali metal Ions/H+ on monoclinic antimonic acid. *Solvent Extraction and Ion Exchange* 7:721–33.

Chitrakar, R., H. Kanoh, Y. Miyai, and K. Ooi. 2000. A new type of manganese oxide (MnO2⊙ 0.5 H2O) derived from Li1. 6Mn1. 6O4 and its lithium ion-sieve properties. *Chemistry of Materials* 12:3151–57.

Chitrakar, R., Y. Makita, K. Ooi, and A. Sonoda. 2013. Magnesium-doped manganese oxide with lithium ion-sieve property: Lithium adsorption from salt lake brine. *Bulletin of the Chemical Society of Japan* 86:850–55.

Chitrakar, R., Y. Makita, K. Ooi, and A. Sonoda. 2014. Synthesis of iron-doped manganese oxides with an ion-sieve property: Lithium adsorption from Bolivian brine. *Industrial & Engineering Chemistry Research* 53:3682–88.

Choubey, P. K., K.-S. Chung, M.-S. Kim, J.-C. Lee, and R. R. Srivastava. 2017. Advance review on the exploitation of the prominent energy-storage element Lithium. Part II: From sea water and spent lithium ion batteries (LIBs). *Minerals Engineering* 110:104–21.

Choubey, P. K., M.-S. Kim, R. R. Srivastava, J.-C. Lee, and J.-Y. Lee. 2016. Advance review on the exploitation of the prominent energy-storage element: Lithium. Part I: From mineral and brine resources. *Minerals Engineering* 89:119–37.

Cisternas, L. A., J. I. Ordóñez, R. I. Jeldres, and R. Serna-Guerrero. 2021. Toward the implementation of circular economy strategies: An overview of the current situation in mineral processing. *Mineral Processing and Extractive Metallurgy Review* 1–23.

Clearfield, A., and J. Troup. 1970. Mechanism of ion exchange in crystalline zirconium phosphate. II. Lithium ion exchange of. alpha.-zirconium phosphate. *The Journal of Physical Chemistry* 74:314–17.

Clearfield, A., and D. A. Tuhtar. 1976. The mechanism of ion exchange in zirconium phosphates. 15. The effect of crystallinity of the exchange on lithium (1+)/hydrogen (1+) exchange of. alpha.-zirconium phosphate. *The Journal of Physical Chemistry* 80:1296–301.

Cole, K. E., Y. Paik, R. J. Reeder, M. Schoonen, and C. P. Grey. 2004. 2H MAS NMR studies of deuterated goethite (α-FeOOD). *The Journal of Physical Chemistry. B* 108:6938–40.

Colella, C. 1996. Ion exchange equilibria in zeolite minerals. *Mineralium Deposita* 31:554–62.

Collins, A. G. E. N. E., and J. D. Vine. 1976. Lithium abundance in oilfield waters. *Lithium Resources and Requirements by the Year 2000* 1005:116–23.

Condie, K. C. 1993. Chemical composition and evolution of the upper continental crust: Contrasting results from surface samples and shales. *Chemical Geology* 104:1–37.

Corma, A. 2003. State of the art and future challenges of zeolites as catalysts. *Journal of Catalysis* 216:298–312.

Danisi, R. M., and F. R. Schilling. 2021. Dehydration and lithium ion-exchange of the open framework vanadium silicate VSH-16Na. *Microporous and Mesoporous Materials* 319:111064.

Dodbiba, G., P. Keeratithakul, Y. Kanemitsu, and T. Fujita. 2014. Optimization of lithium electrosorption from brine deposit. *Geosystem Engineering* 17:157–62.

Dodd, J. L., B. Fultz, and R. Yazami. 2006. Determining the phase diagram of LixFePO4. *ECS Transactions* 1:27.

Eckstein, Y., D. H. Yaalon, and S. Yariv. 1970. The effect of lithium on the cation exchange behaviour of crystalline and amorphous clays. *Israel Journal of Chemistry* 8:335–42.

Epstein, J. A., E. M. Feist, J. Zmora, and Y. Marcus. 1981. Extraction of lithium from the dead sea. *Hydrometallurgy* 6:269–75.

Erdem, E., N. Karapinar, and R. Donat. 2004. The removal of heavy metal cations by natural zeolites. *Journal of Colloid and Interface Science* 280:309–14.

Evans, R. K. 2008. *An abundance of lithium*. Santiago: World Lithium.

Fasel, D., and M. Q. Tran. 2005. Availability of lithium in the context of future D–T fusion reactors. *Fusion Engineering and Design* 75:1163–68.

Feng, Q., H. Kanoh, Y. Miyai, and K. Ooi. 1995a. Alkali metal ions insertion/extraction reactions with hollandite-type manganese oxide in the aqueous phase. *Chemistry of Materials* 7:148–53.

Feng, Q., H. Kanoh, Y. Miyai, and K. Ooi. 1995b. Hydrothermal synthesis of lithium and sodium manganese oxides and their metal ion extraction/insertion reactions. *Chemistry of Materials* 7:1226–32.

Feng, Q., Y. Miyai, H. Kanoh, and K. Ooi. 1992. Lithium (1+) extraction/insertion with spinel-type lithium manganese oxides. Characterization of redox-type and ion-exchange-type sites. *Langmuir* 8:1861–67.

Ferreira, C. A. M., J. A. C. Ponciano, D. S. Vaitsman, and D. V. Pérez. 2007. Evaluation of the corrosivity of the soil through its chemical composition. *Science of the Total Environment* 388:250–55.

Flexer, V., C. F. Baspineiro, and C. I. Galli. 2018. Lithium recovery from brines: A vital raw material for green energies with a potential environmental impact in its mining and processing. *Science of the Total Environment* 639:1188–204.

Fukuda, H. 2019. Lithium extraction from brine with ion exchange resin and ferric phosphate. Vancouver: University of British Columbia.

Gaikwad, R. W., S. A. Misal, and D. V. Gupta. 2011. Removal of metal from acid mine drainage (AMD) by using natural zeolite of Nizarneshwar Hills of Western India. *Arabian Journal of Geosciences* 4:85–89.

Gao, A., X. Hou, Z. Sun, S. Li, H. Li, and J. Zhang. 2019. Lithium-desorption mechanism in LiMn 2 O 4, Li 1.33 Mn 1.67 O 4, and Li 1.6 Mn 1.6 O 4 according to precisely controlled acid treatment and density functional theory calculations. *Journal of Materials Chemistry A* 7:20878–90.

Garcia, M. G., L. G. Borda, L. V. Godfrey, R. L. L. Steinmetz, and A. Losada-Calderon. 2020. Characterization of lithium cycling in the Salar De Olaroz, Central Andes, using a geochemical and isotopic approach. *Chemical Geology* 531:119340.

Gaskova, O. L., and M. B. Bukaty. 2008. Sorption of different cations onto clay minerals: Modelling approach with ion exchange and surface complexation. *Physics and Chemistry of the Earth, Parts A/B/C* 33:1050–55.

Gast, R. G., and W. D. Klobe. 1971. Sodium-lithium exchange equilibria on vermiculite at 25 and 50 C. *Clays and Clay Minerals* 19:311–19.

Gentili, V., S. Brutti, L. J. Hardwick, A. R. Armstrong, S. Panero, and P. G. Bruce. 2012. Lithium insertion into anatase nanotubes. *Chemistry of Materials* 24:4468–76.

Goldberg, V., D. Winter, F. Nitschke, M. Rath, S. Held, L. Spitzmüller, I. Budach, M. Pavez, D. Morata, and J. Koschikowski. 2021. The potential of raw material extraction from thermal brines–successful milestones of the BrineMine project. *Oil Gas-European Magazine* 47:26–33 .

Gorham, E. 1956. The chemical composition of some western Irish fresh waters. *Proceedings of the Royal Irish Academy. Section B: Biological, Geological and Chemical Science* 58:237–243.

Gourcerol, B., E. Gloaguen, J. Melleton, J. Tuduri, and X. Galiegue. 2019. Re-assessing the European lithium resource potential–A review of hard-rock resources and metallogeny. *Ore Geology Reviews* 109:494–519.

Greene-Kelly, R. 1955. Lithium absorption by kaolin minerals. *The Journal of Physical Chemistry* 59:1151–52.

Gruber, P. W., P. A. Medina, G. A. Keoleian, S. E. Kesler, M. P. Everson, and T. J. Wallington. 2011. Global lithium availability: A constraint for electric vehicles? *Journal of Industrial Ecology* 15:760–75.

Gu, D., W. Sun, G. Han, Q. Cui, and H. Wang. 2018. Lithium ion sieve synthesized via an improved solid state method and adsorption performance for West Taijinar Salt Lake brine. *Chemical Engineering Journal* 350:474–83.

Guneysu, S. 2020. Lithium sorption from aqueous solution with cationic resins. *Desalination and Water Treatment* 177:102–08.

Haas-Nüesch, R., F. Heberling, D. Schild, J. Rothe, K. Dardenne, S. Jähnichen, E. Eiche, C. Marquardt, V. Metz, and T. Schäfer. 2018. Mineralogical characterization of scalings formed in geothermal sites in the Upper Rhine Graben before and after the application of sulfate inhibitors. *Geothermics* 71:264–73.

Haklıdır, F. S. T., and T. Ö. Balaban. 2019. A review of mineral precipitation and effective scale inhibition methods at geothermal power plants in West Anatolia (Turkey). *Geothermics* 80:103–18.

Han, Y., H. Kim, and J. Park. 2012. Millimeter-sized spherical ion-sieve foams with hierarchical pore structure for recovery of lithium from seawater. *Chemical Engineering Journal* 210:482–89.

Harvianto, G. R., S.-H. Kim, and C.-S. Ju. 2016. Solvent extraction and stripping of lithium ion from aqueous solution and its application to seawater. *Rare Metals* 35:948–53.

Hawash, S., E. Abd El Kader, and G. El Diwani. 2010. Methodology for selective adsorption of lithium ions onto polymeric aluminium (III) hydroxide. *Journal of American Science* 6:301–09.

Heidari, N., and P. Momeni. 2017. Selective adsorption of lithium ions from Urmia Lake onto aluminum hydroxide. *Environmental Earth Sciences* 76:1–8.

Heidary, F., A. R. Khodabakhshi, and A. N. Kharat. 2016. Novel ion-exchange nanocomposite membrane containing in-situ formed FeOOH nanoparticles: Synthesis, characterization and transport properties. *Korean Journal of Chemical Engineering* 33:1380–90.

Helfferich, F. G. 1995. *Ion exchange*. New York, USA: Dover Publications, Inc.

Helmke, P. A., and D. L. Sparks. 1996. Lithium, sodium, potassium, rubidium, and cesium. *Methods of Soil Analysis: Part 3 Chemical Methods* 5:551–74.

Hong, H.-J., T. Ryu, I.-S. Park, M. Kim, J. Shin, B.-G. Kim, and K.-S. Chung. 2018. Highly porous and surface-expanded spinel hydrogen manganese oxide (HMO)/Al2O3 composite for effective lithium (Li) recovery from seawater. *Chemical Engineering Journal* 337:455–61.

Hoshino, T. 2013. Preliminary studies of lithium recovery technology from seawater by electrodialysis using ionic liquid membrane. *Desalination* 317:11–16.

Houston, J. 2010. Technical report on the Cauchari Project, Jujuy Province, Argentina. ed. Orocobre Ltd. Queensland: FloSolutions.

Hoyer, M., N.-A. Kummer, and B. Merkel. 2015. Sorption of lithium on bentonite, kaolin and zeolite. *Geosciences* 5:127–40.

Hunter, J. C. 1981. Preparation of a new crystal form of manganese dioxide: λ-MnO2. *Journal of Solid State Chemistry* 39:142–47.

Inglezakis, V. J., A. A. Zorpas, M. D. Loizidou, and H. P. Grigoropoulou. 2005. The effect of competitive cations and anions on ion exchange of heavy metals. *Separation and Purification Technology* 46:202–07.

Inoue, Y., and M. Abe. 1996. Synthetic inorganic ion exchange materials. XLIII. Ion exchange mechanism of lithium ions on cubic tantalic acid. *Solvent Extraction and Ion Exchange* 14:507–18.

Intaranont, N., N. Garcia-Araez, A. L. Hector, J. A. Milton, and J. R. Owen. 2014. Selective lithium extraction from brines by chemical reaction with battery materials. *Journal of Materials Chemistry A* 2:6374–77.

Ji, Z.-Y., F.-J. Yang, -Y.-Y. Zhao, J. Liu, N. Wang, and J.-S. Yuan. 2017. Preparation of titanium-base lithium ionic sieve with sodium persulfate as eluent and its performance. *Chemical Engineering Journal* 328:768–75.

Jiang, H., Y. Yang, S. Sun, and J. Yu. 2020a. Adsorption of lithium ions on lithium-aluminum hydroxides: Equilibrium and kinetics. *The Canadian Journal of Chemical Engineering* 98:544–55.

Jiang, H., Y. Yang, and J. Yu. 2020b. Application of concentration-dependent HSDM to the lithium adsorption from brine in fixed bed columns. *Separation and Purification Technology* 241:116682.

Joshi, D. R., and N. Adhikari. 2019. An overview on common organic solvents and their toxicity. *Journal of Pharmaceutical Research International* 28:1–18.

Kamran, U., and S.-J. Park. 2020. Functionalized titanate nanotubes for efficient lithium adsorption and recovery from aqueous media. *Journal of Solid State Chemistry* 283:121157.

Kaunda, R. B. 2020. Potential environmental impacts of lithium mining. *Journal of Energy & Natural Resources Law* 38:237–44.

Kawamoto, H., and W. Tamaki. 2011. *Trends in supply of lithium resources and demand of the resources for automobiles*.Tokyo, Japan: NISTEP Science & Technology Foresight Center.

Kaya, E., S. J. Zarrouk, and M. J. O'Sullivan. 2011. Reinjection in geothermal fields: A review of worldwide experience. *Renewable and Sustainable Energy Reviews* 15:47–68.

Kelly, J. C., M. Wang, Q. Dai, and O. Winjobi. 2021. Energy, greenhouse gas, and water life cycle analysis of lithium carbonate and lithium hydroxide monohydrate from brine and ore resources and their use in lithium ion battery cathodes and lithium ion batteries. *Resources, Conservation and Recycling* 174:105762.

Kesler, S. E., P. W. Gruber, P. A. Medina, G. A. Keoleian, M. P. Everson, and T. J. Wallington. 2012. Global lithium resources: Relative importance of pegmatite, brine and other deposits. *Ore Geology Reviews* 48:55–69.

Kim, J., and C. P. Grey. 2010. 2H and 7Li solid-state MAS NMR study of local environments and lithium adsorption on the iron (III) oxyhydroxide, akaganeite (β-FeOOH). *Chemistry of Materials* 22:5453–62.

Kim, J., U. G. Nielsen, and C. P. Grey. 2008. Local environments and lithium adsorption on the iron oxyhydroxides lepidocrocite (γ-FeOOH) and goethite (α-FeOOH): A 2H and 7Li solid-state MAS NMR study. *Journal of the American Chemical Society* 130:1285–95.

Kloprogge, J. T., S. Komarneni, and J. E. Amonette. 1999. Synthesis of smectite clay minerals: A critical review. *Clays and Clay Minerals* 47:529–54.

Kudryavtsev, P. G. 2016. Lithium in nature, application, methods of extraction. *Journal" Scientific Israel-Technological Advantages* 18:63–83.

Kuss, C., M. Carmant-Dérival, N. D. Trinh, G. Liang, and S. B. Schougaard. 2014. Kinetics of heterosite iron phosphate lithiation by chemical reduction. *The Journal of Physical Chemistry C* 118:19524–28.

Lagaly, G., and S. Ziesmer. 2003. Colloid chemistry of clay minerals: The coagulation of montmorillonite dispersions. *Advances in Colloid and Interface Science* 100:105–28.

Lawagon, C. P., G. M. Nisola, J. Mun, A. Tron, R. E. C. Torrejos, J. G. Seo, H. Kim, and W.-J. Chung. 2016. Adsorptive Li+ mining from liquid resources by H2TiO3: Equilibrium, kinetics, thermodynamics, and mechanisms. *Journal of Industrial and Engineering Chemistry* 35:347–56.

Lee, D. A., W. L. Taylor, W. J. McDowell, and J. S. Drury. 1968. Solvent extraction of lithium. *Journal of Inorganic and Nuclear Chemistry* 30:2807–21.

Lemaire, J., L. Svecova, F. Lagallarde, R. Laucournet, and P.-X. Thivel. 2014. Lithium recovery from aqueous solution by sorption/desorption. *Hydrometallurgy* 143:1–11.

Li, N. N., R. P. Cahn, D. Naden, and R. W. M. Lai. 1983. Liquid membrane processes for copper extraction. *Hydrometallurgy* 9:277–305.

Li, X., Y. Chao, L. Chen, W. Chen, J. Luo, C. Wang, P. Wu, H. Li, and W. Zhu. 2020. Taming wettability of lithium ion sieve via different TiO2 precursors for effective Li recovery from aqueous lithium resources. *Chemical Engineering Journal* 392:123731.

Li, Z., C. Li, X. Liu, L. Cao, P. Li, R. Wei, X. Li, D. Guo, K.-W. Huang, and Z. Lai. 2021. Continuous electrical pumping membrane process for seawater lithium mining. *Energy & Environmental Science* 14:3152–59.

Li, W., and X.-M. Liu. 2020. Experimental investigation of lithium isotope fractionation during kaolinite adsorption: Implications for chemical weathering. *Geochimica et cosmochimica acta* 284:156–72.

Li, L., W. Qu, F. Liu, T. Zhao, X. Zhang, R. Chen, and F. Wu. 2014. Surface modification of spinel λ-MnO2 and its lithium adsorption properties from spent lithium ion batteries. *Applied Surface Science* 315:59–65.

Limousin, G., J.-P. Gaudet, L. Charlet, S. Szenknect, V. Barthes, and M. Krimissa. 2007. Sorption isotherms: A review on physical bases, modeling and measurement. *Applied Geochemistry* 22:249–75.

Liu, W., D. B. Agusdinata, and S. W. Myint. 2019d. Spatiotemporal patterns of lithium mining and environmental degradation in the Atacama Salt Flat, Chile. *International Journal of Applied Earth Observation and Geoinformation* 80:145–56.

Liu, X., X. Chen, Z. Zhao, and X. Liang. 2014. Effect of Na+ on Li extraction from brine using LiFePO4/FePO4 electrodes. *Hydrometallurgy* 146:24–28.

Liu, D.-F., S.-Y. Sun, and J.-G. Yu. 2019a. A new high-efficiency process for Li+ recovery from solutions based on LiMn2O4/λ-MnO2 materials. *Chemical Engineering Journal* 377:119825.

Liu, K., Q. Tan, L. Liu, and J. Li. 2019c. Acid-free and selective extraction of lithium from spent lithium iron phosphate batteries via a mechanochemically induced isomorphic substitution. *Environmental Science & Technology* 53:9781–88.

Liu, W., H. Xu, X. Shi, and X. Yang. 2017. Fractional crystallization for extracting lithium from Cha'erhan tail brine. *Hydrometallurgy* 167:124–28.

Liu, L., H. Zhang, Y. Zhang, D. Cao, and X. Zhao. 2015. Lithium extraction from seawater by manganese oxide ion sieve MnO2· 0.5 H2O. *Colloids and Surfaces. A, Physicochemical and Engineering Aspects* 468:280–84.

Liu, G., Z. Zhao, and A. Ghahreman. 2019b. Novel approaches for lithium extraction from salt-lake brines: A review. *Hydrometallurgy* 187:81–100.

Liu, G., Z. Zhao, and L. He. 2020. Highly selective lithium recovery from high Mg/Li ratio brines. *Desalination* 474:114185.

Marazuela, M. A., E. Vázquez-Suñé, C. Ayora, and A. García-Gil. 2020. Towards more sustainable brine extraction in salt flats: Learning from the Salar de Atacama. *Science of the Total Environment* 703:135605.

Marion, G. M., F. J. Millero, M. F. Camões, P. Spitzer, R. Feistel, and C.-T. A. Chen. 2011. pH of seawater. *Marine Chemistry* 126:89–96.

Marthi, R., H. Asgar, G. Gadikota, and Y. R. Smith. 2021. On the structure and lithium adsorption mechanism of layered H2TiO3. *ACS Applied Materials & Interfaces* 13:8361–69.

McCauley, A., C. Jones, and J. Jacobsen. 2009. Soil pH and organic matter. *Nutrient Management Module* 8:1–12.

Melnikov, S., N. Sheldeshov, V. Zabolotsky, S. Loza, and A. Achoh. 2017. Pilot scale complex electrodialysis technology for processing a solution of lithium chloride containing organic solvents. *Separation and Purification Technology* 189:74–81.

Meng, F., J. McNeice, S. S. Zadeh, and A. Ghahreman. 2021. Review of lithium production and recovery from minerals, brines, and lithium-ion batteries. *Mineral Processing and Extractive Metallurgy Review* 42:123–41.

Meroufel, B., O. Benali, M. Benyahia, M. Zenasni, A. Merlin, and B. George. 2013. Removal of Zn (II) from aqueous solution onto kaolin by batch design. *Journal of Water Resource and Protection* 5:669–80.

Meshram, P., and B. D. Pandey. 2018. Advanced review on extraction of nickel from primary and secondary sources. *Mineral Processing and Extractive Metallurgy Review* 40:157–193.

Millennial Lithium Corp. 2020. *Millennial Lithium Corp. Announces commissioning of lithium carbonate pilot plant at its pastos grandes project in Salta, Argentina.*West Vancouver, BC: Millennial Lithium.

Mimura, K., K. Nakamura, K. Yasukawa, S. Machida, J. Ohta, K. Fujinaga, and Y. Kato. 2019. Significant impacts of pelagic clay on average chemical composition of subducting sediments: New insights from discovery of extremely rare-earth elements and yttrium-rich mud at Ocean Drilling Program Site 1149 in the western North Pacific Ocean. *Journal of Asian Earth Sciences* 186:104059.

The Mineral Corporation. 2019. Mineral Resource estimates for the Falchani Lithium Project in the Puno District of Peru. 76.

Mining Data Online. 2021. Sal de vida project. https://miningdataonline.com/property/3228/Sal-de-Vida-Project.aspx

Miyai, Y., K. Ooi, and S. Katoh. 1988. Recovery of lithium from seawater using a new type of ion-sieve adsorbent based on MgMn2O4. *Separation Science and Technology* 23:179–91.

Moazeni, M., H. Hajipour, M. Askari, and M. Nusheh. 2015. Hydrothermal synthesis and characterization of titanium dioxide nanotubes as novel lithium adsorbents. *Materials Research Bulletin* 61:70–75.

Moazzam, P., Y. Boroumand, P. Rabiei, S. S. Baghbaderani, P. Mokarian, F. Mohagheghian, L. J. Mohammed, and A. Razmjou. 2021. Lithium bioleaching: An emerging approach for the recovery of Li from spent lithium ion batteries. *Chemosphere* 277:1–20.

Mohr, S. H., G. M. Mudd, and D. Giurco. 2012. Lithium resources and production: Critical assessment and global projections. *Minerals* 2:65–84.

Moran, S. 2018. Clean water characterization and treatment objectives. An applied guide to water effluent treatment plant design. United States of American. Elsevier BV Inc., 978-0-12-811309-7 Chap 6, 61–67.

Morcos, S. A. 1970. Chemical composition of seawater and the variation of calcium and alkalinity. *ICES Journal of Marine Science* 33:126–33.

Nan, J., D. Han, and X. Zuo. 2005. Recovery of metal values from spent lithium-ion batteries with chemical deposition and solvent extraction. *Journal of Power Sources* 152:278–84.

Navarrete-Casas, R., A. Navarrete-Guijosa, C. Valenzuela-Calahorro, J. D. López-González, and A. García-Rodríguez. 2007. Study of lithium ion exchange by two synthetic zeolites: Kinetics and equilibrium. *Journal of Colloid and Interface Science* 306:345–53.

Nie, X.-Y., S.-Y. Sun, X. Song, and J.-G. Yu. 2017. Further investigation into lithium recovery from salt lake brines with different feed characteristics by electrodialysis. *Journal of Membrane Science* 530:185–91.

Nielsen, U. G., Y. Paik, K. Julmis, M. A. A. Schoonen, R. J. Reeder, and C. P. Grey. 2005. Investigating sorption on iron– oxyhydroxide soil minerals by solid-state NMR spectroscopy: A 6Li MAS NMR Study of Adsorption and Absorption on Goethite. *The Journal of Physical Chemistry. B* 109:18310–15.

Nir, S., D. Hirsch, J. Navrot, and A. Banin. 1986. Specific adsorption of lithium, sodium, potassium, and strontium to montmorillonite: Observations and predictions. *Soil Science Society of America Journal* 50:40–45.

Obaid, S. S., D. K. Gaikwad, M. I. Sayyed, A. L.-R. Khader, and P. P. Pawar. 2018. Heavy metal ions removal from waste water by the natural zeolites. *Materials Today: Proceedings* 5:17930–34.

Odom, I. E. 1984. Smectite clay minerals: Properties and uses. *Philosophical Transactions of the Royal Society of London. Series A: Mathematical and Physical Sciences* 311:391–409.

Ogawa, Y., H. Koibuchi, K. Suto, and C. Inoue. 2014. Effects of the chemical compositions of S alars de U yuni and A tacama Brines on lithium concentration during evaporation. *Resource Geology* 64:91–101.

Ohashi, F., and Y. Tai. 2019. Lithium adsorption from natural brine using surface-modified manganese oxide adsorbents. *Materials Letters* 251:214–17.

Oi, T., M. Endoh, M. Narimoto, and M. Hosoe. 2000. Ion and lithium isotope selectivity of monoclinic antimonic acid. *Journal of Materials Science* 35:509–13.

Olson, C. L., J. Nelson, and M. S. Islam. 2006. Defect chemistry, surface structures, and lithium insertion in anatase TiO2. *The Journal of Physical Chemistry. B* 110:9995–10001.

Ooi, K., Y. Makita, A. Sonoda, R. Chitrakar, Y. Tasaki-Handa, and T. Nakazato. 2016. Modelling of column lithium adsorption from pH-buffered brine using surface Li+/H+ ion exchange reaction. *Chemical Engineering Journal* 288:137–45.

Ooi, K., Y. Miyai, and S. Katoh. 1987. Lithium-ion sieve property of λ;-type manganese oxide. *Solvent Extraction and Ion Exchange* 5:561–72.

Ooi, K., Y. Miyai, S. Katoh, H. Maeda, and M. Abe. 1989. Topotactic lithium (1+) insertion to. lambda.-manganese dioxide in the aqueous phase. *Langmuir* 5:150–57.

Ooi, K., Y. Miyai, and J. Sakakihara. 1991. Mechanism of lithium (1+) insertion in spinel-type manganese oxide. Redox and ion-exchange reactions. *Langmuir* 7:1167–71.

Palagonia, M. S., D. Brogioli, and F. La Mantia. 2020. Lithium recovery from diluted brine by means of electrochemical ion exchange in a flow-through-electrodes cell. *Desalination* 475:114192.

Palmer, A. N., and M. V. Palmer. 2003. Geochemistry of capillary seepage in Mammoth Cave. *Speleogenesis and Evolution of Karst Aquifers* 1:1–8.

Park, H., N. Singhal, and E. H. Jho. 2015. Lithium sorption properties of HMnO in seawater and wastewater. *Water Research* 87:320–27.

Pauwels, H., M. Brach, and C. Fouillac. 1990. Lithium recovery from geothermal waters of Cesano (Italy) and Cronenbourg (Alsace, France). *Geochimica et Cosmochimica Acta* 57 :2737–2749.

Pauwels, H., M. Brach, and C. Fouillac. 1993. Chemistry and isotopes of deep geothermal saline fluids in the Upper Rhine Graben: Origin of compounds and water-rock interactions. *Geochimica et cosmochimica acta* 57:2737–49.

Peerawattuk, I., and E. R. Bobicki. 2018. Lithium Extraction and Utilization: A Historical Perspective. In *Extraction 2018. The Minerals, Metals & Materials Series. Springer, Cham* 2209–2224.

Pirajno, F. 2012. *Hydrothermal mineral deposits: Principles and fundamental concepts for the exploration geologist*. Berlin Heidelberg: Springer Science & Business Media.

Prodromou, K. P. 2016. Lithium adsorption on amorphous aluminum hydroxides and gibbsite. *Eurasian Journal of Soil Science* 5:13–16.

Pueyo, J. J., G. Chong, and C. Ayora. 2017. Lithium saltworks of the Salar de Atacama: A model for MgSO4-free ancient potash deposits. *Chemical Geology* 466:173–86.

Qian, F., M. Guo, Z. Qian, Q. Li, Z. Wu, and Z. Liu. 2019. Highly lithium adsorption capacities of H1. 6Mn1. 6O4 ion-sieve by ordered array structure. *ChemistrySelect* 4:10157–63.

Qiao, D., G. Wang, T. Gao, B. Wen, and T. Dai. 2021. Potential impact of the end-of-life batteries recycling of electric vehicles on lithium demand in China: 2010–2050. *Science of the Total Environment* 764:142835.

Rao, G. P. C., S. Satyaveni, A. Ramesh, K. Seshaiah, K. S. N. Murthy, and N. V. Choudary. 2006. Sorption of cadmium and zinc from aqueous solutions by zeolite 4A, zeolite 13X and bentonite. *Journal of Environmental Management* 81:265–72.

Reidel, F., and P. Ehren. 2018. Technical report: Lithium and potassium resources. Cauchari Project, Jujuy Province, Argentina.

Rio Tinto. 2020. *Rio Tinto declares maiden Ore Reserve at Jadar*. Melbourne, Australia: Rio Tinto Limited. https://www.riotinto.com/news/releases/2020/Rio-Tinto-declares-maiden-Ore-Reserve-at-Jadar

Rydberg, J. 2004. *Solvent extraction principles and practice, revised and expanded*. New York, USA: CRC press.

Ryu, T., J. C. Ryu, J. Shin, D. H. Lee, Y. H. Kim, and K.-S. Chung. 2013. Recovery of lithium by an electrostatic field-assisted desorption process. *Industrial & Engineering Chemistry Research* 52:13738–42.

Ryu, T., J. Shin, D.-H. Lee, J. Ryu, I. Park, H. Hong, Y. S. Huh, B.-G. Kim, and K.-S. Chung. 2015. Development of multi-stage column for lithium recovery from an aqueous solution. *Hydrometallurgy* 157:39–43.

Safari, S., B. G. Lottermoser, and D. S. Alessi. 2020. Metal oxide sorbents for the sustainable recovery of lithium from unconventional resources. *Applied Materials Today* 19:100638.

Sakamoto, H., K. Kimura, and T. Shono. 1987. Lithium separation and enrichment by proton-driven cation transport through liquid membranes of lipophilic crown nitrophenols. *Analytical Chemistry* 59:1513–17.

Salakjani, N. K., P. Singh, and A. N. Nikoloski. 2021. Production of lithium–A literature review. Part 2. Extraction from spodumene. *Mineral Processing and Extractive Metallurgy Review* 42:268–83.

Sanjuan, B., R. Millot, C. Innocent, C. Dezayes, J. Scheiber, and M. Brach. 2016. Major geochemical characteristics of geothermal brines from the Upper Rhine Graben granitic basement with constraints on temperature and circulation. *Chemical Geology* 428:27–47.

Sato, K., D. M. Poojary, A. Clearfield, M. Kohno, and Y. Inoue 1997. The surface structure of the proton-exchanged lithium manganese oxide spinels and their lithium-ion sieve properties. *Journal of Solid State Chemistry* 131:84–93.

Savannah Resources Plc. 2010-2021. Press release: Mina do Barroso Project, Portugal. https://www.savannahresources.com/assets/mina-do-barroso

Schmidt, M. 2017. *Rohstoffrisikobewertung - Lithium* . Berlin: DERA Rohstoffinformationen 33.

Shi, C., Y. Jing, J. Xiao, X. Wang, Y. Yao, and Y. Jia 2017. Solvent extraction of lithium from aqueous solution using non-fluorinated functionalized ionic liquids as extraction agents. *Separation and Purification Technology* 172:473–79.

Shi, X.-C., Z.-B. Zhang, D.-F. Zhou, L.-F. Zhang, B.-Z. Chen, and L.-L. Yu. 2013. Synthesis of Li+ adsorbent (H2TiO3) and its adsorption properties. *Transactions of Nonferrous Metals Society of China* 23:253–59.

Slunitschek, K., J. Kolb, and E. Eiche. 2021. Lithium extraction from geothermal brines. *GIT Laborfachzeitschrift* 7-8: 14–16.

Somrani, A. A. H. H., A. H. Hamzaoui, and M. Pontie 2013. Study on lithium separation from salt lake brines by nanofiltration (NF) and low pressure reverse osmosis (LPRO). *Desalination* 317:184–92.

Song, J. F., L. D. Nghiem, X.-M. Li, and T. He 2017. Lithium extraction from Chinese salt-lake brines: Opportunities, challenges, and future outlook. *Environmental Science: Water Research & Technology* 3:593–97.

Stober, I., and K. Bucher. 2012. *Geothermie*. Berlin: Springer.

Stringfellow, W. T., and P. F. Dobson 2021. Technology for the Recovery of Lithium from Geothermal Brines. *Energies* 14:6805.

Su, H., Z. Li, J. Zhang, Z. Zhu, L. Wang, and T. Qi. 2020. Recovery of lithium from salt lake brine using a mixed ternary solvent extraction system consisting of TBP, FeCl3 and P507. *Hydrometallurgy* 197:105487.

Sullivan, E. J., P. W. Reimus, S. J. Chipera, and D. Counce 2003. Effects of mineralogy, exchange capacity, surface area and grain size on lithium sorption to zeolitic alluvium near Yucca Mountain, Nevada. *Clays and Clay Minerals* 51:634–43.

Sun, S.-Y., L.-J. Cai, X.-Y. Nie, X. Song, and J.-G. Yu. 2015. Separation of magnesium and lithium from brine using a Desal nanofiltration membrane. *Journal of Water Process Engineering* 7:210–17.

Sun, S., X. Yu, M. Li, J. Duo, Y. Guo, and T. Deng 2020. Green recovery of lithium from geothermal water based on a novel lithium iron phosphate electrochemical technique. *Journal of Cleaner Production* 247:119178.

Sverjensky, D. A., E. L. Shock, and H. C. Helgeson 1997. Prediction of the thermodynamic properties of aqueous metal complexes to 1000 C and 5 kb. *Geochimica et cosmochimica acta* 61:1359–412.

Swain, B. 2016. Separation and purification of lithium by solvent extraction and supported liquid membrane, analysis of their mechanism: A review. *Journal of Chemical Technology and Biotechnology* 91:2549–62.

Swain, B. 2017. Recovery and recycling of lithium: A review. *Separation and Purification Technology* 172:388–403.

Sykes, J. 2019. A global overview of the geology and economics of lithium production.

Tadesse, B., F. Makuei, B. Albijanic, and L. Dyer 2019. The beneficiation of lithium minerals from hard rock ores: A review. *Minerals Engineering* 131:170–84.

Taghvaei, N., E. Taghvaei, and M. Askari 2020. Synthesis of anodized TiO2 nanotube arrays as ion sieve for lithium extraction. *ChemistrySelect* 5:10339–45.

Takeno, N. 2005. Atlas of Eh-pH diagrams. *Geological Survey of Japan Open File Report* 419:102.

Tian, L., W. Ma, and M. Han 2010. Adsorption behavior of Li+ onto nano-lithium ion sieve from hybrid magnesium/lithium manganese oxide. *Chemical Engineering Journal* 156:134–40.

US Geological Survey. 2021. *Mineral commodity summaries 2021: Lithium*. (Reston, VA: U.S. Geological Survey)

Valdez, S. K., H. R. Flores, and A. Orce. 2016. Influence of the evaporation rate over lithium recovery from brines. *World Journal of Research and Review* 3:66–70 .

Hoek, E.M., Tarabara, V.V. and Van der Bruggen, B. 2013. Nanofiltration. In *Encyclopedia of Membrane Science and Technology* (eds E.M. Hoek and V.V. Tarabara). https://doi.org/10.1002/9781118522318.emst077)

Ventura, S., S. Bhamidi, M. Hornbostel, and A. Nagar, International, SRI. 2020. *Selective Recovery of Lithium from Geothermal Brines: Final Project Report.*California, USA: California Energy Commission.

Ventura, S., S. Bhamidi, M. Hornbostel, A. Nagar, and E. Perea 2016. *Selective recovery of metals from geothermal brines*. Menlo Park, CA (United States): SRI International.

Wang, S., Li, P., Cui, W., Zhang, H., Wang, H., Zheng, S., and Zhang, Y. 2016. Hydrothermal synthesis of lithium-enriched β-Li2TiO3 with an ion-sieve application: excellent lithium adsorption. *RSC advances* 6:102608–102616.

Wang, L., C. G. Meng, M. Han, and W. Ma 2008. Lithium uptake in fixed-pH solution by ion sieves. *Journal of Colloid and Interface Science* 325:31–40.

Wang, S., M. Zhang, Y. Zhang, Y. Zhang, S. Qiao, and S. Zheng 2019. High adsorption performance of the Mo-doped titanium oxide sieve for lithium ions. *Hydrometallurgy* 187:30–37.

Warnock, S. J., R. Sujanani, E. S. Zofchak, S. Zhao, T. J. Dilenschneider, K. G. Hanson, S. Mukherjee, V. Ganesan, B. D. Freeman, and M. M. Abu-Omar 2021. Engineering Li/Na selectivity in 12-Crown -4–functionalized polymer membranes. *Proceedings of the National Academy of Sciences* 118:1–8 .

Warren, I. 2021. Techno-economic analysis of lithium extraction from geothermal brines. National Renewable Energy Lab.(NREL), Golden, CO (United States).

Wedepohl K. H. (1995). The composition of the continental crust. *Geochimica et Cosmochimica Acta*, 59:1217–1232.

Wei, S., Y. Wei, T. Chen, C. Liu, and Y. Tang 2020. Porous lithium ion sieves nanofibers: General synthesis strategy and highly selective recovery of lithium from brine water. *Chemical Engineering Journal* 379:122407.

Wen, X., P. Ma, C. Zhu, Q. He, and X. Deng 2006. Preliminary study on recovering lithium chloride from lithium-containing waters by nanofiltration. *Separation and Purification Technology* 49:230–36.

Weng, D., H. Duan, Y. Hou, J. Huo, L. Chen, F. Zhang, and J. Wang 2020. Introduction of manganese based lithium-ion Sieve-A review. *Progress in Natural Science: Materials International* 30:139–52.

Wenger, M., and T. Armbruster 1991. Crystal chemistry of lithium: Oxygen coordination and bonding. *European Journal of Mineralogy* 3:387–400.

Williams, L. B., and R. L. Hervig 2005. Lithium and boron isotopes in illite-smectite: The importance of crystal size. *Geochimica et cosmochimica acta* 69:5705–16.

Wiśniewska, M., G. Fijałkowska, I. Ostolska, W. Franus, A. Nosal-Wiercińska, B. Tomaszewska, J. Goscianska, and G. Wójcik 2018. Investigations of the possibility of lithium acquisition from geothermal water using natural and synthetic zeolites applying poly (acrylic acid). *Journal of Cleaner Production* 195:821–30.

Wunder, B., A. Meixner, R. L. Romer, A. Feenstra, G. Schettler, and W. Heinrich 2007. Lithium isotope fractionation between Li-bearing staurolite, Li-mica and aqueous fluids: An experimental study. *Chemical Geology* 238:277–90.

Xiang, W., S. Liang, Z. Zhou, W. Qin, and W. Fei 2016. Extraction of lithium from salt lake brine containing borate anion and high concentration of magnesium. *Hydrometallurgy* 166:9–15.

Xiao, J., X. Nie, S. Sun, X. Song, P. Li, and J. Yu 2015b. Lithium ion adsorption–desorption properties on spinel Li4Mn5O12 and pH-dependent ion-exchange model. *Advanced Powder Technology* 26:589–94.

Xiao, J.-L., S.-Y. Sun, X. Song, P. Li, and Y. J-g. 2015a. Lithium ion recovery from brine using granulated polyacrylamide–MnO2 ion-sieve. *Chemical Engineering Journal* 279:659–66.

Xiao, G., K. Tong, L. Zhou, J. Xiao, S. Sun, P. Li, and J. Yu 2012. Adsorption and desorption behavior of lithium ion in spherical PVC–MnO2 ion sieve. *Industrial & Engineering Chemistry Research* 51:10921–29.

Xu, X., Y. Chen, P. Wan, K. Gasem, K. Wang, T. He, H. Adidharma, and M. Fan 2016. Extraction of lithium with functionalized lithium ion-sieves. *Progress in Materials Science* 84:276–313.

Xu, C., Q. Dai, L. Gaines, M. Hu, A. Tukker, and B. Steubing 2020. Future material demand for automotive lithium-based batteries. *Communications Materials* 1:1–10.

Xue, F., X. Zhang, Y. Niu, C. Yi, S. Ju, and W. Xing 2020. Preparation and evaluation of α-Al2O3 supported lithium ion sieve membranes for Li+ extraction. *Chinese Journal of Chemical Engineering* 28:2312–18.

Yaksic, A., and J. E. Tilton 2009. Using the cumulative availability curve to assess the threat of mineral depletion: The case of lithium. *Resources Policy* 34:185–94.

Yang, X., Y. Makita, J. Hosokawa, K. Sakane, and K. Ooi 2005. Preparation and alkali metal ion exchange properties of protonated Rb8Nb22O59 compound. *Chemistry of Materials* 17:5420–27.

Yang, Y., X. Meng, H. Cao, X. Lin, C. Liu, Y. Sun, Y. Zhang, and Z. Sun 2018. Selective recovery of lithium from spent lithium iron phosphate batteries: A sustainable process. *Green Chemistry* 20:3121–33.

Yoshinaga, T., K. Kawano, and H. Imoto 1986. Basic study on lithium recovery from lithium containing solution. *Bulletin of the Chemical Society of Japan* 59:1207–13.

Yoshizuka, K., S. Nishihama, M. Takano, and S. Asano. 2021. Lithium recovery from brines with Novel λ-MnO2 adsorbent synthesized by hydrometallurgical method. *Solvent Extraction and Ion Exchange* 39:604–621.

Zamzow, M. J., B. R. Eichbaum, K. R. Sandgren, and D. E. Shanks 1990. Removal of heavy metals and other cations from wastewater using zeolites. *Separation Science and Technology* 25:1555–69.

Zamzow, M. J., and J. E. Murphy 1992. Removal of metal cations from water using zeolites. *Separation Science and Technology* 27:1969–84.

Zandvakili, S., and M. Ranjbar 2018. Preparation and characterisation of lithium ion exchange composite for the recovery of lithium from brine. *Mineral Processing and Extractive Metallurgy* 127:176–81.

Zhang, Y., Y. Hu, L. Wang, and W. Sun 2019. Systematic review of lithium extraction from salt-lake brines via precipitation approaches. *Minerals Engineering* 139:105868.

Zhang, Q.-H., S.-P. Li, S.-Y. Sun, X.-S. Yin, and J.-G. Yu. 2010b. LiMn2O4 spinel direct synthesis and lithium ion selective adsorption. *Chemical Engineering Science* 65:169–73.

Zhang, Q.-H., S.-P. Li, S.-Y. Sun, X.-S. Yin, and J.-G. Yu. 2010c. Lithium selective adsorption on low-dimensional titania nanoribbons. *Chemical Engineering Science* 65:165–68.

Zhang, Q.-H., S. Sun, S. Li, H. Jiang, and J.-G. Yu. 2007. Adsorption of lithium ions on novel nanocrystal MnO2. *Chemical Engineering Science* 62:4869–74.

Zhang, D., C.-H. Zhou, C.-X. Lin, D.-S. Tong, and Y. W-h. 2010a. Synthesis of clay minerals. *Applied Clay Science* 50:1–11.

Zhao, Q., J.-M. Gao, Y. Guo, and F. Cheng 2018. Facile synthesis of magnetically recyclable Fe-doped lithium ion sieve and its Li adsorption performance. *Chemistry Letters* 47:1308–10.

Zhao, Z., X. Si, X. Liu, L. He, and X. Liang 2013. Li extraction from high Mg/Li ratio brine with LiFePO4/FePO4 as electrode materials. *Hydrometallurgy* 133:75–83.

Zhou, C., A. Alshameri, C. Yan, X. Qiu, H. Wang, and Y. Ma 2013. Characteristics and evaluation of synthetic 13X zeolite from Yunnan's natural halloysite. *Journal of Porous Materials* 20:587–94.

Zhu, Q., Aller, R. C., and Fan, Y. 2006. Two-dimensional pH distributions and dynamics in bioturbated marine sediments. *Geochimica et Cosmochimica Acta* 70:4933–4949.

Zhu, G., P. Wang, P. Qi, and C. Gao 2014. Adsorption and desorption properties of Li+ on PVC-H1. 6Mn1. 6O4 lithium ion-sieve membrane. *Chemical Engineering Journal* 235:340–48.

Ziemann, S., D. B. Müller, L. Schebek, and M. Weil 2018. Modeling the potential impact of lithium recycling from EV batteries on lithium demand: A dynamic MFA approach. *Resources, Conservation and Recycling* 133:76–85.

Study II

Structural and compositional variation of zeolite 13X in lithium sorption experiments using synthetic solutions and geothermal brine

Rebekka Reich, Rosa Micaela Danisi, Tobias Kluge, Elisabeth Eiche & Jochen Kolb

This work has been published in Microporous and Mesoporous Materials

published online: 03 May 2023

available online:

https://www.sciencedirect.com/science/article/abs/pii/S1387181123001944?via%3Dihub

DOI: 10.1016/j.micromeso.2023.112623

Microporous and Mesoporous Materials 359 (2023) 112623

Contents lists available at ScienceDirect

Microporous and Mesoporous Materials

journal homepage: www.elsevier.com/locate/micromeso

Structural and compositional variation of zeolite 13X in lithium sorption experiments using synthetic solutions and geothermal brine

Rebekka Reich [a,b,*], Rosa Micaela Danisi [c], Tobias Kluge [a,b], Elisabeth Eiche [a,b], Jochen Kolb [a,b]

[a] Geochemistry and Economic Geology, Institute of Applied Geosciences, Karlsruhe Institute of Technology, Adenauerring 20b, 76131, Karlsruhe, Germany
[b] Laboratory for Environmental and Raw Materials Analysis, Institute of Applied Geosciences, Adenauerring 20b, 76131, Karlsruhe, Germany
[c] Technical Petrophysics, Institute of Applied Geosciences, Karlsruhe Institute of Technology, Adenauerring 20b, 76131, Karlsruhe, Germany

ARTICLE INFO

Keywords:
Ion-exchange
Geothermal brine
Batch experiment
Desorption
Competing ions

ABSTRACT

This study provides insight into the potential application of zeolite 13X powder and beads for direct lithium extraction. The impact of variable stirring time, pH and temperature is investigated. The major ion-exchange process is found to be Li^+ vs. Na^+ or H^+, reaching a maximum sorption capacity of 20.3 mg/g using 13X powder whereas only 8.6 mg/g Li is sorbed to 13X beads. Equilibrium between sorbent and fluid is reached within 1 min and 9 h contact time for powder and beads, respectively. The temperature effect on Li sorption is negligible, whereas pH adjustment to more acidic conditions decreases the Li sorption capacity by up to 68% compared to non-adjusted conditions. Chemical data fits well with changes in crystal parameters confirming the data's significance. Different sorption processes like physisorption, ion exchange of Na^+ and H^+ with Li^+, and different Li sorption sites on zeolite 13X sorbent are indicated. Solutions of different concentrations have been tested for desorption. Lithium recovery from the previously loaded sorbent reaches 94–100%. Aiming at a direct Li extraction technique from geothermal brines in the future, this study shows that zeolite 13X is a promising sorbent although challenges regarding higher selectivity for Ca, K, Mn, Ba, and As need to be resolved for its application in a high saline environment.

1. Introduction

1.1. Economic geology of lithium

Lithium is characterized as critical metal by the European Union and gains increasing interest due to its importance for batteries in mobile phones, cars, and local energy storage solutions [1]. The world's Li resources are estimated to comprise 55–99 Mt Li [2,3]. Currently, Li is mainly mined in southern America (i.e., Chile and Argentina) and Australia, producing 32200 and 55000 t Li in 2021, respectively [3]. In Chile and Argentina, Li is hosted in brines, whereas hard rock ores are mined in Australia and a spodumene concentrate is shipped to and refined in China [4]. Due to the ongoing energy transition and the resulting increase in lithium ion battery use, a significant increase in the global Li demand is expected in the future [5,6]. Models predict a required annual production of 316307–558780 t Li in 2030 [4]. Geothermal brines are known to represent potential new Li sources if Li can be extracted selectively and sustainably in the future [7]. The development of direct Li extraction (DLE) techniques from unconventional sources is thus essential to support the raw materials supply [8].

1.2. Direct lithium extraction

Besides many Li extraction technologies, such as evaporation, precipitation, membrane-related processes and solvent extraction, sorption and ion exchange are regarded as a promising technology for direct Li extraction (DLE) from operating geothermal power plants [9,10]. The salinity of brines is up to 300 g/L TDS (i.e. total dissolved solids). The brines are characterized by high concentrations of Na^+ (<135 g/L) and Cl^- (<180 g/L), and lower concentrations of K^+ (<27 g/L), Ca^{2+} (<16 g/L), Mg^{2+} (<17 g/L) and SO_4^{2-} (<62 g/L) [8]. The highest Li concentrations at 480 mg/L are found in the Campi Flegrei geothermal field in Italy [4]. In geothermal power plants, the brine is typically pumped at 20–50 bar at flow rates of max. 90 L/s with temperatures >60 °C after heat extraction.

The extraction of other raw materials from brine is already being used commercially where e.g., Si, B, and Mg are mined. The potential for

* Corresponding author. Karlsruhe Institute of Technology, Campus Süd, Adenauerring 20b, Gebäude 50.40, 76131 Karlsruhe, Germany.
E-mail address: rebekka.reich@kit.edu (R. Reich).

https://doi.org/10.1016/j.micromeso.2023.112623
Received 10 February 2023; Received in revised form 17 April 2023; Accepted 25 April 2023
Available online 3 May 2023

raw material extraction from geothermal brines and challenges regarding the used materials due to the corrosivity of geothermal brines has already been investigated since the 1980s [11–14]. Especially for DLE, high Mg^{2+} concentrations pose a challenge, as this makes separation from Li^{+} difficult, because both have similar properties [15]. Currently, pilot plant tests are performed for the DLE at Salton Sea, facing problems with dropping water level, the formation of scales and temperatures of 250 °C that increase the requirements for any used material, like pipes and Li selective sorbents or resins [14,16]. Consequently, the physicochemical parameters at the geothermal power plants determine the requirements for the sorbents regarding selectivity, kinetic properties, chemical stability, and sorption capacity [8]. Lithium-manganese oxide, titanium oxide, and aluminum hydroxide are well-known inorganic sorbents. Other inorganic sorbents like zeolite group minerals are already used in industrial applications e.g., water treatment, air conditioning and catalyst industry, where large-scale synthesis and market availability are ensured [17,18].

1.3. Zeolite group minerals

Zeolite group minerals are aluminosilicates that are characterised by a pore architecture built by a three-dimensional framework of linked (Si, Al)O_4 tetrahedra. The group comprises more than 230 minerals differing in chemical composition and framework structure type, which determines their various pore size and accessibility of guest species [19]. Lithium is generally sorbed to the negatively charged surface of the zeolite, forming inner- or outer-sphere surface complexes. This process is positively influenced by a high Al^{3+}/Si^{4+} ratio that enhances the negative charge of the sorbent [18]. This resulting negative charge enables cations to occupy sites in proximity of the Si–$O^{(-)}$-Al bridging groups [20]. Structurally, zeolite 13X is characterized by a cubic faujasite-type framework in the space group F*d*-3*m* and ring sizes of 12, 6, and 4 T-atoms [21]. The zeolite's three-dimensional framework is composed of one large supercage of approximately 13 Å and the sodalite cages. Access to the supercages is by four 12-membered ring windows of about 7.4–8.0 Å in diameter, which are distributed around the centre of the supercages. The diameter of the 6-membered ring windows, accessing the sodalite cages, is 2.2 Å [20,22]. Extra-framework cations can occupy three positions in the zeolite. Site SI is located in the hexagonal prism, whereas site SI' is located at the interface to the sodalite cage. Sites SII and SII' are located on the open hexagonal faces. Site SII is located in the centre of the six-membered rings at the interface between the supercage and the sodalite cage. Site SII' is near the interface but within the sodalite cage. Site SIII is located on the walls of the supercage [20,23]. The lattice parameters are $a = 24.7400$ Å and $V = 15142.55$ $Å^3$ [24]. Advantageous for the physisorbed portion of Li is the large negatively charged surface area of up to ~600–800 m^2/g of zeolite 13X powder [25–27]. Substitution of protons and alkali earth elements with Li in the crystal lattice enables zeolite to perform as an ion exchanger [28]. Lithium exchanges with H^{+} in many inorganic ion exchangers, resulting in the necessity of using acids for desorption [29–31]. However, literature data on the elution of Li from zeolite 13X is lacking [32,33]. Zeolite can be used in NH_4^{+}-, Na^{+}-, or other alkaline earth ion-exchanged forms. The capture of Li^{+} is then controlled by physisorption in combination with ion exchange between Li^{+} and Na^{+} or alkaline earth ions, rather than Li^{+} and H^{+} [34,35]. This enables the desorption of Li^{+} using e.g. NaCl instead of acids [28,36–38].

Zeolite is known to reach a high Li sorption capacity of up to 25 mg/g at short reaction times e.g., less than 15 min are necessary to reach equilibrium [34,39]. Short reaction times are favourable for the DLE from geothermal brines [8]. The sorption capacity is expected to increase with increasing temperature due to faster diffusion. The sorption capacity has been investigated for T = 10, 20, 30, and 40 °C [34], but lacks information at higher temperatures relevant to geothermal systems. The point of zero charge (pH_{pzc}) is determined to be 10.2–11.0 for zeolite 13X [32,40]. At pH = 9, > 0.4 mg/g Li is sorbed whereas only < 0.1 mg/g Li is sorbed at pH = 3 from a solution containing 10 mg/L Li initially [32], however, volume and temperature data have not been defined for these experiments. The Li sorption capacity increases with increasing pH and the chemical stability of zeolite is good at moderate pH [41]. Other studies, however, postulate acid and alkali resistance [26]. Wang and Peng [38] show that chemical stability is good for natural zeolite applied in wastewater treatment after 12 sorption/desorption cycles and elution with 0.5 M HCl. Sorption/desorption characteristics have been investigated for gases, such as N_2 and CO_2, and indicate good stability after five cycles [27,42]. However, Li desorption data are lacking for zeolite 13X and recyclability has not been investigated yet. The selectivity for Li has been stated to be low and the selectivity sequence for most zeolite materials is found to be Cs > Rb > K > Na > Li as well as Ba > Sr > Ca > Mg [28]. The use of additives e.g., polyacrylic acid appears to increase the Li selectivity [32], however, important experimental data are not given.

The large field of potential applications of zeolite for DLE motivates a closer examination of the properties. The potential and limitation of zeolite in the purpose of raw materials extraction from an unconventional resource, like geothermal brine, is addressed in this study. Of particular interest is the investigation of the following questions: (1) Is the chosen calcination temperature and duration appropriate? What is the effect on the zeolite? (2) Does Li sorb to zeolite 13X under the physical and technical conditions (e.g. temperature, pH, flow rate, Li concentration) usually ambient and relevant in geothermal power plants? (3) Do commercially available zeolite 13X powder and beads show the same Li sorption behavior? (4) What are the relevant sorption processes? (5) Which are the main competing ions in geothermal brine? (6) How can Li be eluted after sorption to recover Li? (7) Are Li sorption to and desorption from zeolite 13X fully reversible processes on a compositional and structural scale?

2. Experimental

The zeolite 13X powder (product No. A10378, lot: 10229992) and bead (product No. B21109, lot: 10227590) samples, retrieved from Alfa Aesar, have been investigated regarding their optical (SEM) and structural properties (XRD, DTA-DSC, FT-IR-ATR) and chemical characteristics (XRF, acid digestion, ICP-OES). BSE images and SEM analyses have been performed using a TESCAN VEGA II combined with an EDX INCA X-act device from Oxford Instruments at the Chair of Mineralogy and Petrology, Karlsruhe Institute of Technology, Germany.

For XRD analyses, bead samples with comparably large grain sizes of 1.6–2.5 mm have been milled before analyses. No special preparation step was necessary for the powder. A sample mass of both materials of 1.8 g was mixed with 0.2 g silicon standard material and put in sample carriers with a sample diameter of 20 mm. The Si internal standard was introduced for phase quantification and to account for possible preferential orientation of the samples. The material from experiments was attached to the silica wafer using X-ray amorphous petroleum jelly, due to a reaction of the zeolite powder with acetone during previous preparation with solvents. The conditions for the XRD analyses, using a D8 Discover diffractometer from Bruker with CuKα radiation (Kα1 λ = 1.54060 Å and Kα2 λ = 1.5444 Å) attached to an LYNXEYE XE-T linear detector, were 2–82° 2Θ, 1 s/step and 0.02° increment. The sample rotation was 30 rpm and the airscatter was on automatic mode. The X-ray tube operates at 40 kV and 40 mA. Phase identification was carried out using the Bruker Diffrac.EVA V4.1.1 software package and the database PDF2 of 2002 [43]. The lattice parameters were determined using the Rietveld method [44] provided by the software Topas 5, Bruker AXS, (2011). Peak shapes were fitted using fundamental parameters, while the background was fitted with a 5-term Chebyshev polynomial. The refinement of the zeolite 13X structure was performed starting from the model of Bergerhoff et al [24].

For XRF analyses, the samples have been grinded and calcined at 950 °C for 3 h to determine the loss of ignition (LOI). A sample amount

of 0.5 g of the calcined material was mixed with 5 g Spectroflux 110 (Alfa Aesar) and molten at 1000–1100 °C to produce fused beads. Triplicates of each sample have been prepared for the analysis in wavelength-dispersive mode, using a S4 Explorer from Bruker AXS coupled with a Rh-X-ray tube. The maximum operating voltage was 50 keV. Detection was done in an argon-methane-gas flow using a scintillation counter. Analysing crystals were XS-55, LIF2000 and PET. The used standards to check for accuracy were AGV-1 (andesite powder), G-2 (granite powder) and RGM-1 (rhyolite powder) [45]. Matrix correction was done by alpha-factors.

In preparation for the sorption experiments, the zeolite was calcined at 400 °C for 3 h. The effect of calcination has been investigated using DTA-DSC using sintered corundum as standard reference material. For analysis, powdered samples were filled in a Pt–Rh crucible and heated in a N_2 atmosphere using a STA 409 PC Luxx system from Netzsch. The measurement started at 20 °C, followed by heating to 30 °C (heating rate of 50 K/min) which was kept for 10 min. Thereafter, heating to 400 °C was carried out at 7 K/min and the temperature maximum was kept constant for 3 h. All analyses described have been performed at the Laboratory for Environmental and Raw Materials Analyses (LERA), Karlsruhe Institute of Technology, Germany.

FT-IR-ATR analyses have been performed using a Nicolet iS50 instrument at the Institute of Nanotechnology, Karlsruhe Institute of Technology, Germany. Analyses have been performed with powder samples at wavenumbers between 400 cm^{-1} and 4000 cm^{-1} at contact with a diamond crystal. Each sample was measured using 20 repetitions and then referenced to a background analysis in air. Minimum shifts are 3 cm^{-1}, which is well above the resolution of the instrument [46].

The batch sorption and desorption experiments have been performed in HDPE vessels to prevent Li sorption on amorphous materials such as glass vessels [47] using a sorbent mass of 1 g and a volume of 200 mL solution. The zeolite was always rinsed with 100 mL MilliQ® after each experiment. Parameters potentially influencing the Li sorption behaviour e.g., temperature, pH, solution/sorbent ratio and stirring time were investigated. A synthetic LiCl solution was used. The kinetic experiments were conducted at a fixed Li concentration of 200 mg/L. Stirring times varied between 1, 5, 15, 30, 45, 60, 120, 180, 540, and 1440 min at a constant stirring rate of approximately 300 rpm. For some experiments, additional one- and two-week runs have been performed. To specify the sorption isotherms, a fixed stirring time of 45 min, determined from the kinetic experiments, was chosen. Lithium concentrations varied between 10 and 500 mg/L whereas the temperature was fixed to 25, 40, 60 and 80 °C in an oven, respectively. Experimental batches have been performed without pH adjustment to study endmember cases. In a similar setup, however, the pH was adjusted to 5–6 by buffering with KH_2PO_4 (pro analysis, Merck) and 1 M NaOH (titripur®, Merck) solutions. For geothermal water experiments, the brine was depleted in Fe due to precipitation caused by contact with the atmosphere. The pH was adjusted to 5 using 0.5 M HCl (titripur®, Merck) solution. After the experiments, the material was vacuum filtered through a cellulose acetate filter (0.45 μm mesh size). The filtrate was rinsed with 100 mL Milli-Q® water and afterwards dried at 60 °C for 24 h.

A grinded sorbent mass of 100 mg from each experiment was digested in 1 mL Milli-Q® water, 2 mL 65% HNO_3 (subboiled), 1 mL 65% $HClO_4$ (normatom) and 5 mL 40% HF (suprapur). The samples were heated in a closed Teflon vessel for 16 h at 120 °C. After evaporation of the acids to incipient dryness, the residue was dissolved in 2 mL 65% HNO_3 (subboiled) and evaporated another three times for purification. The final residue was dissolved in 2 mL 65% HNO_3 (subboiled) and diluted with MilliQ® water to a total volume of 50 mL.

The initial solutions, equilibrium solutions and solutions from the acid digestion have been analysed using an ICP-OES iCAP 7000 from Thermo Fisher and an ICP-MS iCAP RQ (C2) with an iMR_1000 gas kit (Thermo Fisher) at the Laboratory for Environmental and Raw Materials Analyses (LERA), Karlsruhe Institute of Technology, Germany. From these solutions, the concentration of Li and, depending on the experiment, Na, K, Rb, Mg, Ca, Sr, Ba, Mn, Fe, Cu, Zn, Al, Si, Pb, P, As, and S have been determined. Information on the relative precision and accuracy can be found in the supplementary data. Quality was assured by analysis of duplicates and certified standards, like ROTI®Star 1000 g/L Y in 2% HNO_3 solution (as an internal standard for diluted samples) and a multi-element aqueous VHG-MISA6-500 standard. Additional blanks have been analysed to determine the detection limit (3 times sigma) and the limit of quantification (10 times sigma).

Sorption capacity, i.e. the load, has been calculated according to the equation $Q_i = (C_0 - C_{Equ}) * \frac{V}{m}$. In this equation, Q is the sorption capacity/load of the sorbate (i) to the sorbent in mg/g (in case of comparison between different sorbates, Q was recalculated to mmol/g), C_0 is the initial concentration of the sorbate in the solution given as mg/L, C_{Equ} is the equilibrium concentration of the sorbate in the solution expressed in mg/L after the experiment, V is the volume of the solution in L and m is the sorbent mass in g used in the experiments [48].

3. Results and discussion

3.1. Sample characterization and the effect of calcination

The zeolite 13X powder has a white colour (Fig. 1a), whereas the zeolite 13X beads appear beige in colour with grain sizes varying between 1.6 and 2.5 mm (Fig. 1b). In BSE images, the powder is homogeneously constituted by mostly euhedral grains and has a grain size of 1–30 μm (Fig. 1c). Zeolite grains of the beads are more subhedral and an additional phase can be observed, presumably acting as a binder for the single zeolite 13X crystals (Fig. 1d).

X-ray diffraction patterns indicate that the powder and bead samples are composed of Na-exchanged varieties of zeolite X which are well-crystalline (Fig. 2a). The XRD patterns include an internal silicon standard (Fig. 2a). The bead samples are predominantly Na-exchanged zeolite X but additional phases, such as muscovite (~6 wt%) and minor amounts of clay minerals (~1 wt%) are also found (Fig. 2a, Table 1). The refined lattice parameters of the Na-exchanged zeolite X phase are $a = 24.9786(4)$ Å, V = 15584.8(8) $Å^3$ and $a = 24.9805(5)$ Å, V = 15588.5(9) $Å^3$ for the powder and bead samples, respectively (Table 1).

Synthetic zeolite 13X yields mean concentrations of 16.39 wt% and 13.30 wt% Na_2O for powder and bead samples, respectively. The Si/Al ratio of zeolite 13X powder is 1.2 and 1.5 for zeolite 13X beads. Higher MgO, CaO, TiO_2 and Fe_2O_3 concentrations of the beads compared to the powder (Table 2) indicate the presence of additional phases related to the synthesis of beads when compared to the pure powder. From the dehydrated formulae for a Si/Al ratio of 1.2 and 1.5 of faujasite zeolite [23,49], the maximum theoretical Li sorption capacity can be determined. For Si/Al = 1.2 ($Li_{76.8}[Si_{115.2}Al_{76.8}]O_{384}$), the highest theoretical load is 6.4 mmol/g (44.5 mg/g) and for Si/Al = 1.5 ($Li_{48}[Si_{144}Al_{48}]O_{384}$) the highest theoretical load is 4.4 mmol/g (30.4 mg/g).

The FT-IR-ATR spectrum of zeolite 13X powder shows bands at 447 cm^{-1}, 567 cm^{-1}, 675 cm^{-1}, 756 cm^{-1}, 958 cm^{-1}, 1650 cm^{-1}, and 3340 cm^{-1} (Fig. 3). The broad band at 3340 cm^{-1} characteristically represents the inner-surface OH^- stretching vibrations, indicating the presence of crystal water or physisorbed water molecules [50]. This is also confirmed by the presence of the 1650 cm^{-1} vibration band related to physisorbed water [26,35,50]. The characteristic framework of zeolite 13X is indicated by the bands at 958 cm^{-1} and 675 cm^{-1} assigned to symmetric and asymmetric vibration of the $(Al,Si)O_4$ bonds, respectively [26]. The 756 cm^{-1} band is related to Si(Al)–O vibration whereas the band at 567 cm^{-1} is assigned to Si–O–Si vibrations and Si–O vibration at 447 cm^{-1} in the double six-membered rings [26,35].

The effect of calcination has been investigated by DTA-DSC analysis of zeolite 13X powder. During heating in a N_2-atmosphere, an endothermic peak occurs at 152 °C related to dehydration (Fig. 4) [26,51]. The total mass difference is −17.8% after calcination at 400 °C. This,

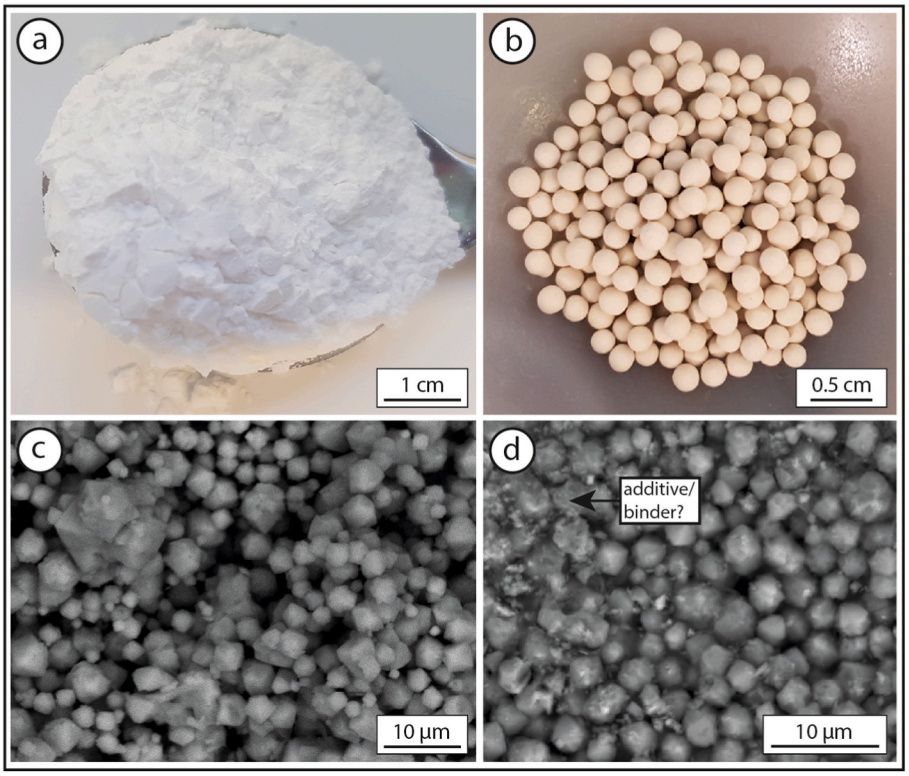

Fig. 1. Pictures of zeolite 13X samples: a) Zeolite 13X powder and b) Zeolite 13X beads. c) Back-scattered electron (BSE) image of zeolite 13X powder. Euhedral cubic crystals of 1–30 µm grain size are homogeneously distributed. d) BSE image of zeolite 13X beads shows subhedral to euhedral crystals, very similar to (c). Left part in the picture shows a rough surface, probably the binder/additive for the synthesis of the beads.

however, changes for the DTA-DSC analyses with previously calcined zeolite 13X powder: The endothermic peaks occur then at 202 and 225 °C, with beginning mass loss at 152–170 °C, respectively (Fig. 4). The total mass loss varies between −9.1 and −11.3%. The changes in temperature and total mass loss indicate that calcination leads to stabilization of the crystal structure at higher temperatures and indicates a reduced sorption affinity to volatiles (e.g. water, CO_2 or N_2) after the first calcination. This is consistent with sintering effects observed during calcination that affect Si–OH bonds [51].

3.2. Kinetics and sorption capacity

Batch experiments have been used to evaluate the relation between stirring time, i.e. contact time, and Li loading (Fig. 5a). A relatively constant sorption capacity of 12 ± 1 mg/g Li for zeolite 13X powder is already reached within the first minute (Fig. 5a), indicating that Li sorption kinetics are extremely fast. The kinetic properties of zeolite 13X beads, however, are much slower compared to the powder samples. No Li sorption occurs within the first minute. Instead, an increase is observed within the first 9 h with a local minimum between 15 and 30 min (Fig. 5a). Equilibrium is reached after 9 h contact time using the zeolite 13X beads with a plateau at ~8 ± 2 mg/g (Fig. 5a). The longer time needed to reach equilibrium is explained by the correlation of Li diffusivity and grain size. Among various grain sizes, compositional differences between the beads and the powder (Fig. 1, Tables 1 and 2) contribute to the variation in sorption properties, known for ion exchange of Ca^{2+}, Sr^{2+}, and Ba^{2+} with Na^{+} in zeolite [52]. An equilibration time of 9 h, however, is not unusual and comparable to sorbents like Mn-oxide and Al-hydroxide [53,54].

Sorption isotherm data allow to determine the maximum sorption capacity (Q_{max}) (Fig. 5b). The shape of the sorption isotherms is mostly concave and can be described by the term L isotherm [55]. The isotherm displaying the Li sorption to the beads reaches a plateau that is not reached for the powder at the highest Li concentrations tested (Fig. 5b). A sharp increase in sorption capacity can be observed at low initial Li concentrations up to 150 mg/L (Fig. 5b). At higher Li concentrations, beads reach Q_{max} of 8.6 mg/g at 60 °C. The decreased Q_{max} of beads compared to powder highlights the relevance of grain size and compositional differences. Increasing initial Li concentrations are not influencing the sorption capacity (Fig. 5b), indicating that equilibrium is reached already in the experiments with beads. The powder reaches a higher Q_{max} value, e.g. 20.3 mg/g, at an initial Li concentration of 500 mg/L in the fluid at 40 °C (Fig. 5b). This sorption isotherm, however, shows non-equilibrium by not reaching an asymptotic plateau [48], indicating that higher loads may be achieved when increasing the initial Li-concentration or the sorbent mass. An inflexion point occurs at an initial Li concentration of 150 mg/L for both zeolite 13X forms, presumably due to more than one underlying sorption process. Similar inflexion points are visible in sorption isotherms in the literature, e.g. for F^{-} sorption to clinoptilolite [56].

3.3. Influence of temperature and pH

The influence of temperature on the Li sorption on zeolite 13X powder has been investigated between 25 and 80 °C. The sorption isotherms for 25, 40, 60 and 80 °C are very similar and only show marginal differences at initial Li concentration higher than 200 mg/L (Fig. 5c). The general shape of the isotherms is concave and can be described as L isotherms [55]. The sorption isotherms obtained at 25 °C and 80 °C show a plateau at Q_{max}, which is less clear for the 40 °C and 60 °C sorption isotherms (Fig. 5c). At 25 °C slightly lower Q_{Li} with maximum sorption of 15.6 mg/g is reached than in the 40, 60 and 80 °C experiments. However, no systematic variations are observed in Q_{Li}, since Q_{max} = 20.3 mg/g is reached at 40 °C whereas Q_{Li} at 60 and 80 °C reach 17.2 and 17.5 mg/g, respectively. A clear relationship between T and Q_{Li} is therefore not recognizable. The highest Q_{Li} is reached at medium

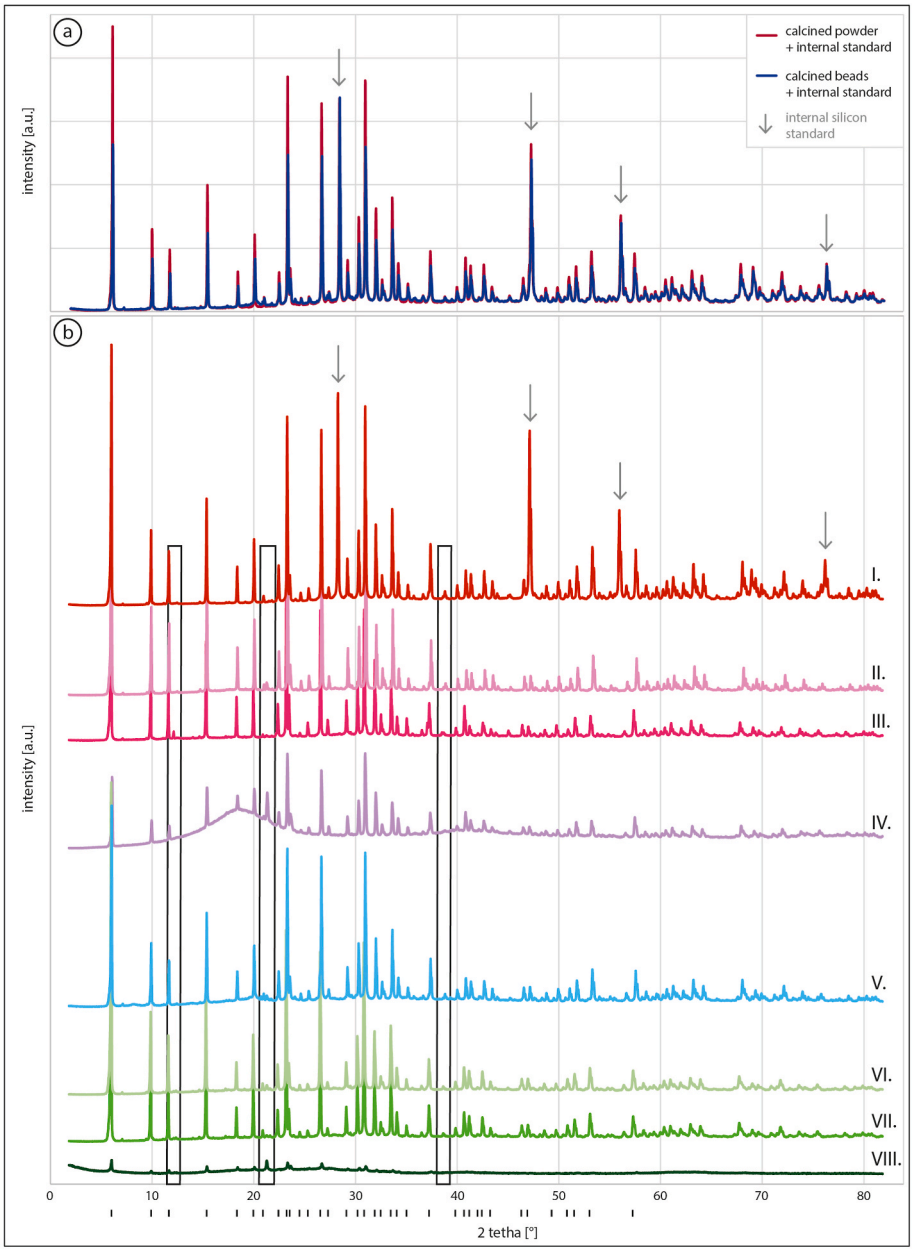

Fig. 2. X-ray diffraction (XRD) patterns of a) calcined zeolite 13X powder (red) and beads (blue) including an internal silicon standard (grey arrows). b) XRD patterns of differently treated samples: I. Li-loaded powder prepared for desorption experiments analysed with internal standard, II. Li-loaded powder unbuffered at 60 °C, III. Li- and K-loaded powder pH adjusted to 6 using KH_2PO_4 at 60 °C, IV. Ca-, K-, Sr-, Mn-, Ba and As-loaded powder from experiments with natural geothermal brine from Bruchsal (Germany) pH adjusted using HCl at 60 °C, V. Li-loaded beads unbuffered at 60 °C. The three lowermost patterns show desorption experiments with material from I. using VI. 1 M CH_3COONa, VII. 1 M NaCl and VIII. 0.1 M CH_3COOH solutions. Lines below the data show theoretical signal positions of zeolite X (Na) with a = 24.99 Å.

temperature while lower and higher temperatures result in lower Q_{Li} (Fig. 5c). These results indicate that the temperature dependence of Li sorption to zeolite 13X may be negligible, which differs from literature data [38,57].

The high TDS content in geothermal fluids leads to the necessity of keeping the natural pH value of the brine constant at slightly acidic conditions to avoid scaling [8,58]. To study the influence of pH variation on the sorption characteristics, unbuffered and KH_2PO_4-buffered as well as HCl-adjusted experiments with pure LiCl solution and geothermal brine have been performed. The unbuffered experiments are in the pH range of 6.7–9.9 (Fig. 5a–c). Kinetic data always show a positive correlation between pH value and contact time even when equilibrium has already been reached (Fig. 5a). Changes in pH are independent of Li sorption as the equilibrium Q_{Li} has been reached for the powder within the first minute whereas the pH increase continues. Dealumination of the zeolite increases with increasing contact time (supplementary data). Thereby, Al–OH-complexes are eluted that increase the pH of the solution, Lewis acid sites and framework defects in the zeolite [49,59]. This effect is contrasting for sorption isotherms: During Li sorption, the pH value decreases with increasing Q_{Li} and/or increasing initial Li concentration (Fig. 5b and c). Since zeolite 13X is a Na-exchanged sorbent, it is expected to substitute Na^+ by Li^+ rather than H^+ by Li^+ [36,60]. From other inorganic sorbents, however, a decrease in pH is expected during Li sorption since the main process of Li incorporation is the substitution of protons that are released into the brine and thereby reduce the pH (e.g., Ref. [61]. The decreasing pH can therefore be explained by the substitution of protons with Li.

By buffering the pH to 6, the shape of the isotherms changes drastically and the maximum sorption capacity decreases by 68% to 6.5 mg/g using zeolite 13X powder (Fig. 5d). The sorption isotherms from the buffered experiments do not show a nice concave curve as the unbuffered sorption isotherms. In comparison, the Li load increases more linearly at c(Li) < 150 mg/L (Fig. 5d). Among the decrease in Q_{Li}, a distinct decrease in Q_{Li} followed by a prompt increase (in the following referred to as inflexion point) is observed at 150–200 mg/L initial Li concentration, prevalent for all (25, 40, 60 and 80 °C) isotherms

Table 1
Identified phases by XRD analysis and their relevant crystal lattice parameters.

sample	ref. Fig. 2	identified phase	space group	a [Å]	V [Å^3]
Initial calcined zeolite 13X powder	a	Si Silicon, internal standard			
		zeolite X, (Na)	Fd-3m	24.9786 (4)	15584.8 (8)
Initial calcined zeolite 13X beads	a	Si Silicon, internal standard			
		zeolite X, (Na)	Fd-3m	24.9805 (5)	15588.5 (9)
		muscovite clay minerals	C2/c		
Li-loaded powder	b, I	Si Silicon, internal standard			
		zeolite X, (Li)	Fd-3m	24.8771 (3)	15395.7 (6)
Li-loaded powder, unbuffered, 60 °C	b, II	zeolite X, (Li)	Fd-3m	24.8470 (4)	15339.8 (8)
Li–K-loaded powder, pH = 6 using KH_2PO_4, 60 °C	b, III	zeolite X, (Li)	Fd-3m	24.8432 (3)	15332.9 (6)
Ca–K–Sr–Mn–Ba–As-loaded powder, geothermal brine, pH = 5 using HCl, 60 °C	b, IV	zeolite X, (Ca)	Fd-3m	24.945 (3)	15522 (2)
		unnamed K–Na–Mg-silicate	P6/mcc		
Li-loaded beads, unbuffered, 60 °C	b, V	zeolite X, (Li)	Fd-3m	24.8828 (5)	15406.3 (9)
Recycled 13X powder using 1 M CH_3COONa	b, VI	zeolite X, (Na)	Fd-3m	24.9739 (5)	15576.1 (9)
Recycled 13X powder using 1 M NaCl	b, VII	zeolite X, (Na)	Fd-3m	24.9704 (5)	15569.6 (9)
Recycled 13X powder using 0.1 M CH_3COOH	b, VIII	zeolite X, (Na)	Fd-3m	24.844 (2)	15334 (3)
		not specified SiO_2-phase	–		

(Fig. 5d). From these experiments, however, we cannot deduce that only the pH reduction is responsible for the reduction in sorption capacity and change of the shape of the isotherm since KH_2PO_4 was used as a buffering agent and K^+ is known to be a competitor for Li^+ [62]. Note that inflexion points are observed in buffered and unbuffered sorption isotherms at all investigated temperatures (Fig. 5b,d,e) but are prominent at 60 and 80 °C for all samples (Fig. 5e). Combined changes in pH and sorption capacity point towards different Li sorption processes. The point of zero charge (pzc) of zeolite 13X is 10.2–11.0 [32,40]. Although zeolite 13X mainly substitutes Na^+ with Li^+, it cannot be excluded that H^+ and Li^+ also exchange in a separate process. The abrupt decrease in pH at c(Li) ~ 100 mg/L (Fig. 5e) may indicate that H^+ substitution with Li^+ becomes a relevant process at high Li concentrations. At high pH, the surface is less protonated [56] and physisorption may be significant, which might be the reason that $Q_{max,Li}$ is distinctly decreased at more acidic pH (Fig. 5c and d). Our data and the occurrence of inflexion points indicate concentration-dependent sorption processes (e.g. physisorption and ion exchange) and different Li sorption sites in the zeolite 13X framework like H^+ and Na^+ sites.

3.4. Influence of competing ions

Using KH_2PO_4-buffered synthetic LiCl solutions, the zeolites show desorption of Na while K and Li are sorbed (Fig. 5f). The maximum amount of K sorbed to zeolite 13X is 1.86 mmol/g whereas Li only reaches 0.82 mmol/g. Sorption of P is within analytical uncertainty and therefore negligible. The major sorption process is the cation exchange of Na^+ with alkaline ions, accompanied by a decrease in pH (Fig. 5f). Calculation of mass balance between Na release and Li + K (+P) uptake reveals that 35% excess Na is released into the fluid with 3.56 mmol/g. Whereas an inflexion point in the Li sorption isotherms is visible, no inflexion point is observed for K and Na (Fig. 5f). Therefore, Li sorption is probably controlled by at least two major sorption processes whereas sorption and desorption of other alkali ions result from a single process or presumably affects other sites in the zeolite framework.

To study the implication for DLE from geothermal brines, we investigated the sorption characteristics of Li using natural brine from the Bruchsal power plant, located in the Upper Rhine Valley in southwestern Germany (Table 3). The high TDS content, accompanied by high ionic activity and the presence of competing ions influence the sorption properties [38]. Lithium sorption for zeolite in contact with the brine is within analytical uncertainty and not detectable for any contact time used (Fig. 6). Sodium data shows mostly desorption with Q_{Na} = -14.7 – 1.4 mmol/g (-339 mg/g – 33 mg/g; Fig. 6) and reach more negative values at longer contact time. No equilibrium is reached for Na in these experiments. Other ions, like Ca, K, Sr, Ba and Mn are sorbed to zeolite 13X powder. They reach an intermediate maximum and loads decrease afterwards for contact times longer than 1000 min (Fig. 6). Calcium reaches highest loads with values up to 1.3 mmol/g (54 mg/g) after 180 min, K after 180 min at 0.5 mmol/g (21.3 mg/g) and Sr at 0.06 mmol/g

Table 2
Sample composition derived from XRF analysis.

Sample	SiO_2 [wt%]	TiO_2 [wt%]	Al_2O_3 [wt%]	Fe_2O_3 [wt%]	MgO [wt%]	CaO [wt%]	MnO [wt%]	Na_2O [wt%]	K_2O [wt%]	P_2O_5 [wt%]	LOI [wt %]	sum [wt %]	Si/Al ratio
13X powder	41.1	0.02	29.41	0.18	0.26	0.26	0.00	16.49	0.20	0.01	11.10	99.02	1.2
13X powder duplicate	40.8	0.02	29.26	0.21	0.26	0.27	0.00	16.29	0.31	0.01	11.19	98.64	1.2
13X powder triplicate	40.6	0.02	29.22	0.22	0.26	0.28	0.00	16.39	0.19	0.01	11.19	98.42	1.2
Mean	40.9	0.02	29.30	0.20	0.26	0.27	0.00	16.39	0.23	0.01	11.16	98.69	1.2
Standard deviation	0.13	0.00	0.03	0.02	0.00	0.01	0.00	0.07	0.06	0.00	0.04	–	–
13X beads	44.2	0.19	25.49	1.30	2.41	0.62	0.04	13.39	0.32	0.05	11.11	98.01	1.5
13X beads duplicate	43.8	0.19	25.30	1.29	2.39	0.62	0.04	13.24	0.31	0.05	11.18	98.39	1.5
13X beads triplicate	44.1	0.19	25.44	1.28	2.40	0.63	0.04	13.28	0.36	0.05	10.05	98.87	1.5
Mean	44.0	0.19	25.41	1.29	2.40	0.62	0.04	13.30	0.33	0.05	10.78	98.42	1.5
Standard deviation	0.11	0.00	0.06	0.00	0.00	0.01	0.00	0.01	0.02	0.00	0.52	–	–

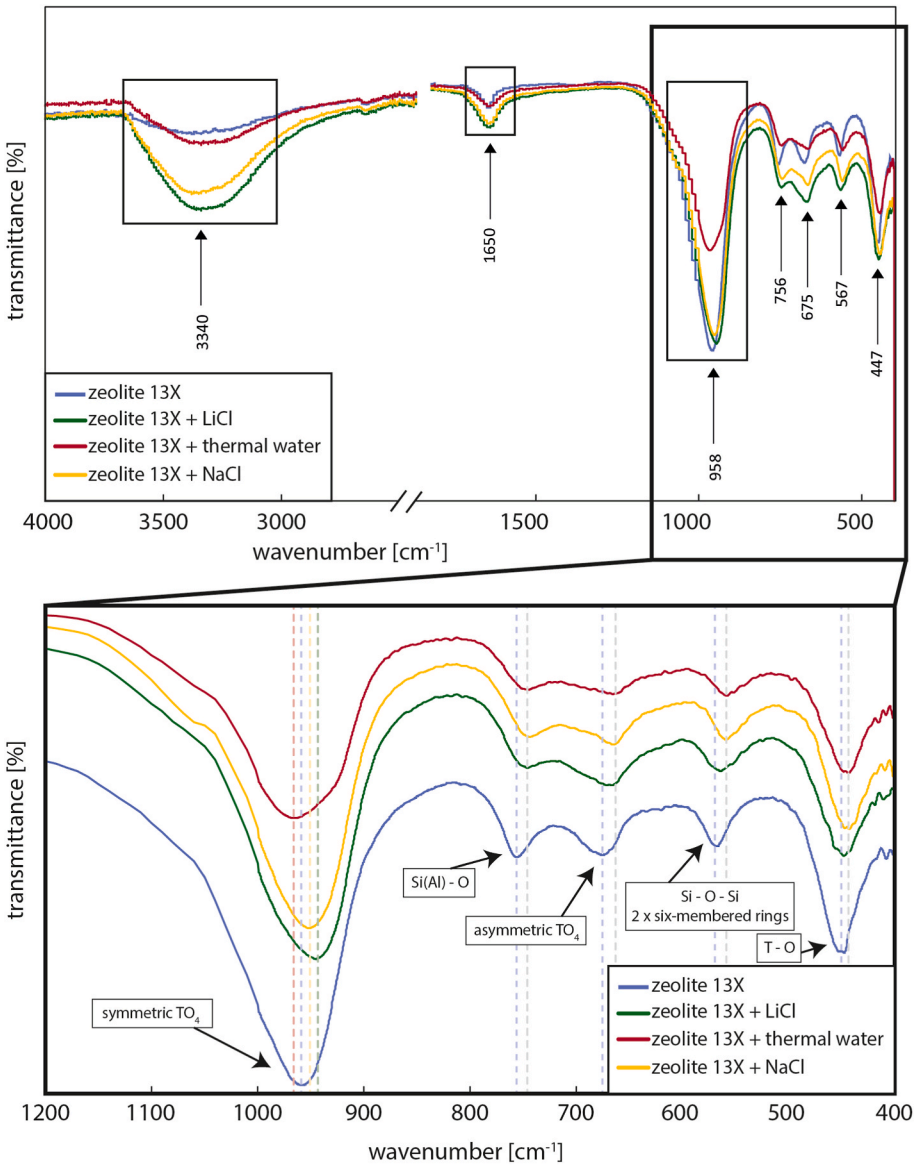

Fig. 3. FT-IR-ATR spectra of zeolite 13X powder. Calcined zeolite 13X sample (blue), Li-loaded zeolite 13X (green), sample mainly loaded with competing ions (red) and Li-desorbed zeolite 13X (yellow). The lower graph shows a detailed sample-characteristic spectrum between 400 and 1200 cm^{-1}. Shifting of the bands, assigned to sample treatment, is highlighted by dashed lines.

(5.4 mg/g) after 45 min. The equilibria for Ba and Mn are reached after 5 min with $Q_{Ba} = 0.003$ mmol/g (0.4 mg/g) and $Q_{Mn} = 0.004$ mmol/g (0.2 mg/g). Calcium, K, Sr, Ba and Mn show a local minimum in the load between 45 and 120 min contact time. Sorption of As is significant but variations are within analytical uncertainty (Fig. 6). The maximum load of As is 0.001 mmol/g (0.05 mg/g) after 15 min.

The experiments with geothermal brine reveal a limited Li selectivity. Sodium is released to the brine during the sorption of competing ions (Ca, K, Sr, Ba, Mn, and As). The distribution coefficients (K_d) have been determined according to the equation $K_d = \frac{Q_{Equ}}{C_{Equ}}$ [48,63,64]. The K_d values have only been determined for elements that sorbed significantly to the samples and are prevalent in natural geothermal brines (Table 3). The K_d values (Table 4) indicate the selectivity order K > Ca > Mn > As > Sr > Ba. This order is inconsistent with literature data, where selectivity for natural zeolite is given as Ba > Sr > Ca > K > Na > Li [28,65]. It has been observed in the experiments with the brine that competing ions instead of Li^+ are sorbed to zeolite 13X (Fig. 6). Generally, materials with higher framework charge capture smaller monovalent cations preferentially [62]. According to Ref. [66]; the pzc decreases due to the presence of divalent cations, indicating that Ca^{2+} presence favours a more negative surface charge of zeolite 13X and, therefore, increases Li sorption capability. By Ca^{2+} sorption, however, the sorption sites for Li^+ might already be occupied. Monovalent cations have lower hydration free energies than divalent ions (Table 5). It is therefore likely that sorption of Li^+, Na^+ and K^+ is controlled by their hydrated radii whereas divalent cations have higher hydration free energies (Table 5) and are therefore more likely present as ionic species. The hydrated radii of monovalent cations and ionic radii of divalent cations in geothermal brine, e.g. 3.4 Å for hydrated Li^+ and 1.14 Å for Ca^{2+} (Table 5), reveal significant differences that could be the explanation for the observed preferred Ca^{2+} sorption. The higher ionic potential of Ca^{2+} (1.754) compared to Li^+ (1.370 ionic and 0.294 hydrated) also supports this interpretation (Table 5). For the hydrated Li^+ ion, only sites SII and SIII are potential sorption sites as it cannot access the sodalite cages through the 6-membered ring windows that are only 2.2 Å in diameter [20].

For clarification of the role of Ca^{2+}-sorption, experiments with synthetic brine (Table 3) have been performed to check whether Li^+ is sorbed to zeolite 13X at Ca^{2+} absence. The tests confirmed that the

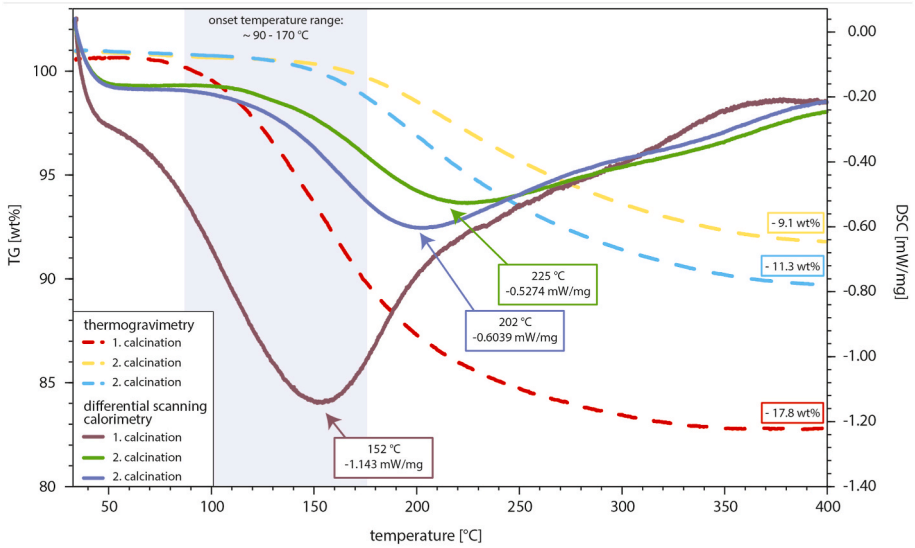

Fig. 4. DTA-DSC results of zeolite 13X powder show the effects of calcination on thermal gravimetry (TG wt%) and differential scanning calorimetry (DSC mW/mg). Red and brown: first calcination. Yellow, light blue, green and dark blue show the second calcination.

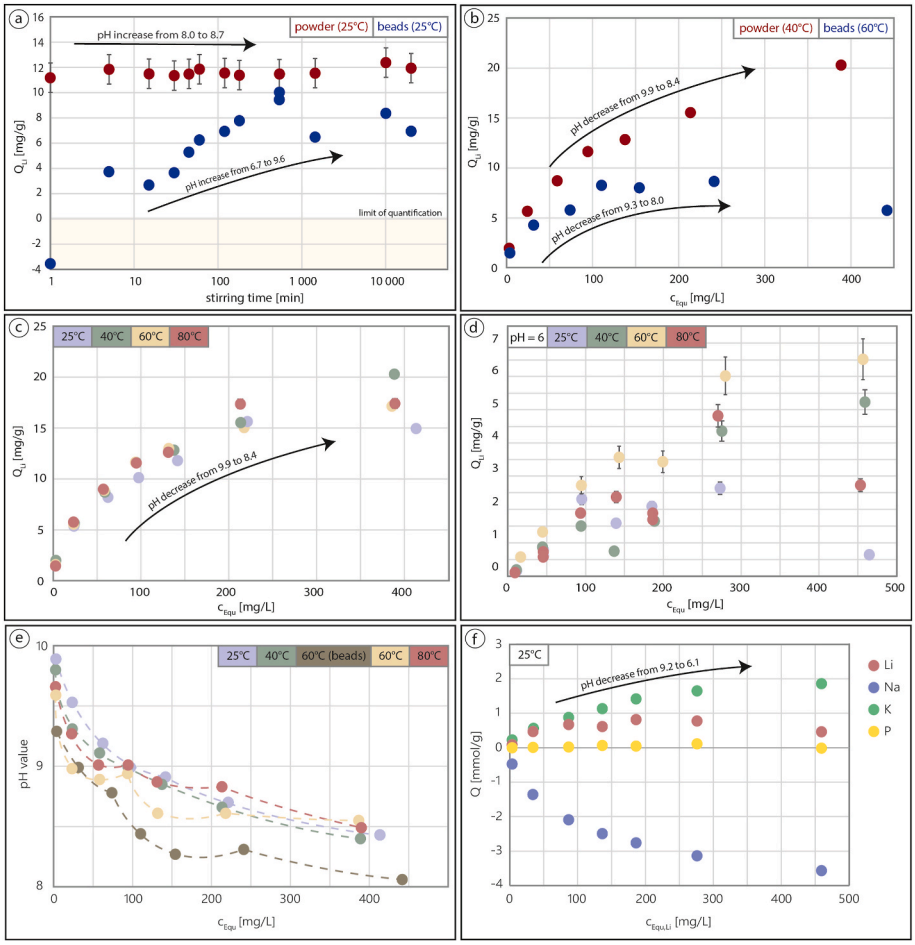

Fig. 5. Sorption kinetics and (non-equilibrium) sorption isotherms for Li-sorption to zeolite 13X powder and beads. If no error bar is visible, the uncertainty is smaller than the symbol. Arrows are labelled with pH values. a) Sorption kinetics at 25 °C, b) maximum sorption capacity in mg/g reached in the batch experiments at 40 °C and 60 °C, c) temperature dependency of Li sorption on zeolite 13X powder at T = 25, 40, 60 and 80 °C. The black arrow displays the pH variations. d) Influence of lowered pH (adjusted using KH_2PO_4 buffer) on sorption isotherms of 13X powder at T = 25, 40, 60 and 80 °C. e) variability of pH values with residual Li concentration in mg/L and f) sorption of Li, Na, K and P in mmol/g at 25 °C, showing sorption of K and Li at the excess release of Na.

major competing ions are Ca^{2+}, K^{+} and Sr^{2+}, reaching maximum loads of 0.88 mmol/g, 0.43 mmol/g and 0.11 mmol/g (supplementary data), respectively. The high sorption capacity for K^{+} and Sr^{2+} is only reached at Ca^{2+} absence, indicating that the high Ca^{2+} concentrations in the geothermal brine and its preferred sorption to zeolite 13X is disadvantageous for the direct extraction of other ions. In any experiment with synthetic geothermal brine, independent from Ca^{2+} concentration, Al^{3+} (−0.16 mmol/g) and Si^{4+} (−0.24 mmol/g) elution occur. This is attributed to the low pH of the synthetic geothermal brines (pH = 2, Bruchsal; pH = 5 Neustadt-Glewe) as well as limited sorbent stability

Table 3
Fluid composition of natural, Fe-depleted and synthetic geothermal brine from Bruchsal and Neustadt-Glewe (Germany). Aluminum and phosphate data are below the detection limit (b.d.l.).

Analyte [mg/L]	Geothermal brine Bruchsal[a] (Germany)	Geothermal brine Bruchsal (Germany)	Synthetic geothermal brine Bruchsal	Synthetic geothermal brine Bruchsal (without Ca)	Geothermal brine Neustadt-Glewe[a] (Germany)	Synthetic geothermal brine Neustadt-Glewe	Synthetic geothermal brine Neustadt-Glewe (without Ca)
Li	155	155	153	152	11.4	9.8	10.1
Na	35606	35943	34557	34479	74700	69202	70183
K	3241	3133	3529	3277	831	847	846
Rb	22.7	<0.4	–	–	1.3	–	–
Mg	347	362	365	370	1340	1368	1376
Ca	7437	7399	7761	1.18	8300	8417	1.22
Sr	354	380	375	368	501	501	514
Ba	8.6	9.0	9.3	11.3	5.2	9.7	2.5
SiO_2	90.4	58.2	<0.01	<0.01	31.9	<0.01	<0.01
Pb	3.6	<0.008	8.0	4.0	0.4	3.4	1.4
As	7.8	4.0	8.9	9.0	<0.0001	<0.0006	<0.0006
Mn	24.3	24.4	24.3	23.6	12.4	12.0	13.0
Fe	44.3	<0.001	<0.002	<0.002	76.9	<0.002	<0.002
Cu	0.02	3.2	–	–	<0.0001	–	–
Zn	15.0	13.7	15.9	14.3	3.0	3.0	4.3

- not analysed.
< below detection limit.
[a] No experiments performed. Data are given for comparison.

during ion exchange. The results are inconclusive for Li^+ due to the necessary strong dilution of highly saline fluids for analysis, causing a higher analytical uncertainty. Both tests with synthetic Bruchsal and Neustadt-Glewe geothermal brine, however, indicate that Li^+ sorption potentially occurs at Ca^{2+} absence, although it varies within analytical uncertainty. This shows that, in any case, the amount of sorption is insignificant and not directly applicable to DLE.

3.5. Desorption

For Li recovery from the powder, different solutions have been tested with a focus on desorption agents that can donate protons or monovalent cations, such as Milli-Q® water, NaCl, HCl, CH_3COOH and CH_3COONa solution (Fig. 7). Lithium-free zeolite 13X powder initially contains 5.2 mmol/g Na and 3.2 mmol/g Al. The Si content could not be determined by acid digestion since SiF_4 evaporates [75]. The zeolite 13X powder sorbs 1.7 mmol/g Li and releases 2.3 mmol/g Na into the fluid phase whereas other constituents do not change. Desorption with Milli-Q® water does not affect the sorbent but using any other tested desorption solutions of different concentrations, 1.6–1.7 mmol/g Li are eluted (Fig. 7), corresponding to a desorption efficiency of 94–100%. Sodium values scatter due to dilution effects during analysis. Sodium-bearing desorption solutions, except for 2 M and 3 M NaCl, show that Na is always sorbed to zeolite 13X when Li is desorbed (Fig. 7a), indicating ion exchange of Na^+ and Li^+. The unit-cell parameters are restored to the initial $a = 24.98$ Å indicating that the crystal structure is not affected by the treatment (Table 1). Discrepancies in the data of 2 M and 3 M NaCl solutions reveal analytical limitations because of necessarily high dilution factors of 500. Although analytical uncertainty seems to account for 0.5 mmol/g, the real uncertainty for the 3 M duplicate is 6 mmol/L for these high Na concentrations which equals 100% uncertainty for the Na load. When using acids, 100% Li are desorbed but Na and Al are released at 2.8–3.3 mmol/g and 2.6–5.4 mmol/g, respectively. Traces of Ca and Mn (≤0.05 mmol/g) are desorbed and Si is dissolved at 3.2–6.2 mmol/g (Fig. 7c and d). During the desorption of Ca, Mn and Al higher concentrations than the initial composition of zeolite 13X powder were measured, indicating that the digestion of the pure zeolite 13X powder was potentially incomplete.

Lithium is successfully desorbed with any tested solution. When using acids, however, Al^{3+} and Si^{4+} have been eluted additionally (Fig. 7c and d). The unit-cell parameters are not restored at the initial a ~24.98 Å but remain at $a = 24.844(2)$ Å indicating that the framework is affected by the acid treatment (Table 1). Elution of Al^{3+} and Si^{4+} from the framework $(Al,Si)O_4$-tetrahedra indicates dissolution of the sorbent itself. The sorbent's dissolution thereby releases Li^+ into the solution rather than exclusively eluting Li^+ by simple ion exchange. This demonstrates that zeolite 13X is not acid resistant and that the use of acids should be avoided for any raw material desorption from zeolite 13X. The use of Na^+-donating solutions, in contrast, is favourable, reaching desorption rates of 94–100% at chemical stability of the sorbent (Fig. 7a and b). The best results have been achieved using 1 M NaCl and 1 M CH_3COONa solution due to complete Li recovery at best chemical stability and lowest investment of chemicals.

3.6. Structural implications

Shifts of the bands in the FT-IR-ATR spectra are observed depending on sample treatment. Analyses have been performed for Li-loaded zeolite 13X ("zeolite 13X + LiCl"; Fig. 3), zeolite 13X that sorbed competing ions ("zeolite 13X + thermal water"; Fig. 3), and samples that previously sorbed Li which was desorbed by using NaCl solution ("zeolite 13X + NaCl"). All treated zeolites show shift of the bands at 447 cm^{-1}, 567 cm^{-1}, 675 cm^{-1} and 756 cm^{-1} to 444 cm^{-1}, 558 cm^{-1}, 665 cm^{-1} and 744 cm^{-1}, respectively. The shift of the symmetric vibration of the $(Al,Si)O_4$ bond at 958 cm^{-1} is different for each sample. Compared to the untreated zeolite 13X powder, zeolite 13X + LiCl and zeolite 13X + NaCl samples are shifted to lower wave numbers (945 and 951 cm^{-1}), whereas the zeolite 13X + thermal water sample shifted to higher wave numbers of 966 cm^{-1} (Fig. 3). The shift of zeolite 13X + LiCl to lower wavenumbers compared to the untreated zeolite 13X sample is attributed to dealumination of framework Al during sorption of Li causing lattice defects and potentially the relaxation of the unit cell [76,77]. By desorption of Li from zeolite 13X using a NaCl solution (zeolite 13X + NaCl), the observations indicate that the changes in the crystal lattice are not fully reversible and therefore the zeolite 13X + NaCl spectrum shows back-shifting to higher wavenumbers but not to the initial wavenumber as no re-substitution of Al takes place [76]. Presumably, we additionally observe a conditioning effect due to dealumination of framework Al when using NaCl as a desorption agent without re-substitution during the sorption of Li [76,77]. However, at the long-range scale, the XRD data show that the unit-cell parameters are restored indicating the reversibility of the sorption/desorption process. The shift to a higher wavenumber of the 958 cm^{-1} band of zeolite 13X + thermal water is attributed to the sorption of divalent Ca^{2+}, bridging two Li^+ exchange sites in proximity, resulting in stiffer (Al,Si)–O–Ca–O-(Al,Si) bonds compared to (Al,Si)–O–Li or (Al,Si)–O–Na bonds

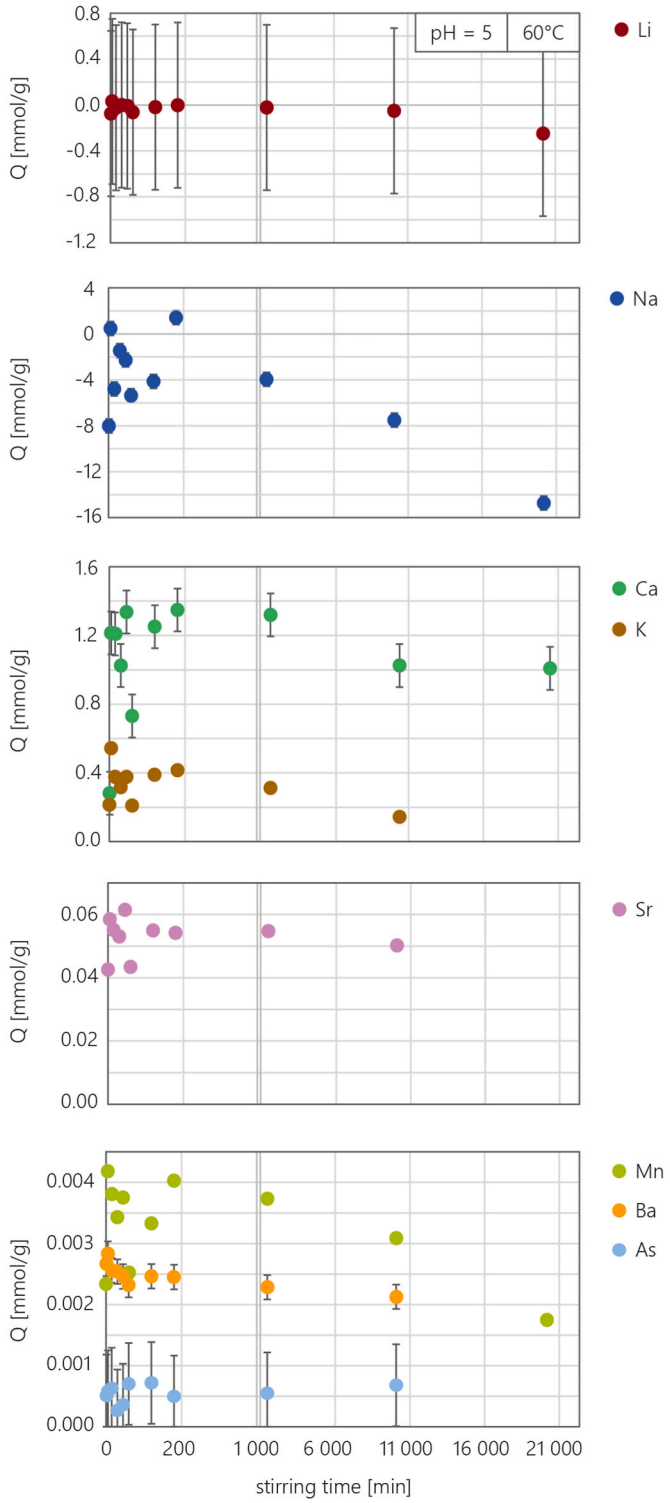

Fig. 6. Kinetic data from batch sorption experiments with zeolite 13X powder and geothermal brine at 60 °C and pH value adjusted to 5. From top to bottom: Li, Na, Ca, K, Sr, Mn, Ba and As load in mmol/g.

(Fig. 5f) [78–80].

The sorption of Li from pure LiCl solution on both, powder and beads, is confirmed by the formation of zeolite X, (Li) phase accompanied by shrinking unit-cell parameters from initially $a = 24.98$ Å to $a = 24.84–24.88$ Å depending on the reaction conditions (Table 1, Fig. 2bI, II,III,V). In the refined structural model, the sorbed Li resides in the centre of the distorted six-membered rings of zeolite X, i.e. cation site

Table 4
Kd values for competing ions were calculated according to Ref. [48].

Sorbate	K_d value
K^+	46
Ca^{2+}	45
Sr^{2+}	12
Ba^{2+}	2
Mn	26
As	18

SII, formed by $(Si,Al)O_4$ tetrahedra [23]. The maximum theoretically possible Li sorption capacity determined by the Si/Al ratio is not reached for any sample. A reason may be the limited accessibility of sorption sites SI, SI' and SII' for fairly large hydrated Li^+ ions (3.4 Å ionic radius, Table 5) through the 6-membered ring windows of 2.2 Å diameter [20]. Minor changes also occur when adding competing ions. Interaction with geothermal brine, however, results structurally in the Ca-exchanged zeolite 13X form, as well as an additional hexagonal phase, i.e. a not further specified K–Na–Mg-silicate, was identified (Table 1). Desorption with a Na-donating solution, like 1 M CH_3COONa or NaCl, is structurally fully reversible (Table 1, Fig. 2bVI,VII), although a conditioning effect already discussed from FT-IR-ATR data is indicated. Acid treatment, however, significantly affects the XRD pattern (Fig. 2bVIII). The partial dissolution of zeolite 13X in 0.1 M CH_3COOH shows few reflexes that can be assigned to a not specified SiO_2 phase and zeolite X, (Na) (Table 1). Comparison of all obtained patterns points out differences in presence and intensity of the reflexes at 12°, 21° and 38–39° 2tetha (Fig. 2b). These reflexes, however, cannot be assigned to a specific phase and presumably represent impurities. A more detailed crystallographic discussion is beyond the scope of this paper.

4. Conclusions

The main conclusions from our study are:

- Zeolite calcination before sorption experiments at 400 °C for 3 h leads to the stabilization of the crystal structure and reduces the sorption affinity to volatiles.
- Lithium sorption from aqueous solution to zeolite takes place under conditions typically occurring in geothermal power plants regarding fast equilibration time (1 min – 9 h), ambient Li concentration (150–200 mg/L), high temperature (60–80 °C) and moderate to slightly acidic pH (5–7).
- Increase in grain size from powder to beads and slight compositional differences reduce the sorption capacity by 58% at 20.3 mg/g to 8.6 mg/g.
- Three different sorption processes are suggested: (1) ion exchange of $Li^+ – Na^+$ is dominant at Li concentrations < ~100–200 mg/L, (2) ion exchange of $H^+ – Na^+$ is dominant at Li concentrations > ~100–200 mg/L, and (3) physisorption is more dominant at high pH.
- Structural investigations confirm the sorption of Li at the centre of the distorted six-membered rings, i.e. cation site SII, of zeolite 13X accompanied by a reduction of the unit cell size.
- The temperature influence at 25–80 °C is negligible whereas pH reduction significantly affects sorption properties and sorbent stability, disqualifying any acid solution for desorption.
- Zeolite 13X is not selective for Li but preferentially sorbs Ca, K, Sr, Ba, Mn and As. Calcium, leading to bridging of Li^+ sorption sites in proximity, is the most challenging competitor due to its high concentration in the geothermal brines tested in this study.
- Desorption using a NaCl or CH_3COONa solution is successful but the dealumination of framework Al during Li sorption is not fully reversible.

Application of zeolites for DLE is nevertheless promising to fluids

Table 5
(Hydrated) ionic radius, mean ion-water nuclear distance, hydration free energy and (hydrated) ionic potential obtained from[1] [67];[2] [68];[3] [69];[4] [70];[5] [71];[6] [72];[7] [73];[8] [74].

Sorbate	Ionic radius [Å]	Hydrated radius [Å]	Mean ion-water nuclear distance [Å]	Hydration free energy [kJ/mol]	Ionic potential[a] [e/Å]	Hydrated ionic potential[a] [e/Å]
Li^+	0.73[8]	3.4[6]	2.080[4]	−515[6]	1.370	0.294
Na^+	1.13[8]	2.99[6]	2.356[4]	−405[6]	0.885	0.334
K^+	1.51[8]	2.75[6]	2.798[4]	−295[6]	0.662	0.364
Ca^{2+}	1.14[8]	4.12[6]	2.422[4]	−1306[6]	1.754	0.485
Sr^{2+}	1.32[8]	4.12[1]	2.640[4]	−1443[3]	1.515	0.485
Ba^{2+}	1.49[8]	4.04[1]	2.965[7]	−1305[3]	1.342	0.495
$Mn^{2+/3+/4+}$	0.80[8]/0.72[8]/0.53[8]	4.38[1]/?/?	2.192[4]/?/?	−1841[3]/-4544[3]/?	2.500/4.167/7.547	0.457/?/?
$As^{3+/5+}$	0.72[8]/0.475[8]	?/?	?/?	?/?	4.167/10.526	–
O^{2-}	1.40[2]	(3.0 OH^-)[1]	?	–	–	–
Cl^-	1.98[5]	3.24[6]	3.187[4]	−355[6]	–	–

?) no value.
[a] Calculated: q/r.

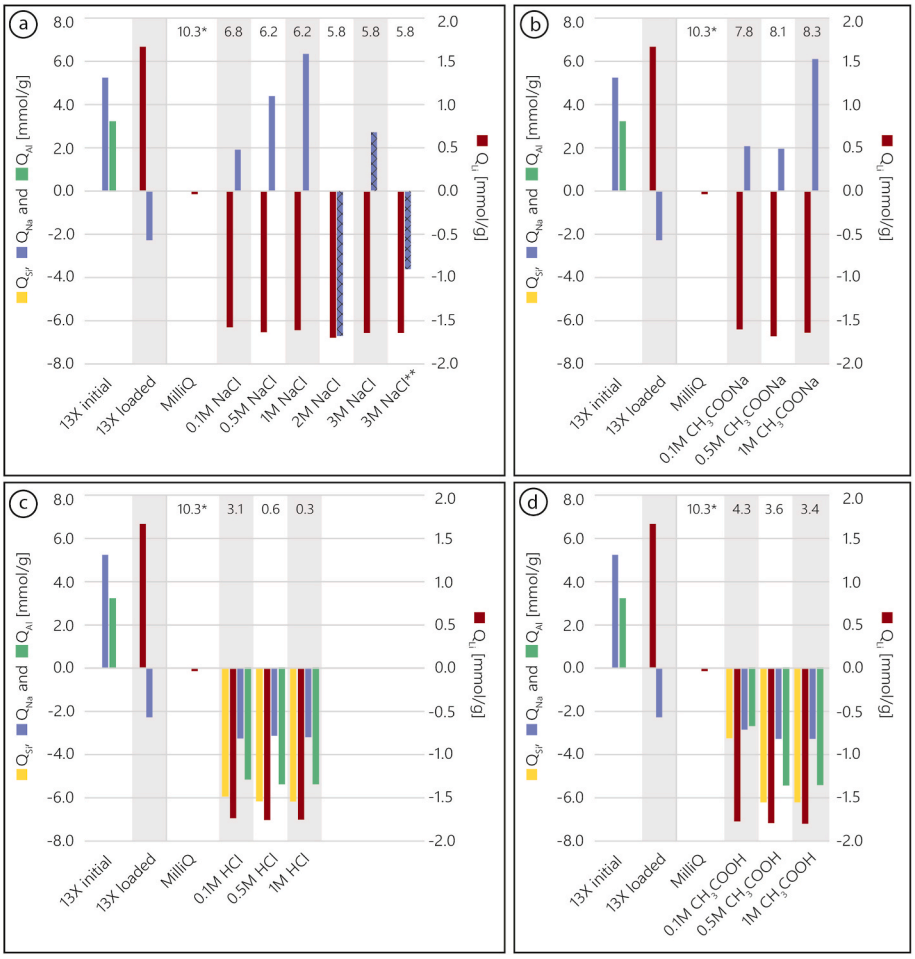

Fig. 7. Desorption of Li and main constituents (Si, Na, Al) of zeolite 13X powder using different solutions of varying concentrations compared to initial and loaded sorbent composition. a) Desorption using different concentrations of NaCl solution. b) Desorption using different concentrations of CH_3COONa solution. c) Desorption using different concentrations of HCl solution. d) Desorption using different concentrations of CH_3COOH solution. Positive values imply sorption to zeolite 13X whereas negative values imply desorption. Silicon could not be analysed for the initial 13X composition due to SiF_4 degassing during sample digestion. Textured bars have high uncertainty of Na data ~6 mmol/g *) pH value after desorption **) analytical duplicate.

with minor concentrations of Ca^{2+} and other competing ions, like battery manufacturing wastewaters, battery recycling or low-saline mine waters. In high saline geothermal applications, the fluid may be pre-purified by removing competitors, mainly Ca^{2+}, before Li extraction using zeolite 13X. After the DLE, the previously removed components could be re-added to the brine before re-injection to the subsurface. Apart from that, the zeolite modification or the use of additives, like anionic polymers that boost the selectivity towards Li, should be investigated to improve the zeolite's selectiveness for Li. The influence of high salinity, pressure, pH and temperature on other zeolitic materials is not fully understood yet and provides a large new research area in raw materials extraction.

CRediT authorship contribution statement

Rebekka Reich: Writing – review & editing, Writing – original draft, Visualization, Methodology, Investigation. **Rosa Micaela Danisi:** Writing – original draft, Investigation. **Tobias Kluge:** Writing – original draft, Supervision. **Elisabeth Eiche:** Writing – original draft, Supervision, Methodology, Funding acquisition, Conceptualization. **Jochen Kolb:** Writing – original draft, Supervision, Project administration, Funding acquisition, Conceptualization.

Declaration of competing interest

The authors declare that they have no known competing financial interests or personal relationships that could have appeared to influence the work reported in this paper.

Data availability

The data that has been used is confidential.

Acknowledgements

We thank Klemens Slunitschek and Michèle Jungmann for helpful discussions during all stages of this work. Beate Oetzel, Janine Wagner and Chantal Kotschenreuther are gratefully thanked for their assistance and advice during XRD and ICP-OES analyses, respectively. Janine Wagner is also acknowledged for her help with the acid digestion of the sorbents. We thank Kristian Nikoloski for providing the oven for zeolite calcination and for his help with grinding the samples in terms of analytical preparation. Kirsten Drüppel is thanked for her help with the SEM analyses and her contributions during writing and XRD data interpretation. Furthermore, Laura Spitzmüller is gratefully acknowledged for performing the FT-IR-ATR analysis and data discussion. The authors additionally thank Andrea Seibt for the performance of experiments with synthetic geothermal brine. We thank Editor Eder Claudio Lima and three anonymous reviewers for their comments that helped to significantly improve the quality of this study. This research is part of the project “UnLimited”, which is funded by the German Federal Ministry for Economic Affairs and Climate Action under Grant O3EE4023D.

Appendix A. Supplementary data

Supplementary data to this article can be found online at https://doi.org/10.1016/j.micromeso.2023.112623.

References

[1] A.J. Whitworth, et al., Review on advances in mineral processing technologies suitable for critical metal recovery from mining and processing wastes, Cleaner Engineering and Technology (2022), 100451.
[2] H. Ambrose, A. Kendall, Understanding the future of lithium: Part 1, resource model, J. Ind. Ecol. 24 (1) (2020) 80–89.
[3] US Geological Survey, Mineral Commodity Summaries: Lithium, 2022.
[4] M. Schmidt, Rohstoffrisikobewertung - Lithium. Rohstoffinformationen 54. Deutsche Rohstoffagentur (DERA) der Bundesanstalt für Geowissenschaften und Rohstoffe (BGR), 2023, p. 81. Berlin.
[5] S. Ziemann, et al., Modeling the potential impact of lithium recycling from EV batteries on lithium demand: a dynamic MFA approach, Resour. Conserv. Recycl. 133 (2018) 76–85.
[6] C. Xu, et al., Future material demand for automotive lithium-based batteries, Communications Materials 1 (1) (2020) 1–10.
[7] S. Ventura, et al., Selective Recovery of Metals from Geothermal Brines, SRI International, Menlo Park, CA (United States), 2016.
[8] R. Reich, et al., Lithium extraction techniques and the application potential of different sorbents for lithium recovery from brines, Miner. Process. Extr. Metall. Rev. (2022) 1–20.
[9] X. Xu, et al., Extraction of lithium with functionalized lithium ion-sieves, Prog. Mater. Sci. 84 (2016) 276–313.
[10] G. Neupane, D. Wendt, Assessment of mineral resources in geothermal brines in the US, in: Proceedings of the 42nd Workshop on Geothermal Reservoir Engineering, Stanford University, Stanford, CA, USA, 2017.
[11] J. Carter, F. McCawley, Corrosion tests in brine and steam from the Salton sea KGRA, J. Mater. Energy Syst. 3 (4) (1982) 30–38.
[12] A. Maimoni, Minerals recovery from Salton Sea geothermal brines: a literature review and proposed cementation process, Geothermics 11 (4) (1982) 239–258.
[13] L. Schultze, D. Bauer, "Comparison of methods for recovering metal values from Salton Sea KGRA brines.", Trans.-Geotherm. Resour. Counc. 6 (1982). United States).
[14] M. Al Radi, et al., Recent progress, economic potential, and environmental benefits of mineral recovery geothermal brine treatment systems, Arabian J. Geosci. 15 (9) (2022) 832.
[15] V. Lundaev, et al., Material extraction potential of desalination brines: a technical and economic evaluation of brines as a possible new material source, Miner. Eng. 185 (2022), 107652.
[16] M.A. McKibben, et al., Lithium and other geothermal mineral and energy resources beneath the Salton Sea, Crisis at the Salton Sea: Res. Gaps and Opportun. (2021) 107–122.
[17] J. Pérez Pariente, M. Martínez Sánchez, Zeolites and Ordered Porous Solids: Fundamentals and applications.", 2011.
[18] S. Obaid, et al., Heavy metal ions removal from waste water bythe natural zeolites, Mater. Today: Proc. 5 (9) (2018) 17930–17934.
[19] H. Robson, Verified Synthesis of Zeolitic Materials, Gulf Professional Publishing, 2001.
[20] A. Habrowska, E. Popiel, Positron annihilation in zeolite 13X, J. Appl. Phys. 62 (6) (1987) 2419–2423.
[21] Structure Commission of the International Zeolite Association, Database of Zeolite Structures, I.-S, 2017, p. 2021. from, https://europe.iza-structure.org/IZA-SC/ftc_table.php.
[22] L. Puppe, Zeolithe–Eigenschaften und technische Anwendungen, Chem. Unserer Zeit 20 (4) (1986) 117–127.
[23] H. Herden, et al., Location of Li-ions in synthetic zeolites X and Y, Zeolites 2 (2) (1982) 131–134.
[24] G. Bergerhoff, et al., "Über die kristallstrukturen des faujasits.", N Jahrb Min. Mh 1958 (1958) 193–200.
[25] L. Andersson, et al., Colloidal processing and CO2-capture performance of hierarchically porous Al2O3-zeolite 13X composites, J. Ceram. Sci. Technol. 3 (1) (2012) 9–16.
[26] C. Zhou, et al., Characteristics and evaluation of synthetic 13X zeolite from Yunnan's natural halloysite, J. Porous Mater. 20 (4) (2013) 587–594.
[27] J.T. Soe, et al., CO2 capture and Ca2+ exchange using Zeolite A and 13X prepared from power plant fly ash, Bull. Kor. Chem. Soc. 37 (4) (2016) 490–493.
[28] C. Colella, Ion exchange equilibria in zeolite minerals, Miner. Deposita 31 (6) (1996) 554–562.
[29] N. Heidari, P. Momeni, Selective adsorption of lithium ions from Urmia Lake onto aluminum hydroxide, Environ. Earth Sci. 76 (16) (2017) 1–8.
[30] F. Qian, et al., Highly lithium adsorption capacities of H1. 6Mn1. 6O4 ion-sieve by ordered array structure, ChemistrySelect 4 (34) (2019) 10157–10163.
[31] S. Wang, et al., Application of citric acid as eluting medium for titanium type lithium ion sieve, Hydrometallurgy 183 (2019) 166–174.
[32] M. Wiśniewska, et al., Investigations of the possibility of lithium acquisition from geothermal water using natural and synthetic zeolites applying poly (acrylic acid), J. Clean. Prod. 195 (2018) 821–830.
[33] T. Belova, Adsorption of heavy metal ions (Cu2+, Ni2+, Co2+ and Fe2+) from aqueous solutions by natural zeolite, Heliyon 5 (9) (2019), e02320.
[34] R. Navarrete-Casas, et al., Study of lithium ion exchange by two synthetic zeolites: kinetics and equilibrium, J. Colloid Interface Sci. 306 (2) (2007) 345–353.
[35] C. Qin, et al., Characteristics of calcium adsorption by Ca-Selectivity zeolite in fixed-pH and in a range of pH, Chem. Eng. J. 156 (3) (2010) 540–545.
[36] R. Accardi, R. Lobo, Accessibility of lithium cations in high-silica zeolites investigated using the NMR paramagnetic shift effect of adsorbed oxygen, Microporous Mesoporous Mater. 40 (1–3) (2000) 25–34.
[37] V. Inglezakis, et al., The effect of competitive cations and anions on ion exchange of heavy metals, Sep. Purif. Technol. 46 (3) (2005) 202–207.
[38] S. Wang, Y. Peng, Natural zeolites as effective adsorbents in water and wastewater treatment, Chem. Eng. J. 156 (1) (2010) 11–24.
[39] J. Lemaire, et al., Lithium recovery from aqueous solution by sorption/desorption, Hydrometallurgy 143 (2014) 1–11.
[40] M. Bautista-Toledo, et al., Influence of the physicochemical properties of inorganic supports on the activity of immobilized bacteria for water denitrification, J. Environ. Manag. 156 (2015) 81–88.
[41] M. Hoyer, et al., Sorption of lithium on bentonite, kaolin and zeolite, Geosciences 5 (2) (2015) 127–140.
[42] S. Cavenati, et al., Adsorption equilibrium of methane, carbon dioxide, and nitrogen on zeolite 13X at high pressures, J. Chem. Eng. Data 49 (4) (2004) 1095–1101.
[43] JCPDS-ICDD, PDF-2 Release 2002, ICDD, Newton Square, Pennsylvania, USA, 2002.
[44] H.M. Rietveld, The rietveld method, Phys. Scripta 89 (9) (2014), 098002.
[45] K.P. Jochum, et al., GeoReM: a new geochemical database for reference materials and isotopic standards, Geostand. Geoanal. Res. 29 (3) (2005) 333–338.
[46] Thermo Fisher Scientific Inc, A Tutorial on Spectral Resolution for the Nicolet iS, FTIR, 2013.
[47] S. Li, et al., Comparison of amorphous, pseudohexagonal and orthorhombic Nb 2 O 5 for high-rate lithium ion insertion, CrystEngComm 18 (14) (2016) 2532–2540.
[48] H.N. Tran, et al., Mistakes and inconsistencies regarding adsorption of contaminants from aqueous solutions: a critical review, Water Res. 120 (2017) 88–116.
[49] K.T. No, et al., Theoretical studies on acidity and site selectivity of cations in faujasite zeolite, J. Phys. Chem. A 85 (14) (1981) 2065–2070.
[50] L. Deng, et al., Effects of calcination and acid treatment on improving benzene adsorption performance of halloysite, Appl. Clay Sci. 181 (2019), 105240.
[51] M. Camblor, et al., Characterization of nanocrystalline zeolite Beta, Microporous Mesoporous Mater. 25 (1–3) (1998) 59–74.
[52] H.S. Sherry, Ion-exchange properties of zeolites. IV. Alkaline earth ion exchange in the synthetic zeolites Linde X and Y, J. Phys. Chem. A 72 (12) (1968) 4086–4094.
[53] H. Jiang, et al., Adsorption of lithium ions on lithium-aluminum hydroxides: equilibrium and kinetics, Can. J. Chem. Eng. 98 (2) (2020) 544–555.
[54] H. Wang, et al., Selective recovery of lithium from geothermal water by EGDE cross-linked spherical CTS/LMO, Chem. Eng. J. 389 (2020), 124410.

[55] G. Limousin, et al., Sorption isotherms: a review on physical bases, modeling and measurement, Appl. Geochem. 22 (2) (2007) 249–275.
[56] P. Ghomashi, et al., Removal of fluoride from wastewater by natural and modified nano clinoptilolite zeolite, J. Water and Environ. Nanotechnol. 5 (3) (2020) 270–282.
[57] F.W. Leavitt, Thermally-driven Ion-Exchange Process for Lithium Recovery, Google Patents, 1997.
[58] F. Haklıdır, T. Balaban, A review of mineral precipitation and effective scale inhibition methods at geothermal power plants in West Anatolia (Turkey), Geothermics 80 (2019) 103–118.
[59] E. Kianfar, A. Mahler, Zeolites: Properties, Applications, Modification and Selectivity, 2020. Chapter. **1**.
[60] M. Akgül, et al., Removal of silver (I) from aqueous solutions with clinoptilolite, Microporous Mesoporous Mater. 94 (1–3) (2006) 99–104.
[61] H. Park, et al., Lithium sorption properties of HMnO in seawater and wastewater, Water Res. 87 (2015) 320–327.
[62] R. Barrer, et al., Comparison of the ion exchange properties of zeolites X and Y, J. Inorg. Nucl. Chem. 31 (8) (1969) 2599–2609.
[63] J. Biggar, M. Cheung, Adsorption of picloram (4-amino-3, 5, 6-trichloropicolinic acid) on panoche, ephrata, and palouse soils: a thermodynamic approach to the adsorption mechanism, Soil Sci. Soc. Am. J. 37 (6) (1973) 863–868.
[64] A.A. Khan, R. Singh, Adsorption thermodynamics of carbofuran on Sn (IV) arsenosilicate in H+, Na+ and Ca2+ forms, Colloid. Surface. 24 (1) (1987) 33–42.
[65] F. Helfferich, Ion Exchange, Courier Corporation, 1995.
[66] R. Panek, et al., Simultaneous removal of Pb2+ and Zn2+ heavy metals using fly ash Na-X zeolite and its carbon Na-X (C) composite, Materials 14 (11) (2021) 2832.
[67] E. Nightingale Jr., Phenomenological theory of ion solvation. Effective radii of hydrated ions, J. Phys. Chem. A 63 (9) (1959) 1381–1387.
[68] R.D. Shannon, Revised effective ionic radii and systematic studies of interatomic distances in halides and chalcogenides, Acta Crystallogr. Sect. A Cryst. Phys. Diffr. Theor. Gen. Crystallogr. 32 (5) (1976) 751–767.
[69] D.W. Smith, Ionic hydration enthalpies, J. Chem. Educ. 54 (9) (1977) 540.
[70] Y. Marcus, Ionic radii in aqueous solutions, Chem. Rev. 88 (8) (1988) 1475–1498.
[71] J. Zhou, et al., Molecular dynamics study on ionic hydration, Fluid Phase Equil. 194 (2002) 257–270.
[72] B. Tansel, Significance of thermodynamic and physical characteristics on permeation of ions during membrane separation: hydrated radius, hydration free energy and viscous effects, Sep. Purif. Technol. 86 (2012) 119–126.
[73] O.C. Gagné, F.C. Hawthorne, Bond-length distributions for ions bonded to oxygen: alkali and alkaline-earth metals, Acta Crystallogr. B: Struct. Sci. Cryst. Eng. Mater. 72 (4) (2016) 602–625.
[74] A.F. Holleman, N. Wiberg, Grundlagen und Hauptgruppenelemente, Walter de Gruyter GmbH & Co KG, 2016.
[75] I.W. Croudace, A possible error source in silicate wet-chemistry caused by insoluble fluorides, Chem. Geol. 31 (1980) 153–155.
[76] J. Datka, et al., Dealumination of zeolite Y by H4EDTA, Catal. Lett. 19 (2) (1993) 159–165.
[77] D.P. Siantar, W.S. Millman, Structural defects and cation exchange capacity in dealuminated Y zeolites, Zeolites 15 (6) (1995) 556–560.
[78] Y.-R. Luo, Comprehensive Handbook of Chemical Bond Energies, CRC press, 2007.
[79] M. Król, et al., Influence of alkali metal cations/type of activator on the structure of alkali-activated fly ash–ATR-FTIR studies, Spectrochim. Acta Mol. Biomol. Spectrosc. 198 (2018) 33–37.
[80] L. Spitzmueller, et al., Selective silica removal in geothermal fluids: implications for applications for geothermal power plant operation and mineral extraction, Geothermics 95 (2021), 102141.

Study III

Delithiation and lithiation of $LiFePO_4$: Implications for direct Li extraction from synthetic solutions and geothermal brines

Rebekka Reich, Elisabeth Eiche & Jochen Kolb

This work has been published in Desalination

published online: 26 Jun 2024

available online:

https://www.sciencedirect.com/science/article/pii/S0011916424005940

DOI: 10.1016/j.desal.2024.117883

Desalination 586 (2024) 117883

Contents lists available at ScienceDirect

Desalination

journal homepage: www.elsevier.com/locate/desal

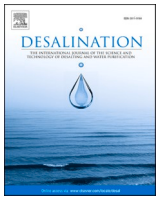

Delithiation and lithiation of $LiFePO_4$: Implications for direct Li extraction from synthetic solutions and geothermal brines

Rebekka Reich *, Elisabeth Eiche, Jochen Kolb

Chair of Geochemistry and Economic Geology, Institute of Applied Geosciences, Karlsruhe Institute of Technology, Adenauerring 20b, 76131 Karlsruhe, Germany
Laboratory for Environmental and Raw Materials Analysis, Institute of Applied Geosciences, Adenauerring 20b, 76131 Karlsruhe, Germany

HIGHLIGHTS

- Chemical and mineralogical characterization of nanocrystalline $LiFePO_4$ powder
- Fast and complete delithiation of $LiFePO_4$ using 0.1 M $Na_2S_2O_8$
- High Li selectivity in geochemically complex fluid compositions
- >99 % Li recovery from geothermal brines

GRAPHICAL ABSTRACT

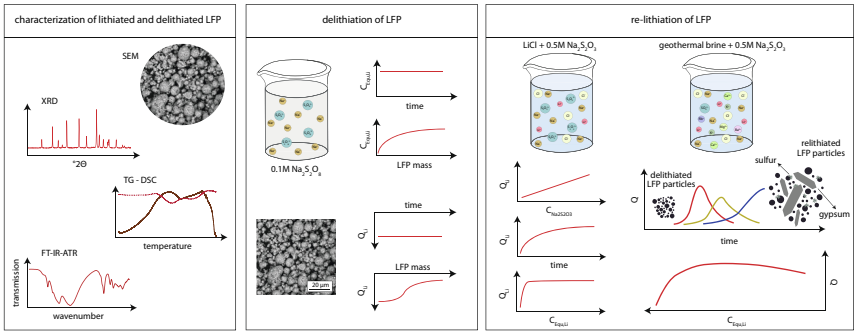

ARTICLE INFO

Keywords:
Lithium iron phosphate
Geothermal brine
Redox additive
Direct lithium extraction (DLE)
Selectivity

ABSTRACT

The demand for Li is and will be increasing in the future, and the development of a direct Li extraction (DLE) technology from unconventional resources, like geothermal brines, may contribute to a resilient supply in the future. This study investigates the deintercalation from and intercalation of Li in $LiFePO_4$ (LFP) at 25–80 °C, near neutral to acidic pH and the effect of high salinity on the Li extraction performance. The (de-)lithiation is a fully reversible redox process between triphylite and heterosite. Lithium is delithiated from LFP using 0.1 M $Na_2S_2O_8$ at 42–43 mg/g. The lithiation kinetics increase with temperature, but show a complex relationship to reducing agent ($Na_2S_2O_3$) concentration. The maximum re-intercalation is achieved in synthetic LiCl + 0.5 M $Na_2S_2O_3$ solution at 39 mg/g, 25 °C and 7 days, whereas 27 mg/g and 1.3 mg/g Li are intercalated to LFP within 3–4 h in experiments with Bruchsal and synthetic Neustadt-Glewe geothermal brines at 60 °C, respectively. At optimal parameters, >99 % Li are recovered from both geothermal brines in laboratory experiments. This shows that LFP can be used for DLE from geothermal brines under specific conditions in a purely chemical process.

* Corresponding author at: Karlsruhe Institute of Technology, Adenauerring 20b, Gebäude 50.40, 76131 Karlsruhe, Germany.
E-mail address: rebekka.reich@kit.edu (R. Reich).

https://doi.org/10.1016/j.desal.2024.117883
Received 25 April 2024; Received in revised form 21 June 2024; Accepted 25 June 2024
Available online 26 June 2024

1. Introduction

Lithium iron phosphate (LFP) is widely used as cathode material in Li-ion batteries in the form of triphylite [1]. LFP batteries are claimed to be eco-friendly, non-toxic, cheap and fulfil higher safety standards than batteries with comparable cathode materials, like $LiCoO_2$ (LCO) or $LiNiMnCoO_2$ (NMC), and are, therefore, expected to replace them in the future [1–3].

The olivine-type $LiFePO_4$ (triphylite) – $FePO_4$ (heterosite) phases are built of FeO_6 octahedra and PO_4 tetrahedra with interstitial Li showing mobility in the *b* direction [2,4–6]. Both phases are orthorhombic in the *Pnma* space group [2,6,7]. In the olivine structure, $M1M2TO_4$ monovalent cations, like Li^+ or Na^+, only occupy the octahedral M1 site whereas divalent cations, like Fe^{2+}, Mg^{2+} or Mn^{2+} occupy the slightly distorted octahedral M2 site [6–8]. The tetrahedral site T is occupied by P, Si or Ge [8].

A miscibility gap between triphylite and heterosite is postulated at temperatures <200 °C [9], becoming smaller with increasing temperature and decreasing grain size [2,10]. The miscibility gap is found for nanoparticle size >15 nm at room temperature and >25 nm at 45 °C, respectively [11]. For macroscopic grains at room temperature, the miscibility gap results in phase compositions of $Li_{1.00–0.05}FePO_4$ triphylite and $Li_{0.00–0.17}FePO_4$ heterosite, respectively [5]. The miscibility gap shrinks, e.g. by doping triphylite with V^{3+}, Mo^{6+}, Ti^{4+}, Al^{3+} or Zr^{4+} [12,13]. The substitution of Fe^{2+} by V^{3+} in the M2 site reduces the Li intercalation capacity because V^{3+} does not participate in the Fe^{+III} – Fe^{+II} redox reaction and remains trivalent in triphylite [12,13]. Lithium diffusion in *b* direction, however, remains unaffected [12,13].

The phase transformation of triphylite to heterosite during delithiation results in a decrease of the unit cell volume by 6.8 % [2]. The unit cell parameters of triphylite are $a = 10.338(1)$ Å, $b = 6.011(1)$ Å and $c = 4.695(1)$ Å [7]. After delithiation, the lattice shrinks at −5.6 % and −4.3 % in the *a* and *b* direction, respectively, whereas it increases in *c* direction by 1.5 % [7]. The resulting heterosite has crystal lattice parameters of $a = 9.760(1)$ Å, $b = 5.752(1)$ Å and $c = 4.756(1)$ Å, and the FeO_6 octahedral site is more distorted than in triphylite [7]. The intercalation of Na in $FePO_4$, however, results in the increase of the unit cell parameters by 16.6 vol% [14]. Oxidation of Fe^{2+} in triphylite may either be accompanied by a vacancy in the M2 site for charge balance ($3Fe^{2+} \rightarrow 2Fe^{3+}$) or in the M1 site (due to lacking substitution of Li) in heterosite [15].

Phase transition between triphylite and heterosite is reversible [15]. The kinetics, however, depend on the Li diffusion along the $LiFePO_4$/$FePO_4$ interface [15]. The mean Fe – O distances vary at a maximum of 0.28 Å after delithiation of triphylite (2.17 Å) to heterosite (2.04 Å) [15]. The reduction of amorphous $FePO_4$, however, is accompanied by the formation of a $Fe_2P_2O_7$ phase which is lacking when crystalline $FePO_4$ is reduced [16].

Calcination of $FePO_4$ at temperatures higher than 300 °C removes the Brønsted acid sites from the surface by evaporation of adsorbed water [16]. As a result, only Lewis acid sites remain [16].

Due to its application as cathode material in Li-ion batteries, the electrochemical properties and the Li recycling potential of LFP are being intensely investigated [e.g., 17,18,19]. The good performance and safety standards of LFP in batteries lead to increasing interest in investigating the electrochemical Li extraction from aqueous solutions using LFP [20,21]. Liu et al. [20] found an average Li^+ capacity of 39 mg/g and a positive correlation between kinetics and applied voltage. A maximum recovery of 91 % is reached after 8 cycles from a brine with 2.5 g/L total dissolved solids (TDS) and 26 mg/L Li [21]. At 1 *V* applied, the Li capacity reaches 11 mg/g, but increases to 17 mg/g by adding polyethylene glycol to the electrode, i.e. a long-chain polymer that increases electrode porosity [21]. The equilibrium time for extraction is 1.5 h [21]. Using a LiCl solution with 220 mg/L Li concentration, the Li capacity reaches 41 mg/g [22]. The presence of Na^+ ions in solution, however, significantly reduces the Li^+ extraction but may be controlled by adjustment of the applied voltage to <0.3 *V* [20]. The selectivity for Li over Mg may be achieved by voltage adjustment to <1 V [22].

Only sparse work has been done addressing the potential application of LFP in direct Li extraction (DLE) from geothermal brines in a purely chemical approach. To extract Li from brines, LFP needs to be delithiated prior to extraction, which can either be achieved by ion exchange or oxidation of Fe^{+II} to Fe^{+III} in the LFP [23,24]. Lithium is isomorphically substituted by Na^+ in a mechanochemical process without using acid [23]. By co-grinding LFP with NaCl, a maximum Li recovery of 12 mg/g is achieved at high $FePO_4$ stability [23]. Lithium is also recovered by Fe oxidation using a solution of 2.4 % H_2O_2 and 0.1 % CH_3COOH, a mixture of H_2O_2 and CO_2, or in a sulfate solution by oxidation of $LiFePO_4$ using $K_2S_2O_8$ or $Na_2S_2O_8$ [19,24–27]. Using a mixture of 1 % H_2O_2 and 3 % CH_3COOH, a complete delithiation is achieved after approximately 400 s using particles of 300 nm diameter [26]. The delithiation kinetics, however, depend on the oxidizing agent concentration, e.g. equilibrium is reached after 20 min using 0.017 M H_2O_2 and after ~15 min using 0.043 M H_2O_2 [19]. Higher oxidation agent concentration increases the delithiation efficiency as well [28]. Using a mixture of 6 % H_2O_2 + 0.8 M CH_3COOH, 94 % Li are recovered at <1 % dissolution of Fe after 60 min [28]. Another significant parameter is the solid-liquid ratio, which should be <100–120 g/L, since higher slurry density decreases the Li elution efficiency [19,28]. Increasing temperature, i.e. 40–60 °C, increases the Li desorption kinetics and capacity, tested for solutions including CH_3COOH and H_2O_2, but behaves inversely if CO_2 is introduced [19,28]. Carbon-coating of LFP has a negligible effect on the delithiation performance [26].

After delithiation of LFP, Fe^{+III} must be reduced during Li extraction. $NaFePO_4$ is successfully synthesized by reduction of heterosite using NaI for 40 h at 60 °C [14]. Complete lithiation of $FePO_4$ was achieved after 300 s at ~60 °C by reduction using 13.4 mmol/L LiI in acetonitrile [25]. Decreasing temperature negatively affects the intercalation of Li, tested in experiments at $T = 7–58$ °C [25]. The lithiation kinetics increase with increasing initial Li concentration and increasing reducing agent concentration [24]. Equilibrium is achieved after 3 h at >0.7 mol/L concentration of both ions in solution at good chemical sorbent stability [24], at least within 50 cycles [25]. A maximum Li uptake of ~46 mg/g $FePO_4$ was achieved by reduction of 0.6–1 g $FePO_4$ with 0.3 M $Na_2S_2O_3$ after 24 h in lithiation experiments with synthetic 0.06–0.2 M LiCl solutions including some competing ions like 2.4–4 M NaCl, 0.2 M KCl or 0.3 M K_2SO_4 and 0.3–1.3 M $MgCl_2$ [24]. The concentration of competing ions sorbed to $FePO_4$ is <3 mg/g after 24 h using 0.3 M $Na_2S_2O_3$ and Li and Na concentrations varying between 0.10 and 0.01 mol/L [24]. A high Li selectivity was also achieved in experiments using a $C_6H_7O_6Na$ reducing agent for DLE from artificial salt lake brine comprising 100 mg/L Li, 82.3 g/L Na, 13.2 g/L Mg and 4.7 g/L K, reaching a maximum Li uptake of 9 mg/g [27]. However, the influence of other (trace) elements on the Li intercalation in LFP for DLE, like Ca, Sr, Ba, B, Pb, As, S, Mn or Zn, usually present at variable concentrations in natural geothermal brines, remains uninvestigated.

Detailed information about quantitative sorbent dissolution and dissolution rates under specific process conditions, the influence of temperature and reaction times >24 h on the extraction process or preferred operating pH, sorption isotherms and underlying sorption processes for Li and competing ions, however, is lacking [24,27]. To directly recover Li from geothermal brines, sorption is regarded as promising technique. Fast sorption and desorption kinetics and a high Li selectivity are indispensable for an efficient extraction process at high ambient flow rates of typically 30–80 L/s and a complex geochemical brine composition [e.g., 29].

In this study, commercially available, carbon-coated LFP cathode material is characterized for its geochemistry and mineralogy. Furthermore, (de-)lithiation kinetics and (de-)lithiation capacity of the nanocrystalline powder are evaluated in a redox process in synthetic $Na_2S_2O_8$ and $Na_2S_2O_3$ + LiCl solutions. The effects of physicochemical parameters, like temperature and pH, on extraction performance and LFP

stability are evaluated. Experiments with pre-precipitated, Fe-depleted natural geothermal brine from the Bruchsal geothermal power plant, operated by EnBW AG, and synthetic geothermal brine similar to the one at Neustadt-Glewe geothermal power plant, operated by Erdwärme Neustadt-Glewe GmbH, in Germany have been conducted to study the material's potential for DLE and its appropriateness regarding stability and Li selectivity.

2. Materials and methods

The Li-Fe-phosphate (IBUvolt® LFP400) was provided by IBU-tec, Weimar, Germany. The samples were investigated optically (SEM), structurally (XRD, TG-DSC, FT-IR-ATR, BET) and chemically (EDX, acid digestion, ICP-OES, ICP-MS). The BSE images and SEM analyses were conducted using a PhenomXL G2 Desktop-SEM from ThermoFisher Scientific at the Department for Petrology and Mineral Resources, Eberhard Karls University Tübingen, Germany.

Two samples that were available at large quantity were analysed by XRD including an internal silicon standard. Therefore, 1.8 g were homogeneously mixed with 0.2 g of standard material and put in sample carriers of 20 mm diameter. The internal silicon standard was introduced to identify texture effects. Samples that were only available at small quantities were attached to a silica wafer with acetone. The XRD analyses were performed with a D8 Discover diffractometer from Bruker with CuKα radiation (Kα1 λ = 1.54060 Å and Kα2 λ = 1.5444 Å) attached to a LYNX-EYE XE-T linear detector at the Laboratory for Environmental and Raw Materials Analyses (LERA), Karlsruhe Institute of Technology, Germany. The conditions were 2–82°2Θ, 1 s/step and 0.02° increment. The sample rotation was 30 rpm, the airscatter was on automatic mode and the X-ray tube operated at 40 kV and 40 mA. The software package Bruker Diffrac.EVA V4.1.1 and the database PDF2 of 2002 were used for phase identification [30].

For the 5-point-BET method with N_2 ($0.05 < p/p0 < 0.35$), the LFP powder was dried at 105 °C under vacuum overnight. Subsequently, the specific surface area (SSA) was determined with a Quantachrome NOVA 4000e instrument at the Institute for Technical Chemistry, Karlsruhe Institute of Technology, Germany. An external Al_2O_3 standard (SSA = 5.1 m^2/g) was used for quality control and the analytical uncertainty was determined to 4 %.

FT-IR-ATR analyses were conducted using a Nicolet iS50 instrument at the Institute of Nanotechnology, Karlsruhe Institute of Technology, Germany. Analyses were performed at wavenumbers between 400 cm^{-1} and 4000 cm^{-1} at contact with a diamond crystal. Each sample was measured using 20 repetitions that were referenced to a background analysis in air.

The phase stability was investigated by TG-DSC analysis with a sintered corundum standard reference material. The powder was filled in a ceramic crucible and heated to 1000 °C in a N_2 atmosphere using a STA 409 PC Luxx system from Netzsch at the LERA. The measurement started at room temperature, followed by heating to 30 °C (heating rate of 10 K/min) which was kept for 10 min. Thereafter, heating to 1000 °C was carried out at 5 K/min. After reaching the maximum temperature, the analysis was stopped.

A sorbent mass of 0.1 g LFP was digested in 2.5 mL 65 % HNO_3 (suprapur®), 0.6 mL 30 % HCl (suprapur®, Merck) and 2.5 mL millipore water. The samples were digested using a Multiwave 5000 instrument from Anton Paar Germany GmbH with a 20SVT50 rotor. The temperature was increased to 100 °C within 5 min. Afterward, the system was heated to 230 °C within 25 min and held for 15 min. After cooling to room temperature, the solution was diluted in millipore water to a total volume of 50 mL.

All solutions (from experiments and digestions) were analysed with an ICP-OES (iCAP 7000, Thermo Fisher) at LERA. The solutions from the acid digestion of sample material from the experiments with geothermal brine were additionally analysed for trace element content using an ICP-MS iCAP RQ (C2) with an iMR_1000 gas kit (Thermo Fisher) at LERA. Lithium, Na, P, S and Fe were analysed in all solutions. The samples related to experiments with geothermal brines were additionally analysed for K, Rb, Cs, Mg, Ca, Sr, Ba, B, Al, Si, Pb, As, Sb, Ti, *V*, Cr, Mn, Co, Ni, Cu, Zn, and Cd. Solutions containing $Na_2S_2O_3$ additive cause analytical difficulties since they cannot be analysed in an 1 % HNO_3 matrix due to acid sensitivity of $Na_2S_2O_3$. The analyses have been performed in millipore water, which leads to potential underestimation of metal concentrations, like As, Pb and Fe. Duplicates and certified standards (e.g., a multi-element aqueous VHG-MISA6–500 standard, a high-purity multi-element standard CRM-TMDW-A for trace metals in drinking water, and an internal standard ROTI®Star 1000 mg/L Y in 2 % HNO_3 for diluted samples) were analysed for quality control and estimation of the analytical uncertainty. Additionally, blanks were analysed to determine the detection limit (LOD, 3 times sigma) and the limit of quantification (LOQ, 10 times sigma; supplementary data).

The (de-)lithiation capacity is calculated using the equation $Q_i = \left(C_0 - C_{Equ}\right) * \frac{V}{m}$. Q is the amount of sorbate (i) in the sorbent in mg/g (when different sorbates are compared, the value is recalculated to mmol/g), C_0 is the initial concentration of the sorbate in the solution in mg/L, C_{Equ} is the equilibrium concentration of the sorbate in the solution after the experiment in mg/L, *V* is the volume of the solution in L and m is the sorbent mass in g used in the experiment or the digestion [31].

2.1. Experimental

The batch (de-)lithiation experiments were performed after the procedure described in Reich et al. [32]. In initial delithiation experiments, 1 g LFP and 200 mL of different solutions in variable concentrations (e.g. 0.01–0.50 M HCl (pro analysis, Merck), 0.1–3.0 M NaCl (pro analysis, Merck), mixtures of H_2O_2 (pro analysis, Roth) and CH_3COOH (pro analysis, Merck) and 0.1–1.0 M $Na_2S_2O_8$ (normapur™, VWR)) were used. The experiments were stirred for 45 min and 24 h (for HCl). Best performance was reached for a 0.1 M $Na_2S_2O_8$ solution, which was used with the same sorbent/fluid ratio at variable stirring time (delithiation kinetics), and a variable sorbent/fluid ratio at a fixed stirring time of 60 min (delithiation isotherm).

For the lithiation experiments, variable concentrations of 0.1–1.5 M $Na_2S_2O_3$ (pro analysis, Merck) were used with a fixed sorbent/fluid ratio (1 g/200 mL) and Li concentration (200 mg/L) in synthetic LiCl – $Na_2S_2O_3$ solutions. A 0.5 M $Na_2S_2O_3$ matrix was used, which is advantageous for ICP-OES analyses since higher $Na_2S_2O_3$ concentration would require higher dilution of samples, making trace element analysis challenging. The kinetic experiments with synthetic solutions were conducted at 25 °C and a Li concentration of 200 mg/L. The stirring time varied between 1 min and 2 weeks. For the lithiation isotherm experiments in synthetic LiCl solution, the Li concentration was varied between 10 and 1000 mg/L and the stirring time was seven days. Experimental batches have been performed at 25, 40, 60 and 80 °C to study the temperature influence.

All experiments with geothermal brine were conducted at 60 °C. In kinetic experiments, the stirring time was varied between 1 min and 2 weeks. A constant stirring rate of ~300 rpm was used in Bruchsal brine experiments. The experiments with synthetic geothermal brine (Neustadt-Glewe) were shaken. The sorbent mass was varied in the isotherm experiments (between 0.2 and 75 g/L) that were stirred for 3 h and 4 h using geothermal brine from Bruchsal and the synthetic geothermal brine of Neustadt-Glewe composition, respectively. For quality control, blank experiments were conducted in each experimental run.

3. Results

3.1. Material characterization

Both, LFP cathode material (initial $LiFePO_4$) and its delithiated form ($FePO_4$) are used as starting material in the experiments. The initial

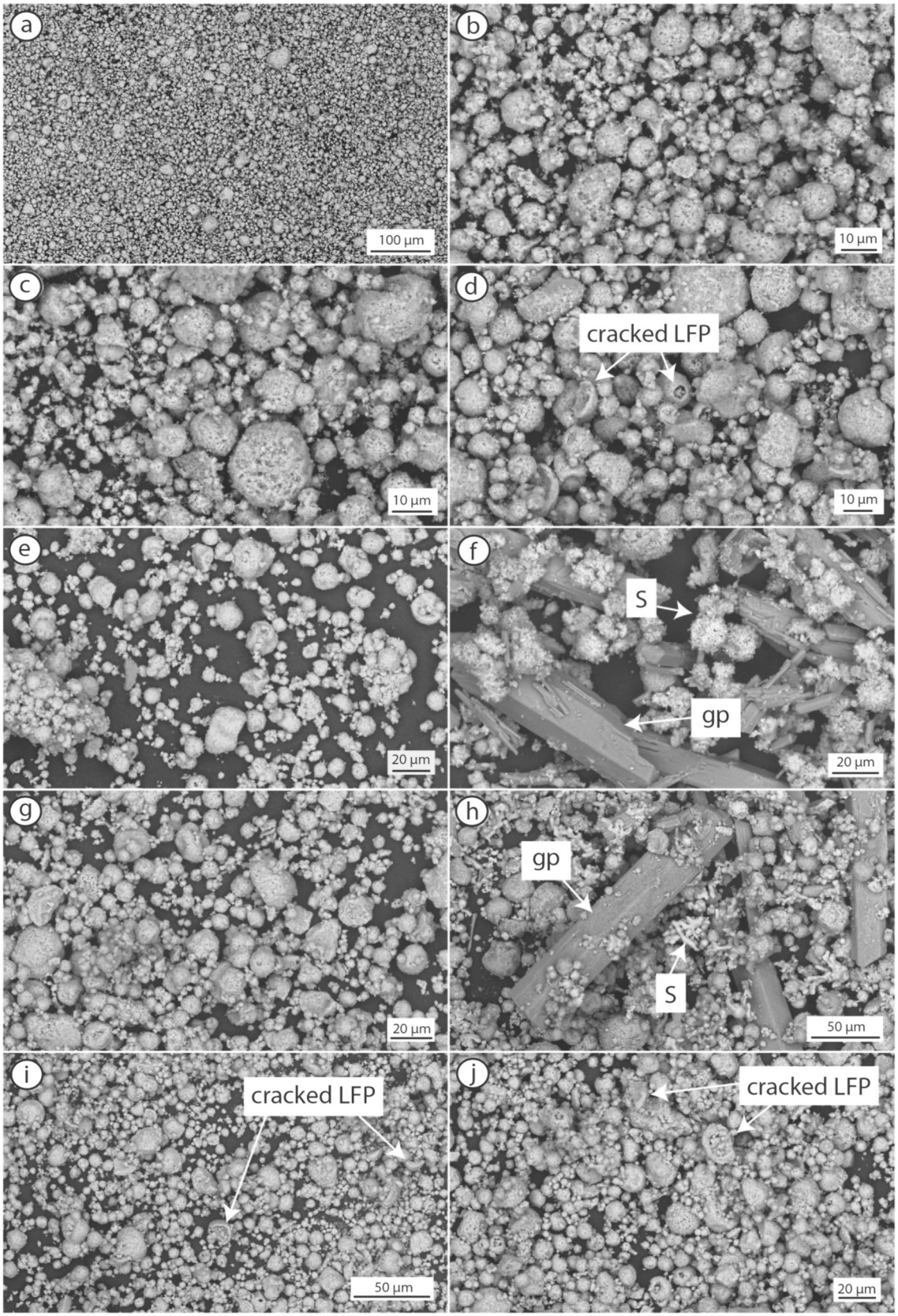

Fig. 1. BSE images of LFP samples. a) and b) initial $LiFePO_4$ powder, c) $FePO_4$ sample after delithiation using 0.1 M $Na_2S_2O_8$, d) sample after synthetic LiCl + $Na_2S_2O_3$ solution treatment, e) sample after geothermal brine + $Na_2S_2O_3$ treatment (1 g, 3 h, Bruchsal), f) sample after two weeks reaction time with geothermal brine + $Na_2S_2O_3$ (Bruchsal), g) sample after 4 h reaction time with synthetic brine + $Na_2S_2O_3$ (Neustadt-Glewe), h) sample after one week reaction time with synthetic brine + $Na_2S_2O_3$ (Neustadt-Glewe), i) sample after brine + $Na_2S_2O_3$ treatment (5 g, 3 h, Bruchsal) and j) sample after brine + $Na_2S_2O_3$ treatment (10 g, 3 h, Bruchsal).

Table 1
Chemical composition of initial $LiFePO_4$ starting material and $FePO_4$.

	$LiFePO_4$ [mg/g]	$FePO_4$ [mg/g]
Li	43	1.7
Fe	266	247
P	161	145
Na	<0.3	0.98
K	0.09	<0.05
Mg	0.11	0.12
Al	0.08	0.07
Si	0.05	0.08
S	0.86	1.02
Ti	0.02	0.02
Mn	0.46	0.42
Co	0.05	0.05
Ni	0.06	0.07
Cu	0.10	0.10
Zn	0.06	0.07
Rb	<0.0005	<0.0005
Cs	<0.0005	<0.0005
Ca	<0.1	<0.1
Sr	<0.0002	<0.0002
Ba	<0.0003	<0.0003
B	<0.005	<0.005
Pb	<0.0005	<0.0005
As	<0.01	<0.01
Sb	<0.0005	<0.0005
V	<0.003	<0.003
Cr	<0.006	0.01
Cd	<0.0009	<0.0009

$LiFePO_4$ is composed of rounded nanoparticles that appear homogeneous with a grain size ranging between approximately 1–20 μm (Fig. 1a). A distinct micro porosity is visible on the surface of each particle (Fig. 1b). The initial $LiFePO_4$ has a specific surface area of 21.5 m^2/g. Its Li content is 43 mg/g (Table 1).

Iron and P concentrations are 266 mg/g and 161 mg/g, respectively. The $FePO_4$, in contrast, contains 1.7 mg/g Li, 247 mg/g Fe and 145 mg/g P (Table 1). The mineral formulae for $LiFePO_4$ and $FePO_4$ are approximately $Li_{1.000}Fe_{0.996}Mg_{0.001}Mn_{0.002}PO_4$ and $Li_{0.051}Na_{0.009}Fe_{0.936}Mg_{0.001}Mn_{0.002}PO_4$, respectively. The XRD data confirm that the initial $LiFePO_4$ is well crystalline and identifies it as orthorhombic triphylite endmember (Fig. 2I.). The $FePO_4$ is the orthorhombic heterosite endmember (Fig. 2II.).

TG-DSC data show minor mass variation (±3 %) between 30 and 1000 °C in $LiFePO_4$, whereas $FePO_4$ loses 10 % total mass by heating to 1000 °C with strongest mass loss (~8 %) starting at approximately 530 °C (Fig. 3a). The $LiFePO_4$ shows, after an initial mass loss of ~2 %, a two-step mass increase starting at ~550 °C (Fig. 3a). The DSC curve of the $LiFePO_4$ shows an endothermic peak at 55 °C (−0.04 mW/mg), and three exothermic peaks at 538 °C (+1.51 mW/mg), 652 °C (+1.25 mW/mg) and 863 °C (+1.56 mW/mg), respectively. The $FePO_4$ sample shows a similar DSC curve with an endothermic peak at 58 °C (−0.05 mW/mg) and two sharp exothermic peaks at 573 °C (+1.31 mW/mg) and 654 °C (+1.25 mW/mg), respectively.

The FT-IR-ATR spectra of the $LiFePO_4$ sample have characteristic bands at 460 cm^{-1}, 496 cm^{-1}, 545 cm^{-1}, 574 cm^{-1}, 633 cm^{-1}, 927 cm^{-1}, 1030 cm^{-1}, 1138 cm^{-1}, 1205 cm^{-1} and 3430 cm^{-1}, respectively (Fig. 4).

3.2. Delithiation

Different solutions have been tested for delithiation of $LiFePO_4$ to produce $FePO_4$ that is needed for the DLE process. Delithiation can either be performed by Fe oxidation or by ion-exchange. Different oxidizing solutions, like 1 % H_2O_2 + 3 % CH_3COOH [26], 2.4 % H_2O_2 + 0.1 % CH_3COOH [25], 0.1 % H_2O_2 + 1 % CH_3COOH and 0.1 M, 0.5 M and 1.0 M $Na_2S_2O_8$ are tested. For delithiation by ion exchange, 0.1–3.0 M NaCl and 0.01–0.50 M HCl are used. The efficiency of delithiation and the elution of Fe and P are checked by determining the amount of each element eluted from $LiFePO_4$ by the respective solution.

A small amount of Li (1–3 mg/g) and P (5–7 mg/g) are rinsed from $LiFePO_4$ in blank experiments using millipore water (Fig. 5). Using different mixtures of H_2O_2 + CH_3COOH (i.e., oxidation agents), 81–99 % of Li is eluted (5.02–6.14 mmol/g; 35–43 mg/g) (Fig. 5). Phosphorous and Fe are eluted at 0.2–0.3 mmol/g (7–9 mg/g) and 0.003–0.03 mmol/g (0.2–2.0 mg/g), respectively, only slightly more than using millipore water. The Li elution is less variable using 0.1–1.0 M $Na_2S_2O_8$ solutions: 96–99 % (5.98–6.14 mmol/g; 41–43 mg/g) Li are recovered from $LiFePO_4$ powder, whereas Fe and P loss are low at <0.01 mmol/g (<0.4 mg/g) and 0.22 mmol/g (<7 mg/g), respectively (Fig. 5). With 0.1–3.0 M NaCl, Li, Fe and P are eluted at 0.14–0.25 mmol/g (1–2 mg/g), <0.001 mmol/g (<0.05 mg/g) and 0.10–0.18 mmol/g (3–6 mg/g), respectively. In contrast, 36–98 % (15–42 mg/g) Li, 0–100 % Fe and 6–100 % P are eluted using 0.01–0.50 M HCl (Fig. 5).

The delithiation kinetics is investigated using a 0.1 M $Na_2S_2O_8$ solution. Equilibrium is reached within 1 min reaction time and the delithiation capacity reaches 42–43 mg/g (Figs. 6a, 7a, b) at low Fe and P loss (1–2 mg/g and 5–7 mg/g, respectively). The starting pH is 3.1–3.6 in both, kinetic and isotherm delithiation experiments. The pH increases to 5.3 within 5 min and decreases exponentially to 2.3 after 2 weeks reaction time (Fig. 6b).

The maximum concentration of Li in the delithiation solution after the reaction is approximately 1.5 g/L Li at an optimal $LiFePO_4$/fluid ratio of <35 g/L (Fig. 7a, b). At higher $LiFePO_4$/fluid ratios, the Li concentration in the solution only slightly increases but the $LiFePO_4$ is not fully delithiated (Fig. 7a, b). At $LiFePO_4$/fluid ratios <0.5 g/L, the Fe and P loss are highest, at maximum 0.07–0.09 mmol/g (4–5 mg/g) and 0.23–0.26 mmol/g (7–8 mg/g), respectively. Sodium and S are sorbed to $LiFePO_4$ at 0.03–0.10 mmol/g (0.6–2.0 mg/g) and 0.01–0.08 mmol/g (0.2–3.0 mg/g), respectively (Fig. 7a, b). The pH increases with higher $LiFePO_4$/fluid ratios to pH = 8, with an increase in slope at a $LiFePO_4$/fluid ratio of 25 g/L and pH = 3.9 (Fig. 7c).

The delithiation of $LiFePO_4$ using a 0.1 M $Na_2S_2O_8$ solution does not change the particle shape at micro scale (Fig. 1c). The round grains and the micro porosity seem unchanged compared to the initial $LiFePO_4$ sample (Fig. 1b, c). However, structural changes are identified by XRD and FT-IR-ATR (Figs. 2II., 4). An orthorhombic heterosite phase is identified but the specific reflexes that are expected at 30.64°2Θ, 40.68°2Θ, 54.29°2Θ are shifted to 30.90°2Θ, 40.79°2Θ, 54.56°2Θ, respectively. An additional reflex at 64.35°2Θ occurs in the pattern that is not identified (Fig. 2II.). The bands in the FT-IR-ATR spectrum that were identified at 1030 cm^{-1}, 927 cm^{-1} and 633 cm^{-1} are shifted to 1067 cm^{-1}, 902 cm^{-1} and 646 cm^{-1}, respectively. An additional band at 514 cm^{-1} is identified. The tiny band, initially present at 1205 cm^{-1}, became a strong band at 1238 cm^{-1} (Fig. 4).

3.3. Lithiation experiments with pure LiCl – $Na_2S_2O_3$ solution

In lithiation experiments using a solution of 200 mg/L LiCl and 0.1–1.5 M $Na_2S_2O_3$, the sorption of Li shows a near-linear behaviour correlating positively with the $Na_2S_2O_3$ concentration (Fig. 8a). The Li sorption capacity in mg/g and mmol/g, i.e. the intercalated amount of Li in $FePO_4$ within 24 h, are estimated as a function of additive concentration:

$$Q_{Li}\left[\frac{mg}{g}\right] = 15.093{*}c(Na_2S_2O_3)\left[\frac{mol}{L}\right] - 0.6282, \text{or} \quad \text{(F.1)}$$

$$Q_{Li}\left[\frac{mmol}{g}\right] = 2.1745{*}c(Na_2S_2O_3)\left[\frac{mol}{L}\right] - 0.0905. \quad \text{(F.2)}$$

At 1.5 M $Na_2S_2O_3$, the Li sorption capacity reaches 3 mmol/g (21 mg/g), whereas only 0.04 mmol/g (0.3 mg/g) Li are sorbed to $FePO_4$ using 0.1 M $Na_2S_2O_3$ (Fig. 8a). Sulfur and Na sorption capacities increase

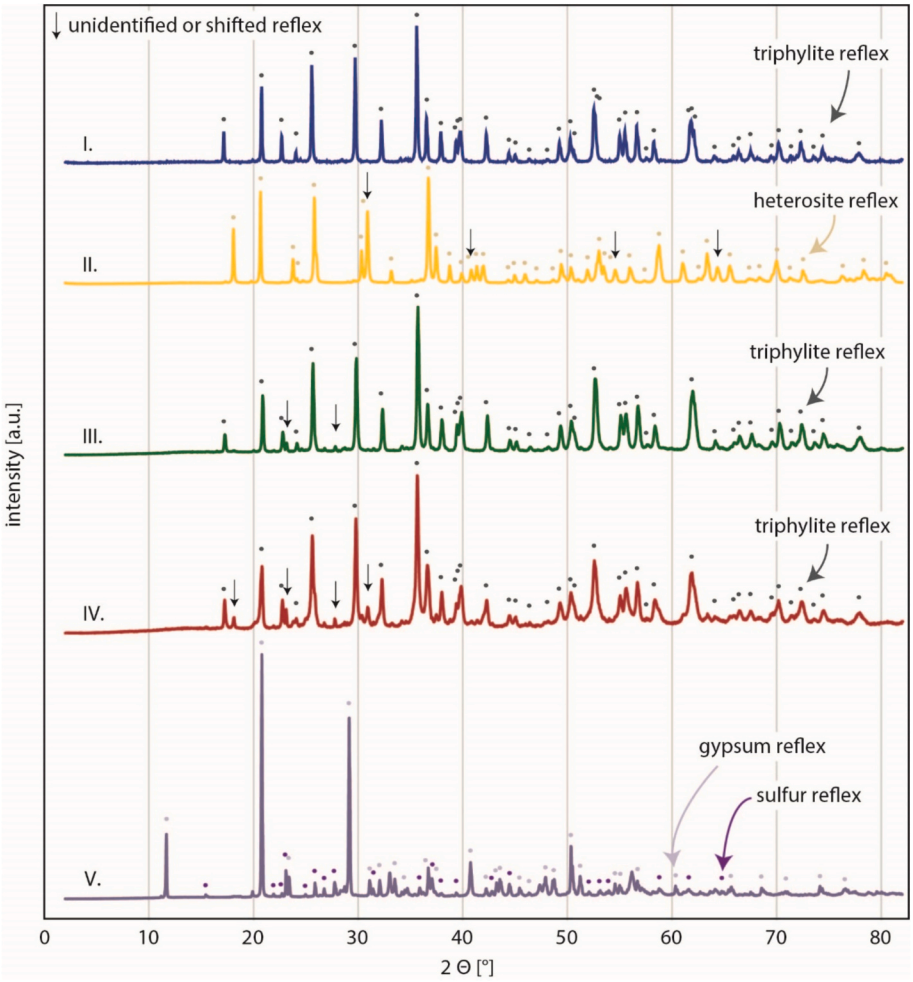

Fig. 2. XRD patterns. Reflexes of the identified phase are highlighted by dots. Arrows highlight reflexes that could not be related to the identified phases or shifts of single reflexes compared to the initial $LiFePO_4$ material. I.) orthorhombic triphylite initial material, II.) orthorhombic heterosite after delithiation, III.) orthorhombic triphylite re-lithiated by LiCl +0.5 M $Na_2S_2O_3$ solution (25 °C, 7 days, 5 g/L $FePO_4$, 1000 mg/L initial Li concentration), *IV.*) orthorhombic triphylite re-lithiated by geothermal brine +0.5 M $Na_2S_2O_3$ (60 °C, 3 h, 5 g/L $FePO_4$, 160 mg/L initial Li concentration) and *V.*) gypsum and native sulfur in LFP sample after two weeks reaction time with Bruchsal geothermal brine +0.5 M $Na_2S_2O_3$ (60 °C, 2 weeks, 5 g/L $FePO_4$, 160 mg/L initial Li concentration).

with increasing $Na_2S_2O_3$ concentration, reaching 0.8 mmol/g (26 mg/g) and 0.9 mmol/g (20 mg/g) at maximum, respectively (Fig. 8a).

After seven days reaction time at 25 °C using a 0.5 M $Na_2S_2O_3$ matrix, Li sorption reaches equilibrium (Fig. 8b). The maximum Li sorption capacity is at 6.35 mmol/g (44 mg/g), which corresponds to 100 % lithiation within analytical uncertainty. The elution of Fe and P is below detection limit at reaction times shorter than 24 h. At longer reaction times, elution of Fe and P starts and is at maximum after two weeks (0.63 mmol/g (35 mg/g) Fe and 0.71 mmol/g (22 mg/g) P). Sodium sorption is not detected during the first two days reaction time, but reaches a maximum of 0.34 mmol/g (8 mg/g) after two weeks. Sulfur sorption is observed within the first five minutes, at 0.004 mmol/g (0.1 mg/g), increasing to 2.58 mmol/g (83 mg/g) after two weeks (Fig. 8b). The starting pH in experiments with 0.5 M $Na_2S_2O_3$ matrix is 9.0–9.4. After 1 min – 5 days reaction time, the pH varies between 6.8 and 7.7 (Fig. 8b). A reaction time of 5 days – 2 weeks leads to a pH decrease to 5.5 and elution of P starts. The P and Fe elution reaches its maximum at the lowest pH (Fig. 8b). Maximum Li sorption capacity is reached at 25 °C with 39 mg/g, whereas only 31 mg/g is sorbed to $FePO_4$ at 40 °C and no Li sorption was detectable at 60 and 80 °C (Fig. 8c).

Lithiation of $FePO_4$ does not affect the particles at micro-scale, except of few cracks (Fig. 1d). Two minor additional reflexes at 23.14°2Θ and 27.79°2Θ are visible in the XRD pattern, not related to triphylite (Fig. 2III.). The re-lithiated $FePO_4$ shows the same FT-IR-ATR bands as the initial $LiFePO_4$ sample (Fig. 4), with only a minor shift of the bands at 1030 cm^{-1} and 927 cm^{-1} to 1040 cm^{-1}, 937 cm^{-1}.

3.4. Lithiation kinetics with geothermal brine and $Na_2S_2O_3$ additive

The Neustadt-Glewe geothermal brine has significantly lower concentrations of Li, K, B, SiO_2 and As than the Bruchsal geothermal brine, i.e. 11 mg/L vs. 155 mg/L Li, 830 mg/L vs. 3240 mg/L K, 0.05 mg/L vs. 41 mg/L B, 32 mg/L vs. 90 mg/L $SiO_{2(aq)}$ and <0.0001 mg/L vs. 7.8 mg/L As (Table 2). The Na and Mg concentrations, however, are higher in the Neustadt-Glewe brine than in the Bruchsal geothermal brine (74,700 mg/L vs. 35,600 mg/L and 1320 mg/L vs. 340 mg/L, respectively; Table 2).

3.4.1. Bruchsal geothermal brine

The Li sorption increases quickly in kinetic experiments at short reaction times using Bruchsal geothermal brine, reaching a maximum and thereafter, the Li sorption slowly decreases at longer reaction times (Fig. 9a). Maximum Li sorption of 23 mg/g (3.37 mmol/g) is reached after 3 h. Lithiation does not affect the material at micro-scale until the maximum sorption capacity is reached (Fig. 1e). The XRD data confirm the formation of orthorhombic $LiFePO_4$ after lithiation (Fig. 2IV.). Additional reflexes are identified at 18.10°2Θ, 23.10°2Θ, 27.73°2Θ and 30.89°2Θ that cannot be related to a coexisting heterosite phase. The FT-

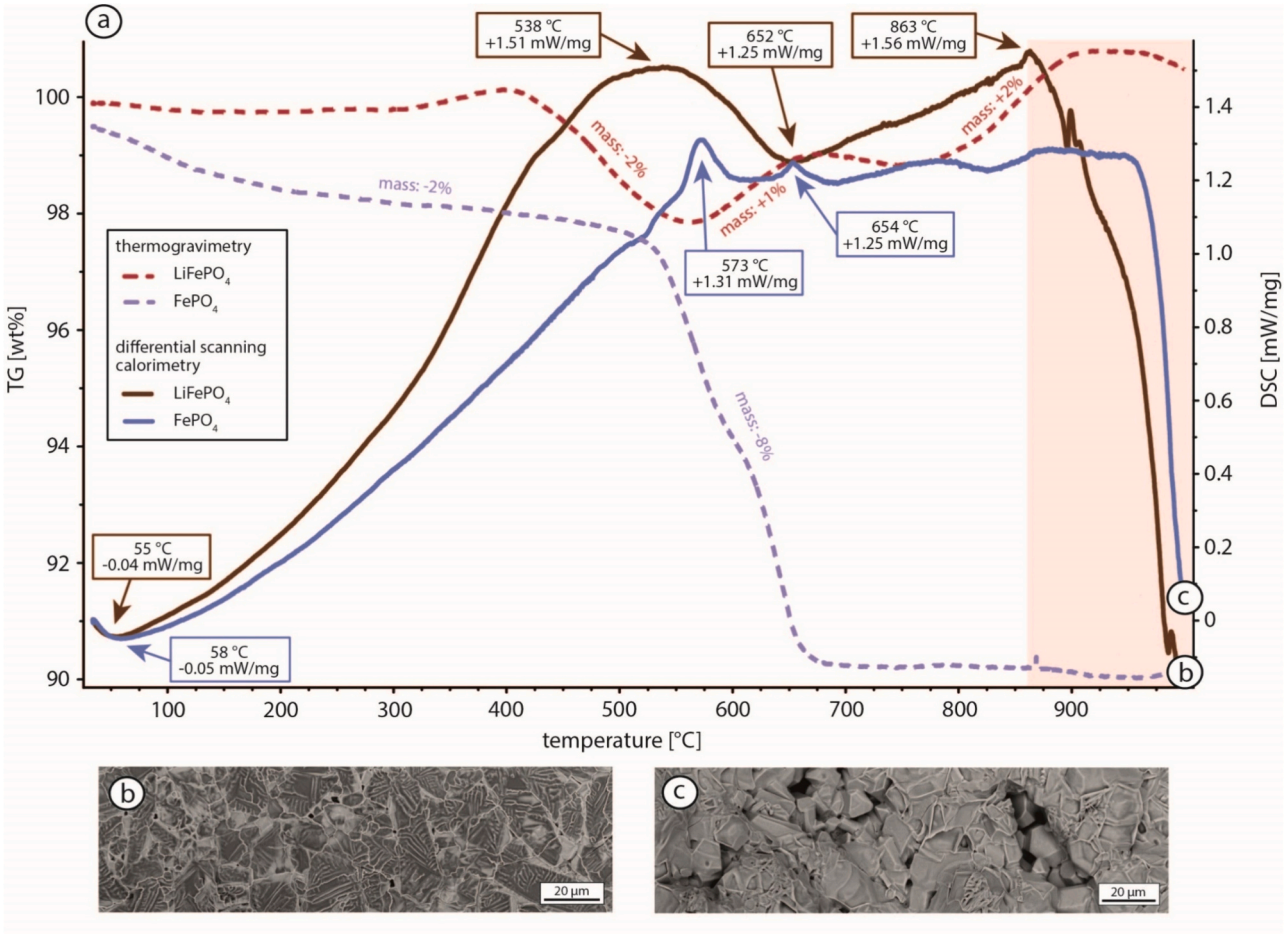

Fig. 3. a) TG-DSC results for $LiFePO_4$ and $FePO_4$. The mass change [wt%] during heating is illustrated by dashed lines, whereas the solid lines reflect the DSC results [mW/mg] during heating. b) BSE image of crystallized $LiFePO_4$ melt and c) BSE image of crystallized $FePO_4$ melt.

IR-ATR spectrum is similar to the initial $LiFePO_4$ and the $FePO_4$ sample re-lithiated from the synthetic $LiCl + Na_2S_2O_3$ solution (Fig. 4). Only the band at 927 cm^{-1} shows a shift beyond the analytical uncertainty to 934 cm^{-1}.

Sodium shows a similar behaviour as Li, but the maximum Na sorption capacity is reached later (after 24 h) (Fig. 9a). The elution of Fe and P is low until the maximum Li sorption capacity is reached and increases to −123 mg/g (−2.2 mmol/g) Fe after 3 days reaction time and −114 mg/g (−3.7 mmol/g) P loss after one week reaction time (Fig. 9a). The starting pH is 6.9–7.3. It decreases exponentially with stirring time, until equilibrium is reached at pH = 3.7–4.1 after 24 h (Fig. 10).

Sorption of S and Ca increases with reaction time and is at maximum with 10.7 mmol/g (344 mg/g) S and 3.8 mmol/g (154 mg/g) Ca after 2 weeks (Fig. 9a). Strong increase in S and Ca sorption correlates with the decrease in Fe elution. In BSE images, elongated, euhedral crystals are observed after long stirring time (Fig. 1f) and the surface of the LFP particles is rough (Fig. 1b, f).

At short reaction time, Sr is already sorbed to $FePO_4$ with 0.003–0.007 mmol/g (0.2–0.6 mg/g) and reaches maximum at 0.02 mmol/g (1.4 mg/g) after 3 days. Sorption of Ba is generally low, at 0.001 mmol/g (0.05–0.08 mg/g) at the start and increases to 0.002 mmol/g (0.2 mg/g) after 1–3 days. The sorption of both elements is low until Fe and P elution starts (Fig. 9a).

Sorption of other elements reaches maximum values of 0.004–0.015 mmol/g (0.1–0.6 mg/g) for K and 0.002 mmol/g (0.10 mg/g) for Mg. At maximum, As sorption is 0.004 mmol/g (0.3 mg/g) after 5 days. The sorption kinetics of Mn, Si, Zn and Pb are inconclusive (Fig. 9a). In general, however, the sorption capacities are low. Zink and Pb are extracted from the brine with a maximum of 0.005 mmol/g (0.3 mg/g) and 0.0001 mmol/g (0.01 mg/g), respectively. Manganese is partially eluted from $FePO_4$, but also shows positive sorption values depending on the reaction times and varies between −0.006–0.001 mmol/g (−0.3–0.1 mg/g). Silica shows low elution from $FePO_4$ at −0.003 mmol/g (−0.08 mg/g).

3.4.2. *Synthetic Neustadt-Glewe geothermal brine*

The kinetics is similar to the results for the Bruchsal brine, but Li sorption is at maximum after 4 h (Fig. 9b). Sodium shows a similar behaviour as Li and reaches the maximum sorption capacity after 24 h, i. e. the same as observed for the Bruchsal brine. The Fe and P elution is at maximum at −98 mg/g (−1.7 mmol/g) after 3 days and −65 mg/g (−2.1 mmol/g) after 5 days, respectively (Fig. 9b). The starting pH is 7.0–7.7. The pH decreases with time, reaching an equilibrium pH = 3.8–4.0 after 24 h (Fig. 10).

Sorption of S and Ca increases with long reaction times and is at maximum with 8.3 mmol/g (265 mg/g) S and 3.5 mmol/g (139 mg/g) Ca after 2 weeks (Fig. 9b). As already observed in the Bruchsal kinetic experiments (Section 3.4.1), short reaction times do not affect the $FePO_4$ particles at micro-scale (Fig. 1g), but elongated, euhedral crystals form after long stirring time (Fig. 1h) and the surface of the LFP particles is rough (Fig. 1b, h).

Strontium is sorbed at the start of the experiment with 0.002–0.005 mmol/g (0.2–0.4 mg/g) and reaches maximum at 0.01 mmol/g (1.2 mg/g) after 3 days. Barium is generally low at the start, with 0.001 mmol/g (0.03–0.08 mg/g), and increases to 0.002 mmol/g (0.1–0.3 mg/g) after

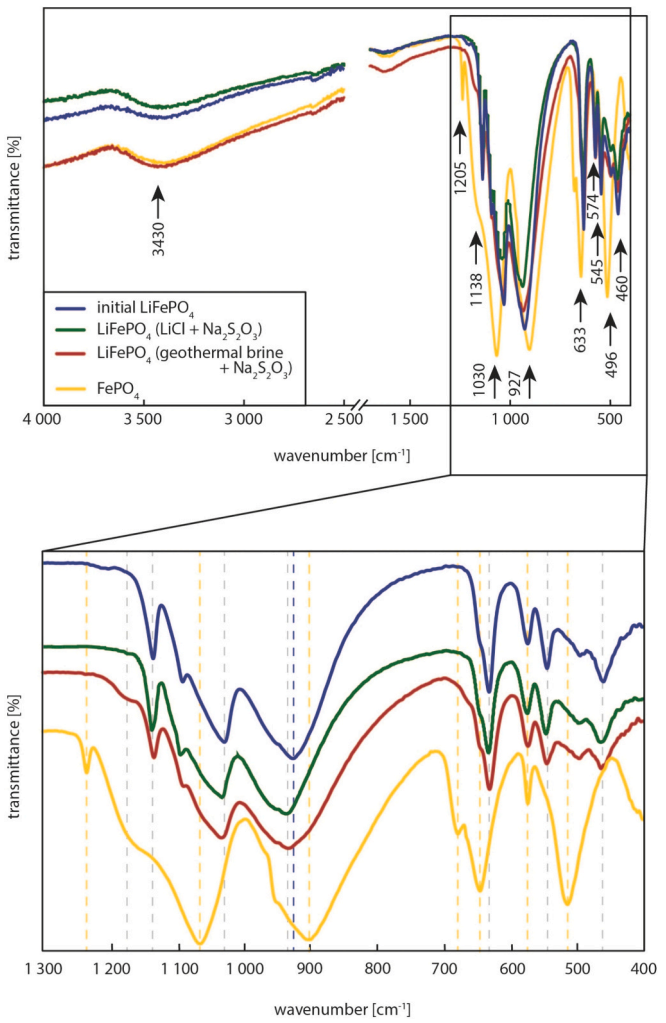

Fig. 4. FT-IR-ATR spectra in the range of 400–4000 cm^{-1} of initial $LiFePO_4$ (blue), $FePO_4$ (yellow), re-lithiated sample using LiCl +0.5 M $Na_2S_2O_3$ solution (green; 25 °C, 7 days, 5 g/L $FePO_4$, 1000 mg/L initial Li concentration) and re-lithiated sample using Bruchsal geothermal brine (red; 60 °C, 3 h, 5 g/L $FePO_4$, 160 mg/L initial Li concentration). The identified bands for the initial $LiFePO_4$ sample are labelled in the upper graph. The dashed lines in the lower graph highlight the shift of characteristic bands in the range of 400–1300 cm^{-1}.

1–3 days. The sorption behaviour of Sr and Ba is the same as already observed in experiments with Bruchsal brine (Section 3.4.1).

Sorption reaches maximum values of 0.003 mmol/g (0.1 mg/g) for K and 0.01 mmol/g (0.3 mg/g) for Mg. The kinetics of Mn, Si, Zn and Pb are inconclusive and behave differently than observed in the kinetic experiments with Bruchsal brine (Fig. 9). In general, however, the sorption capacities are low. Zink and Pb are extracted from the brine with a maximum of 0.001 mmol/g (0.1 mg/g) and 0.001 mmol/g (0.1 mg/g), respectively. Manganese is partially eluted from $FePO_4$, but also shows positive sorption values depending on the reaction time and varies between −0.003–0.001 mmol/g (−0.2–0.2 mg/g).

3.5. Lithiation isotherms with geothermal brine and $Na_2S_2O_3$ additive

3.5.1. Bruchsal geothermal brine

The isotherm shows a typical Langmuir behaviour, with increasing Li sorption capacity at increasing residual Li concentration. At residual Li concentrations >80 mg/L, however, the Li sorption decreases (Fig. 11a). The maximum Li sorption capacity reaches 3.9 mmol/g (27 mg/g). After the strong increase, the Li sorption decreases at $FePO_4$/brine ratios >2.5 g/L (Fig. 11b). The equilibrium Li concentration at $FePO_4$/brine ratios >25 g/L is below the detection limit. A maximum Na sorption of 4.7 mmol/g (107 mg/g) is reached at the smallest tested $FePO_4$/brine ratio of 0.25 g/L. Sorption of S reaches maximum of 1.8 mmol/g (58 mg/g) at a $FePO_4$/brine ratio of 0.25 g/L and decreases with increasing $FePO_4$/brine ratios (Fig. 11b).

Calcium, Sr, Mg, Mn, Si, As, Zn and B show a similar sorption behaviour, reaching high sorption capacities at an $FePO_4$/brine ratio of 0.25 g/L and a decreasing capacity at higher $FePO_4$/brine ratios (Fig. 11b). The maximum capacities are 0.3 mmol/g (14 mg/g) Ca, 0.009 mmol/g (0.8 mg/g) Sr, 0.03 mmol/g (0.6 mg/g) Mg, 0.001 mmol/g (0.1 mg/g) Mn, 0.01 mmol/g (0.3 mg/g) Si, 0.005 mmol/g (0.3 mg/g) As, 0.02 mmol/g (1.4 mg/g) Zn and 0.04 mmol/g (0.5 mg/g) B. The sorption capacities of K and Ba are low at small $FePO_4$/brine ratios <5 g/L, before reaching equilibrium at $FePO_4$/brine ratios >5 g/L at approximately 0.01 mmol/g (0.4 mg/g) K and 0.001 mmol/g (0.13 mg/g) Ba (Fig. 11b). The elution of Fe and P is not continuous, reaching a maximum at −0.04 mmol/g (−2 mg/g) and −0.03 mmol/g (−1 mg/g), respectively.

In the Bruchsal isotherm experiments, the pH value progressively decreases with increasing Li extraction to pH = 3.6. The pH decreases exponentially with increasing $FePO_4$/brine ratio, reaching equilibrium at $FePO_4$/brine ratios >25 g/L and pH = 3.6–3.9 (Fig. 10).

3.5.2. Synthetic Neustadt-Glewe geothermal brine

The lithiation isotherm from the Neustadt-Glewe brine is different compared to the Bruchsal brine experiments (Fig. 11a, c). No typical sorption behaviour, as described by Henry, Langmuir or BET can be identified and the sorption capacities are relatively constant with increasing residual Li concentration (Fig. 11c). The total Li sorption is lower due to the lower initial Li concentration (Table 2, Fig. 11a, c). The maximum Li sorption capacity is 0.2 mmol/g (1.3 mg/g) at an $FePO_4$/brine ratio of 2 g/L (Fig. 11d). Sodium shows the opposite behaviour but not as distinctly as observed in the Bruchsal isotherm (Fig. 11b, d). The maximum Na sorption capacity is 1.7 mmol/g (38 mg/g) at an $FePO_4$/brine ratio of 8 g/L. A typical L isotherm shape is observed for S, reaching a mean equilibrium sorption capacity of 0.4 mmol/g (14 mg/g) at 8–60 g/L. The capacities of Ca, Mg, Zn and Pb decrease after the initial maximum at 0.2 g/L $FePO_4$/brine ratio at 0.1 mmol/g (4.4 mg/g), 0.02 mmol/g (0.4 mg/g), 0.01 mmol/g (0.9 mg/g) and 0.01 mmol/g (1.7 mg/g), respectively (Fig. 11d). The elution of Fe and P are higher in the Neustadt-Glewe than in the Bruchsal experiments and the mean dissolution rates at −0.09 mmol/g (−5.2 mg/g) Fe elution and −0.07 mmol/g (−2.2 mg/g) P elution stay constant over all tested $FePO_4$/brine ratios >8 g/L. The pH progressively decreases with progressing Li extraction to 3.6 and exponentially decreases with increasing $FePO_4$/brine ratio, reaching the equilibrium at $FePO_4$/brine ratios >16 g/L and pH = 3.6–3.9 (Fig. 10).

3.6. LFP selectivity

No robust distribution coefficients (K_d) for the different elements can be calculated because the isotherms do not fit known sorption models, like Henry, Langmuir or BET. Distribution coefficients, however, can be calculated for different points of the isotherms by Eq. (F.3) [31]. The calculated distribution coefficients are thus only valid for the specific conditions under which the experiments have been performed.

$$K_d \left[\frac{L}{g}\right] = \frac{Q_{Equ}\left[\frac{mg}{g}\right]}{C_{Equ}\left[\frac{mg}{L}\right]} \tag{F.3}$$

Different distribution coefficients are calculated for the lithiation peak in kinetic experiments with Bruchsal geothermal brine (Fig. 12a; Table 3), the maximum Li sorption capacity in isotherm experiments from Bruchsal geothermal brine (Fig. 12b; Table 3), the peak lithiation in kinetic experiments from synthetic Neustadt-Glewe geothermal brine

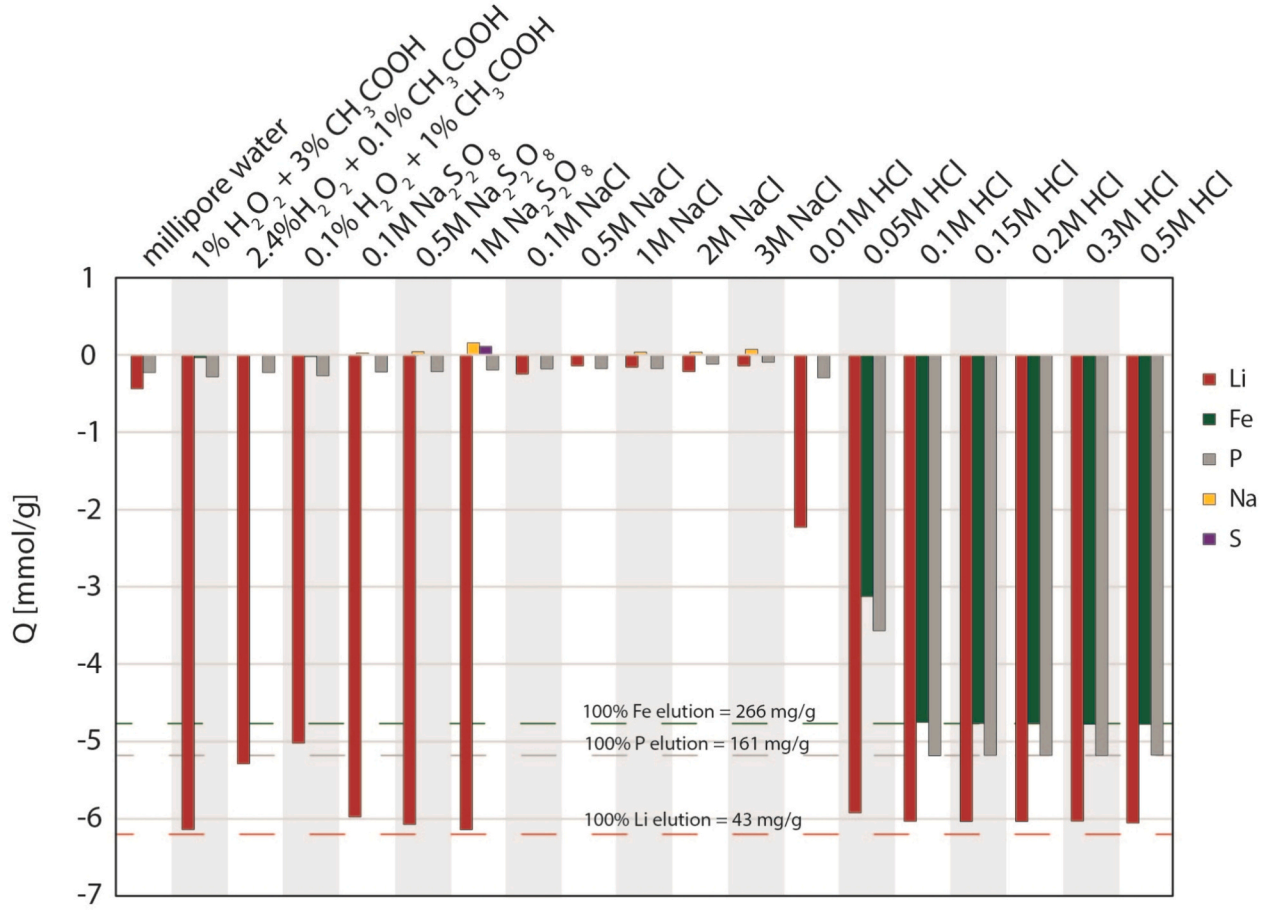

Fig. 5. Preliminary delithation experiments testing redox and ion exchange. Plot of different solutions vs. elution of Li, Fe and P and sorption of Na and S [mmol/g]. The experiments were conducted at 25 °C, 5 g/L $LiFePO_4$ and 45 min (24 h for HCl experiments).

(Fig. 12c; Table 3) and the maximum Li sorption capacity in isotherm experiments with synthetic Neustadt-Glewe geothermal brine (Fig. 12d; Table 3). At all investigated conditions, Li has an approximately 10 times higher affinity for $FePO_4$ than the other elements, with K_d values of 0.1–0.8 (Fig. 12, Table 3). In the Neustadt-Glewe experiments, Na and S concentrations in $FePO_4$ are much higher than Li (Fig. 11d). The K_d values of Li are, however, still higher than those of Na and S (Fig. 12d, Table 3). Although As and Pb are sorbed to $FePO_4$ occasionally, it was not possible to calculate K_d values for these elements because of lacking fluid data due to analytical difficulties with the $Na_2S_2O_3$ additive. Different selectivity orders are identified: (1) Li>Ba>As>Zn>Mn>Sr>S>Ca>Na>Mg>K (3 h, Bruchsal kinetics); (2) Li>Ba>Zn>Mn>B>S>Si>Sr>Ca>Na>Mg>K (2.5–5.0 g/L $FePO_4$/brine ratio, Bruchsal isotherm); (3) Li>Ba>Mn>Sr>S>Ca>Na>Mg>K>Zn (4 h, Neustadt-Glewe kinetics); and (4) Li>Zn>Ba>Mn>Sr>Ca>Na>S>Mg>K (2.0 g/L $FePO_4$/brine ratio, Neustadt-Glewe isotherm). Iron and P are disregarded for the selectivity sequence since K_d values would reflect the dissolution of $FePO_4$. Initial P concentration in the sample is below detection limit (Table 2) and Fe concentration is depleted compared to the original brine composition due to ferric oxyhydroxide precipitation under laboratory conditions. The different selectivity sequences are summarized qualitatively to Li>Ba>Mn>Sr>Ca>Na>Mg>K. The K_d values of Zn and S are variable. Sulfur likely has a similar selectivity as Ca and Na (Fig. 12a, c, d). Arsenic, B and Si are only extracted in the Bruchsal experiments, robust data on their selectivity is therefore not generated by our experiments.

The complete dataset for all experiments performed with (synthetic) geothermal brine (supplementary data) shows that Li has the highest affinity to $FePO_4$, i.e. higher K_d values than other elements, at reaction times between 15 min – 5 days and an $FePO_4$/brine ratio of 0.25–25 g/L (Bruchsal), or 60 min – 3 days and 0.4–16 g/L (Neustadt-Glewe). Although K_d values are highest for Li in these ranges, a higher purity of the re-lithiated $FePO_4$ is reached in Bruchsal using a $FePO_4$/brine ratio of 2.5–10 g/L. At lower and higher $FePO_4$/brine ratios, a higher total amount of Na is extracted (Fig. 11b).

4. Discussion

4.1. Mineralogical implications

The 3430 cm^{-1} band in the $LiFePO_4$ FT-IR-ATR spectrum represents OH^- vibrations and its presence indicates adsorbed water vapor [33]. The bands at 1138 cm^{-1} (ν_3), 1030 cm^{-1} (ν_3) and 927 cm^{-1} (ν_1) are assigned to antisymmetric P – O stretching vibrations of the PO_4^{3-} anion [18,34]. The bands at 633 cm^{-1} (ν_4), 574 cm^{-1} ($\nu_4 + \nu_2$) and 545 cm^{-1} ($\nu_4 + \nu_2$) are assigned to O – P – O stretching vibrations of the PO_4^{3-} anion [18,35]. The vibration at wavenumber 633 cm^{-1}, however, may also be assigned to FeO_6 [36]. The occurrence of the vibration at 1238 cm^{-1} has been previously discussed by Ait-Salah et al. [36] and is assumed to represent a unique stretching vibration of the PO_4^{3-} anion, only occurring in the $FePO_4$ phase. The minor shift of bands in the FT-IR-ATR spectrum of the re-lithiated $FePO_4$ compared to the initial $LiFePO_4$ material may indicate the formation of defects or distortion of the PO_4 units, e.g. the shift of the band at 927 cm^{-1} to 934 cm^{-1}. The formation of defects in the crystal lattice is of importance regarding the sorbent reuse in multiple cycles, potentially affecting the Li diffusivity in *b* direction, which may reduce the Li sorption capacity of $FePO_4$ after multiple sorption – desorption cycles.

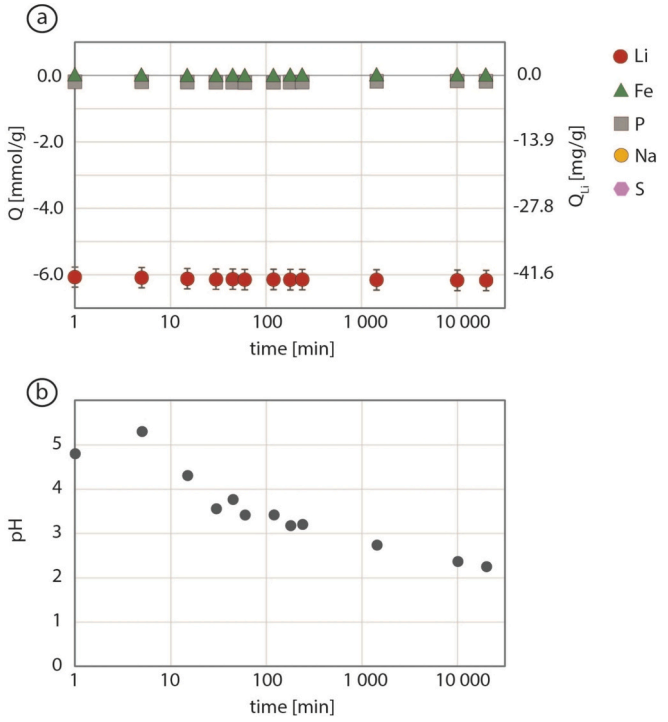

Fig. 6. Delithiation kinetics of $LiFePO_4$. a) Plot of sorption capacity [mmol/g] vs. reaction time [min] and b) pH value vs. reaction time [min]. The experiments were conducted at 25 °C, 0.1 M $Na_2S_2O_8$ and 5 g/L $LiFePO_4$.

The vibrations at low wavenumbers, i.e. at 496 cm^{-1} and 460 cm^{-1} are related to translational vibrations of Li^+ ions [18,35,36]. The bands that indicate the presence of Li^+ ions at 496 cm^{-1} and 460 cm^{-1}, disappear in the $FePO_4$ FT-IR-ATR spectrum (Fig. 4). Phase transition between $LiFePO_4$ and $FePO_4$ is complete since Li^+-ion characteristic bands are present or absent from the respective FT-IR-ATR spectra (Fig. 4).

The reversibility of delithiation – lithiation of LFP is also confirmed by the XRD data, because the pattern of re-lithiated $FePO_4$ is indistinguishable from orthorhombic triphylite from the initial $LiFePO_4$ (Fig. 2). The strong shift of some reflexes in the heterosite XRD pattern (Fig. 2II.), however, may indicate lattice distortion, possibly resulting from residual Li (Table 1) or the formation of crystal defects during phase transition. The occurrence of minor additional reflexes in the XRD patterns of re-lithiated samples (Fig. 2III., IV.) may indicate the formation of defects and/or mineral alteration. Thus, complete phase transition may induce structural defects that indicate aging of the material, which could be of significant importance for their application during numerous phase transition cycles. Mechanical cracking of LFP particles is interpreted as a result of stirring during the experiments (Fig. 1d, i, j). The mechanism of delithiation and lithiation of LFP is a reversible redox process and thus generally suitable for DLE.

The TG-DSC data indicate that $LiFePO_4$ and $FePO_4$ are stable under the specific DLE conditions between 60 and 80 °C (Fig. 3). The mass loss at temperatures <450 °C visible in both samples results from evaporation of adsorbed interparticle and crystal water from the nanocrystalline powder [1]. The presence of water is also evident from FT-IR-ATR spectra (Fig. 4). The two exothermic peaks at 573 °C and 654 °C (Fig. 3) reflect phase transitions in the $FePO_4$ lattice [1]. The increased mass loss at T >550 °C coincides with the exothermic peak indicating that this is linked to recrystallization potentially resulting from evaporation of more strongly bound crystal water [37]. The exothermic peak at 654 °C also coincides with a slight change in the mass loss, supporting further changes in the crystal lattice at these temperatures.

The mass of $LiFePO_4$ remains quite constant until ~420 °C,

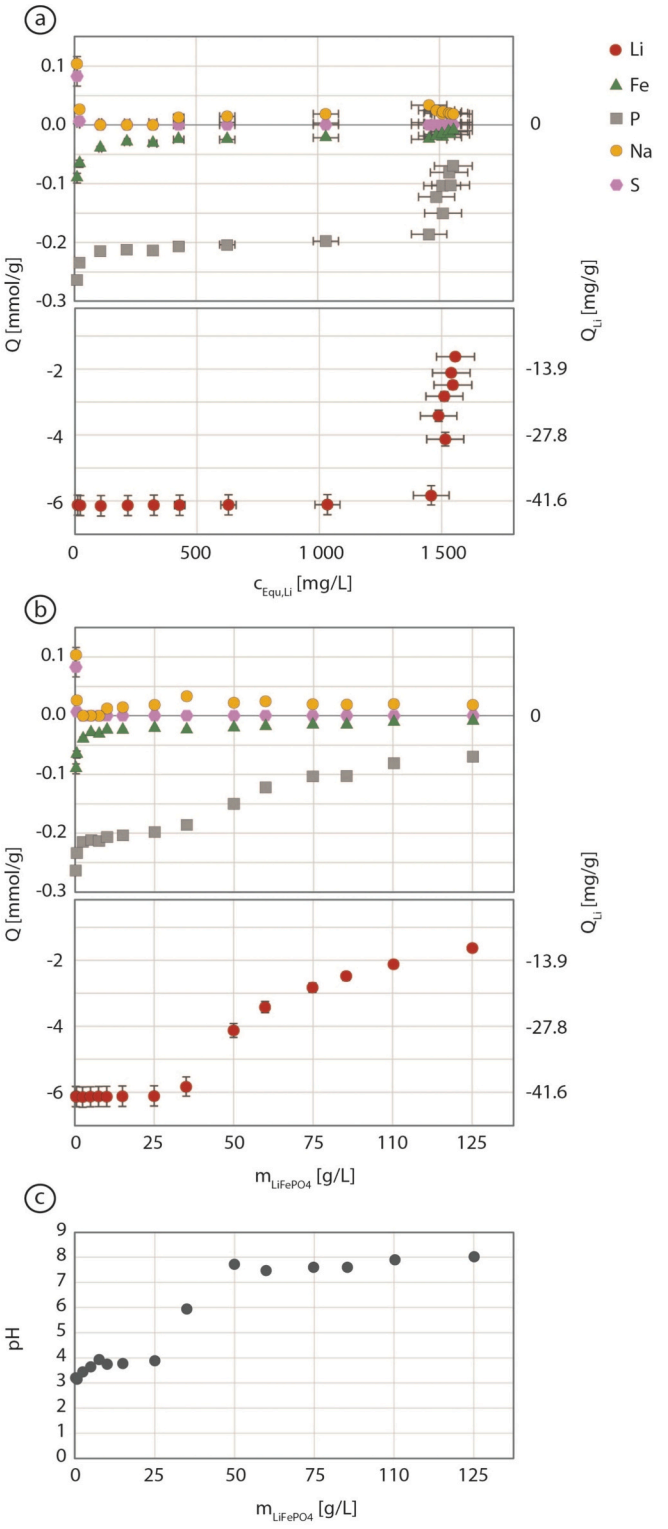

Fig. 7. Delithiation isotherm plot of a) sorption capacity [mmol/g] vs. equilibrium Li concentration [mg/L], b) $LiFePO_4$/fluid ratio [g/L] and c) pH value vs. $LiFePO_4$/fluid ratio [g/L]. The experiments were conducted at 25 °C, 0.1 M $Na_2S_2O_8$ and 60 min.

indicating that it contains less adsorbed interparticle water than $FePO_4$, which was produced by $LiFePO_4$ oxidation in aqueous solution. Mass loss between 420 and 550 °C contradicts the exothermic behaviour with a peak at 538 °C. The mass loss may result from water evaporation but endothermic peaks are lacking. The exothermic peak may be linked to

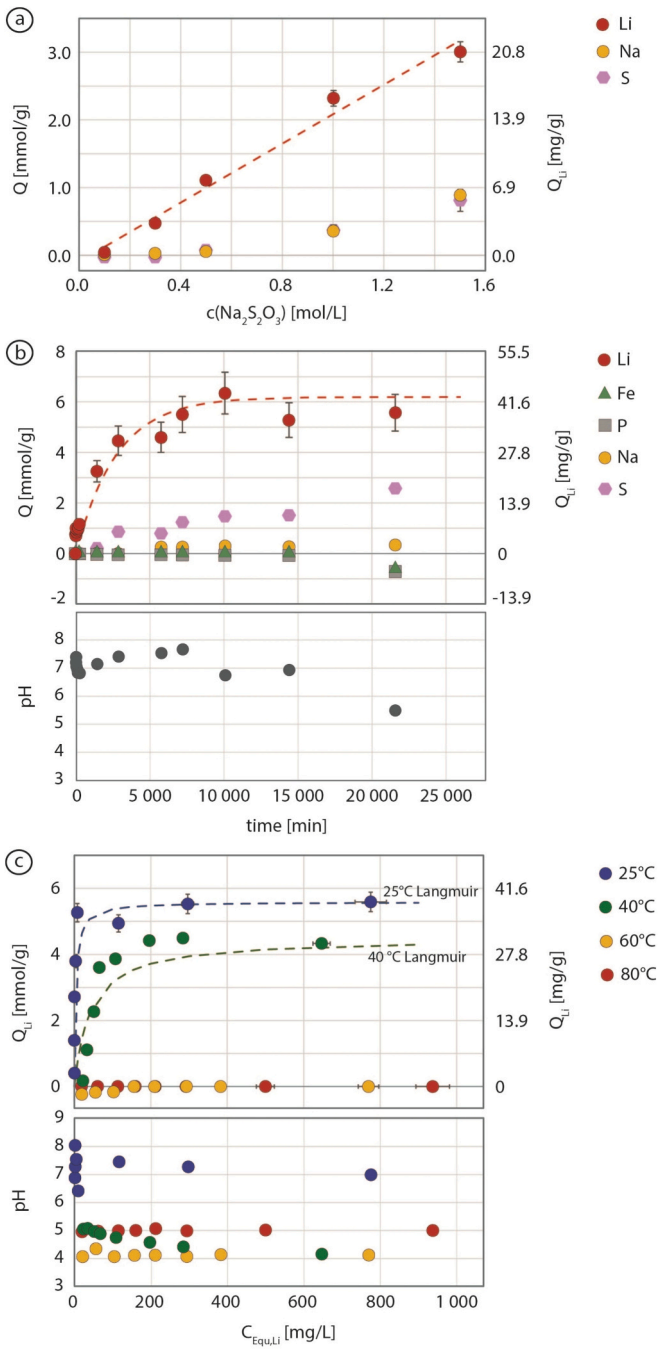

Fig. 8. Isotherms derived from experiments of synthetic LiCl + $Na_2S_2O_3$ solutions. a) Li, Na and S sorption capacity [mmol/g] vs. $Na_2S_2O_3$ concentration [mol/L]. The dashed line shows the linear relationship between lithiation and additive concentration. The experiments were conducted at 25 °C, 5 g/L $FePO_4$, 24 h and 200 mg/L initial Li concentration, b) lithiation kinetics in sorption capacity [mmol/g] vs. reaction time [min] and pH value vs. reaction time [min] at 25 °C, 5 g/L $FePO_4$/volume ratio and 200 mg/L initial Li concentration. The dashed line represents the PFO kinetic model and c) lithiation isotherm, plotted with sorption capacity [mmol/g and mg/g] vs. equilibrium Li concentration [mg/L] and pH value vs. equilibrium Li concentration [mg/L] at 25, 40, 60 and 80 °C. The experiments were conducted with 5 g/L $FePO_4$ for 7 days. The dashed lines illustrate the Langmuir models at 25 and 40 °C.

recrystallization processes, potentially caused by the loss of strongly bound crystal water [37]. This, however, is difficult to interpret and remains unclear without further analyses and detailed structural information. At higher temperatures, $LiFePO_4$ shows endothermic behaviour

Table 2
Chemical composition of the natural and synthetic geothermal brines from Bruchsal and Neustadt-Glewe before and after mixing with 0.5 M $Na_2S_2O_3$.

Analyte [mg/L]	Geothermal brine Bruchsal, Germany	Bruchsal brine + additive, before DLE	Geothermal brine Neustadt-Glewe, Germany	Synthetic Neustadt-Glewe brine + additive, before DLE
Li	155	158	11	11
Na	35,600	57,390	74,700	98,530
K	3240	3250	830	920
Mg	340	340	1340	1320
Ca	7440	7270	8300	8200
S	130	32,900	260	32,360
Rb	24	–	1.3	–
Cs	13	–	0.1	–
Sr	350	360	500	490
Ba	8.6	5.9	5.2	3.9
B	41	37	0.05	<0.009
SiO_2	90	45	32	<0.007
Pb	3.6	–	0.4	–
As	7.8	2.8	<0.0001	<0.002
Mn	24	21	12	7.9
Zn	14	7.1	3	2.1
Al	0.03	<0.07	<0.0002	<0.07
P	<0.0003	<0.003	<0.0003	<0.003
Sb	0.2	–	<0.000009	–
Ti	<0.0001	–	<0.0001	–
V	0.002	–	0.004	–
Cr	0.002	<0.003	0.004	<0.003
Fe	44	<0.0001	77	<0.0001
Co	0.005	<0.0003	<0.000009	<0.0003
Ni	0.005	<0.007	<0.00003	<0.007
Cu	0.02	<0.003	<0.00006	<0.003
Cd	0.08	<0.0002	0.005	<0.0002

up to 652 °C resulting from changed thermal conductivity properties of $LiFePO_4$ after previous water loss. This is followed by an exothermic behaviour with a two-step mass increase until 863 °C, potentially reflecting Fe oxidation and further recrystallization or N_2 sorption, followed by subsequent recrystallization. Melting of $LiFePO_4$ begins at 860 °C, whereas $FePO_4$ is more stable and starts melting at approximately 950 °C. After heating to 1000 °C and cooling to room temperature, the BSE images of the sample material confirm melt formation in both materials (Fig. 3b, c). Spinifex textures, also typically occurring in olivine-rich samples in the nature that indicate cooling under low nucleation rates and fast crystal growth rates [38] are visible in the $LiFePO_4$ sample (Fig. 3b). The phases that crystallized from the $FePO_4$ sample during heating to 1000 °C, are orthorhombic and triclinic (Fig. 3c). The orthorhombic crystals may represent euhedral heterosite, whereas the triclinic crystals may either represent kabalovite ($Fe_3^{+II}Fe^{+III}_4(PO_4)_6$) or nabateaite ($Fe_2P_2O_7$) [39,40].

4.2. Delithiation

Delithiation using NaCl does not elute Li significantly by ion exchange and $LiFePO_4$ is dissolved using HCl. Therefore, oxidation agents are regarded as most promising for $LiFePO_4$ delithiation. The oxidation agent $Na_2S_2O_8$ is proven to provide the highest delithiation capacity at the highest $LiFePO_4$ stability (Fig. 5).

The delithiation of $LiFePO_4$ is complete, reaching the maximum delithiation capacity of 42–43 mg/g (Fig. 7a, b), equal to the concentration of Li in $LiFePO_4$, supporting the crystallographic data (Figs. 2, 4). This indicates that the amount of anti-site defects in the initial $LiFePO_4$ sample is low [26].

Elution of P, Fe and Li is an effect occurring at low $LiFePO_4$/fluid ratios and pH <4 (Fig. 7b, c). No linear correlation is observed between elution and $LiFePO_4$/fluid ratio (Fig. 7b), and no increased Fe and P elution is observed during kinetic delithiation experiments at pH as low as 2.3 (Fig. 6b). Thus, both a $LiFePO_4$/fluid ratio <25 g/L and pH <4

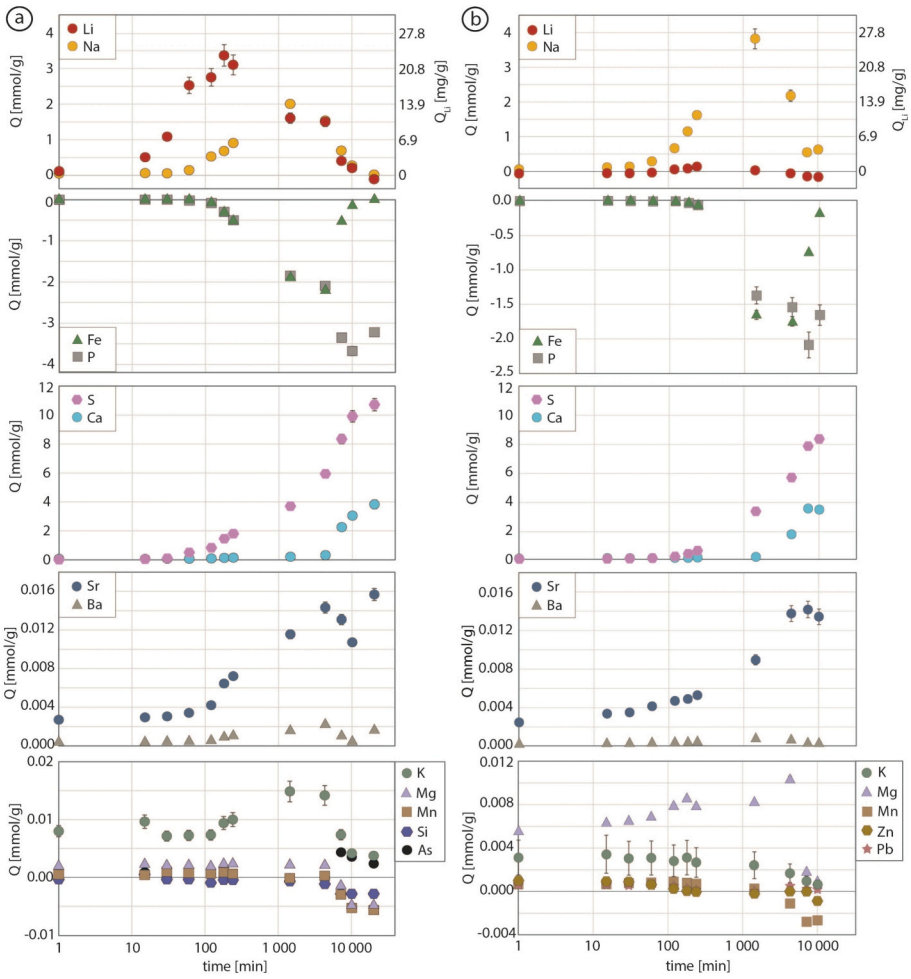

Fig. 9. Lithiation kinetics from geothermal brines plotted as sorption capacity [mmol/g] vs. reaction time [min]. The experiments were conducted at 60 °C, 5 g/L $FePO_4$, 160 mg/L and 10 mg/L initial Li concentration for a) Bruchsal and b) Neustadt-Glewe geothermal brines, respectively.

seem to affect $LiFePO_4$ stability negatively and should be avoided in DLE.

4.3. Lithiation experiments with pure LiCl – $Na_2S_2O_3$ solution

$FePO_4$ lithiation is a redox reaction of $Fe^{+III} \rightarrow Fe^{+II}$ under consumption of $Na_2S_2O_3$ (F.4) [24].

$$2\,Li^{+} + 2\,Fe^{+III}PO_4 + 2\,\left[S_2^{+II}O_3\right]^{2-} \rightarrow 2\,LiFe^{+II}PO_4 + \left[S_2^{0}\left(S^{+V}O_3\right)_2\right]^{2-} \quad \text{(F.4)}$$

Li sorption increases within 24 h with increasing $Na_2S_2O_3$ concentration (Fig. 8a). Thus, the mechanism of lithiation shows positive correlation of sorption kinetics and sorption capacity with increasing reducing agent concentration.

$FePO_4$ is not affected by the $Na_2S_2O_3$ additive since Fe and P loss is below the detection limit during 24 h reaction time at 25 °C. The increasing sorption of Na and S with increasing $Na_2S_2O_3$ concentration may indicate insufficient rinsing of the $FePO_4$ after filtration, rather than sorption to $FePO_4$ (Fig. 8a). However, in kinetic experiments using 0.5 M $Na_2S_2O_3$, Na and S are progressively sorbed to $FePO_4$ with longer reaction time (Fig. 8b). The observation cannot be explained by rinsing effects since the initial concentration of $Na_2S_2O_3$ and the $FePO_4$/fluid ratio are constant. In a DLE process, lithiation should thus be stopped immediately after reaching equilibrium, reducing the sorbed amount of Na and S and avoiding $FePO_4$ dissolution (Fig. 8b).

The rather long equilibration time of seven days (Fig. 8b) results from the low, 0.5 M additive concentration and will be faster if a higher concentration of $Na_2S_2O_3$ is used (Fig. 8a). The lithiation kinetics fit well with a pseudo-first-order (PFO) kinetic model (F.5), with the variables $k_1 = 0.00036248\ min^{-1}$ (rate constant in the PFO equation), $Q_{Equ} = 43$ mg/g (maximum Li uptake) and Q_t (Li uptake at any time t) [31].

$$Q_t = Q_{Equ}\left(1 - e^{-k_1 t}\right). \quad \text{(F.5)}$$

The Li sorption at 25 and 40 °C (Fig. 8c) is described by a Langmuir isotherm with the K_L values 0.2445 (25 °C) and 0.0239 (40 °C) derived from the Scratchard linearization of the Langmuir model [31]. The steep initial slope of the isotherm at 25 °C indicates a high affinity of $FePO_4$ to Li [31], which is for a prerequisite of DLE. Temperatures >40 °C have a negative influence on the process (Fig. 8c). The sorption of Li to $FePO_4$ is thus different from many other sorption processes, where kinetics are slowest at low temperatures due to slower ion diffusion rates and equilibrium is identified by a stable plateau with longer reaction time [e.g., 41,42]. At 25 °C, the initial pH is 9.0–9.1, whereas the initial pH of the solution at 40 °C is 8.5–9.0, at 60 °C pH = 5.0–5.3 and at 80 °C pH = 5.0–5.5. The pH ≤5.5 at 60 and 80 °C may be the reason for Li not intercalating into $FePO_4$ at these temperatures. After the experiments, the pH is 6.4–8.0 (25 °C), 4.2–5.1 (40 °C), 4.1–4.4 (60 °C) and 5.0 (80 °C), respectively (Fig. 8c). The acidification during the experiments, however, does not correlate with the (equilibrium) Li concentration and is thus not a result of a potential additional $Li^+ - H^+$ ion exchange process. It seems more likely that the $Na_2S_2O_3$ additive becomes unstable during Li extraction and/or at elevated temperatures, leading to acidification during heating already prior to the start of the experiments.

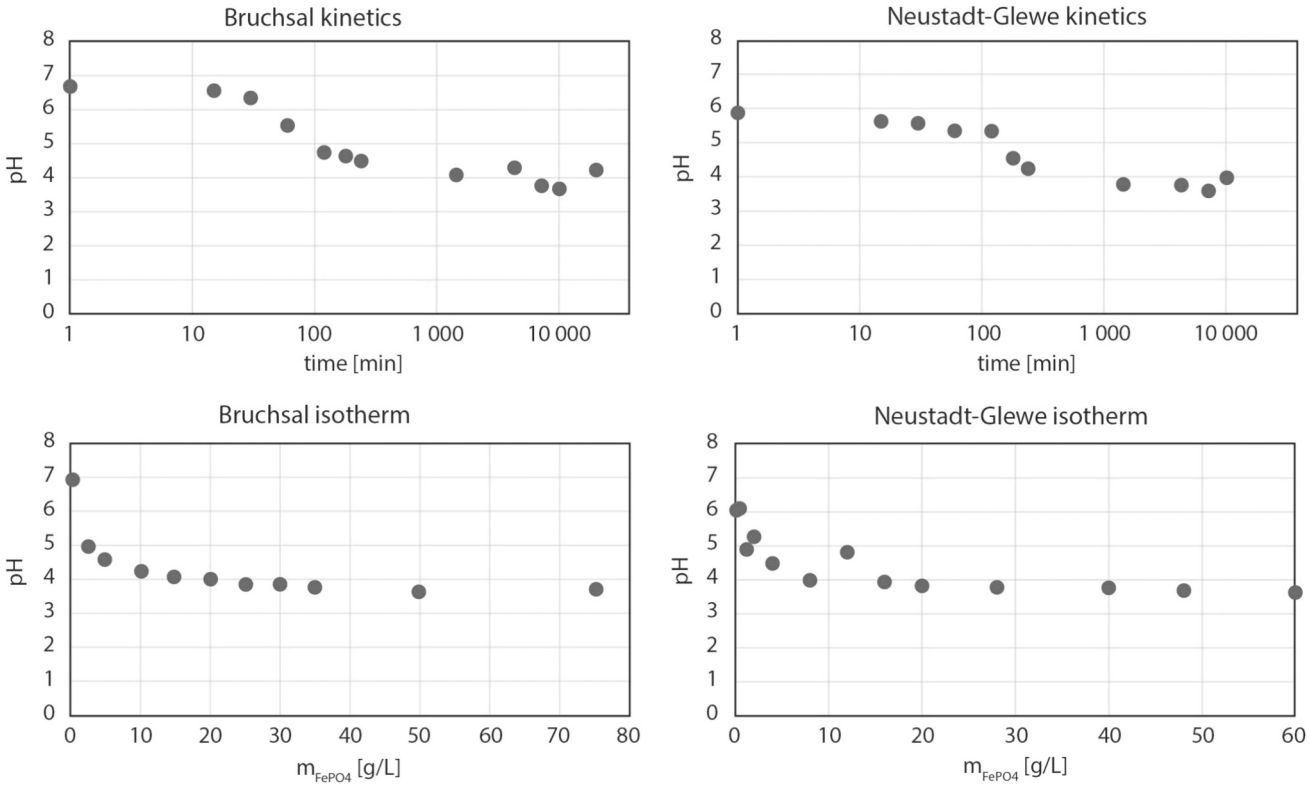

Fig. 10. pH variations in DLE experiments with geothermal brines. The experiments were conducted at 60 °C and initial Li concentrations of 160 mg/L (Bruchsal) and 10 mg/L (Neustadt-Glewe). A $FePO_4$/brine ratio of 5 g/L was used in kinetic experiments and the stirring time in isotherm experiments was 3 h (Bruchsal) and 4 h (Neustadt-Glewe).

4.4. *Lithiation from geothermal brines*

The Li sorption kinetics in experiments using both brines does not reach a plateau (Fig. 9), known from sorption kinetics in general [e.g., 41,42]. Lithium and Na show the same sorption behaviour, indicating that they are both intercalated into $FePO_4$, sharing the same sorption site in M1. The time gap between Li and Na sorption may be a result of different diffusivity. Possibly the Li diffusivity in *b* direction during phase transformation of $FePO_4$ to $LiFePO_4$, progressively expands the unit cell up to 6.8 vol% [2] and thereby opens the pathway for Na to intercalate into LFP in *b* direction.

The Bruchsal lithiation isotherm is described by a Langmuir sorption behaviour for equilibrium Li concentrations of <80 mg/L (Fig. 11a). In the isotherm experiments, Na shows a contradictory behaviour to Li (Fig. 11b), confirming that Na and Li are competing ions in the M1 sorption site. After the maximum Li sorption in kinetic experiments, $FePO_4$ dissolution starts and Li is eluted into the brine (Fig. 9). Iron and P dissolution starts after 1–2 h reaction time, i.e. shortly after Na starts to intercalate into $FePO_4$ (Fig. 9), and is at maximum when Na sorption is at maximum. Similar to the kinetic experiments, the $FePO_4$ dissolution positively correlates with the Na sorption and decreases at $FePO_4$/brine ratios >5 g/L, (Fig. 11b). Since the intercalation of Na into $FePO_4$ leads to an expansion of the unit cell volume by 16.6 vol% [14], the stability of $FePO_4$ may be negatively influenced by Na intercalation, leading to its dissolution.

The observed surface roughness of the LFP particles is the result of daughter crystals that nucleate on their surface. EDX and XRD data indicate that native sulfur may occur on the surface of the LFP, whereas the euhedral crystals are identified as gypsum (Fig. 2V.). The samples from experiments with synthetic geothermal brine of Neustadt-Glewe composition show the same: No secondary phases are visible until the maximum sorption capacity is reached (Fig. 1g). At longer reaction time, however, native sulfur and gypsum precipitate like in the other samples (Fig. 1f, h). In the experiments with synthetic brine, native sulfur does not occur on the LFP surface but forms larger aggregates (Fig. 1f, h). The precipitation of gypsum and native sulfur explains the S and Ca geochemical data (Fig. 9) and confirms that S and Ca are not mainly sorbed to $FePO_4$, but precipitated in other phases.

The extracted amount of Ba and Sr is similar for both tested brine compositions, which is explained by similar starting concentrations (Table 2). Due to the similar geochemical behaviour of Sr, Ba and Ca, the increase in Sr and Ba extraction may be an effect of progressing gypsum precipitation, rather than sorption to $FePO_4$. Gypsum and native sulfur are known to precipitate due to decreasing pH [43–45]. The extraction of Ca, S, Ba and Sr, i.e. gypsum and sulfur precipitation, already occurs before the dissolution of $FePO_4$ starts (Fig. 9); and the dissolution of Fe and P starts before the equilibrium pH at ~5.5 is reached. This indicates limited $FePO_4$ stability at pH <5.5 (Fig. 10). The decrease in pH is a function of the $FePO_4$/brine ratio (Fig. 10) and the sorbent stability behaves differently compared to delithiation experiments, due to the different matrices, i.e. $Na_2S_2O_8$ for delithiation and $Na_2S_2O_3$ for lithiation.

It is likely that the decrease in pH leading to $FePO_4$ dissolution and co-precipitation of secondary phases is a result of $Na_2S_2O_3$ instability. Disproportionation of $Na_2S_2O_3$ (F.6) [45] leads to SO_4^{2-} formation and H_2S degassing, recognized by the characteristic smell in the laboratory during pre-heating and during the experiments. Since the reaction vessels are closed during the experiments, a liquid/vapor equilibrium may form, leading to brine acidification (F.7) [45]. Disproportionation may be the reason that no Li was extracted from LiCl solutions at 60–80 °C since degassing of H_2S may be catalyzed by increasing temperature. Thus, $Na_2S_2O_3$ may already be fully consumed during the seven days reaction time at high temperatures or during pre-heating of the partially closed vessels (to prevent overpressure), not being able to support the redox reaction. The SO_4^{2-} species forms gypsum in reaction with Ca^{2+} ions from the geothermal brine. Thus, gypsum precipitation is not

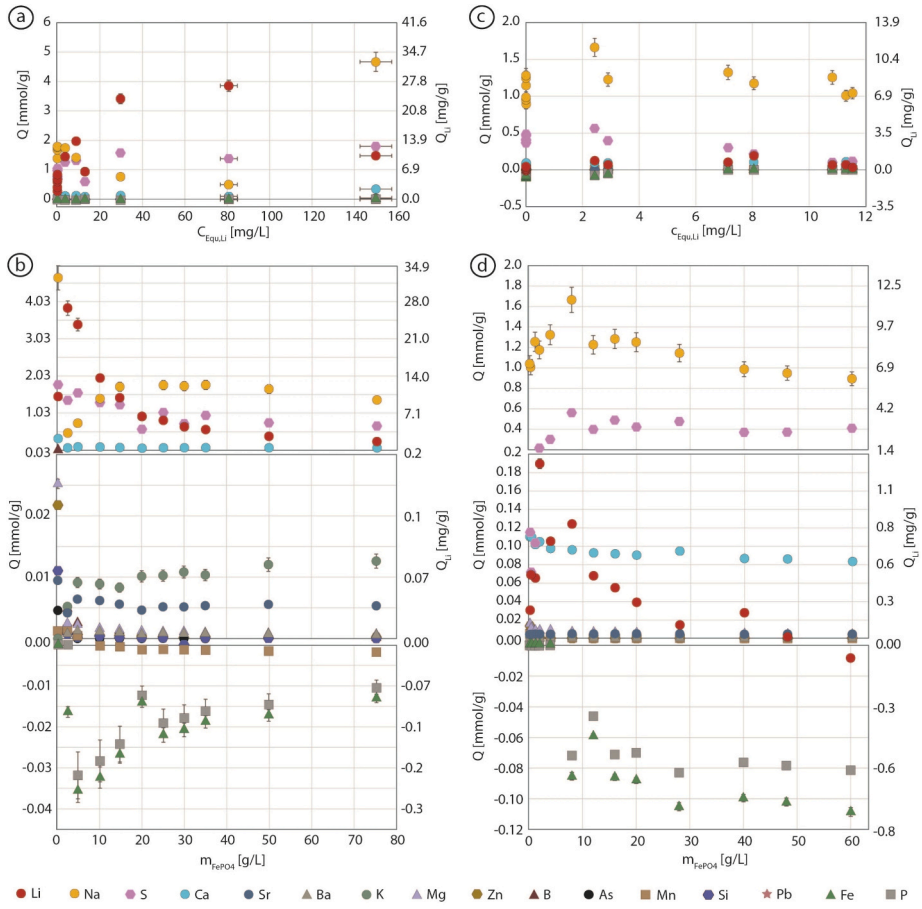

Fig. 11. Lithiation isotherms from geothermal brines. a) Sorption capacity (Q) in mmol/g vs. equilibrium Li concentration ($C_{Equ,Li}$) in mg/L (Bruchsal), b) sorption capacity (Q) in mmol/g vs. $FePO_4$/brine ratio [g/L] (Bruchsal), c) sorption capacity (Q) in mmol/g vs. equilibrium Li concentration ($C_{Equ,Li}$) in mg/L (Neustadt-Glewe) and d) sorption capacity (Q) in mmol/g vs. $FePO_4$/brine ratio [g/L] (Neustadt-Glewe). The experiments were conducted at 60 °C, 160 mg/L and 10 mg/L initial Li concentration for a + b) Bruchsal and c + d) Neustadt-Glewe geothermal brines, respectively. The reaction time was 3 h with Bruchsal and 4 h with Neustadt-Glewe geothermal brine.

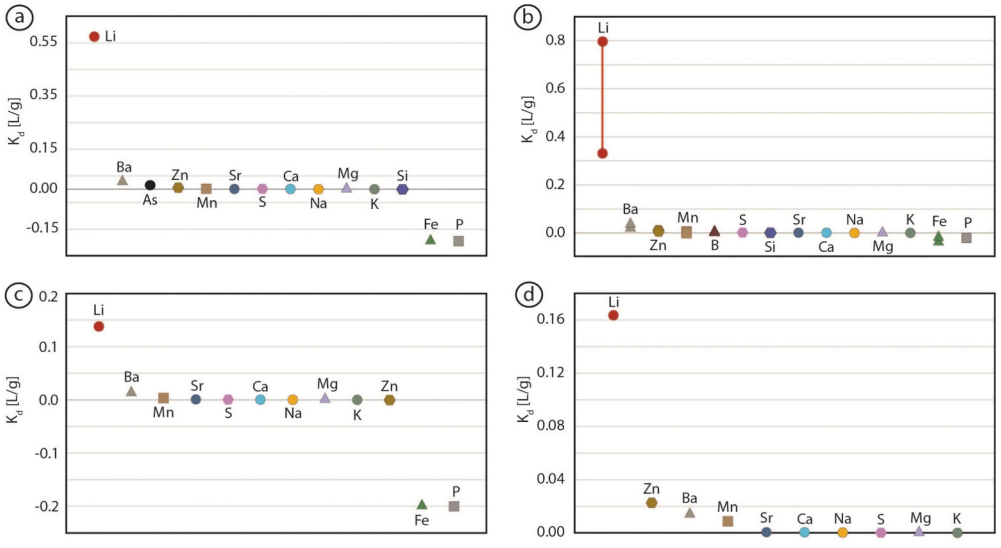

Fig. 12. Distribution coefficients for optimal Li extraction conditions. The experiments were conducted at 60 °C and initial Li concentrations of 160 mg/L (Bruchsal) and 10 mg/L (Neustadt-Glewe). a) Three hours reaction time (Bruchsal), b) 2.5–5 g/L $FePO_4$/brine ratio in isotherm experiments (Bruchsal), c) four hours reaction time (Neustadt-Glewe) and d) 2 g/L $FePO_4$/brine ratio in isotherm experiments (Neustadt-Glewe).

Table 3
Equilibrium Li concentration, sorption capacity [mg/g and mmol/g], K_d value and selectivity estimation for different elements at maximum Li intercalation in kinetics and isotherm experiments with geothermal brines.

	Li	Na	K	Mg	Ca	Sr	Ba	B	Si	Pb	P	As	S	Mn	Fe	Zn
Bruchsal kinetics, 3 h																
C_{Equ} [mg/L]	41	58,640	3240	330	7390	360	4.7	36	22	–	47	3.0	32,530	21	90	9.3
Load [mg/g]	23	16	0.4	0.06	5.4	0.6	0.1	<002	−0.01	<LOQ	−9.2	0.05	47	0.05	−17	0.06
Load [mmol/g]	3.37	0.68	0.01	0.002	0.13	0.01	0.001	<0.0002	−0.0004	<LOQ	−0.3	0.001	1.46	0.001	−0.31	0.001
K_d value [L/g]	0.5729	0.0003	0.0001	0.0001	0.0007	0.0016	0.0267	–	−0.0005	–	−0.1947	0.0157	0.0014	0.0023	−0.1947	0.0059
Selectivity order	1	9	11	10	8	6	2	–	12	–	14	3	7	5	13	4
Bruchsal isotherm, 2.5–5 g/L LFP/brine ratio																
C_{Equ} [mg/L]	30–81	54,890–55,020	3100	330	6910–6940	350	5.3–5.8	37	19–20	–	<LOQ – 48	<LOQ	32,910–33,130	19	23–97	6.0–6.1
Load [mg/g]	24–27	11–17	0.2–0.4	0.06	3.8–5.0	0.4–0.6	0.1–0.2	0.03–0.05	0.01–0.02	<LOQ	<LOQ – −1	<LOQ – 0.1	44–50	0.03–0.08	−1 to −2	0.04–0.06
Load [mmol/g]	3.41–3.85	0.49–0.76	0.01	0.02	0.09–0.12	0.004–0.01	0.001	0.003–0.005	0.000–0.001	<LOQ	<LOQ – −0.03	<LOQ – 0.001	1.37–1.57	0.0005–0.001	−0.02 to −0.04	0.001
K_d value [L/g]	0.3313–0.7965	0.0002–0.0003	0.0001	0.0001	0.0005–0.0007	0.001–0.0016	0.0183–0.0314	0.0007–0.0015	0.0003–0.0011	–	−0.0204	–	0.0013–0.0015	0.0013–0.0042	−0.0204 to −0.0393	0.0067–0.0097
Selectivity order	1	10	12	11	9	8	2	5	7	–	14	–	6	4	13	3
Neustadt-Glewe kinetics, 4 h																
C_{Equ} [mg/L]	6.9	99,630	890	1300	8330	510	4.7	–	–	–	9.7	–	32,810	12	18	2.7
Load [mg/g]	1.0	37	0.1	0.2	4.1	0.5	0.1	–	–	0.02	−1.9	–	19	0.04	−3.7	−0.0003
Load [mmol/g]	0.14	1.62	0.003	0.01	0.10	0.01	0.0004	–	–	0.0001	−0.06	–	0.58	0.001	−0.07	−0.0000
K_d value [L/g]	0.1381	0.0004	0.0001	0.0001	0.0005	0.0009	0.01246	–	–	–	−0.2	–	0.0006	0.0033	−0.2	−0.0001
Selectivity order	1	7	9	8	6	4	2	–	–	–	12	–	5	3	11	10
Neustadt-Glewe isotherm, 2 g/L LFP/brine ratio																
C_{Equ} [mg/L]	8.1	97,970	950	1330	8050	460	2.9	–	–	–	<LOD	–	32,440	11	<LOQ	2.5
load [mg/g]	1.3	27	0.1	0.2	4.2	0.4	0.04	–	–	0.2	<LOD	–	6.9	0.1	<LOQ	0.1
load [mmol/g]	0.19	1.18	0.003	0.01	0.1	0.005	0.0003	–	–	0.001	<LOD	–	0.22	0.002	<LOQ	0.001
K_d value [L/g]	0.1636	0.0003	0.0001	0.0002	0.0005	0.0009	0.0138	–	–	–	–	–	0.0002	0.0087	–	0.0227
selectivity order	1	7	10	9	6	5	3	–	–	–	–	–	8	4	–	2

observed in the experiments with LiCl + $Na_2S_2O_3$ solution. According to (F.8), H_2S can react with SO_4^{2-} and H^+ to precipitate native sulfur [44]. An additional reaction that may take place is the decomposition of $Na_2S_2O_3$ with protons (e.g., from H_2S equilibrium in the closed vessels) that causes native sulfur precipitation (F.9) [45]. The combination of all the described reactions explains the processes observed in our experiments.

$$[S_2O_3]^{2-} + H_2O \rightleftarrows H_2S\uparrow + SO_4^{2-} \quad \text{(F.6)}$$

$$H_2S \rightleftarrows H^+ + HS^- \rightleftarrows 2H^+ + S^{2-} \quad \text{(F.7)}$$

$$3H_2S + SO_4^{2-} + 2H^+ \rightarrow 4S^0\downarrow + 4H_2O \quad \text{(F.8)}$$

$$Na_2S_2O_3 \xrightarrow{+2HCl,\,-2NaCl} H_2S_2O_3 \xrightarrow{-H_2SO_3} \frac{1}{n}S_n \quad \text{(F.9)}$$

No secondary phases, like gypsum or native sulfur are, however, observed in the isotherm experiments. The dissolution of Fe and P is significantly lower than in kinetic experiments which may result from higher $FePO_4$ stability due to minor Na intercalation and lattice expansion at shorter reaction times. In addition, the solution acidifies with increasing $FePO_4$/brine ratio to the same degree as in kinetic experiments (Fig. 10). Native sulfur and gypsum precipitation are thus not solely controlled by pH decrease but also by kinetics.

The strong decrease in Fe elution in kinetic experiments after the maximum (Fig. 9) may be explained by the formation of a new phase, which is, however, not detected by XRD or visible in SEM. It is more likely that Fe is a trace compound in the gypsum precipitate [46], since P elution remains at maximum at long stirring times.

A pH adjustment during lithiation of $FePO_4$ is not necessary since maximum Li intercalation is achieved at short reaction times, where Fe and P elution is low and the extraction process should be immediately stopped due to decreasing Li selectivity at longer reaction times, as discussed previously (Fig. 9). To improve stability of $FePO_4$ at reaction times >24 h, however, buffering may be advantageous due to $Na_2S_2O_3$ decomposition and brine acidification.

Since Na and S are already compounds in the geothermal brine, the increase in Na and S concentration in the geothermal brine by using $Na_2S_2O_3$ as reducing agent is regarded as uncritical. To overcome the challenge regarding limited $Na_2S_2O_3$ stability, another reducing agent may be used instead, e.g. ascorbate, iodide or hydride compounds, like NaI, $(AlH_3)_x$ or $NaBH_4$ [14,25,27,47]. The use of an ascorbate reducing agent, however, might be challenging for the DLE application in geothermal brines since ascorbic acid degrades with increasing fluid temperature [48]. Oxidation of ascorbate forms dehydroascorbate, which further degrades into different products, e.g. furan-2-carboxylic acid or furan-2-carbaldehyde [49,50]. Both are hazardous to water and the latter is potentially carcinogenic, which is disadvantageous for DLE from geothermal brines [51,52]. Iodine concentration in the geothermal brines is usually below detection limit and the introduction of iodine into the brine might be critical with respect environmental and legal aspects [53,54]. Aluminium hydride is thermally stable to up to 160 °C [55]. However, it is sensitive to moisture, i.e. it reacts strongly with water forming $Al(OH)_3$ and H_2 [45,55]. Sodium and B are components of geothermal brines, rendering $NaBH_4$ a potential option. Furthermore, hydrogen gas may be applied as reducing agent. Therefore, experiments to test the applicability of hydrides or hydrogen are suggested to substitute $Na_2S_2O_3$.

The kinetics of different elements, like Li and Na, Fe and P or Ca, S, Ba and Sr, is similar in extraction experiments from brines that have significantly different initial Li concentrations, i.e. Bruchsal and Neustadt-Glewe (Table 2). This emphasizes the reproducibility of the results and similar underlying extraction mechanisms. In electrochemical Li extraction, the selectivity is controlled by adjustment of the applied voltage [20,22]. The selectivity of the chemical DLE process using $FePO_4$ may be controlled by adjusting the reaction time, instead. The steep initial slope of the isotherms derived from experiments using LiCl + $Na_2S_2O_3$ solutions (Fig. 8c) and the successful extraction of Li from saline geothermal brine (Section 3.5) confirm high Li selectivity of $FePO_4$. The DLE process, however, should be adjusted to optimal conditions to successfully extract Li among other elements, i.e. 3–4 h reaction time and an $FePO_4$/brine ratio of 2–10 g/L is determined in our experiments. Minor Fe and P loss, the potential formation of defects in the crystal lattice and variations in the maximum Li sorption capacity of LFP depend on the experimental setup and geochemical brine composition. This might affect the recycling potential of the sorbent and is of significance for the LFP reuse in multiple DLE cycles. Since the results for both brine compositions are similar, the data and identified optimal conditions are likely also applicable to other (unbuffered) brines, but should, however, be tested and verified.

The lithiation isotherms for the Bruchsal and Neustadt-Glewe geothermal brines show that the Li extraction using $FePO_4$ is successful for brines with initial Li concentrations between 10 and 160 mg/L (Table 2), reaching a Li recovery of >99 % within one extraction cycle (Fig. 11a, c). This is an advantage for a chemical DLE process using LFP compared to electrochemical DLE using LFP. Comparably high Li recoveries of 98 % can be reached by electrochemical techniques, but several delithiation – lithiation cycles are needed, e.g. 3 cycles from a LiCl solution containing 60 mg/L Li [22]. Eight extraction cycles are needed to recover 91 % Li from a low saline brine [21]. Thus, more cycles may be required to reach as high Li recoveries from high saline geothermal brines, but experimental data is sparse [20,22].

5. Conclusions

Lithium completely de-intercalates from and re-intercalates into $LiFePO_4$ (LFP) in a mineralogically and chemically fully reversible redox process. This study investigates the application of LFP for the direct Li extraction (DLE) from two chemically different geothermal brines in Germany. The Li-poor phase, used for DLE, is orthorhombic heterosite $FePO_4$. The Li-rich phase is orthorhombic triphylite $LiFePO_4$.

A starting LFP cathode material is delithiated using 0.1 M $Na_2S_2O_8$. Within 1 min reaction time, 43 mg/g Li are successfully extracted at an $LiFePO_4$/volume ratio of 0.5–35 g/L. Lithiation of $FePO_4$ is positively correlating with the concentration of the reducing agent ($Na_2S_2O_3$). For optimal Li extraction in a 0.5 M $Na_2S_2O_3$ matrix, a reaction time of 3–4 h and an $FePO_4$/brine ratio of 2–10 g/L is estimated. The Li extraction process should immediately be stopped when the highest Li sorption capacity is achieved. Otherwise, Li extraction is inefficient, $FePO_4$ stability decreases and secondary phases, like gypsum and native sulfur, precipitate. >99 % Li are recovered from the Bruchsal geothermal brine and the synthetic brine of Neustadt-Glewe in the laboratory, confirming a similar elemental behaviour and the reproducibility of the results for different brines.

We show that LFP is successfully used for Li extraction from geothermal brine in Germany in a purely chemical DLE process with very high recovery and high Li-load within one cycle. Limitations are few crystal defects that are imposed during the process, which indicates potential sorbent aging, and the $Na_2S_2O_3$ redox agent that causes side reactions and that better would be replaced by an alternative material during up-scaling. A major challenge for upscaling the presented technique to industrial scale is the handling of nanoparticles in a high flow regime like geothermal power plants. Technical solutions or formulation approaches and the investigation of the Li sorption performance of novel LFP-based materials are thus required.

CRediT authorship contribution statement

Rebekka Reich: Conceptualization, Methodology, *V*alidation, Formal analysis, Investigation, Resources, Writing - Original Draft, Writing - Review & Editing, Visualization, Project administration. **Elisabeth Eiche:** Conceptualization, Methodology, Resources, Writing -

Original Draft, Writing - Review & Editing, Supervision, Project administration, Funding acquisition. **Jochen Kolb:** Conceptualization, Methodology, Resources, Writing - Original Draft, Writing - Review & Editing, Supervision, Project administration, Funding acquisition.

Declaration of competing interest

The authors declare that they have no known competing financial interests or personal relationships that could have appeared to influence the work reported in this paper.

Data availability

Data will be made available on request.

Acknowledgements

We thank IBU-tec AG, Weimar, Germany for providing the LFP cathode material. We thank Julia Podszuweit and Günter Beuchle for the BET analysis. Laura Spitzmüller is acknowledged for performing FT-IR-ATR analyses. We thank Andrea Seibt for the experiments with synthetic Neustadt-Glewe geothermal brine. Nadine Hüll and Janine Wagner are acknowledged for sample digestion. Chantal Kotschenreuther and Maya Denker are acknowledged for their assistance with the ICP-OES and ICP-MS analyses, respectively. We thank Janine Wagner for her help during XRD data acquisition. Michèle Jungmann and the UnLimited project team members are thanked for their helpful contributions during all stages of this study. This research is part of the "UnLimited" project, funded by the German Federal Ministry for Economic Affairs and Climate Action under Grant O3EE4023D.

Appendix A. Supplementary data

Supplementary data to this article can be found online at https://doi.org/10.1016/j.desal.2024.117883.

References

[1] S.M. Zhang, J.X. Zhang, S.J. Xu, X.J. Yuan, T. Tian, Synthesis of nano-sized FePO4 cathode material via a microemulsion technique, Appl. Mech. Mater. 320 (2013) 675–682, https://doi.org/10.4028/www.scientific.net/AMM.320.675.
[2] A. Banday, R. Shahid, S.S. Meena, S. Yusuf, S. Murugavel, Effect of crystallite size on the phase transition behavior of heterosite FePO 4, Phys. Chem. Chem. Phys. 22 (2020) 15478–15487, https://doi.org/10.1039/D0CP02387F.
[3] J. Lee, P. Kumar, J. Lee, B.M. Moudgil, R.K. Singh, ZnO incorporated LiFePO4 for high rate electrochemical performance in lithium ion rechargeable batteries, J. Alloys Compd. 550 (2013) 536–544, https://doi.org/10.1016/j.jallcom.2012.10.092.
[4] A. Mauger, A. Ait-Salah, M. Massot, F. Gendron, K. Zaghib, C. Julien, Characterization of LiFePO4 at a Nanoscopic scale in relation to the mode of preparation, ECS Trans. 3 (2007) 57, https://doi.org/10.1149/1.2795106.
[5] C. Zhu, K. Weichert, J. Maier, Electronic conductivity and defect chemistry of heterosite FePO4, Adv. Funct. Mater. 21 (2011) 1917–1921, https://doi.org/10.1002/adfm.201002059.
[6] T. Maxisch, G. Ceder, Elastic properties of olivine Li x FePO 4 from first principles, Phys. Rev. B 73 (2006) 174112, https://doi.org/10.1103/PhysRevB.73.174112.
[7] G. Rousse, J. Rodriguez-Carvajal, S. Patoux, C. Masquelier, Magnetic structures of the triphylite LiFePO4 and of its delithiated form FePO4, Chem. Mater. 15 (2003) 4082–4090, https://doi.org/10.1021/cm0300462.
[8] A. Losey, J. Rakovan, J.M. Hughes, C.A. Francis, M.D. Dyar, Structural variation in the lithiophilite–triphylite series and other olivine-group structures, Can. Mineral. 42 (2004) 1105–1115, https://doi.org/10.2113/gscanmin.42.4.1105.
[9] J.L. Dodd, B. Fultz, R. Yazami, Determining the phase diagram of LixFePO4, ECS Transactions 1 (2006) 27, https://doi.org/10.1149/1.2209354.
[10] M. Wagemaker, D.P. Singh, W.J. Borghols, U. Lafont, L. Haverkate, V.K. Peterson, F.M. Mulder, Dynamic solubility limits in nanosized olivine LiFePO4, J. Am. Chem. Soc. 133 (2011) 10222–10228, https://doi.org/10.1021/ja2026213.
[11] N. Meethong, H.-Y.S. Huang, W.C. Carter, Y.-M. Chiang, Size-dependent lithium miscibility gap in nanoscale Li1− x FePO4, Electrochem. Solid St. 10 (2007) A134, https://doi.org/10.1149/1.2710960.
[12] F. Omenya, N.A. Chernova, Q. Wang, R. Zhang, M.S. Whittingham, The structural and electrochemical impact of Li and Fe site substitution in LiFePO4, Chem. Mater. 25 (2013) 2691–2699, https://doi.org/10.1021/cm401293r.
[13] A. Moretti, G. Giuli, F. Nobili, A. Trapananti, G. Aquilanti, R. Tossici, R. Marassi, Structural and electrochemical characterization of vanadium-doped LiFePO4 cathodes for lithium-ion batteries, J. Electrochem. Soc. 160 (2013) A940, https://doi.org/10.1149/2.133306jes.
[14] J. Lu, S.C. Chung, S.-i. Nishimura, A. Yamada, Phase diagram of olivine Na x FePO4 (0< x< 1), Chem. Mater., 25 (2013) 4557–4565, doi:https://doi.org/10.1021/cm402617b.
[15] A.S. Andersson, B. Kalska, L. Häggström, J.O. Thomas, Lithium extraction/insertion in LiFePO4: an X-ray diffraction and Mössbauer spectroscopy study, Solid State Ion. 130 (2000) 41–52, https://doi.org/10.1016/S0167-2738(00)00311-8.
[16] M. Gadgil, S. Kulshreshtha, Study of FePO4 catalyst, J. Solid State Chem. 111 (1994) 357–364, https://doi.org/10.1006/jssc.1994.1239.
[17] G. Kobayashi, S.i. Nishimura, M.S. Park, R. Kanno, M. Yashima, T. Ida, A. Yamada, Isolation of solid solution phases in size-controlled LixFePO4 at room temperature, Adv. Funct. Mater. 19 (2009) 395–403, https://doi.org/10.1002/adfm.200801522.
[18] Y. Kuk, J. Hwang, D. Nam, J. Kim, Facile synthesis of high-performance LiFePO4-reduced graphene oxide composites using ball milling, Ionics 26 (2020) 2803–2812, https://doi.org/10.1007/s11581-019-03395-6.
[19] F. Larouche, F. Voisard, K. Amouzegar, G. Houlachi, P. Bouchard, A. Vijh, G. P. Demopoulos, Kinetics, mechanism, and optimization modeling of a green LFP Delithiation process developed for direct recycling of Lithium-ion batteries, Ind. Eng. Chem. Res. 62 (2023) 903–915, https://doi.org/10.1021/acs.iecr.2c03552.
[20] X. Liu, X. Chen, Z. Zhao, X. Liang, Effect of Na+ on Li extraction from brine using LiFePO4/FePO4 electrodes, Hydrometallurgy 146 (2014) 24–28, https://doi.org/10.1016/j.hydromet.2014.03.010.
[21] S. Sun, X. Yu, M. Li, J. Duo, Y. Guo, T. Deng, Green recovery of lithium from geothermal water based on a novel lithium iron phosphate electrochemical technique, J. Clean. Prod. 247 (2020) 119178, https://doi.org/10.1016/j.jclepro.2019.119178.
[22] Z. Zhao, X. Si, X. Liu, L. He, X. Liang, Li extraction from high mg/Li ratio brine with LiFePO4/FePO4 as electrode materials, Hydrometallurgy 133 (2013) 75–83, https://doi.org/10.1016/j.hydromet.2012.11.013.
[23] K. Liu, Q. Tan, L. Liu, J. Li, Acid-free and selective extraction of lithium from spent lithium iron phosphate batteries via a mechanochemically induced isomorphic substitution, Environ. Sci. Technol. 53 (2019) 9781–9788, https://doi.org/10.1021/acs.est.9b01919.
[24] N. Intaranont, N. Garcia-Araez, A. Hector, J. Milton, J. Owen, Selective lithium extraction from brines by chemical reaction with battery materials, J. Mater. Chem. A 2 (2014) 6374–6377, https://doi.org/10.1039/C4TA01101E.
[25] C. Kuss, M. Carmant-Dérival, N.D. Trinh, G. Liang, S.B. Schougaard, Kinetics of Heterosite Iron phosphate Lithiation by chemical reduction, J. Phys. Chem. C 118 (2014) 19524–19528, https://doi.org/10.1021/jp502346f.
[26] D. Lepage, F. Sobh, C. Kuss, G. Liang, S. Schougaard, Delithiation kinetics study of carbon coated and carbon free LiFePO4, J. Power Sources 256 (2014) 61–65, https://doi.org/10.1016/j.jpowsour.2013.12.054.
[27] J. Xiong, Z. Zhao, D. Liu, L. He, Direct lithium extraction from raw brine by chemical redox method with LiFePO4/FePO4 materials, Sep. Purif. Technol. 290 (2022) 120789, https://doi.org/10.1016/j.seppur.2022.120789.
[28] Y. Yang, X. Meng, H. Cao, X. Lin, C. Liu, Y. Sun, Y. Zhang, Z. Sun, Selective recovery of lithium from spent lithium iron phosphate batteries: a sustainable process, Green Chem. 20 (2018) 3121–3133, https://doi.org/10.1039/C7GC03376A.
[29] R. Reich, K. Slunitschek, R.M. Danisi, E. Eiche, J. Kolb, Lithium extraction techniques and the application potential of different sorbents for Lithium recovery from brines, Miner. Process. Extr. Metall. Rev. (2022) 1–20, https://doi.org/10.1080/08827508.2022.2047041.
[30] JCPDS-ICDD, PDF-2 Release 2002, In, ICDD, Newton Square, Pennsylvania, USA, 2002.
[31] H.N. Tran, S.-J. You, A. Hosseini-Bandegharaei, H.-P. Chao, Mistakes and inconsistencies regarding adsorption of contaminants from aqueous solutions: a critical review, Water Res. 120 (2017) 88–116, https://doi.org/10.1016/j.watres.2017.04.014.
[32] R. Reich, R.M. Danisi, T. Kluge, E. Eiche, J. Kolb, Structural and compositional variation of zeolite 13X in lithium sorption experiments using synthetic solutions and geothermal brine, Microporous Mesoporous Mater. 359 (2023) 112623, https://doi.org/10.1016/j.micromeso.2023.112623.
[33] E. Muneyama, A. Kunishige, K. Ohdan, M. Ai, Reduction and reoxidation of iron phosphate and its catalytic activity for oxidative dehydrogenation of isobutyric acid, J. Catal. 158 (1996) 378–384, https://doi.org/10.1006/jcat.1996.0039.
[34] M.T. Paques-Ledent, P. Tarte, Vibrational studies of olivine-type compounds—II orthophosphates,-arsenates and-vanadates AIBIIXVO4, Spectrochim. Acta A: Mol. Spectrosc. 30 (1974) 673–689, https://doi.org/10.1016/0584-8539(74)80190-X.
[35] C.M. Burba, R. Frech, In situ transmission FTIR spectroelectrochemistry: a new technique for studying lithium batteries, Electrochim. Acta 52 (2006) 780–785, https://doi.org/10.1016/j.electacta.2006.06.007.
[36] A. Ait-Salah, J. Dodd, A. Mauger, R. Yazami, F. Gendron, C. Julien, Structural and magnetic properties of LiFePO4 and lithium extraction effects, Z. Anorg. Allg. Chem. 632 (2006) 1598–1605, https://doi.org/10.1002/zaac.200600090.
[37] N. Rajić, R. Gabrovšek, V. Kaučič, Thermal investigation of two FePO materials prepared in the presence of 1, 2-diaminoethane, Thermochim. Acta 359 (2000) 119–122, https://doi.org/10.1016/S0040-6031(00)00512-8.
[38] F. Faure, N. Arndt, G. Libourel, Formation of spinifex texture in komatiites: an experimental study, J. Petrol. 47 (2006) 1591–1610, https://doi.org/10.1093/petrology/egl021.

[39] R. Miyawaki, F. Hatert, M. Pasero, S.J. Mills, IMA Commission on new minerals, nomenclature and classification (CNMNC) – newsletter 67, Eur. J. Mineral. 34 (2022) 359–364, https://doi.org/10.5194/ejm-34-359-2022.
[40] R. Miyawaki, F. Hatert, M. Pasero, S.J. Mills, IMA Commission on new minerals, nomenclature and classification (CNMNC) – newsletter 62, Eur. J. Mineral. 33 (2021) 479–484, https://doi.org/10.5194/ejm-33-479-2021.
[41] J. Lemaire, L. Svecova, F. Lagallarde, R. Laucournet, P.-X. Thivel, Lithium recovery from aqueous solution by sorption/desorption, Hydrometallurgy 143 (2014) 1–11, https://doi.org/10.1016/j.hydromet.2013.11.006.
[42] G. Limousin, J.-P. Gaudet, L. Charlet, S. Szenknect, V. Barthes, M. Krimissa, Sorption isotherms: a review on physical bases, modeling and measurement, Appl. Geochem. 22 (2007) 249–275, https://doi.org/10.1016/j.apgeochem.2006.09.010.
[43] Y.O. Rosenberg, I.J. Reznik, S. Zmora-Nahum, J. Ganor, The effect of pH on the formation of a gypsum scale in the presence of a phosphonate antiscalant, Desalination 284 (2012) 207–220, https://doi.org/10.1016/j.desal.2011.08.061.
[44] J. Alonso-Azcárate, S. Bottrell, J. Tritlla, Sulfur redox reactions and formation of native sulfur veins during low grade metamorphism of gypsum evaporites, Cameros Basin (NE Spain), Chem. Geol. 174 (2001) 389–402, https://doi.org/10.1016/S0009-2541(00)00286-2.
[45] A.F. Holleman, N. Wiberg, Grundlagen und Hauptgruppenelemente, Walter de Gruyter GmbH & Co KG, 2016.
[46] L. Chang, R. Howie, J. Zussman, Rock-Forming Minerals, Volume 5B, Non-Silicates, Sulphates, Carbonates, Phosphates and Halides. Second Edition, The Geological Society, London, 1996.
[47] E. Walker, The functional group selectivity of complex hydride reducing agents, Chem. Soc. Rev. 5 (1976) 23–50, https://doi.org/10.1039/CS9760500023.
[48] B.G. Ruiz, S. Roux, F. Courtois, C. Bonazzi, Kinetic modelling of ascorbic and dehydroascorbic acids concentrations in a model solution at different temperatures and oxygen contents, Food Res. Int. 106 (2018) 901–908, https://doi.org/10.1016/j.foodres.2018.01.051.
[49] E. Kimoto, H. Tanaka, T. Ohmoto, M. Choami, Analysis of the transformation products of dehydro-L-ascorbic acid by ion-pairing high-performance liquid chromatography, Anal. Biochem. 214 (1993) 38–44, https://doi.org/10.1006/abio.1993.1453.
[50] J.-P. Yuan, F. Chen, Degradation of ascorbic acid in aqueous solution, J. Agric. Food Chem. 46 (1998) 5078–5082, https://doi.org/10.1021/jf9805404.
[51] IFA, GESTIS-Substance Database: 2-Furaldehyde, (2024) https://gestis.dguv.de/data?name=025010&lang=en (11.04.2024).
[52] ThermoFisher Scientific, Sicherheitsdatenblatt gemäß Verordnung (EG) Nr. 1907/2006: Brenzschleimsaeure, (2023) https://www.fishersci.ch/store/msds?partNumber=10309323&countryCode=CH&language=de (11.04.2024).
[53] R. Fuge, C.C. Johnson, Iodine and human health, the role of environmental geochemistry and diet, a review, Appl. Geochem. 63 (2015) 282–302, https://doi.org/10.1016/j.apgeochem.2015.09.013.
[54] S.A. Patil, R.R. Rodriguez-Berrios, D. Chavez-Flores, D.V. Wagle, A. Bugarin, Recent advances in the removal of radioactive iodine and iodide from the environment, ACS ES&T Water 3 (2023) 2009–2023, https://doi.org/10.1021/acsestwater.3c00111.
[55] P. Yao, H. Zhao, M. Zhang, C. Xia, T. Yang, Q. Li, Synthesis of α-AlH3 by organic liquid reduction method and its hydrogen desorption performance, Int. J. Hydrogen Energy (2023), https://doi.org/10.1016/j.ijhydene.2023.05.170.

6. Discussion

6.1 Comparison of synthetic zeolite 13X and LFP

Synthetic zeolite 13X and LFP are novel Li sorbents, which have been investigated for their applicability in DLE from geothermal brines in laboratory experiments using synthetic LiCl solutions and geothermal brines. The sorption kinetics in experiments with synthetic zeolite 13X are extremely fast, reaching equilibrium within one minute. In comparison, the reaction time required with LFP is much longer and is strongly dependent on the process temperature. Although an increased temperature has a positive effect on the sorption kinetics in LFP, the process requires 3 h for maximum Li extraction, i.e. still much longer than zeolite 13X.

Zeolite 13X has a lower maximum Li sorption capacity than LFP, but the maximum sorption capacity for both sorbents is rather high at 20.3 and 43 mg/g, respectively. The Li sorption capacity of zeolite 13X, however, decreases at slightly acidic pH. The decrease in maximum Li sorption capacity of LFP is not only a function of decreasing pH. Sodium intercalation decreases LFP stability and Li is simultaneously eluted by Fe and P dissolution. The decrease in pH in LFP experiments, however, may be minimized by using a reducing agent that is either more stable at the elevated ambient temperature of 60°C and the required reaction time or by using a reducing agent that does not decrease the pH during its decomposition as opposed to $Na_2S_2O_3$.

The Li sorption processes of both tested sorbents are different. The main sorption process of Li in zeolite 13X is a cation exchange of Na^+ by Li^+. Thereby, the Na concentration in the brine progressively increases with progressing Li extraction. The initial Na concentration of NaCl-dominated geothermal brines in Germany is usually high, e.g. 28 – 135 g/L (Reich et al., 2022; Sanjuan et al., 2016). A post-treatment would not be necessary, since Na concentrations by the Li^+ – Na^+ ion exchange are, assuming that all theoretically available Na sites in zeolite 13X are substituted by Li, only increased by at maximum 147 mg/g, i.e. 6.4 mmol/g (Reich et al., 2023). No chemicals are added when using zeolite 13X except for the potential addition of a buffering agent

or HCl or NaOH for pH adjustment. Thus, Na and Cl concentrations of the reinjected brine would be slightly higher, but Na and Cl are major brine components, anyway. The increase in concentration, however, cannot be quantified as it depends on the used sorbent/brine ratio.

The sorption process of Li to LFP, in contrast, is controlled by the reduction of Fe^{+III} to Fe^{+II}. Although the reduction of Fe does not lead to a change in brine chemistry during the extraction, the use of a reducing agent as an additive in this process is indispensable. By using 0.5M $Na_2S_2O_3$, the brine chemistry is strongly changed by an increase in Na and S concentration by a factor of 1.3 – 1.6 and 124 – 253, respectively (Reich et al., 2024). The decreasing pH during the decomposition of the additive is within an uncritical range, i.e. the pH value decreases from ~ 7 to ~ 4 (Reich et al., 2024) compared to the natural geothermal brine pH between 5 and 6 but the geothermal brine that was used in the laboratory experiments already had a starting pH of ~7. The higher pH is a result of degassing and previous mineral precipitation after sampling and brine storage in the laboratory. To conclusively estimate if the pH variation is critical at the industrial scale, on-site experiments with continuous pH monitoring, keeping the brine pressure constant to avoid brine degassing, must be performed. With the results, the decision for buffering or pH adjustment can be made. A post-treatment of the brine is necessary in case of reinjection, anyway, due to the change in Na and S concentration of the brine.

The limited Li selectivity of zeolite 13X is a crucial parameter that renders it inappropriate for DLE from geothermal brines. As long as the zeolite 13X cannot be modified towards higher Li selectivity, its application is limited to low saline fluids or fluids that do not contain competing ions, like Ca, K, Sr, Ba, Mn and As. LFP, in contrast, has a very high selectivity for Li, making it a suitable sorbent for selective Li extraction from fluids with a complex chemical composition.

6.2 Importance of novel sorbents

Synthetic zeolite 13X and LFP are novel sorbents that are competitive with commonly investigated sorbents like lithium-manganese oxide (LMO), lithium-titanium oxide (LTO) and lithium-aluminum hydroxide (often LADH). Zeolite 13X and LFP are both available on the market and do not require a complex, expensive or time-consuming synthesis that still needs to be established at an industrial scale (Reich et al., 2022; Xiao et al., 2015; Zhang et al., 2010).

The applicability of each sorbent for DLE from geothermal brines can be evaluated regarding Li selectivity, maximum Li sorption capacity, optimal temperature, sorbent stability, optimal pH and equilibration time (Figure 9, Table 2). The comparison of different sorbents based on literature data is challenging, because experiments with different sorbents have been conducted in different experimental setups and fluids. For Li^+ - H^+ exchanging sorbents, DLE experiments are often performed in synthetic LiOH solutions at alkaline pH (improving their sorption performance), although natural brines are usually NaCl dominated. The use of LiCl solutions is thus more convenient in DLE experiments. Furthermore, sorption experiments are conducted with different initial Li concentrations and higher initial Li concentrations usually increase the Li sorption capacity (e.g., Tian et al., 2010). For comparability, DLE research would benefit from a common standard for the conduction of experiments, although site-specific conditions must be considered as well. Similarly, experiments with natural brines are hardly comparable, because brine chemistries vary, which influences the sorption behavior, at least regarding selectivity estimations due to variable concentrations of competing ions (Intaranont et al., 2014; Reich et al., 2023; Reich et al., 2024).

Nonetheless, it is possible to summarize maximum or minimum values achieved for each parameter with different sorbents to illustrate general strengths and weaknesses of sorbents (Figure 9). A high Li selectivity, high maximum Li sorption capacity, sorbent stability and a short equilibration time are advantageous for DLE. A high Li selectivity is required to recover Li among competing ions. A high maximum sorption capacity is advantageous because less sorbent is needed to extract Li

efficiently. A high chemical stability increases the number of sorption – desorption cycles in which the sorbent can be reused and reduces the contamination of the brine by elements that are eluted from the sorbent. Fast sorption kinetics are especially required in DLE from geothermal brines as long-time brine storage at the surface bears the risk for scaling which needs to be minimized. Furthermore, due the high flow rates in geothermal power plants, pilot plants for DLE are currently often designed as flow-through reactors, which also benefit from fast sorption kinetics. An optimal DLE temperature between 60 – 80°C is in line with the temperature in the reinjection pipe of geothermal power plants and an operating pH at near natural brine pH ~ 5 – 6 is favorable.

Table 2. Parameters for the estimation of the sorbent applicability for geothermal brines in Figure 9. Data of different experimental conditions for LMO, LTO, LADH any amorphous/polymeric $Al(OH)_3$ compiled from (Bajestani et al., 2019; Choubey et al., 2017; Han et al., 2012; Hawash et al., 2010; Heidari and Momeni, 2017; Herrmann et al., 2022; Isupov et al., 1999; Lawagon et al., 2016; Orooji et al., 2022; Paranthaman et al., 2017; Prodromou, 2016; Qian et al., 2019; Seip et al., 2021; Shi et al., 2013; Zhang et al., 2023; Zhang et al., 2010). Data for zeolite 13X and LFP compiled from Reich et al. (2023) and Reich et al. (2024).

parameter	Li sorption capacity	optimal operating temperature	sorbent stability	optimal operating pH	equilibration time	Li selectivity
unit	mg/g	°C	–	–	h	–
LMO	53.5	70	poor	alkaline	24	good
LTO	94.5	60	very good	alkaline	10 – 192	good
LADH	13.4	90	moderate	3 – 8	1	good
$Al(OH)_3$	123	neglectable	poor	alkaline	24	good
Zeolite 13X	20.3	neglectable	moderate	8 – 9	0.02	bad
LFP	43	60	good	5 – 7	3 – 4	very good
abbreviation in Figure 9	$Q_{max,Li}$	optimal T	stability	optimal pH	t_{Equ}	selectivity
low applicability	0	0	poor	alkaline	210	low
high applicability	140	100	very good	acidic	0	very high

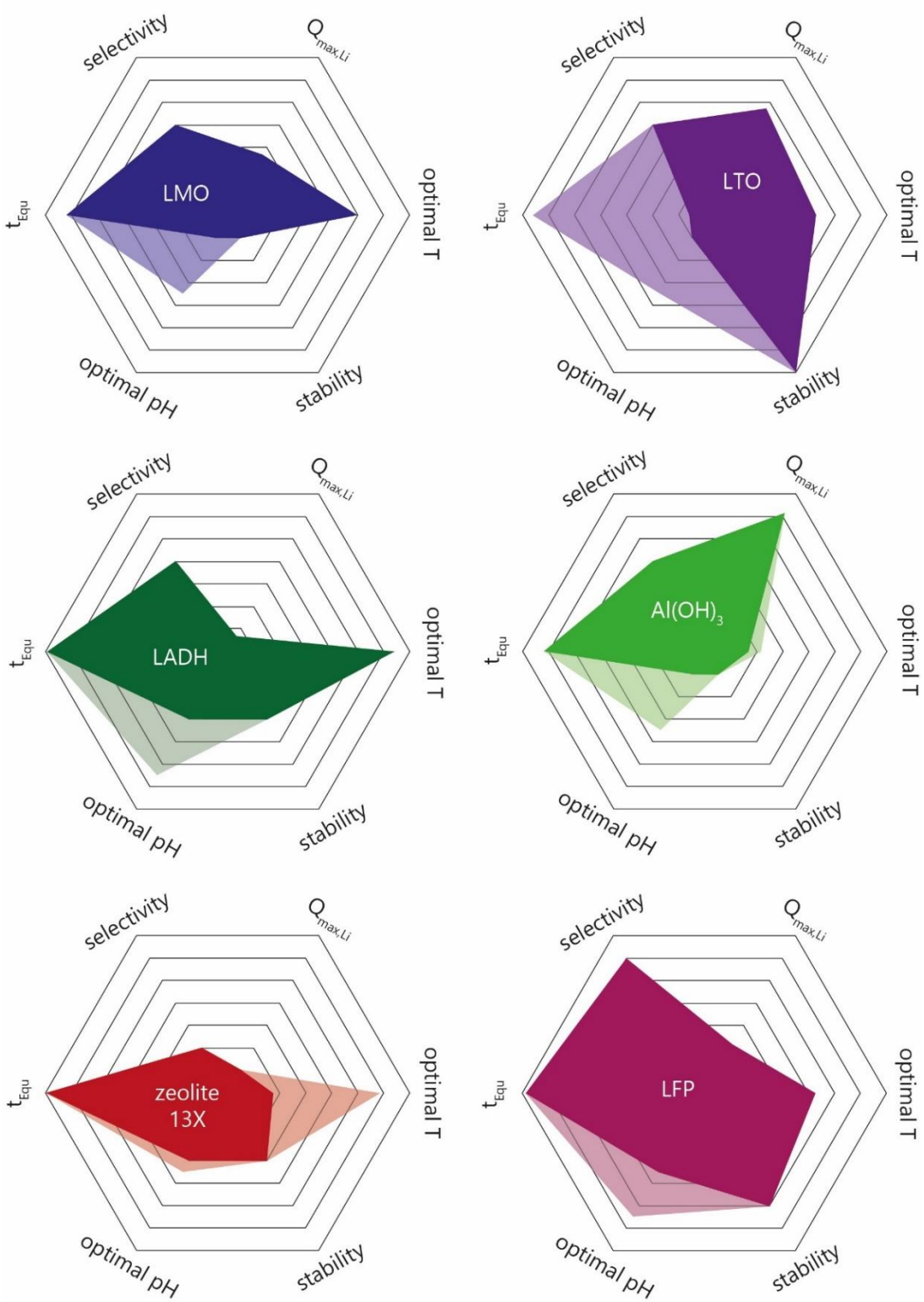

Figure 9. Comparison of different sorbents regarding Li selectivity, maximum Li sorption capacity ($Q_{max,Li}$), optimal T, sorbent stability, optimal pH and required equilibration time (t_{Equ}). Underlying data is given in Table 2. Larger fields indicate higher application potential in DLE from geothermal brines. Transparent fields illustrate the variability of one parameter. Data of different experimental conditions for LMO, LTO, LADH and amorphous/polymeric $Al(OH)_3$ sorbents compiled from Bajestani et al. (2019); Choubey et al. (2017); Han et al. (2012); Hawash et al. (2010); Heidari and Momeni (2017); Herrmann et al. (2022); Isupov et al. (1999); Lawagon et al. (2016); Orooji et al. (2022); Paranthaman et al. (2017); Prodromou (2016); Qian et al. (2019); Seip et al. (2021); Shi et al. (2013); Zhang et al. (2023); Zhang et al. (2010). Data for zeolite 13X and LFP compiled from Reich et al. (2023) and Reich et al. (2024).

For DLE from resources other than geothermal brines, e.g. salt lake brines, salars, seawater or industrial (waste) waters, fast sorption kinetics may be less important, because of less fluid volume that has to be processed or when fluid storage is uncritical. High Li selectivity may not be required in less complex fluid compositions, e.g. for Mg^{2+} – Li^{+} separation, the sorbent does not need to have a high Li selectivity compared to Na^{+}. The decision on a sorbent is thus very important and can only be made for the specific fluid composition and local conditions. The process temperature, operating pH and sorbent stability will always be important parameters for DLE and are regarded to have a higher influence on DLE performance than maximum sorption capacity, which, however, must be considered from an economic perspective.

In DLE from geothermal brines, the parameters are not regarded to be equally important for the selection of a sorbent. The limited Li selectivity of zeolite 13X for instance disqualifies it for DLE from complex brine compositions, although equilibration time and temperature are in line with ambient conditions in geothermal power plants. A low Li sorption capacity can well be compensated by a high Li selectivity and fast kinetics. Furthermore, the design of the extraction facility, as well as economic parameters, may render a sorbent with a lower sorption capacity more appropriate than a sorbent that has a high sorption capacity but requires strong acids for desorption (Hawash et al., 2010) or very long reaction times (Shi et al., 2013), where only a small amount of brine can be processed in the same time.

LMO and LTO exchange H^{+} by Li^{+} during sorption, thereby the pH is reduced, occasionally to pH ~ 1 (Chitrakar et al., 2012), which makes brine buffering indispensable. These sorbents usually have a high extraction efficiency at alkaline pH, which is unfavorable for DLE from geothermal brines, since alkaline pH may lead to scaling (Reich et al., 2022). This is at least not necessary when using LFP, operating at pH ~ 7. The equilibrium time strongly depends on the sorbent used. LMO usually needs to react for 24 h to reach Li sorption equilibrium, whereas LTO requires reaction times between 10 – 192 h and the kinetics of lithium-aluminum hydroxide vary between 1 – 24 h (Table 2). The high variability in equilibration time is a result of different

experimental conditions and slightly different materials used, e.g. regarding temperature, pH, fluid composition and mineralogical and trace element composition of the sorbent (Bajestani et al., 2019; Li et al., 2020; Prodromou, 2016; Shi et al., 2013; Zhang et al., 2023). Zeolite 13X and LFP both have very fast kinetics, favorable for a DLE process avoiding long time brine storage at the surface.

The maximum Li sorption capacity at equilibrium reaches ~ 50 – 123 mg/g when using LMO, LTO and polymeric $Al(OH)_3$ (Reich et al., 2022). Zeolite 13X and LFP do not reach as high Li sorption capacities, but many LADH, have significantly lower sorption capacities, i.e. 8 – 13.4 mg/g (Isupov et al., 1999; Zhang et al., 2023), and the reported maximum sorption capacities have been obtained in experiments under optimal pH and temperature conditions, not necessarily in line with ambient conditions for geothermal power plants (Reich et al., 2022). Thus, the sorption capacity is not as a critical parameter as Li selectivity and kinetics when deciding for a sorbent.

7. Conclusions

The present thesis shows that DLE by sorption is not limited to intensely investigated lithium-manganese oxide, lithium-titanium oxide or lithium-aluminium hydroxide sorbents that are usually considered for the Li extraction from geothermal brines. Novel materials, like synthetic zeolite 13X and lithium-iron-phosphate that are commercially used for other purposes, like wastewater treatment or in the battery industry are also able to sorb Li. Although zeolite 13X in its current form has a low Li selectivity hindering its application for DLE from geothermal brines, it might still be considered for Li extraction from low saline fluids or fluids that contain only small amounts of competing ions, e.g. in battery recycling. Lithium-iron-phosphate, in contrast, is identified as a very promising material to be used as a novel sorbent in DLE. Challenges regarding the use of a reducing agent and undesired co-precipitation of phases need to be addressed, but some solutions are already suggested in this thesis.

The new results obtained for the novel materials are of high importance for the future Li-supply from unconventional resources. DLE in general is considered as technology with lower environmental impact and the used sorbents must contribute to a more sustainable Li extraction. Novel sorbents which overcome limitations of LMO, LTO and Al-hydroxides, like limited commercial availability, or challenges regarding pH and sorbent stability, must be considered in DLE technology. The findings may thus be a game-changer in developing and upscaling the DLE technology.

Some new research questions, however, must be addressed in the future. DLE by sorption, independent of the used sorbent, changes the chemistry of geothermal brines at minimum in pH and/or Li concentration. At which amount it is changed by DLE can hardly be generalized as this depends on the used sorbent, the local brine composition, the used sorbent/brine ratio and the finalized technical design of the extraction facility. Details must be discussed with the authorities since regulations are lacking so far. Further research on reservoir fluid-rock interaction is necessary for clarification. Thus, the reinjection of the Li-poor brine is under investigated and should

be a focus of future research. The effect of the reinjected brine on the geochemistry of the reservoir, mixing of different bine compositions and water-rock-interaction processes must be estimated for the specific brine and reservoir.

Most sorbents, including those investigated here, are often tested in their powdery form. The application of a powder in a high-flow regime is challenging and thus one focus must be the material formulation applicable in DLE facilities. Differently formulated materials must be investigated for changes in sorption performance because a limited availability of the sorbent surface due to the accumulation of crystals or the addition of binders likely change the sorbent properties.

All sorbents have different advantages and disadvantages regarding kinetics, sorption capacity, selectivity or economic properties. In DLE from geothermal brines, the different parameters for sorbent selection are found to be of varying importance. The Li selectivity seems to be of highest importance, but kinetics as well as pH, temperature and chemical stability of the sorbent are crucial parameters. The Li sorption capacity, in contrast, is considered to be less decisive as long as Li is sorbed in general. Sorbents are usually classified for their chemical composition, rather than crystallography. The Li-sorption is, however, mainly controlled by mineralogy. Thus, it is recommended to shift the classification of sorbents from their chemical composition to their mineralogy.

In addition to synthetic zeolite 13X and LFP, there may be a variety of novel materials. Therefore, the research field should be widened to sorbents that are already used commercially for wastewater treatment, in biotechnology, raw materials metallurgy or the remediation of contaminated sites and that might be able to sorb Li. This thesis confirms the potential of such an approach for further development in DLE technology.

References

Agusdinata, D.B., Liu, W., Eakin, H. and Romero, H., 2018. Socio-environmental impacts of lithium mineral extraction: towards a research agenda. Environmental Research Letters, 13(12): 123001.

Aljarrah, S., Al-Rawajfeh, A.E., Shahid, M.K. and Islam, Q.U., 2023. Recent Innovations and Patents of Lithium Extraction Techniques from Various Lithium Bearing Solutions. Recent Innovations in Chemical Engineering (Formerly Recent Patents on Chemical Engineering), 16(4): 241-259.

Ambrose, H. and Kendall, A., 2020. Understanding the future of lithium: Part 2, temporally and spatially resolved life-cycle assessment modeling. Journal of Industrial Ecology, 24(1): 90-100.

Amer, A., 2008. The hydrometallurgical extraction of lithium from Egyptian montmorillonite-type clay. JOM, 60(10): 55-57.

An, J., Kang, D., Tran, K., Kim, M., Lim, T. and Tran, T., 2012. Recovery of lithium from Uyuni salar brine. Hydrometallurgy, 117: 64-70.

Australian Government, 2020. Lithium - Resources and Energy Quarterly December 2020. https://publications.industry.gov.au/publications/resourcesandenergyquarterlydecember2020/documents/Resources-and-Energy-Quarterly-Dec-2020-Lithium.pdf (19.05.2021).

Australian Government, 2023. Lithium - Resources and Energy Quarterly December 2023. https://www.industry.gov.au/publications/resources-and-energy-quarterly (24.01.2024).

Bajestani, M., Moheb, A. and Masigol, M., 2019. Simultaneous optimization of adsorption capacity and stability of hydrothermally synthesized spinel ion sieve composite adsorbents for selective removal of lithium from aqueous solutions. Industrial & Engineering Chemistry Research, 58(27): 12207-12215.

Banks, M., 1953. A Method For Concentration of North Carolina Spodumene Ores.

Barandiarán, J., 2019. Lithium and development imaginaries in Chile, Argentina and Bolivia. World Development, 113: 381-391.

Bowell, R., Lagos, L., de los Hoyos, C. and Declercq, J., 2020. Classification and characteristics of natural lithium resources. Elements: An International Magazine of Mineralogy, Geochemistry, and Petrology, 16(4): 259-264.

Bundesverband Geothermie, 2021. Informationsportal tiefe Geothermie. https://www.red-drilling-services.at/fileadmin/user_upload/BVG_Tiefe_Geothermieprojekte_Plakat_2021-22.pdf (10.08.2021).

Chitrakar, R., Makita, Y., Ooi, K. and Sonoda, A., 2012. Selective uptake of lithium ion from brine by H1. 33Mn1. 67O4 and H1. 6Mn1. 6O4. Chemistry Letters, 41(12): 1647-1649.

Chordia, M., Wickerts, S., Nordelöf, A. and Arvidsson, R., 2022. Life cycle environmental impacts of current and future battery-grade lithium supply from brine and spodumene. Resources, Conservation and Recycling, 187: 106634.

Choubey, P., Chung, K.-S., Kim, M.-s., Lee, J.-c. and Srivastava, R., 2017. Advance review on the exploitation of the prominent energy-storage element Lithium. Part II: From sea water and spent lithium ion batteries (LIBs). Minerals Engineering, 110: 104-121.

Choubey, P., Kim, M.-s., Srivastava, R., Lee, J.-c. and Lee, J.-Y., 2016. Advance review on the exploitation of the prominent energy-storage element: Lithium. Part I: From mineral and brine resources. Minerals Engineering, 89: 119-137.

Dahlkamp, J.M., Quintero, C., Videla, Á. and Rojas, R., 2023. Production processes for LiOH–A review. Hydrometallurgy: 106217.

DERA, 2019. Preismonitor April 2019. https://www.deutsche-rohstoffagentur.de/DE/Themen/Min_rohstoffe/Produkte/Preisliste/pm_19_04.pdf?__blob=publicationFile (27.04.2021).

DERA, 2023. Preismonitor Januar 2023. https://www.bgr.bund.de/DERA/DE/Aktuelles/Monitore/2023/01-23/2023-01-preismonitor.pdf?__blob=publicationFile&v=3 (22.01.2024).

DERA, 2024. Preismonitor Januar 2024. https://www.bgr.bund.de/DE/Themen/Min_rohstoffe/Produkte/Preisliste/pm_24_01.pdf?__blob=publicationFile (13.02.2024).
Dill, H., 2020. A geological and mineralogical review of clay mineral deposits and phyllosilicate ore guides in Central Europe–A function of geodynamics and climate change. Ore Geology Reviews, 119: 103304.
Drüppel, K., Stober, I., Grimmer, J. and Mertz-Kraus, R., 2020. Experimental alteration of granitic rocks: Implications for the evolution of geothermal brines in the Upper Rhine Graben, Germany. Geothermics, 88: 101903.
Eckstein, Y., Yaalon, D. and Yariv, S., 1970. The effect of lithium on the cation exchange behaviour of crystalline and amorphous clays. Israel Journal of Chemistry, 8(3): 335-342.
European Commission, 2020. COMMUNICATION FROM THE COMMISSION TO THE EUROPEAN PARLIAMENT, THE COUNCIL, THE EUROPEAN ECONOMIC AND SOCIAL COMMITTEE AND THE COMMITTEE OF THE REGIONS: Critical Raw Materials Resilience: Charting a Path towards greater Security and Sustainability, Brussels.
Everett, D.H., 1972. Manual of symbols and terminology for physicochemical quantities and units, appendix II: Definitions, terminology and symbols in colloid and surface chemistry. Pure and Applied Chemistry, 31(4): 577-638.
Farahbakhsh, J., Arshadi, F., Mofidi, Z., Mohseni-Dargah, M., Kök, C., Assefi, M., Soozanipour, A., Zargar, M., Asadnia, M. and Boroumand, Y., 2023. Direct lithium extraction: A new paradigm for lithium production and resource utilization. Desalination: 117249.
Fasel, D. and Tran, M., 2005. Availability of lithium in the context of future D–T fusion reactors. Fusion engineering and design, 75: 1163-1168.
Flexer, V., Baspineiro, C.F. and Galli, C.I., 2018. Lithium recovery from brines: A vital raw material for green energies with a potential environmental impact in its mining and processing. Science of the Total Environment, 639: 1188-1204.
Gabra, G., Torma, A. and Olivier, C., 1975. Pressure leaching of beta-spodumene by sodium chloride. Canadian Metallurgical Quarterly, 14(4): 355-359.
Gourcerol, B., Gloaguen, E., Melleton, J., Tuduri, J. and Galiegue, X., 2019. Re-assessing the European lithium resource potential–A review of hard-rock resources and metallogeny. Ore Geology Reviews, 109: 494-519.
Gregg, S.J. and Sing, K.S.W., 1982. Adsorption, Surface Area and Porosity. ACADEMIC PRESS INC., London.
Gutiérrez, J.S., Moore, J.N., Donnelly, J.P., Dorador, C., Navedo, J.G. and Senner, N.R., 2022. Climate change and lithium mining influence flamingo abundance in the Lithium Triangle. Proceedings of the Royal Society B, 289(1970): 20212388.
Haklıdır, F. and Balaban, T., 2019. A review of mineral precipitation and effective scale inhibition methods at geothermal power plants in West Anatolia (Turkey). Geothermics, 80: 103-118.
Han, Y., Kim, H. and Park, J., 2012. Millimeter-sized spherical ion-sieve foams with hierarchical pore structure for recovery of lithium from seawater. Chemical engineering journal, 210: 482-489.
Hawash, S., Abd El Kader, E. and El Diwani, G., 2010. Methodology for selective adsorption of lithium ions onto polymeric aluminium (III) hydroxide. Journal of American Science, 6(11): 301-309.
Heidari, N. and Momeni, P., 2017. Selective adsorption of lithium ions from Urmia Lake onto aluminum hydroxide. Environmental Earth Sciences, 76(16): 1-8.
Herrmann, L., Ehrenberg, H., Graczyk-Zajac, M., Kaymakci, E., Kölbel, T., Kölbel, L. and Tübke, J., 2022. Lithium recovery from geothermal brine–an investigation into the desorption of lithium ions using manganese oxide adsorbents. Energy Advances, 1(11): 877-885.
Intaranont, N., Garcia-Araez, N., Hector, A., Milton, J. and Owen, J., 2014. Selective lithium extraction from brines by chemical reaction with battery materials. Journal of Materials Chemistry A, 2(18): 6374-6377.

Isupov, V., Kotsupalo, N., Nemudry, A. and Menzeres, L., 1999. Aluminium hydroxide as selective sorbent of lithium salts from brines and technical solutions. Studies in surface science and catalysis, 120: 621-652.

Jin, J., Zhang, S., Wei, X., Cao, X., Peng, M. and Jiang, L., 2023. Synergistic design of membrane-based ion separation and solar-driven evaporation for direct lithium extraction from salt-lake brine.

Joo, H., Kim, S., Kim, S., Choi, M., Kim, S.-H. and Yoon, J., 2020. Pilot-scale demonstration of an electrochemical system for lithium recovery from the desalination concentrate. Environmental Science: Water Research & Technology, 6(2): 290-295.

Joshi, D.R. and Adhikari, N., 2019. An overview on common organic solvents and their toxicity. Journal of Pharmaceutical Research International: 1-18.

Kelly, J.C., Wang, M., Dai, Q. and Winjobi, O., 2021. Energy, greenhouse gas, and water life cycle analysis of lithium carbonate and lithium hydroxide monohydrate from brine and ore resources and their use in lithium ion battery cathodes and lithium ion batteries. Resources, Conservation and Recycling, 174: 105762.

Kesler, S., Gruber, P., Medina, P., Keoleian, G., Everson, M. and Wallington, T., 2012. Global lithium resources: Relative importance of pegmatite, brine and other deposits. Ore geology reviews, 48: 55-69.

Kessler, T., Mugova, E., Jasnowski-Peters, H., Rinder, T., Stemke, M., Wolkersdorfer, C., Hilberg, S., Melchers, C., Struckmeier, W. and Wieber, G., 2020. Groundwater in former German coal mining areas—a scientific perspective on mine floodings. Grundwasser, 25: 259-272.

Kölbel, L., Kölbel, T., Herrmann, L., Kaymakci, E., Ghergut, I., Poirel, A. and Schneider, J., 2023. Lithium extraction from geothermal brines in the Upper Rhine Graben: A case study of potential and current state of the art. Hydrometallurgy, 221: 106131.

Kölbel, L., Slunitschek, K., Kaymakci, E., Kölbel, T., Reich, R. and Schneider, J., 2024. Lithium recovery from geothermal brines: An investigation into radioactive nuclide uptake on lithium-manganese-oxide (LMO) granules. Hydrometallurgy: 106266.

Kranz, K. and Dillenardt, J., 2010. Mine water utilization for geothermal purposes in Freiberg, Germany: determination of hydrogeological and thermophysical rock parameters. Mine Water and the Environment, 29: 68-76.

Kudryavtsev, P., 2016. Lithium in nature, application, methods of extraction. Journal" Scientific Israel-Technological Advantages, 18(3): 63-83.

Kuss, C., Carmant-Dérival, M., Trinh, N.D., Liang, G. and Schougaard, S.B., 2014. Kinetics of Heterosite Iron Phosphate Lithiation by Chemical Reduction. The Journal of Physical Chemistry C, 118(34): 19524-19528.

Lawagon, C., Nisola, G., Mun, J., Tron, A., Torrejos, R., Seo, J., Kim, H. and Chung, W.-J., 2016. Adsorptive Li+ mining from liquid resources by H2TiO3: Equilibrium, kinetics, thermodynamics, and mechanisms. Journal of industrial and engineering chemistry, 35: 347-356.

Lemaire, J., Svecova, L., Lagallarde, F., Laucournet, R. and Thivel, P.-X., 2014. Lithium recovery from aqueous solution by sorption/desorption. Hydrometallurgy, 143: 1-11.

Li, L. and Stanforth, R., 2000. Distinguishing adsorption and surface precipitation of phosphate on goethite (α-FeOOH). Journal of colloid and interface science, 230(1): 12-21.

Li, R., Wang, Y., Duan, W., Du, C., Tian, S., Ren, Z. and Zhou, Z., 2023. Selective extraction of lithium ions from salt lake brines using a tributyl phosphate-sodium tetraphenyl boron-phenethyl isobutyrate system. Desalination, 555: 116543.

Li, X., Chen, L., Chao, Y., Chen, W., Luo, J., Xiong, J., Zhu, F., Chu, X., Li, H. and Zhu, W., 2020. Amorphous TiO2-Derived Large-Capacity Lithium Ion Sieve for Lithium Recovery. Chemical Engineering & Technology, 43(9): 1784-1791.

Li, Z., Li, C., Liu, X., Cao, L., Li, P., Wei, R., Li, X., Guo, D., Huang, K.-W. and Lai, Z., 2021. Continuous electrical pumping membrane process for seawater lithium mining. Energy & Environmental Science, 14(5): 3152-3159.

Liebetreu, D., 2022. Strategic Competition in South America's Lithium Triangle. InterAgency Journal 12-2.
Limousin, G., Gaudet, J.-P., Charlet, L., Szenknect, S., Barthes, V. and Krimissa, M., 2007. Sorption isotherms: A review on physical bases, modeling and measurement. Applied geochemistry, 22(2): 249-275.
Liu, C., Lowenstein, T.K., Wang, A., Zheng, C. and Yu, J., 2023. Brine: Genesis and Sustainable Resource Recovery Worldwide. Annual Review of Environment and Resources, 48: 371-394.
Liu, W., Xu, H., Shi, X. and Yang, X., 2017. Fractional crystallization for extracting lithium from Cha'erhan tail brine. Hydrometallurgy, 167: 124-128.
Liu, Y.-G., Zhou, M., Zeng, G.-M., Li, X., Xu, W.-H. and Fan, T., 2007. Effect of solids concentration on removal of heavy metals from mine tailings via bioleaching. Journal of Hazardous Materials, 141(1): 202-208.
London Metal Exchange, 2021. The London Metal Exchange - an HKEX Company. https://www.lme.com/Metals/Minor-metals/Lithium-prices (19.05.2021).
Luan, Z., Hartmann, M., Zhao, D., Zhou, W. and Kevan, L., 1999. Alumination and ion exchange of mesoporous SBA-15 molecular sieves. Chemistry of materials, 11(6): 1621-1627.
Lundaev, V., Solomon, A., Caldera, U. and Breyer, C., 2022. Material extraction potential of desalination brines: A technical and economic evaluation of brines as a possible new material source. Minerals Engineering, 185: 107652.
Martin, G., Rentsch, L., Höck, M. and Bertau, M., 2017. Lithium market research–global supply, future demand and price development. Energy Storage Materials, 6: 171-179.
Melnikov, S., Sheldeshov, N., Zabolotsky, V., Loza, S. and Achoh, A., 2017. Pilot scale complex electrodialysis technology for processing a solution of lithium chloride containing organic solvents. Separation and Purification Technology, 189: 74-81.
Meng, F., McNeice, J., Zadeh, S. and Ghahreman, A., 2021. Review of lithium production and recovery from minerals, brines, and lithium-ion batteries. Mineral Processing and Extractive Metallurgy Review, 42(2): 123-141.
Meshram, P., Pandey, B. and Mankhand, T., 2014. Extraction of lithium from primary and secondary sources by pre-treatment, leaching and separation: A comprehensive review. Hydrometallurgy, 150: 192-208.
Mundhenk, N., 2013. Corrosion and scaling in utilization of geothermal energy in the Upper Rhine graben.
Murodjon, S., Yu, X., Li, M., Duo, J. and Deng, T., 2020. Lithium recovery from brines including seawater, salt lake brine, underground water and geothermal water. Thermodynamics and Energy Engineering, 90371.
Nie, X.-Y., Sun, S.-Y., Song, X. and Yu, J.-G., 2017. Further investigation into lithium recovery from salt lake brines with different feed characteristics by electrodialysis. Journal of Membrane Science, 530: 185-191.
Niu, Z., Zou, Y., Xin, B., Chen, S., Liu, C. and Li, Y., 2014. Process controls for improving bioleaching performance of both Li and Co from spent lithium ion batteries at high pulp density and its thermodynamics and kinetics exploration. Chemosphere, 109: 92-98.
No, K.T., Chon, H., Ree, T. and Jhon, M.S., 1981. Theoretical studies on acidity and site selectivity of cations in faujasite zeolite. The Journal of Physical Chemistry, 85(14): 2065-2070.
Ooi, K., Sonoda, A., Makita, Y., Chitrakar, R., Tasaki-Handa, Y. and Nakazato, T., 2017. Recovery of lithium from salt-brine eluates by direct crystallization as lithium sulfate. Hydrometallurgy, 174: 123-130.
Orooji, Y., Nezafat, Z., Nasrollahzadeh, M., Shafiei, N., Afsari, M., Pakzad, K. and Razmjou, A., 2022. Recent advances in nanomaterial development for lithium ion-sieving technologies. Desalination, 529: 115624.
Paranthaman, M.P., Li, L., Luo, J., Hoke, T., Ucar, H., Moyer, B.A. and Harrison, S., 2017. Recovery of lithium from geothermal brine with lithium–aluminum layered double hydroxide chloride sorbents. Environmental science & technology, 51(22): 13481-13486.

Peerawattuk, I. and Bobicki, E., 2018. Lithium Extraction and Utilization: A Historical Perspective, Extraction 2018. Springer, pp. 2209-2224.
Perez, T.C., 2023. A Mini-Review of the Environmental Footprint of Lithium-Ion Batteries for Electric Vehicles. Journal of Computers, Mechanical and Management, 2(3): 43-52.
Petavratzi, E., Sanchez-Lopez, D., Hughes, A., Stacey, J., Ford, J. and Butcher, A., 2022. The impacts of environmental, social and governance (ESG) issues in achieving sustainable lithium supply in the Lithium Triangle. Mineral Economics, 35(3-4): 673-699.
Piedmont Lithium Limited, 2020. Chemical plant PFS demonstrates exceptional economics and optionality of USA location. ASX Release.
Pourret, O., Bollinger, J.-C., Hursthouse, A. and van Hullebusch, E.D., 2022. Sorption vs adsorption: The words they are a-changin', not the phenomena. Science of the Total Environment, 838: 156545.
Prodromou, K., 2016. Lithium adsorption on amorphous aluminum hydroxides and gibbsite. Eurasian Journal of Soil Science, 5(1): 13-16.
Qian, F., Guo, M., Qian, Z., Li, Q., Wu, Z. and Liu, Z., 2019. Highly lithium adsorption capacities of H1. 6Mn1. 6O4 ion-sieve by ordered array structure. ChemistrySelect, 4(34): 10157-10163.
Regenspurg, S., Feldbusch, E., Norden, B. and Tichomirowa, M., 2016. Fluid-rock interactions in a geothermal Rotliegend/Permo-Carboniferous reservoir (north German basin). Applied Geochemistry, 69: 12-27.
Reich, R., Danisi, R.M., Kluge, T., Eiche, E. and Kolb, J., 2023. Structural and compositional variation of zeolite 13X in lithium sorption experiments using synthetic solutions and geothermal brine. Microporous and Mesoporous Materials, 359: 112623.
Reich, R., Eiche, E. and Kolb, J., 2024. Delithiation and lithiation of LiFePO4: Implications for direct Li extraction from synthetic solutions and geothermal brines. Desalination: 117883.
Reich, R., Slunitschek, K., Danisi, R.M., Eiche, E. and Kolb, J., 2022. Lithium Extraction Techniques and the Application Potential of Different Sorbents for Lithium Recovery from Brines. Mineral Processing and Extractive Metallurgy Review: 1-20.
Roy, J., Madhavi, S. and Cao, B., 2021. Metal extraction from spent lithium-ion batteries (LIBs) at high pulp density by environmentally friendly bioleaching process. Journal of Cleaner Production, 280: 124242.
Safari, S., Lottermoser, B. and Alessi, D., 2020. Metal oxide sorbents for the sustainable recovery of lithium from unconventional resources. Applied Materials Today, 19: 100638.
Sanjuan, B., Millot, R., Innocent, C., Dezayes, C., Scheiber, J. and Brach, M., 2016. Major geochemical characteristics of geothermal brines from the Upper Rhine Graben granitic basement with constraints on temperature and circulation. Chemical Geology, 428: 27-47.
Schmidt, M., 2017. Rohstoffrisikobewertung - Lithium. - DERA Rohstoffinformationen 33, Berlin.
Schmidt, M., 2023. Rohstoffrisikobewertung - Lithium, Berlin.
Seip, A., Safari, S., Pickup, D.M., Chadwick, A.V., Ramos, S., Velasco, C.A., Cerrato, J.M. and Alessi, D.S., 2021. Lithium recovery from hydraulic fracturing flowback and produced water using a selective ion exchange sorbent. Chemical Engineering Journal, 426: 130713.
Shi, C., Jing, Y., Xiao, J., Wang, X., Yao, Y. and Jia, Y., 2017. Solvent extraction of lithium from aqueous solution using non-fluorinated functionalized ionic liquids as extraction agents. Separation and Purification Technology, 172: 473-479.
Shi, X.-c., Zhang, Z.-b., Zhou, D.-f., Zhang, L.-f., Chen, B.-z. and Yu, L.-l., 2013. Synthesis of Li+ adsorbent (H2TiO3) and its adsorption properties. Transactions of Nonferrous Metals Society of China, 23(1): 253-259.
Song, Z. and Jia, S., 2023. Municipal water use kuznets curve. Water Resources Management, 37(1): 235-249.
Sposito, G., 1984. The surface chemistry of soils. Oxford university press.
Sposito, G., 1987. Distinguishing adsorption from surface precipitation. ACS Publications.

Statista, 2021. Statista: Global No. 1 Business Data Platform. https://de.statista.com/statistik/daten/studie/979746/umfrage/durchschnittlicher-preis-von-lithium-weltweit/ (19.05.2021).
Steiger, K., Reich, R., Slunitschek, K., Steinmüller, K., Bergemann, C., Hilgers, C. and Kolb, J., 2022. Lithium in Europa, THINKTANK für Industrielle Ressourcenstrategien, Karlsruhe.
Stober, I., Grimmer, J. and Kraml, M., 2023. The Muschelkalk aquifer of the Molasse basin in SW-Germany: implications on the origin and development of highly saline lithium-rich brines in calcareous hydrothermal reservoirs. Geothermal Energy, 11(1): 27.
Stober, I., Wolfgramm, M. and Birner, J., 2014. Hydrochemie der Tiefenwässer in Deutschland—hydrochemistry of deep waters in Germany. Z Geol Wiss, 41(42): 5-6.
Stringfellow, W.T. and Dobson, P.F., 2021. Technology for the Recovery of Lithium from Geothermal Brines. Energies, 14(20): 6805.
Su, H., Li, Z., Zhang, J., Zhu, Z., Wang, L. and Qi, T., 2020. Recovery of lithium from salt lake brine using a mixed ternary solvent extraction system consisting of TBP, FeCl3 and P507. Hydrometallurgy, 197: 105487.
Swain, B., 2017. Recovery and recycling of lithium: A review. Separation and Purification Technology, 172: 388-403.
Tian, L., Ma, W. and Han, M., 2010. Adsorption behavior of Li+ onto nano-lithium ion sieve from hybrid magnesium/lithium manganese oxide. Chemical Engineering Journal, 156(1): 134-140.
Tran, H.N., You, S.-J., Hosseini-Bandegharaei, A. and Chao, H.-P., 2017. Mistakes and inconsistencies regarding adsorption of contaminants from aqueous solutions: a critical review. Water research, 120: 88-116.
Tran, T. and Luong, V., 2015. Lithium production processes, Lithium process chemistry. Elsevier, pp. 81-124.
US Geological Survey, 1996. Mineral Commodity Summaries: Lithium. https://d9-wret.s3.us-west-2.amazonaws.com/assets/palladium/production/mineral-pubs/lithium/lithimcs96.pdf (27.04.2021).
US Geological Survey, 1996-2023. Mineral Commodity Summaries: Lithium. https://www.usgs.gov/centers/national-minerals-information-center/lithium-statistics-and-information (24.01.2024).
US Geological Survey, 2000. Mineral Commodity Summaries: Lithium. https://d9-wret.s3.us-west-2.amazonaws.com/assets/palladium/production/mineral-pubs/lithium/450300.pdf (27.04.2021).
US Geological Survey, 2020. Mineral Commodity Summaries: Lithium. https://pubs.usgs.gov/periodicals/mcs2020/mcs2020-lithium.pdf (27.04.2021).
US Geological Survey, 2021. Mineral Commodity Summaries: Lithium. https://pubs.usgs.gov/periodicals/mcs2021/mcs2021-lithium.pdf (27.04.2021).
US Geological Survey, 2022. Mineral Commodity Summaries: Lithium. https://pubs.usgs.gov/periodicals/mcs2022/mcs2022-lithium.pdf (17.04.2022).
US Geological Survey, 2023. Mineral Commodity Summaries: Lithium. https://pubs.usgs.gov/periodicals/mcs2023/mcs2023-lithium.pdf (22.01.2024).
Ventura, S., Bhamidi, S., Hornbostel, M., Nagar, A. and Perea, E., 2016. Selective recovery of metals from geothermal brines, SRI International, Menlo Park, CA (United States).
Vera, M.L., Torres, W.R., Galli, C.I., Chagnes, A. and Flexer, V., 2023. Environmental impact of direct lithium extraction from brines. Nature Reviews Earth & Environment, 4(3): 149-165.
Vivoda, V., Bazilian, M.D., Khadim, A., Ralph, N. and Krame, G., 2024. Lithium nexus: Energy, geopolitics, and socio-environmental impacts in Mexico's Sonora project. Energy Research & Social Science, 108: 103393.
Warren, I., 2021. Techno-Economic Analysis of Lithium Extraction from Geothermal Brines, National Renewable Energy Lab.(NREL), Golden, CO (United States).
Williams, L. and Hervig, R., 2005. Lithium and boron isotopes in illite-smectite: The importance of crystal size. Geochimica et Cosmochimica Acta, 69(24): 5705-5716.

Wiśniewska, M., Fijałkowska, G., Ostolska, I., Franus, W., Nosal-Wiercińska, A., Tomaszewska, B., Goscianska, J. and Wójcik, G., 2018. Investigations of the possibility of lithium acquisition from geothermal water using natural and synthetic zeolites applying poly (acrylic acid). Journal of Cleaner Production, 195: 821-830.

Wisotzky, F., 2019. Hydrogeochemie der balneologisch genutzten Grundwässer in Deutschland und deren Relevanz für Geothermieprojekte. Grundwasser, 24(2): 101-108.

Xiao, J., Nie, X., Sun, S., Song, X., Li, P. and Yu, J., 2015. Lithium ion adsorption–desorption properties on spinel Li4Mn5O12 and pH-dependent ion-exchange model. Advanced Powder Technology, 26(2): 589-594.

Yi, D., Xiao, L., Wang, B., Tian, Z., Zhu, B. and Yu, H., 2018. Method for quickly extracting lithium carbonate from saline lake water. United States Patent; US9932241B2.

Zhang, L., Zhang, T., Zhao, Y., Dong, G., Lv, S., Ma, S., Song, S. and Quintana, M., 2023. Doping engineering of lithium-aluminum layered double hydroxides for high-efficiency lithium extraction from salt lake brines. Nano Research: 1-9.

Zhang, Q.-H., Li, S.-P., Sun, S.-Y., Yin, X.-S. and Yu, J.-G., 2010. LiMn2O4 spinel direct synthesis and lithium ion selective adsorption. Chemical Engineering Science, 65(1): 169-173.

Zhang, X., Tang, X., Yang, Y., Sun, Z., Ma, W., Tong, X., Wang, C. and Zhang, X., 2021. Responses of the reproduction, population growth and metabolome of the marine rotifer Brachionus plicatilis to tributyl phosphate (TnBP). Environmental Pollution, 273: 116462.

Zhao, Y., Pohl, O., Bhatt, A.I., Collis, G.E., Mahon, P.J., Rüther, T. and Hollenkamp, A.F., 2021. A review on battery market trends, second-life reuse, and recycling. Sustainable Chemistry, 2(1): 167-205.

Appendix

A.1 Preliminary sorption experiments – Supplementary data

montmorillonite								
	T [°C]	pH c0	pH c1	mass [g]	time [min]	C,Li mg/L	C,Equ,Li mg/L	Q,Li mg/g
uncertainty [%]						9.1	9.1	
millipore water	25	5.79				<0.002		
RR-Cl-Mmt01-0001	25	5.95	5.88	1.000	1	215	210	0.9
RR-Cl-Mmt01-0005	25	5.95	5.89	0.995	5	207	205	0.4
RR-Cl-Mmt01-0015	25	5.95	5.9	1.003	15	209	203	1.2
RR-Cl-Mmt01-0030	25	5.95	5.89	1.000	30	215	210	1.0
RR-Cl-Mmt01-0045	25	5.95	5.88	0.997	45	209	208	0.4
RR-Cl-Mmt01-0060	25	5.95	5.88	0.991	60	206	201	1.1
RR-Cl-Mmt01-0120	25	5.95	5.92	1.006	120	215	212	0.3
RR-Cl-Mmt01-0180	25	5.95	5.88	1.006	180	209	212	-0.6
RR-Cl-Mmt01-0540	25	5.95	5.89	0.993	540	211	209	0.3
RR-Cl-Mmt01-1440	25	5.95	5.87	0.996	1440	212	209	0.6
RR-Cl-Mmt01-Blank1	25	5.95	5.94	0	15	213	212	0.8
RR-Cl-Mmt01-Blank2	25	5.95	5.94	0	952	213	211	0.8

zeolite clinoptilolite								
	T [°C]	pH c0	pH c1	mass [g]	time [min]	C,Li mg/L	C,Equ,Li mg/L	Q,Li mg/g
uncertainty [%]						11.1	11.1	
millipore water	25					<0.002		
RR-ZEO-Cpt01-0001	25	4.86	5.1	1.010	1	205	208	-0.6
RR-ZEO-Cpt01-0005	25	4.86	5.1	0.994	5	205	204	0.2
RR-ZEO-Cpt01-0015	25	4.86	5.1	0.996	15	203	202	0.9
RR-ZEO-Cpt01-0030	25	4.86	5.1	1.001	30	205	203	-0.6
RR-ZEO-Cpt01-0045	25	4.86	5.2	0.996	45	204	203	0.3
RR-ZEO-Cpt01-0060	25	4.86	5.1	0.993	60	206	201	0.7
RR-ZEO-Cpt01-0120	25	4.86	5.2	1.003	120	206	205	0.1
RR-ZEO-Cpt01-0180	25	4.86	5.2	0.998	180	199	205	0.2
RR-ZEO-Cpt01-0540	25	4.86	5.3	0.995	540	204	201	-0.4
RR-ZEO-Cpt01-1440	25	4.86	5.4	0.991	1440	204	199	1.0
RR-ZEO-Cpt01-Blank1	25	4.86	4.9	0	15	203	204	-0.2
RR-ZEO-Cpt01-Blank2	25	4.86	4.9	0	890	213	206	1.4

iron phosphate tetrahydrate								
	T [°C]	pH c0	pH c1	mass [g]	time [min]	C,Li mg/L	C,Equ,Li mg/L	Q,Li mg/g
uncertainty [%]						9.1	9.1	
millipore water	25	6.3				<0.002		
RR-EPT01-0001	25	5.93	5.74	0.994	1	213	212	0.2
RR-EPT01-0005	25	5.93	5.76	1.000	5	209	207	0.4
RR-EPT01-0015	25	5.93	5.70	1.000	15	212	208	0.9
RR-EPT01-0030	25	5.93	5.69	1.006	30	210	205	1.0
RR-EPT01-0045	25	5.93	5.68	1.000	45	212	211	0.2
RR-EPT01-0060	25	5.93	5.68	1.000	60	214	211	0.6
RR-EPT01-0120	25	5.93	5.66	0.997	120	222	217	0.9
RR-EPT01-0180	25	5.93	5.65	1.000	180	218	212	1.2
RR-EPT01-0540	25	5.93	5.65	1.000	540	212	210	0.4
RR-EPT01-1440	25	5.93	5.59	1.012	1440	209	209	0.1
RR-EPT01-Blank1	25	5.93	5.93	0	15	218	217	0.3
RR-EPT01-Blank2	25	5.93	5.93	0	900	214	213	0.2

synthetic zeolite 13X								
	T [°C]	pH c0	pH c1	mass [g]	time [min]	C,Li mg/L	C,Equ,Li mg/L	Q,Li mg/g
uncertainty [%]						2.3	2.3	
millipore water	25					0.01		
RR-ZEO-13X01-0001	25	4.95	6.1	1.00062	1	192	176	3.3
RR-ZEO-13X01-0005	25	4.95	6.1	1.00036	5	192	177	3.0
RR-ZEO-13X01-0015	25	4.95	6.2	1.00167	15	192	176	3.2
RR-ZEO-13X01-0030	25	4.95	6.2	1.00127	30	192	177	3.1
RR-ZEO-13X01-0045	25	4.95	6.2	1.00083	45	192	176	3.3
RR-ZEO-13X01-0060	25	4.95	-	1.00039	60	192	178	2.9
RR-ZEO-13X01-0120	25	4.95	6.2	1.00086	120	192	182	2.1
RR-ZEO-13X01-0180	25	4.95	6.2	1.00749	180	192	180	2.4
RR-ZEO-13X01-0540	25	4.95	6.3	1.0016	540	192	179	2.6
RR-ZEO-13X01-1440	25	4.95	6.4	0	1440	192	183	2.0
RR-ZEO-13X01-Blank1	25	4.95	4.9	0	15	192	186	1.2
RR-ZEO-13X01-Blank2	25	4.95	5.0	0	897	192	191	0.3

A.2 Study I – Colour figures

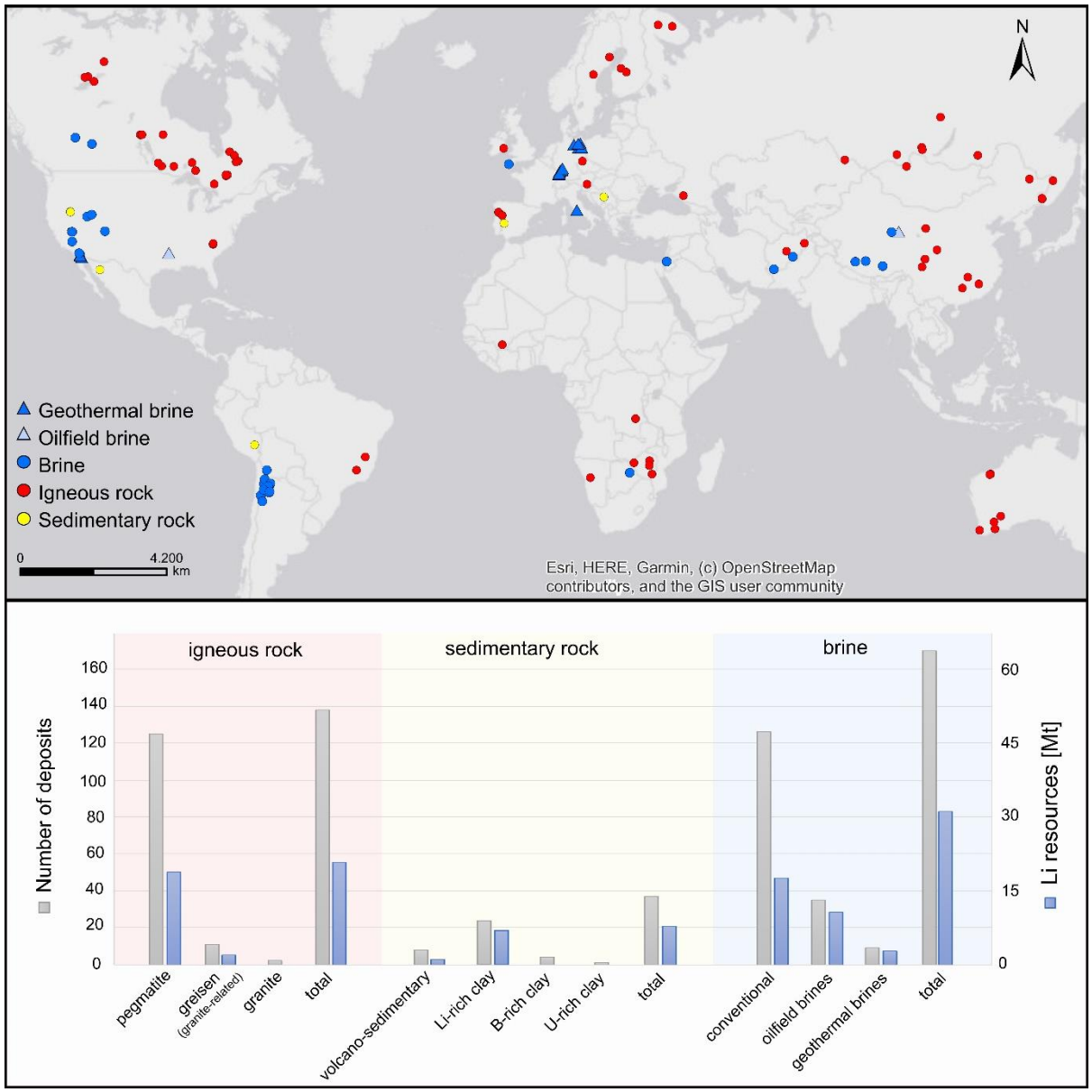

Figure A 1. Global Li deposits and resource distribution between different deposit types (Reich et al., 2022).

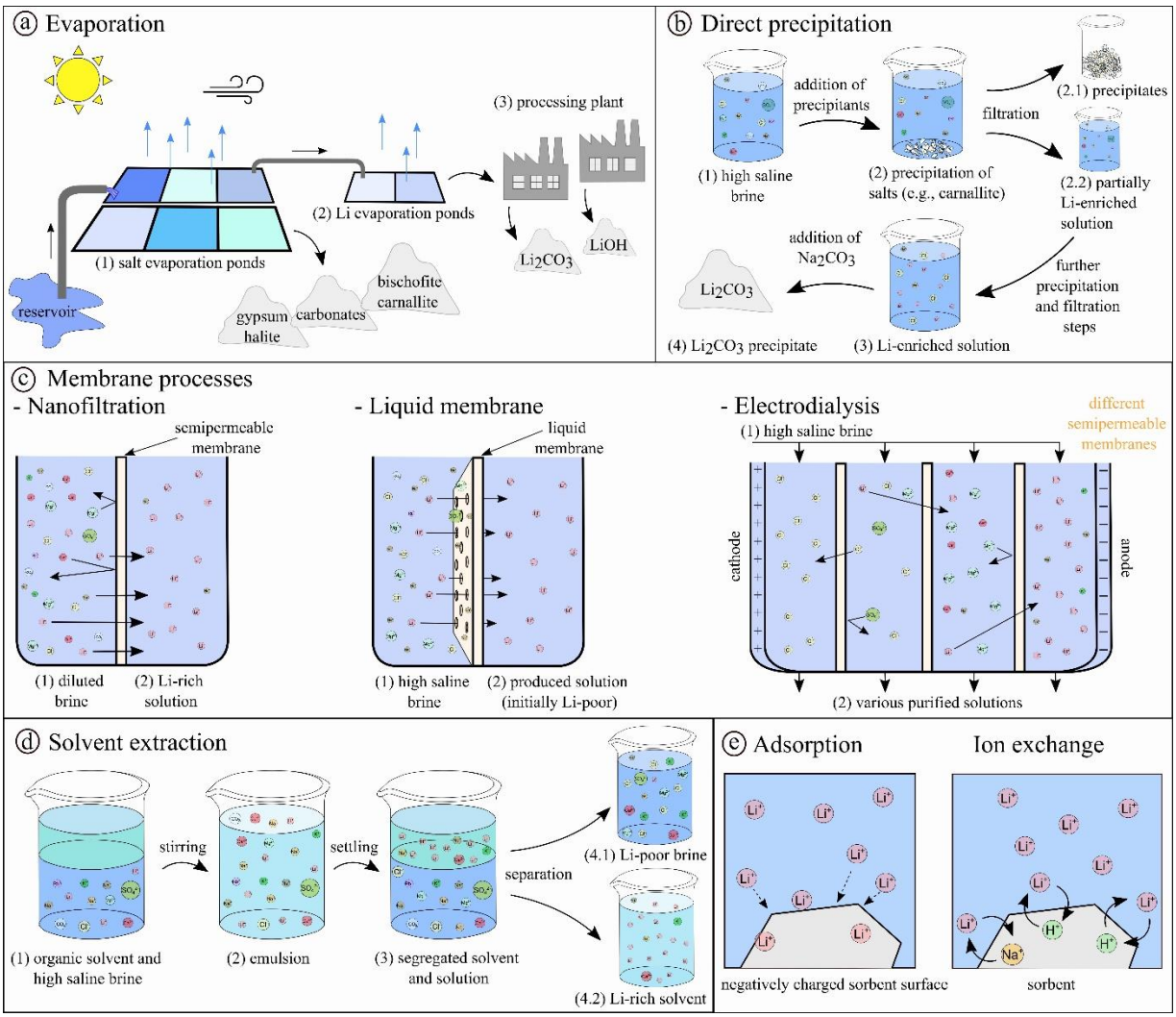

Figure A 2. Sketch of different extraction technologies for Li from aqueous solutions. (a) Evaporation, (b) Direct precipitation, (c) Membrane processes, (d) Solvent extraction and (e) Adsorption and Ion exchange (Reich et al., 2022).

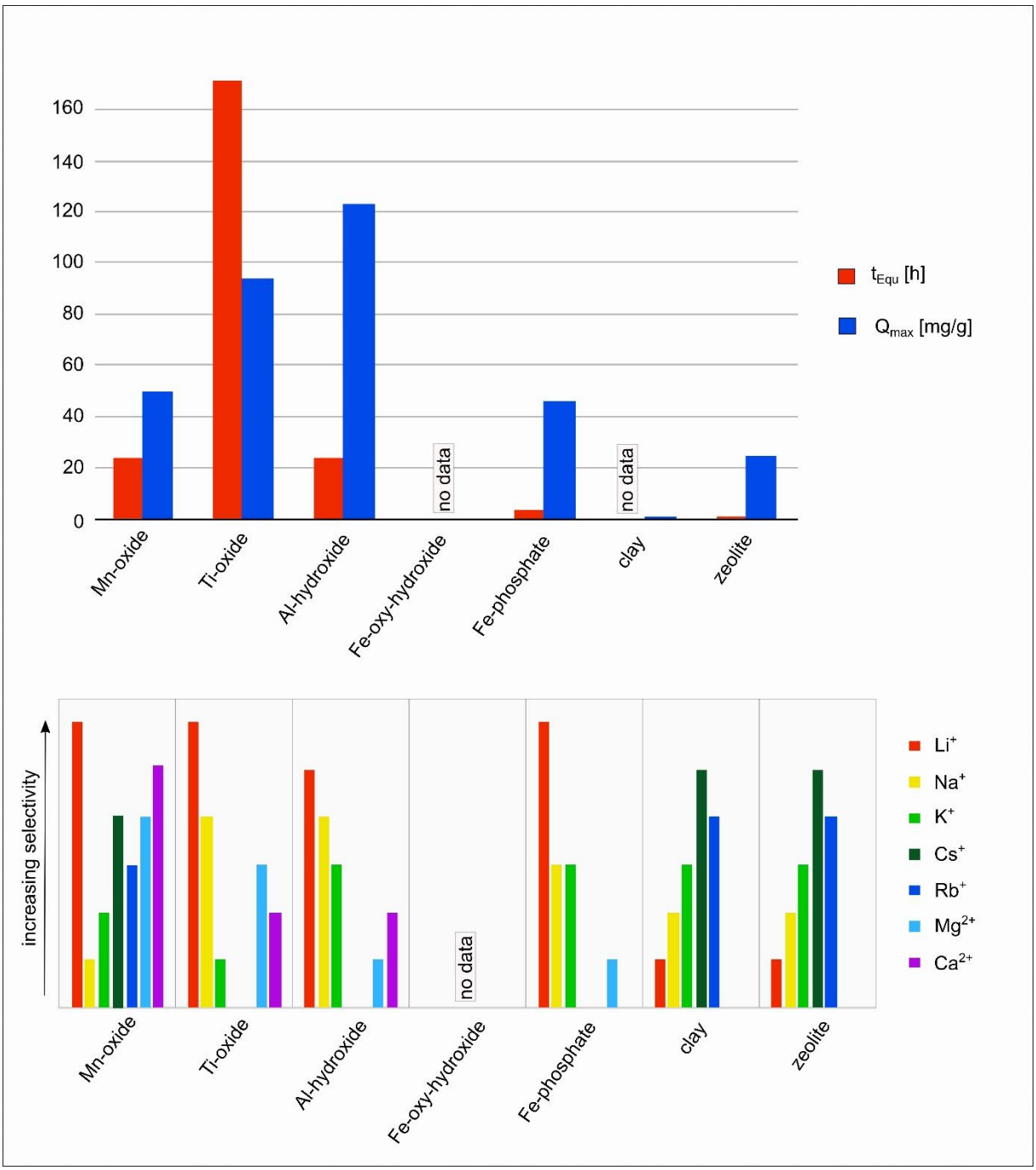

Figure A 3. Comparison between sorbents regarding kinetics (t_{Equ} [h]), maximum sorption capacity (Q_{max} [mg/g]) in the upper graph and relative qualitative selectivity of different ions in the lower graph (Reich et al., 2022).

A.3 Study II – Electronic supplement

	Kinetics zeolite 13X powder 25 °C - unbuffered					Kinetics zeolite 13X beads 25 °C - unbuffered				
	Li	Al	stirring time [min]	pH	sorbent mass [g]	Li	Al	stirring time [min]	pH	sorbent mass [g]
Limit of detection	0.002	0.001				0.001	0.003			
Coefficient of determination	0.9997	1.0000				0.9999	1.0000			
Correlation coefficient	0.9998	1.0000				1.0000	1.0000			
sigma	0.001	0.000				0.000	0.001			
Limit of quantification	0.006	0.003				0.003	0.009			
Accuracy 1/100	92.5	97.8				94.5	96.6			
Accuracy Misa 1/10	98.4	98.9				101.7	97.4			
Accuracy 1/2	99.9	99.7				100.8	98.3			
uncertainty [%]	7.5	2.2				5.5	3.4			
	C [mg/L]					**C [mg/L]**				
MilliQ water	b.d.l.	b.d.l.				b.d.l.	0.0			
C0001	197.4	b.d.l.				198.7	b.d.l.			
C0005	197.1	b.d.l.				202.4	0.1			
C0015	198.5	b.d.l.				192.3	b.d.l.			
C0030	201.3	b.d.l.				194.0	b.d.l.			
C0045	200.3	b.d.l.				193.4	b.d.l.			
C0060	204.2	0.0				194.6	b.d.l.			
C0120	202.8	b.d.l.				194.6	b.d.l.			
C0180	202.0	b.d.l.				197.4	b.d.l.			
C0540	201.5	b.d.l.				194.9	b.d.l.			
C1440	201.7	b.d.l.				190.8	0.1			
C1Wo	207.1	b.d.l.				193.1	0.1			
C2Wo	205.7	b.d.l.				192.5	b.d.l.			
CBlank1	197.5	b.d.l.				194.3	b.d.l.			
CBlank2	202.5	0.0				197.6	0.1			
CBlank3	207.6	b.d.l.				193.6	b.d.l.			
	C(Equ) [mg/L]					**C(Equ) [mg/L]**				
0001a	142.0	0.5		8.04		216.5	b.d.l.		6.14	
0005a	137.9	0.8		8.66		183.5	b.d.l.		6.76	
0015a	140.7	1.1		8.76		178.9	0.1		7.16	
0030a	143.8	1.4		8.76		175.5	0.1		7.33	
0045a	142.3	1.8		8.78		167.0	0.1		7.38	
0060a	144.7	2.0		8.75		163.2	0.2		7.63	
0120a	143.7	2.7		8.82		159.7	0.2		7.66	
0180a	144.5	3.1		8.79		158.6	0.3		7.93	
0540a	142.9	4.3		8.78		147.3	0.8		9.02	
0540a						144.3	0.8		9.02	
1440a	143.8	5.6		8.8		158.4	1.4		9.33	
1Woa	144.3	7.3		8.75		149.5	2.2		9.61	
2Woa	145.3	6.8		8.68		157.3	1.9		9.64	
Blank1a	195.7	0.1		6.06		195.1	0.1		5.69	
Blank2a	200.4	b.d.l.		5.88		197.7	b.d.l.		5.97	
Blank3a	200.0	b.d.l.		6.64		194.9	b.d.l.		6.54	
Blank3a						192.8	0.1		6.54	
	Q [mg/g]					**Q [mg/g]**				
0001	11.2	-0.1	1		0.991	-3.55	b.d.l.	1		1.001
0005	11.8	-0.2	5		1.000	3.74	0.0	5		1.012
0015	11.5	-0.2	15		1.005	2.68	0.0	15		1.001
0030	11.3	-0.3	30		1.013	3.66	0.0	30		1.008
0045	11.5	-0.4	45		1.009	5.29	0.0	45		0.997
0060	11.9	-0.4	60		1.003	6.25	0.0	60		1.007
0120	11.6	-0.5	120		1.023	6.93	0.0	120		1.005
0180	11.4	-0.6	180		1.011	7.78	-0.1	180		0.999
0540	11.5	-0.8	540		1.022	9.44	-0.2	540		1.008
0540						10.03	-0.2	540		1.008
1440	11.5	-1.1	1440		1.004	6.48	-0.3	1440		0.999
1 week	12.4	-1.4	10102		1.015	8.36	-0.4	10055		1.043
2 weeks	11.9	-1.3	20160		1.012	6.95	-0.4	20146		1.014
Blank 1	0.4	0.0	15		0	-0.16	0.0	15		0
Blank 2	0.4	0.0	745		0	-0.02	0.0	1097		0
Blank 3	1.5	b.d.l.	10078		0	-0.27	b.d.l.	10080		0
Blank 3						0.15	0.0	10080		0

	isotherm beads unbuffered						isotherm powder unbuffered					
	Li	Al	stirring time [min]	pH	T [°C]	sorbent mass [g]	Li	Al	stirring time [min]	pH	T [°C]	sorbent mass [g]
Limit of detection	0.001	0.003					0.001	0.002				
Correlation coefficient	1.0000	1.0000					0.9999	1.0000				
sigma	0.000	0.001					0.000	0.001				
Limit of quantification	0.003	0.009					0.005	0.007				
Accuracy 1/100	94.5	96.6					92.8	97.2				
Accuracy 1/50												
Accuracy Misa 10	101.7	97.4					99.3	98.1				
Accuracy 1/5												
Accuracy 1/2	100.8	98.3					99.5	98.6				
uncertainty [%]	5.5	3.4					7.2	2.8				
	C [mg/L]						**C [mg/L]**					
MilliQ water	b.d.l.	0.0					b.d.l.	0.0		6.07		
C0010	11.3	b.d.l.					10.7	0.2				
C0010												
C0050	52.8	b.d.l.					51.9	0.1				
C0050												
C0100	102.5	b.d.l.					102.2	0.2				
C0150	151.4	b.d.l.					152.2	0.1				
C0200	194.3	b.d.l.					201.3	0.1				
C0300	284.5	b.d.l.					291.2	0.1				
C0500	470.5	b.d.l.					489.2	0.2				
CBlank1	48.9	b.d.l.					50.7	0.1				
CBlank1												
CBlank2	289.4	0.1					295.4	0.2				
	C(Equ) [mg/L]						**C(Equ) [mg/L]**					
0010a	3.9	1.4		9.3			2.5	5.6		9.8		
0010a												
0050a	31.5	1.1		9.0			23.7	5.7		9.3		
0050a												
0100a	73.9	1.1		8.8			58.3	6.0		9.1		
0100a												
0150a	110.3	0.8		8.4			94.1	5.9		9.0		
0200a	154.3	0.7		8.3			137.4	5.9		8.9		
0200a												
0300a	241.1	**0.7**		8.3			213.5	5.9		8.7		
0300a												
0500a	441.8	0.7		8.1			388.8	5.4		8.4		
Blank1a	48.3	0.0		6.3			49.2	0.1		6.0		
Blank1a												
Blank2a	286.0	b.d.l.		5.8			290.2	0.2		6.2		
	Q [mg/g]						**Q [mg/g]**					
0010	1.5	-0.3	45		60	1.001	1.6	-1.1	45		40	1.005
0010												
0050	4.3	-0.2	45		60	1.003	5.7	-1.1	45		40	0.992
0050												
0100	5.8	-0.2	45		60	0.993	8.7	-1.2	45		40	1.005
0100												
0150	8.2	-0.2	45		60	0.997	11.7	-1.2	45		40	0.997
0200	8.0	-0.1	45		60	1.001	12.8	-1.2	45		40	0.996
0200												
0300	8.6	-0.1	45		60	1.007	15.5	-1.1	45		40	1.001
0500	5.7	-0.1	45		60	1.002	20.3	-1.1	45		40	0.991
Blank 1	0.1	0.0	45		60	0	0.3	0.0	45		40	0
Blank 1												
Blank 2	0.7	0.0	45		60	0	1.0	0.0	45		40	0

	isotherm powder unbuffered						Isotherm powder unbuffered					
	Li	Al	stirring time [min]	pH	T [°C]	sorbent mass [g]	Li	Al	stirring time [min]	pH	T [°C]	sorbent mass [g]
Limit of detection	0.002	0.001					0.001	0.002				
Correlation coefficient	0.9998	1.0000					0.9999	1.0000				
sigma	0.001	0.000					0.000	0.001				
Limit of quantification	0.006	0.003					0.005	0.007				
Accuracy 1/100	92.5	97.8					92.8	97.2				
Accuracy 1/50												
Accuracy Misa 10	98.4	98.9					99.3	98.1				
Accuracy 1/5												
Accuracy 1/2	99.9	99.7					99.5	98.6				
uncertainty [%]	7.5	2.2					7.2	2.8				
	C [mg/L]						**C [mg/L]**					
MilliQ water	b.d.l.	b.d.l.					b.d.l.	0.0		6.06		
C0010	12.0	b.d.l.					11.3	**0.1**				
C0010												
C0050	50.2	b.d.l.					51.8	0.1				
C0050												
C0100	103.8	b.d.l.					103.6	0.2				
C0150	148.6	0.0					152.3	0.1				
C0200	200.7	b.d.l.					199.3	0.2				
C0300	299.8	b.d.l.					292.8	0.1				
C0500	488.1	b.d.l.					472.1	0.2				
CBlank1	52.3	b.d.l.					51.1	0.1				
CBlank1												
CBlank2	302.6	b.d.l.					293.8	0.1				
	C(Equ) [mg/L]						**C(Equ) [mg/L]**					
0010a	3.0	2.6		9.9			2.8	10.0		9.6		
0010a												
0050a	23.6	3.0		9.5			23.4	9.7		9.0		
0050a												
0100a	62.4	2.8		9.2			58.2	10.5		8.9		
0100a												
0150a	97.3	2.5		9.0			93.9	10.3		8.9		
0200a	141.8	2.6		8.9			131.9	10.5		8.6		
0200a												
0300a	221.3	2.3		8.7			218.1	10.1		8.6		
0300a												
0500a	413.5	2.2		8.4			386.7	9.9		8.6		
Blank1a	51.6	0.0		6.1			51.0	0.1		6.3		
Blank1a												
Blank2a	300.4	b.d.l.		5.9			292.9	**0.2**		6.1		
	Q [mg/g]						**Q [mg/g]**					
0010	1.8	-0.5	45		25	0.999	1.6	-1.9	45		60	1.038
0010												
0050	5.4	-0.6	45		25	0.991	5.6	-1.9	45		60	1.017
0050												
0100	8.2	-0.5	45		25	1.011	8.9	-2.0	45		60	1.022
0100												
0150	10.1	-0.5	45		25	1.018	11.6	-2.0	45		60	1.003
0200	11.8	-0.5	45		25	0.997	13.0	-2.0	45		60	1.036
0200												
0300	15.6	-0.5	45		25	1.005	15.0	-2.0	45		60	0.993
0500	14.9	-0.4	45		25	0.999	17.2	-2.0	45		60	0.997
Blank 1	0.1	0.0	45		25	0	0.0	0.0	45		60	0
Blank 1												
Blank 2	0.4	b.d.l.	45		25	0	0.2	0.0	45		60	0

	Isotherm powder unbuffered						Isotherm powder pH buffered					
	Li	Al	stirring time [min]	pH	T [°C]	sorbent mass [g]	Li	Al	stirring time [min]	pH	T [°C]	sorbent mass [g]
Limit of detection	0.001	0.002					0.001	0.005				
Correlation coefficient	0.9999	1.0000					0.9999	1.0000				
sigma	0.000	0.001					0.000	0.002				
Limit of quantification	0.005	0.007					0.003	0.016				
Accuracy 1/100	92.77	97.2					92.9	98.0				
Accuracy 1/50												
Accuracy Misa 10	99.30	98.1					97.9	98.4				
Accuracy 1/5												
Accuracy 1/2	99.49	98.6					101.9	100.1				
uncertainty [%]	7.23	2.8					7.1	2.0				
	C [mg/L]						**C [mg/L]**					
MilliQ water	b.d.l.	0.0		5.85			b.d.l.	b.d.l.		6.14		
C0010	10.07	0.1					12.1	b.d.l.				
C0010							11.9	b.d.l.				
C0050	51.69	0.1					49.0	b.d.l.				
C0050							49.6	b.d.l.				
C0100	102.38	0.2					106.5	b.d.l.				
C0150	151.79	0.1					147.1	b.d.l.				
C0200	194.24	0.1					195.6	b.d.l.				
C0300	302.25	0.1					286.1	b.d.l.				
C0500	479.45	0.2					467.8	b.d.l.				
CBlank1	52.11	0.1					50.7	b.d.l.				
CBlank1							49.2	b.d.l.				
CBlank2	292.39	0.3					292.8	b.d.l.				
	C(Equ) [mg/L]						**C(Equ) [mg/L]**					
0010a	2	15.2		9.7			11.4	0.2		6.3		
0010a							11.1	0.2		6.3		
0050a	23	15.0		9.3			45.9	0.2		6.3		
0050a							45.7	0.2		6.3		
0100a	57	15.2		9.0			95.0	0.2		6.2		
0100a												
0150a	95	15.5		9.0			139.2	0.2		6.2		
0200a	131	14.7		8.9			185.2	0.2		6.2		
0200a												
0300a	213	15.2		8.8			272.9	0.2		6.2		
0300a												
0500a	390	13.9		8.5			464.6	4.3		6.1		
Blank1a	52	0.2		6.5			49.5	b.d.l.		6.0		
Blank1a							49.7	b.d.l.		6.0		
Blank2a	300	0.3		6.7			287.2	b.d.l.		5.9		
	Q [mg/g]						**Q [mg/g]**					
0010	1.52	-3.0	45		80	1.010	0.1	0.0	45		25	1.002
0010							0.2	0.0	45		25	1.002
0050	5.77	-3.0	45		80	0.998	0.6	0.0	45		25	1.000
0050							0.8	0.0	45		25	1.000
0100	8.98	-3.0	45		80	1.012	2.3	0.0	45		25	1.000
0100												
0150	11.57	-3.1	45		80	0.990	1.6	0.0	45		25	0.994
0200	12.61	-2.9	45		80	1.001	2.1	0.0	45		25	1.002
0200												
0300	17.37	-2.9	45		80	1.023	2.6	0.0	45		25	1.005
0500	17.41	-2.7	45		80	1.029	0.6	-0.9	45		25	1.001
Blank 1	0.06	0.0	45		80	0	0.2	b.d.l.	45		25	0
Blank 1							-0.1	b.d.l.	45		25	0
Blank 2	-1.61	0.0	45		80	0	1.1	b.d.l.	45		25	0

	Isotherm powder pH buffered						Isotherm powder pH buffered					
	Li	Al	stirring time [min]	pH	T [°C]	sorbent mass [g]	Li	Al	stirring time [min]	pH	T [°C]	sorbent mass [g]
Limit of detection	0.001	0.005					0.001	0.001				
Correlation coefficient	0.9999	1.0000					0.9999	0.9999				
sigma	0.000	0.002					0.000	0.000				
Limit of quantification	0.003	0.016					0.002	0.002				
Accuracy 1/100	92.9	98.0										
Accuracy 1/50							90.6	96.4				
Accuracy Misa 10	97.9	98.4					95.9	103.0				
Accuracy 1/5							94.7	102.1				
Accuracy 1/2	101.9	100.1										
uncertainty [%]	7.1	2.0					9.4	3.6				
	C [mg/L]						**C [mg/L]**					
MilliQ water	b.d.l.	b.d.l.					b.d.l.	b.d.l.				
C0010	12.2	b.d.l.					19.3	b.d.l.				
C0010	12.3	b.d.l.										
C0050	48.1	b.d.l.					51.5	0.0				
C0050	47.9	b.d.l.										
C0100	100.4	**b.d.l.**					108.4	b.d.l.				
C0150	140.6	b.d.l.					161.1	0.0				
C0200	197.1	b.d.l.					216.8	b.d.l.				
C0300	297.5	b.d.l.					308.3	0.0				
C0500	485.1	b.d.l.					489.7	0.0				
CBlank1	48.4	b.d.l.					48.3	0.0				
CBlank1	49.0	b.d.l.										
CBlank2	288.8	b.d.l.					304.4	0.0				
	C(Equ) [mg/L]						**C(Equ) [mg/L]**					
0010a	11.2	b.d.l.		6			16.4	0.4		6.5		
0010a	11.4	0.2		6								
0050a	43.8	0.1		6			44.7	0.5		6.5		
0050a	45.8	b.d.l.		6								
0100a	95.7	0.2		6			94.7	0.4		6.5		
0100a	92.9	0.1		6								
0150a	136.8	b.d.l.		6			143.2	0.3		6.4		
0200a	188.7	0.2		6			199.5	0.4		6.4		
0200a												
0300a	275.2	0.2		6			280.0	0.3		6.4		
0300a							277.9	0.3		6.4		
0500a	459.0	0.2		6			457.0	0.3		6.3		
Blank1a	48.1	b.d.l.		6			48.1	b.d.l.		6.1		
Blank1a	48.6	b.d.l.		6								
Blank2a	292.1	b.d.l.		6			298.9	0.0		5.9		
	Q [mg/g]						**Q [mg/g]**					
0010	0.2	b.d.l.	45		40	1.0006	0.6	-0.1	45		60	1.012
0010	0.2	0.0	45		40	1.0006						
0050	0.9	0.0	45		40	0.9912	1.3	-0.1	45		60	1.014
0050	0.4	b.d.l.	45		40	0.9912						
0100	0.9	0.0	45		40	1.0021	2.7	-0.1	45		60	1.003
0100	1.5	0.0	45		40	1.0021						
0150	0.8	b.d.l.	45		40	0.9995	3.6	-0.1	45		60	1.004
0200	1.7	0.0	45		40	1.0161	3.4	-0.1	45		60	1.009
0200												
0300	4.4	0.0	45		40	1.0228	6.0	-0.1	45		60	1.009
0500	5.2	0.0	45		40	0.9998	6.5	-0.1	45		60	1.004
Blank 1	0.1	b.d.l.	45		40	0	0.0	b.d.l.	45		60	0
Blank 1	0.1	b.d.l.	45		40	0						
Blank 2	-0.7	b.d.l.	45		40	0	1.1	0.0	45		60	0

	Isotherm powder pH buffered					
	Li	Al	stirring time [min]	pH	T [°C]	sorbent mass [g]
Limit of detection	0.001	0.005				
Correlation coefficient	0.9999	1.0000				
sigma	0.000	0.002				
Limit of quantification	0.003	0.016				
Accuracy 1/100	92.9	98.0				
Accuracy 1/50						
Accuracy Misa 10	97.9	98.4				
Accuracy 1/5						
Accuracy 1/2	101.9	100.1				
uncertainty [%]	7.1	2.0				
	C [mg/L]					
MilliQ water	b.d.l.	b.d.l.				
C0010	9.8	b.d.l.				
C0010	9.4	b.d.l.				
C0050	48.5	b.d.l.				
C0050	49.2	b.d.l.				
C0100	103.2	**b.d.l.**				
C0150	151.6	b.d.l.				
C0200	195.7	b.d.l.				
C0300	294.9	b.d.l.				
C0500	468.0	b.d.l.				
CBlank1	49.5	b.d.l.				
CBlank1	49.4	b.d.l.				
CBlank2	298.7	b.d.l.				
	C(Equ) [mg/L]					
0010a	9.2	0.2		6.2		
0010a	9.2	0.4		6.2		
0050a	44.8	0.3		6.2		
0050a	46.2	0.4		6.2		
0100a	93.7	0.3		6.2		
0100a						
0150a	139.6	0.4		6.2		
0200a	187.1	**0.5**		6.2		
0200a	186.1	0.5		6.2		
0300a	270.6	0.6		6.2		
0300a						
0500a	454.2	0.5		6.1		
Blank1a	48.9	b.d.l.		6		
Blank1a	48.8	b.d.l.		6		
Blank2a	287.8	b.d.l.		5.9		
	Q [mg/g]					
0010	0.12	0.0	45		80	1.012
0010	0.06	-0.1	45		80	1.012
0050	0.73	-0.1	45		80	1.005
0050	0.58	-0.1	45		80	1.005
0100	1.89	-0.1	45		80	1.004
0100						
0150	2.38	-0.1	45		80	1.002
0200	1.71	-0.1	45		80	1.009
0200	1.90	-0.1	45		80	1.009
0300	4.82	-0.1	45		80	1.007
0500	2.74	-0.1	45		80	1.010
Blank 1	0.13	b.d.l.	45		80	0
Blank 1	0.12	b.d.l.	45		80	0
Blank 2	2.17	b.d.l.	45		80	0

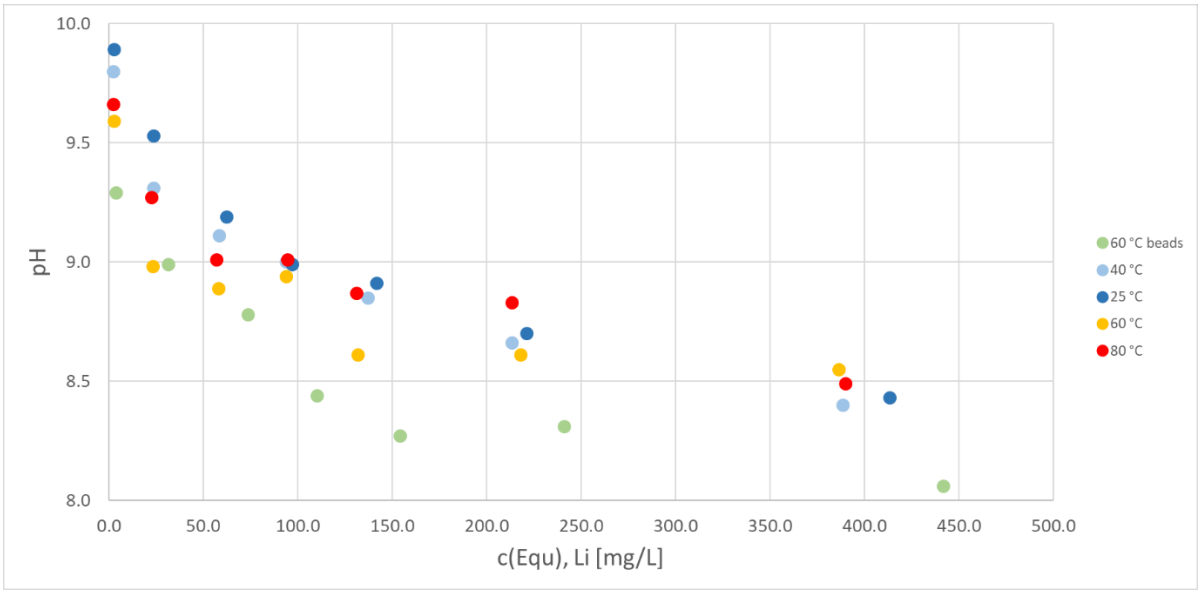
10.0
9.5
9.0
8.5
8.0
pH
0.0
50.0
100.0
150.0
200.0
250.0
300.0
350.0
400.0
450.0
500.0
c(Equ), Li [mg/L]
60 °C beads
40 °C
25 °C
60 °C
80 °C

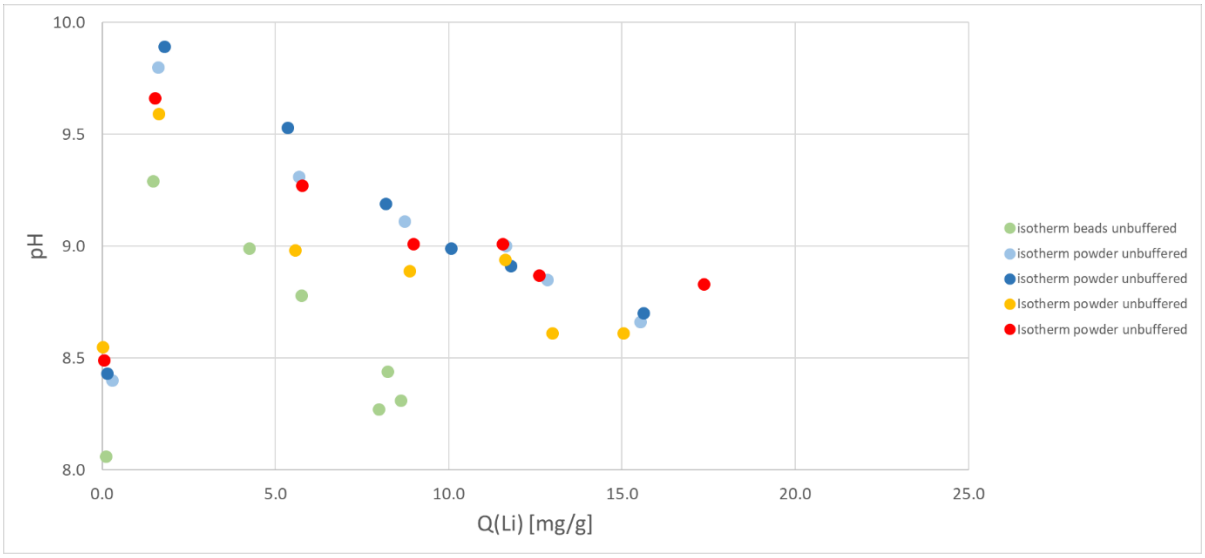
10.0
9.5
9.0
8.5
8.0
pH
0.0
5.0
10.0
15.0
20.0
25.0
Q(Li) [mg/g]
isotherm beads unbuffered
isotherm powder unbuffered
isotherm powder unbuffered
Isotherm powder unbuffered
Isotherm powder unbuffered

	stirring time [min]	pH	Li [mg/L]	Na [mg/L]	K [mg/L]	Ca [mg/L]	Mg [mg/L]	Al [mg/L]	Si [mg/L]	Fe [mg/L]	P [mg/L]	Ba [mg/L]
Limit of detection			0.002	0.017	0.045	0.005	0.000	0.005	0.016	0.003	0.013	0.000
sigma			0.001	0.006	0.015	0.002	0.000	0.002	0.005	0.001	0.004	0.000
Limit of quantification			0.006	0.055	0.150	0.016	0.000	0.017	0.055	0.009	0.043	0.000
Accuracy 1/50			88.9	93.2	94.9	94.2	95.6	97.1	95.5	97.3	96.0	96.2
Accuracy 1/5			93.4	94.9	97.0	100.6	97.5	100.3	96.4	99.0	96.0	96.9
uncertainty [%]			11.1	6.8	5.1	5.8	4.4	2.9	4.5	2.7	4.0	3.8
RR-ZEO-13X02-MilliQ			b.d.l.	b.d.l.	b.d.l.	0.0	b.d.l.	b.d.l.	b.d.l.	b.d.l.	b.d.l.	b.d.l.
RR-ZEO-13X02-C0010			10.8	0.3	20.5	0.0	b.d.l.	b.d.l.	b.d.l.	b.d.l.	16.4	b.d.l.
RR-ZEO-13X02-C0010			11.1	0.2	20.8	b.d.l.	b.d.l.	b.d.l.	b.d.l.	b.d.l.	16.3	b.d.l.
RR-ZEO-13X02-C0050			49.1	1.5	102.0	0.0	b.d.l.	b.d.l.	b.d.l.	b.d.l.	77.7	0.0
RR-ZEO-13X02-C0050			54.4	1.5	102.6	b.d.l.	b.d.l.	b.d.l.	b.d.l.	b.d.l.	82.5	b.d.l.
RR-ZEO-13X02-C0100			110.0	3.0	207.6	b.d.l.	b.d.l.	b.d.l.	b.d.l.	b.d.l.	167.6	b.d.l.
RR-ZEO-13X02-C0150			157.6	4.4	301.6	b.d.l.	b.d.l.	b.d.l.	b.d.l.	b.d.l.	249.8	b.d.l.
RR-ZEO-13X02-C0200			214.3	6.0	411.9	b.d.l.	b.d.l.	b.d.l.	b.d.l.	b.d.l.	330.9	b.d.l.
RR-ZEO-13X02-C0300			302.9	8.8	600.8	b.d.l.	b.d.l.	b.d.l.	b.d.l.	b.d.l.	496.9	b.d.l.
RR-ZEO-13X02-C0300			297.7	8.7	595.9	b.d.l.	b.d.l.	0.1	b.d.l.	b.d.l.	492.3	b.d.l.
RR-ZEO-13X02-C0500			475.3	14.4	978.4	1.4	b.d.l.	b.d.l.	b.d.l.	b.d.l.	808.8	0.1
RR-ZEO-13X02-CBlank1			49.8	1.5	102.8	0.0	b.d.l.	0.0	0.0	b.d.l.	78.0	0.0
RR-ZEO-13X02-CBlank1			55.3	1.4	104.0	b.d.l.	b.d.l.	b.d.l.	b.d.l.	b.d.l.	83.8	b.d.l.
RR-ZEO-13X02-CBlank2			306.0	8.7	593.5	b.d.l.	b.d.l.	b.d.l.	b.d.l.	b.d.l.	491.0	b.d.l.
RR-ZEO-13X02-0010a			3.4	55.0	0.6	0.1	0.0	1.9	2.7	0.0	16.0	b.d.l.
RR-ZEO-13X02-0010a			3.2	51.0	0.7	0.1	b.d.l.	1.7	2.7	b.d.l.	16.4	b.d.l.
RR-ZEO-13X02-0050a			33.9	157.5	10.0	0.0	0.0	0.8	5.0	0.0	76.2	b.d.l.
RR-ZEO-13X02-0050a			34.9	155.8	9.7	b.d.l.	b.d.l.	0.8	5.3	b.d.l.	80.7	b.d.l.
RR-ZEO-13X02-0100a			86.6	242.8	35.9	b.d.l.	b.d.l.	0.9	6.9	b.d.l.	164.4	b.d.l.
RR-ZEO-13X02-0150a			136.2	291.2	79.3	b.d.l.	b.d.l.	0.6	7.8	b.d.l.	239.5	b.d.l.
RR-ZEO-13X02-0200a			185.9	322.3	135.6	b.d.l.	b.d.l.	0.4	8.2	b.d.l.	323.6	b.d.l.
RR-ZEO-13X02-0300a			275.8	371.5	275.8	b.d.l.	b.d.l.	0.1	8.7	b.d.l.	479.3	b.d.l.
RR-ZEO-13X02-0500a			459.2	422.4	616.5	0.1	0.1	0.1	11.0	b.d.l.	810.4	b.d.l.
RR-ZEO-13X02-Blank1a			49.9	1.6	103.8	0.0	b.d.l.	0.0	0.0	b.d.l.	78.1	0.0
RR-ZEO-13X02-Blank1a			53.4	1.5	100.1	b.d.l.	b.d.l.	b.d.l.	b.d.l.	b.d.l.	84.9	b.d.l.
RR-ZEO-13X02-Blank2a			296.0	8.7	589.2	0.1	b.d.l.	0.1	b.d.l.	b.d.l.	492.2	b.d.l.
							Q [mg/g]					
RR-ZEO-13X02-0010	45	9.2	1.5	-10.9	4.0	0.0	0.0	-0.4	-0.5	0.0	0.1	no value
RR-ZEO-13X02-0010	45	9.2	1.6	-10.1	4.0	0.0	no value	-0.3	-0.5	no value	0.0	no value
RR-ZEO-13X02-0050	45	7.8	3.0	-31.2	18.4	0.0	0.0	-0.2	-1.0	0.0	0.3	no value
RR-ZEO-13X02-0050	45	7.8	3.9	-30.9	18.6	no value	no value	-0.2	-1.1	no value	0.4	no value
RR-ZEO-13X02-0100	45	7.2	4.7	-48.0	34.4	no value	no value	-0.2	-1.4	no value	0.6	no value
RR-ZEO-13X02-0150	45	6.9	4.3	-57.3	44.4	no value	no value	-0.1	-1.5	no value	2.1	no value
RR-ZEO-13X02-0200	45	6.7	5.7	-63.4	55.4	no value	no value	-0.1	-1.6	no value	1.5	no value
RR-ZEO-13X02-0300	45	6.4	5.4	-72.1	64.6	no value	no value	0.0	-1.7	no value	3.5	no value
RR-ZEO-13X02-0500	45	6.1	3.2	-81.9	72.7	0.3	0.0	0.0	-2.2	no value	-0.3	no value

	stirring time [min]	sorbent mass [g]	pH	T [°C]	Li [mg/L]	Na [mg/L]	K [mg/L]	Ca [mg/L]	Mg [mg/L]	Al [mg/L]	Si [mg/L]	P [mg/L]	Mn [mg/L]	S [mg/L]	Ba [mg/L]	Rb [mg/L]	Sr [mg/L]	As [mg/L]	Pb [mg/L]	Zn [mg/L]	Cu [mg/L]
Limit of detection					0.004	0.005	0.034	0.009	0.001	0.023	0.015	0.009	0.000	0.003	0.000	0.411	0.000	0.002	0.008	0.000	0.003
Correlation coefficient					1.0000	0.9998	1.0000	0.9999	0.9999	1.0000	1.0000	0.9999	1.0000	0.9999	1.0000	0.9997	1.0000	1.0000	0.9999	0.9999	1.0000
simga					0.001	0.002	0.011	0.003	0.000	0.008	0.005	0.003	0.000	0.001	0.000	0.137	0.000	0.001	0.003	0.000	0.001
Limit of quantification					0.013	0.016	0.113	0.031	0.005	0.075	0.050	0.031	0.001	0.010	0.002	1.371	0.000	0.007	0.027	0.001	0.009
Accuracy 1/100					96.3	96.1	101.0	94.0	93.6	96.8	97.9	97.2	96.8	95.3	99.4	260.4	95.9	98.8	97.3	96.0	101.0
Accuracy Misa					96.8	101.5	101.7	97.8	97.6	100.6		100.3	99.5		99.6	101.8	98.5		103.9	98.9	100.9
Accuracy 1/2					102.3	101.9	103.0	100.4	102.4	99.8	99.9	100.7	102.5	100.8	102.1	103.2	100.7	105.8	104.6	100.6	105.2
uncertainty [%]					3.7	3.9	3.0	6.0	6.4	3.2	2.1	2.8	3.2	4.7	2.1	160.4	4.1	5.8	4.6	4.0	5.2
RR-ZEO-13XTW01-MilliQ				25	b.d.l.	0.0	b.d.l.	0.0	b.d.l.	b.d.l.	b.d.l.	b.d.l.	b.d.l.	b.d.l.	b.d.l.	b.d.l.	b.d.l.	b.d.l.	b.d.l.	b.d.l.	b.d.l.
RR-ZEO-13XTW01-C0				25	154.6	34943.5	3132.5	7399.5	361.6	b.d.l.	27.2	b.d.l.	24.4	113.2	9.0	b.d.l.	379.7	4.0	b.d.l.	13.7	3.1
RR-ZEO-13XTW01-0001a		1.001	5.37	60	157.1	35865.3	3090.2	7342.9	365.6	b.d.l.	30.8	b.d.l.	23.8	113.2	7.1	b.d.l.	361.0	3.8	b.d.l.	13.6	3.1
RR-ZEO-13XTW01-0005a		1.016	5.38	60	153.5	34888.9	3024.4	7152.1	358.1	b.d.l.	28.3	b.d.l.	23.2	111.6	7.0	b.d.l.	353.6	3.8	b.d.l.	13.3	3.0
RR-ZEO-13XTW01-0015a		1.001	5.29	60	155.4	35496.1	3058.6	7156.9	359.3	b.d.l.	30.2	b.d.l.	23.4	111.2	7.2	b.d.l.	355.5	3.8	b.d.l.	13.4	3.2
RR-ZEO-13XTW01-0030a		0.997	5.32	60	154.5	35111.7	3070.6	7194.6	360.3	b.d.l.	30.5	b.d.l.	23.5	111.5	7.2	b.d.l.	356.5	3.9	b.d.l.	15.6	6.1
RR-ZEO-13XTW01-0045a		1.002	5.30	60	154.8	35206.1	3058.3	7131.1	356.4	b.d.l.	30.0	b.d.l.	23.4	112.5	7.3	b.d.l.	352.7	3.9	b.d.l.	13.3	3.0
RR-ZEO-13XTW01-0060a		0.998	5.35	60	156.7	35560.6	3091.5	7253.2	363.6	b.d.l.	31.8	b.d.l.	23.7	112.9	7.4	b.d.l.	360.7	3.7	b.d.l.	13.5	3.4
RR-ZEO-13XTW01-0120a		1.000	5.39	60	155.2	35419.4	3056.3	7148.8	359.0	5.7	30.3	b.d.l.	23.5	111.8	7.3	b.d.l.	355.6	3.7	b.d.l.	13.5	3.1
RR-ZEO-13XTW01-0180a		1.002	5.13	60	154.6	34779.5	3051.0	7128.8	358.9	b.d.l.	31.9	b.d.l.	23.3	110.9	7.3	b.d.l.	355.9	3.8	b.d.l.	13.4	3.1
RR-ZEO-13XTW01-1440a		0.999	5.19	60	155.3	35397.2	3071.6	7135.5	359.5	b.d.l.	27.7	b.d.l.	23.4	111.3	7.4	b.d.l.	355.7	3.8	b.d.l.	13.6	3.2
RR-ZEO-13XTW01-1Woa		1.002	5.38	60	156.3	35809.0	3104.2	7193.8	364.1	b.d.l.	21.2	b.d.l.	23.6	112.5	7.5	b.d.l.	357.6	3.7	b.d.l.	13.8	3.4
RR-ZEO-13XTW01-2Woa		1.014	5.36	60	163.3	36659.5	-	7194.8	362.1	b.d.l.	20.2	b.d.l.	23.9	165.2	-	-	-	-	-	-	-
RR-ZEO-13XTW01-Blank1a			2.71	60	156.4	35404.6	3122.7	7326.1	356.4	b.d.l.	26.4	b.d.l.	24.2	112.6	9.0	b.d.l.	374.0	4.0	b.d.l.	13.7	3.0
RR-ZEO-13XTW01-Blank2a			2.71	60	157.2	35528.1	3144.8	7378.3	360.2	b.d.l.	26.6	b.d.l.	24.4	113.9	9.0	b.d.l.	376.7	4.0	b.d.l.	13.8	3.2

Q		Li [mg/g]	Na [mg/g]	K [mg/g]	Ca [mg/g]	Mg [mg/g]	Al [mg/g]	Si [mg/g]	P [mg/g]	Mn [mg/g]	S [mg/g]	Ba [mg/g]	Rb [mg/g]	Sr [mg/g]	As [mg/g]	Pb [mg/g]	Zn [mg/g]	Cu [mg/g]
RR-ZEO-13XTW01-0001	1	-0.5	-184.2	8.5	11.3	-0.8	-	-0.7	-	0.1	0.0	0.4	-	3.7	0.0	-	0.0	0.0
RR-ZEO-13XTW01-0005	5	0.2	10.7	21.3	48.7	0.7	-	-0.2	-	0.2	0.3	0.4	-	5.1	0.0	-	0.1	0.0
RR-ZEO-13XTW01-0015	15	-0.2	-110.4	14.8	48.4	0.5	-	-0.6	-	0.2	0.4	0.4	-	4.8	0.0	-	0.1	0.0
RR-ZEO-13XTW01-0030	30	0.0	-33.7	12.4	41.1	0.3	-	-0.7	-	0.2	0.3	0.3	-	4.6	0.0	-	-0.4	-0.6
RR-ZEO-13XTW01-0045	45	-0.1	-52.4	14.8	53.5	1.0	-	-0.6	-	0.2	0.1	0.3	-	5.4	0.0	-	0.1	0.0
RR-ZEO-13XTW01-0060	60	-0.4	-123.6	8.2	29.3	-0.4	-	-0.9	-	0.1	0.1	0.3	-	3.8	0.1	-	0.0	0.0
RR-ZEO-13XTW01-0120	120	-0.1	-95.2	15.2	50.1	0.5	-	-0.6	-	0.2	0.3	0.3	-	4.8	0.1	-	0.0	0.0
RR-ZEO-13XTW01-0180	180	0.0	32.7	16.3	54.0	0.6	-	-0.9	-	0.2	0.5	0.3	-	4.8	0.0	-	0.0	0.0
RR-ZEO-13XTW01-1440	1440	-0.2	-90.9	12.2	52.9	0.4	-	-0.1	-	0.2	0.4	0.3	-	4.8	0.0	-	0.0	0.0
RR-ZEO-13XTW01-1Wo	10080	-0.4	-172.8	5.6	41.0	-0.5	-	1.2	-	0.2	0.2	0.3	-	4.4	0.1	-	0.0	0.0
RR-ZEO-13XTW01-2Wo	20160	-1.7	-338.6	-	40.4	-2.0	-	1.6	-	0.1	-10.2	-	-	-	-	-	-	-
RR-ZEO-13XTW01-Blank1	15	-0.4	-92.2	2.0	14.7	1.0	-	0.1	-	0.0	0.1	0.0	-	1.1	0.0	-	0.0	0.0
RR-ZEO-13XTW01-Blank2	1020	-0.5	-116.9	-2.5	4.2	0.3	-	0.1	-	0.0	-0.1	0.0	-	0.6	0.0	-	0.0	0.0

- no value

	used solution	stirring time [min]	T [°C]	pH	sorbent mass [g]	Li [mg/L]	Na [mg/L]	K [mg/L]	Ca [mg/L]	Mg [mg/L]	Al [mg/L]	Si [mg/L]	Fe [mg/L]	P [mg/L]	Ba [mg/L]
Limit of detection						0.002	0.654	0.027	0.003	0.000	0.008	0.025	0.005	0.016	0.000
Correlation coefficient						0.9998	1.0000	0.9999	1.0000	1.0000	1.0000	1.0000	0.9999	0.9999	0.9998
sigma						0.001	0.218	0.009	0.001	0.000	0.003	0.008	0.002	0.005	0.000
Limit of quantification						0.007	2.179	0.089	0.011	0.000	0.028	0.082	0.016	0.053	0.002
Accuracy 1/100						90.4	94.2	95.0	95.8	91.4	97.3	99.6	95.0	98.5	96.1
Accuracy Misa						98.3	99.1	97.0	104.5	102.9	98.9	0.0	102.7	102.2	99.5
Accuracy 1/2						97.6	97.8	96.9	99.0	99.4	97.9	100.1	98.0	98.5	97.6
uncertainty [%]						9.6	5.8	5.0	4.2	8.6	2.7	0.4	5.0	2.2	3.9
zeolite 13X powder for desorption c0						694	b.d.l.	b.d.l.	0.9	0.0	b.d.l.	b.d.l.	b.d.l.	b.d.l.	0.1
zeolite 13X powder for desorption c1						548	662	b.d.l.	1.5	0.1	5.0	b.d.l.	b.d.l.	b.d.l.	b.d.l.
RR-ZEO-13XD01-C01	Milli-Q					b.d.l.	b.d.l.	b.d.l.	0.0	0.0	b.d.l.	b.d.l.	b.d.l.	b.d.l.	b.d.l.
RR-ZEO-13XD01-C02	0.1M NaCl					b.d.l.	2310	b.d.l.	0.2	0.0	b.d.l.	b.d.l.	b.d.l.	b.d.l.	b.d.l.
RR-ZEO-13XD01-C03	0.5M NaCl					b.d.l.	11605	b.d.l.	1.0	0.1	b.d.l.	b.d.l.	b.d.l.	b.d.l.	b.d.l.
RR-ZEO-13XD01-C04	1M NaCl					b.d.l.	22795	b.d.l.	3.9	0.1	b.d.l.	b.d.l.	b.d.l.	b.d.l.	0.2
RR-ZEO-13XD01-C05	2M NaCl					b.d.l.	45842	b.d.l.	4.9	0.2	b.d.l.	b.d.l.	b.d.l.	b.d.l.	b.d.l.
RR-ZEO-13XD01-C06	3M NaCl					b.d.l.	68949	b.d.l.	4.3	0.2	b.d.l.	b.d.l.	b.d.l.	b.d.l.	b.d.l.
RR-ZEO-13XD01-C06	3M NaCl					b.d.l.	68219	b.d.l.	4.7	0.3	b.d.l.	b.d.l.	b.d.l.	b.d.l.	b.d.l.
RR-ZEO-13XD01-C07	0.1M HCl					b.d.l.	1	b.d.l.	0.0	0.0	b.d.l.	b.d.l.	b.d.l.	b.d.l.	b.d.l.
RR-ZEO-13XD01-C08	0.5M HCl					b.d.l.	b.d.l.	b.d.l.	0.0	0.0	b.d.l.	b.d.l.	b.d.l.	b.d.l.	0.0
RR-ZEO-13XD01-C09	1M HCl					b.d.l.	b.d.l.	b.d.l.	0.0	0.0	b.d.l.	b.d.l.	0.0	b.d.l.	b.d.l.
RR-ZEO-13XD01-C10	0.1M CH3COOH					b.d.l.	b.d.l.	b.d.l.	0.0	0.0	b.d.l.	b.d.l.	b.d.l.	b.d.l.	b.d.l.
RR-ZEO-13XD01-C11	0.5M CH3COOH					b.d.l.	b.d.l.	b.d.l.	0.0	0.0	b.d.l.	b.d.l.	b.d.l.	b.d.l.	0.0
RR-ZEO-13XD01-C12	1M CH3COOH					b.d.l.	b.d.l.	b.d.l.	0.0	0.0	0.0	b.d.l.	b.d.l.	b.d.l.	b.d.l.
RR-ZEO-13XD01-C13	0.1M CH3COONa					b.d.l.	2357	b.d.l.	0.2	0.0	b.d.l.	b.d.l.	b.d.l.	b.d.l.	b.d.l.
RR-ZEO-13XD01-C14	0.5M CH3COONa					b.d.l.	11221	b.d.l.	1.4	0.1	b.d.l.	b.d.l.	b.d.l.	b.d.l.	b.d.l.
RR-ZEO-13XD01-C15	1M CH3COONa					b.d.l.	22912	b.d.l.	4.3	0.6	b.d.l.	b.d.l.	b.d.l.	b.d.l.	b.d.l.
RR-ZEO-13XD01-01a	Milli-Q					1.2	1.5	b.d.l.	0.0	0.0	0.4	0.3	0.0	b.d.l.	b.d.l.
RR-ZEO-13XD01-02a	0.1M NaCl					55.0	2088.8	2.1	0.4	0.2	b.d.l.	b.d.l.	b.d.l.	b.d.l.	b.d.l.
RR-ZEO-13XD01-03a	0.5M NaCl					56.4	11104.0	2.9	3.4	1.4	b.d.l.	b.d.l.	b.d.l.	b.d.l.	b.d.l.
RR-ZEO-13XD01-04a	1M NaCl					57.3	22048.1	b.d.l.	5.1	1.5	b.d.l.	b.d.l.	b.d.l.	b.d.l.	b.d.l.
RR-ZEO-13XD01-05a	2M NaCl					59.4	46618.1	b.d.l.	8.6	1.7	b.d.l.	b.d.l.	b.d.l.	b.d.l.	b.d.l.
RR-ZEO-13XD01-06a	3M NaCl					57.2	68635.6	b.d.l.	9.2	1.8	b.d.l.	b.d.l.	b.d.l.	b.d.l.	b.d.l.
RR-ZEO-13XD01-07a	0.1M HCl					60.8	377.8	5.0	7.6	4.6	695.4	841.5	1.0	b.d.l.	0.1
RR-ZEO-13XD01-08a	0.5M HCl					61.3	360.7	b.d.l.	8.0	4.9	723.4	868.7	1.2	b.d.l.	0.1
RR-ZEO-13XD01-09a	1M HCl					61.3	369.8	3.6	8.1	4.9	723.8	871.4	1.3	b.d.l.	0.1
RR-ZEO-13XD01-10a	0.1M CH3COOH					61.2	323.9	b.d.l.	5.3	3.7	353.1	451.2	b.d.l.	b.d.l.	b.d.l.
RR-ZEO-13XD01-11a	0.5M CH3COOH					63.0	380.0	3.0	8.0	4.8	735.6	881.3	1.1	b.d.l.	0.1
RR-ZEO-13XD01-12a	1M CH3COOH					62.0	372.9	2.9	9.0	5.1	719.8	865.5	1.8	b.d.l.	0.1
RR-ZEO-13XD01-13a	0.1M CH3COONa					55.1	2121.0	2.3	0.5	0.2	b.d.l.	b.d.l.	b.d.l.	b.d.l.	b.d.l.
RR-ZEO-13XD01-14a	0.5M CH3COONa					57.7	10999.5	b.d.l.	3.7	1.4	b.d.l.	b.d.l.	b.d.l.	b.d.l.	b.d.l.
RR-ZEO-13XD01-15a	1M CH3COONa					55.9	22222.3	b.d.l.	6.7	1.5	b.d.l.	b.d.l.	b.d.l.	b.d.l.	b.d.l.

Q	used solution	stirring time [min]	T [°C]	pH	sorbent mass [g]	Li [mg/g]	Na [mg/g]	K [mg/g]	Ca [mg/g]	Mg [mg/g]	Al [mg/g]	Si [mg/g]	Fe [mg/g]	P [mg/g]	Ba [mg/g]
zeolite 13X powder for desorption	inital		25			11.6	-52	b.d.l.	0.0	0.0	-0.4	b.d.l.	b.d.l.	b.d.l.	0.0
RR-ZEO-13X06-KXX	calcined initial					0.0	120	1.0	0.9	0.7	85.9	b.d.l.	0.2	b.d.l.	0.0
RR-ZEO-13XD01-01	Milli-Q	45	25	10.27	0.999	-0.2	0	b.d.l.	0.0	0.0	-0.1	-0.1	0.0	b.d.l.	b.d.l.
RR-ZEO-13XD01-02	0.1M NaCl	45	25	6.84	1.007	-10.9	44	-0.4	0.0	0.0	b.d.l.	b.d.l.	b.d.l.	b.d.l.	b.d.l.
RR-ZEO-13XD01-03	0.5M NaCl	45	25	6.23	0.996	-11.3	101	-0.6	-0.5	-0.3	b.d.l.	b.d.l.	b.d.l.	b.d.l.	b.d.l.
RR-ZEO-13XD01-04	1M NaCl	45	25	6.22	1.026	-11.2	146	b.d.l.	-0.2	-0.3	b.d.l.	b.d.l.	b.d.l.	b.d.l.	0.0
RR-ZEO-13XD01-05	2M NaCl	45	25	5.79	1.009	-11.8	-154	b.d.l.	-0.7	-0.3	b.d.l.	b.d.l.	b.d.l.	b.d.l.	b.d.l.
RR-ZEO-13XD01-06	3M NaCl	45	25	5.78	1.005	-11.4	62	b.d.l.	-1.0	-0.3	b.d.l.	b.d.l.	b.d.l.	b.d.l.	b.d.l.
RR-ZEO-13XD01-06	3M NaCl	45	25	5.78	1.005	-11.4	-83	b.d.l.	-0.9	-0.3	b.d.l.	b.d.l.	b.d.l.	b.d.l.	b.d.l.
RR-ZEO-13XD01-07	0.1M HCl	45	25	3.09	1.010	-12.0	-75	-1.0	-1.5	-0.9	-137.7	-166.6	-0.2	b.d.l.	0.0
RR-ZEO-13XD01-08	0.5M HCl	45	25	0.62	1.007	-12.2	-72	b.d.l.	-1.6	-1.0	-143.7	-172.6	-0.2	b.d.l.	0.0
RR-ZEO-13XD01-09	1M HCl	45	25	0.28	1.009	-12.2	-73	-0.7	-1.6	-1.0	-143.5	-172.8	-0.3	b.d.l.	0.0
RR-ZEO-13XD01-10	0.1M CH3COOH	45	25	4.3	0.994	-12.3	-65	b.d.l.	-1.1	-0.7	-71.0	-90.8	b.d.l.	b.d.l.	b.d.l.
RR-ZEO-13XD01-11	0.5M CH3COOH	45	25	3.64	1.014	-12.4	-75	-0.6	-1.6	-0.9	-145.1	-173.9	-0.2	b.d.l.	0.0
RR-ZEO-13XD01-12	1M CH3COOH	45	25	3.36	0.995	-12.5	-75	-0.6	-1.8	-1.0	-144.7	-174.0	-0.4	b.d.l.	0.0
RR-ZEO-13XD01-13	0.1M CH3COONa	45	25	7.82	0.994	-11.1	48	-0.5	0.0	0.0	b.d.l.	b.d.l.	b.d.l.	b.d.l.	b.d.l.
RR-ZEO-13XD01-14	0.5M CH3COONa	45	25	8.11	0.991	-11.7	45	b.d.l.	-0.5	-0.3	b.d.l.	b.d.l.	b.d.l.	b.d.l.	b.d.l.
RR-ZEO-13XD01-15	1M CH3COONa	45	25	8.3	0.985	-11.4	140	b.d.l.	-0.5	-0.2	b.d.l.	b.d.l.	b.d.l.	b.d.l.	b.d.l.

Percentage/Recovery [%]		Li [%]	Na [%]	K [%]	Ca [%]	Mg [%]	Al [%]	Si [%]	Fe [%]	P [%]	Ba [%]
RR-ZEO-13XD01-01	Milli-Q	2	-1	no value	-2	-14	-21	no value	no value	no value	no value
RR-ZEO-13XD01-02	0.1M NaCl	94	84	no value	-86	-1791	no value	no value	no value	no value	no value
RR-ZEO-13XD01-03	0.5M NaCl	98	192	no value	-1079	-12404	no value	no value	no value	no value	no value
RR-ZEO-13XD01-04	1M NaCl	96	278	no value	-524	-12782	no value	no value	no value	no value	-375
RR-ZEO-13XD01-05	2M NaCl	102	-293	no value	-1590	-14484	no value	no value	no value	no value	no value
RR-ZEO-13XD01-06	3M NaCl	98	119	no value	-2133	-14801	no value	no value	no value	no value	no value
RR-ZEO-13XD01-06	3M NaCl	98	-158	no value	-1945	-14602	no value	no value	no value	no value	no value
RR-ZEO-13XD01-07	0.1M HCl	104	-142	no value	-3276	-43156	-34898	no value	no value	no value	246
RR-ZEO-13XD01-08	0.5M HCl	105	-137	no value	-3436	-45414	-36430	no value	no value	no value	243
RR-ZEO-13XD01-09	1M HCl	105	-140	no value	-3494	-45518	-36388	no value	no value	no value	235
RR-ZEO-13XD01-10	0.1M CH3COOH	106	-124	no value	-2315	-34705	-18009	no value	no value	no value	no value
RR-ZEO-13XD01-11	0.5M CH3COOH	107	-143	no value	-3415	-44401	-36789	no value	no value	no value	243
RR-ZEO-13XD01-12	1M CH3COOH	108	-143	no value	-3925	-48235	-36687	no value	no value	no value	249
RR-ZEO-13XD01-13	0.1M CH3COONa	96	91	no value	-106	-2217	no value	no value	no value	no value	no value
RR-ZEO-13XD01-14	0.5M CH3COONa	101	85	no value	-1001	-12396	no value	no value	no value	no value	no value
RR-ZEO-13XD01-15	1M CH3COONa	98	267	no value	-1052	-8845	no value	no value	no value	no value	no value
Recovery [mmol/g]		**Li [mmol/g]**	**Na [mmol/g]**	**K [mmol/g]**	**Ca [mmol/g]**	**Mg [mmol/g]**	**Al [mmol/g]**	**Si [mmol/g]**	**Fe [mmol/g]**	**P [mmol/g]**	**Ba [mmol/g]**
zeolite 13X powder for desorption	powder for desorption	1.67	-2.28	no value	0.00	0.00	-0.01	no value	no value	no value	0.00
RR-ZEO-13X06-KXX	calcined initial	0.00	5.23	no value	0.02	0.03	3.18	no value	0.00	no value	0.00
RR-ZEO-13XD01-01	Milli-Q	-0.04	-0.01	no value	0.00	0.00	0.00	0.00	0.00	no value	no value
RR-ZEO-13XD01-02	0.1M NaCl	-1.57	1.91	no value	0.00	0.00	no value	no value	no value	no value	no value
RR-ZEO-13XD01-03	0.5M NaCl	-1.63	4.38	no value	-0.01	-0.01	no value	no value	no value	no value	no value
RR-ZEO-13XD01-04	1M NaCl	-1.61	6.33	no value	-0.01	-0.01	no value	no value	no value	no value	0.00
RR-ZEO-13XD01-05	2M NaCl	-1.70	-6.69	no value	-0.02	-0.01	no value	no value	no value	no value	no value
RR-ZEO-13XD01-06	3M NaCl	-1.64	2.72	no value	-0.02	-0.01	no value	no value	no value	no value	no value
RR-ZEO-13XD01-06	3M NaCl	-1.64	-3.60	no value	-0.02	-0.01	no value	no value	no value	no value	no value
RR-ZEO-13XD01-07	0.1M HCl	-1.73	-3.24	no value	-0.04	-0.04	-5.10	-5.93	0.00	no value	0.00
RR-ZEO-13XD01-08	0.5M HCl	-1.75	-3.12	no value	-0.04	-0.04	-5.33	-6.14	0.00	no value	0.00
RR-ZEO-13XD01-09	1M HCl	-1.75	-3.19	no value	-0.04	-0.04	-5.32	-6.15	0.00	no value	0.00
RR-ZEO-13XD01-10	0.1M CH3COOH	-1.77	-2.83	no value	-0.03	-0.03	-2.63	-3.23	no value	no value	no value
RR-ZEO-13XD01-11	0.5M CH3COOH	-1.79	-3.26	no value	-0.04	-0.04	-5.38	-6.19	0.00	no value	0.00
RR-ZEO-13XD01-12	1M CH3COOH	-1.80	-3.26	no value	-0.05	-0.04	-5.36	-6.20	-0.01	no value	0.00
RR-ZEO-13XD01-13	0.1M CH3COONa	-1.60	2.07	no value	0.00	0.00	no value	no value	no value	no value	no value
RR-ZEO-13XD01-14	0.5M CH3COONa	-1.68	1.95	no value	-0.01	-0.01	no value	no value	no value	no value	no value
RR-ZEO-13XD01-15	1M CH3COONa	-1.64	6.09	no value	-0.01	-0.01	no value	no value	no value	no value	no value

	stirring time [min]	pH	T [°C]	sorbent mass [g]	Li	Na	K	Ca	Al	Si	Fe	Mg	Mn	Pb	Zn	Ba	Sr	As	S
Limit of detection					0.001	0.006	0.035	0.005	0.008	0.007	0.002	0.002	0.000	1.804E-05	0.001	0.000	0.000	0.001	0.014
Correlation coefficient					1.0000	1.0000	0.9999	0.9999	1.0000	0.9999	1.0000	0.9997	1.0000		1.0000	0.9998	1.0000	0.9999	0.9999
sigma					0.000	0.002	0.012	0.002	0.003	0.002	0.001	0.001	0.000	6.01E-06	0.000	0.000	0.000	0.000	0.005
Limit of quantification					0.004	0.019	0.116	0.017	0.026	0.022	0.008	0.006	0.002	0.000	0.003	0.000	0.000	0.002	0.046
Accuracy 1/100					105.57	102.98	105.13	112.19	106.10	104.42	103.73	109.09	103.11		103.80	105.26	104.97	103.51	99.21
Accuracy Misa 10					95.11	97.51	101.34	103.06	97.60		97.88	103.23	99.26		98.90	103.87	100.11		
Accuracy 1/2					97.32	97.74	101.30	101.72	99.21	100.66	96.42	101.99	96.37		97.09	101.04	99.31	94.00	99.85
uncertainty [%]					5.57	2.98	5.13	12.19	6.10	4.42	3.73	9.09	3.63	2.15	3.80	5.26	4.97	6.00	0.79
absolute uncertainty B [mg/L]					8.5	1035	173	468	0.4	1.3		33.3	0.9	0.1	0.6	0.5	17.6	0.5	1.0
absolute uncertainty NG [mg/L]					4.5	1554	105	511	0.8	1.2		79.1	0.6	0.1	0.3	0.5	20.8	0.5	1.6
	C [mg/L]																		
ZEO-13XORG-B1					152.8	34557	3529	7761	b.d.l.	b.d.l.	b.d.l.	365	24.3	8.0	15.9	9.3	375	8.87	130
ZEO-13XORG-B2					151.6	34479	3277	1	b.d.l.	b.d.l.	b.d.l.	370	23.6	4.0	14.3	11.3	368	9.00	131
ZEO-13XNDB-NG1					9.8	69202	847	8417	b.d.l.	b.d.l.	b.d.l.	1368	12.0	3.4	3.0	9.7	501	b.d.l.	263
ZEO-13XNDB-NG2					10.1	70183	846	1	b.d.l.	b.d.l.	b.d.l.	1376	13.0	1.4	4.3	2.5	514	b.d.l.	259
ZEO-13XORG-B1a					152.9	35264	3462	7584	9.1	33.9	b.d.l.	366	23.9	7.2	15.9	7.9	359	8.64	129
ZEO-13XORG-B2a					150.8	34541	3192	8	4.0	26.3	b.d.l.	366	22.0	2.6	13.8	6.9	318	8.67	131
ZEO-13XNDB-NG1a					9.9	70185	846	8359	21.9	30.0	b.d.l.	1379	11.8	3.3	3.1	8.5	490	b.d.l.	262
ZEO-13XNDB-NG2a					9.9	68417	838	7	2.6	3.9	b.d.l.	1378	11.4	1.2	4.1	8.0	468	b.d.l.	263
	Q [mg/g]																		
ZEO-13XORG-B1 - Ca	45	2.01	60	1.009	0.0	-140	13	35	-1.8	-6.7	b.d.l.	-0.1	0.1	4	0.0	0.3	3.2	0.04	0.3
ZEO-13XORG-B2	45	2.09	60	1.008	0.1	-12	17	-1	-0.8	-5.2	b.d.l.	0.7	0.3	7	0.1	0.9	9.9	0.06	0.0
ZEO-13XNDB-NG1 - Ca	45	5.28	60	1.002	0.0	-196	0	12	-4.4	-6.0	b.d.l.	-2.3	0.0	0	0.0	0.2	2.1	b.d.l.	0.2
ZEO-13XNDB-NG2	45	5.55	60	1.002	0.0	352	2	-1	-0.5	-0.8	b.d.l.	-0.3	0.3	1	0.0	-1.1	9.3	b.d.l.	-0.7
M [g/mol]					6.941	22.990	39.098	40.078	26.982	28.086	55.845	24.305	54.938	207.200	65.380	137.327	87.620	74.922	32.065
	Q [mmol/g]																		
Bruchsal	45	2.01	60	1.009	0.00	-6	0.3	0.9	-0.07	-0.24	b.d.l.	0.00	0.00	0.02	0.000	0.00	0.04	0.00	0.01
Bruchsal (without Ca)	45	2.09	60	1.008	0.02	-1	0.4	0.0	-0.03	-0.19	b.d.l.	0.03	0.01	0.03	0.001	0.01	0.11	0.00	0.00
Neustadt-Glewe	45	5.28	60	1.002	0.00	-9	0.0	0.3	-0.16	-0.21	b.d.l.	-0.09	0.00	0.00	0.000	0.00	0.02	b.d.l.	0.01
Neustadt-Glewe (without Ca)	45	5.55	60	1.002	0.00	15	0.0	0.0	-0.02	-0.03	b.d.l.	-0.01	0.01	b.d.l.	0.001	-0.01	0.11	b.d.l.	-0.02

below limit of quantification

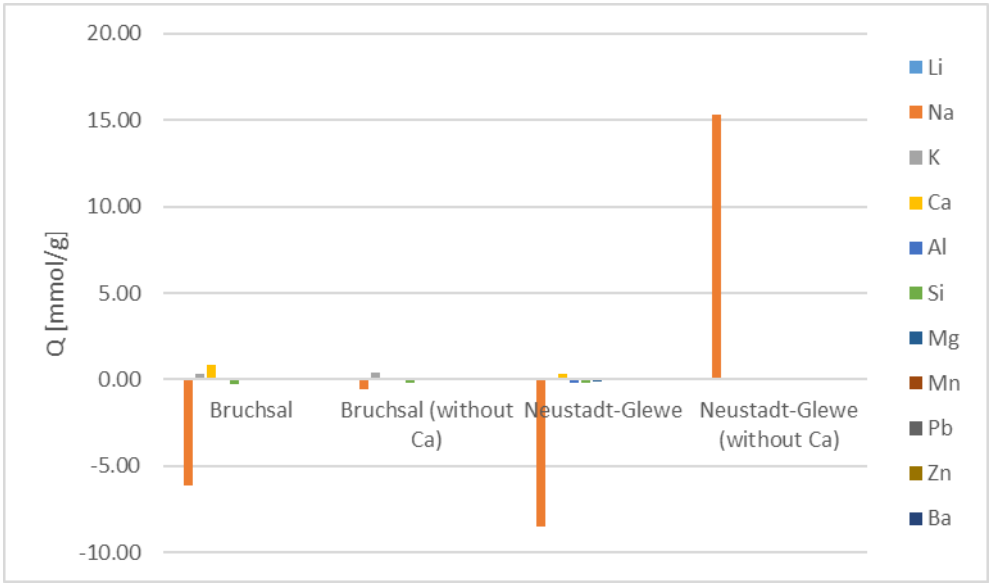
20.00
15.00
10.00
5.00
0.00
-5.00
-10.00
Q [mmol/g]
Bruchsal
Bruchsal (without Ca)
Neustadt-Glewe
Neustadt-Glewe (without Ca)
Li
Na
K
Ca
Al
Si
Mg
Mn
Pb
Zn
Ba

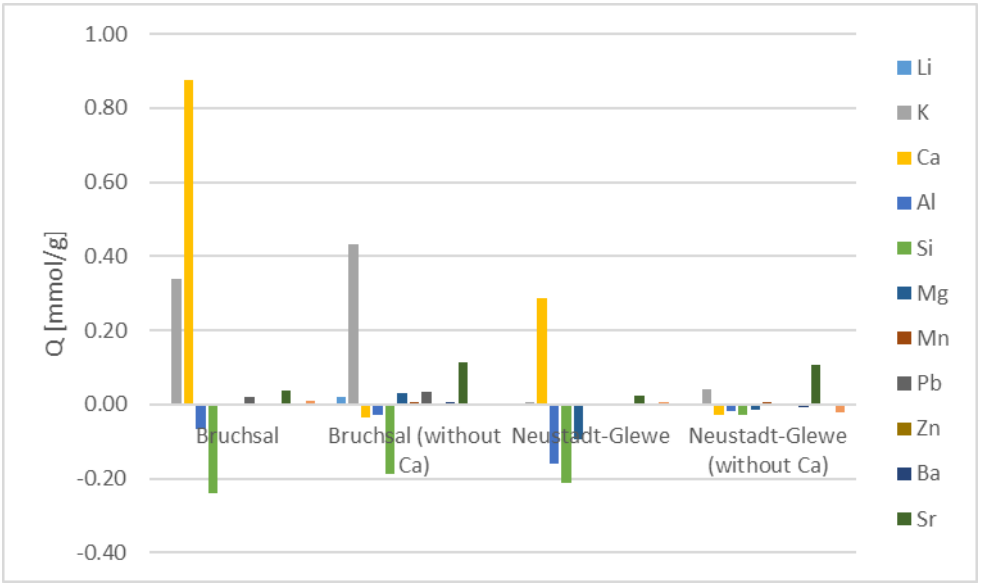
1.00
0.80
0.60
0.40
0.20
0.00
-0.20
-0.40
Q [mmol/g]
Bruchsal
Bruchsal (without Ca)
Neustadt-Glewe
Neustadt-Glewe (without Ca)
Li
K
Ca
Al
Si
Mg
Mn
Pb
Zn
Ba
Sr

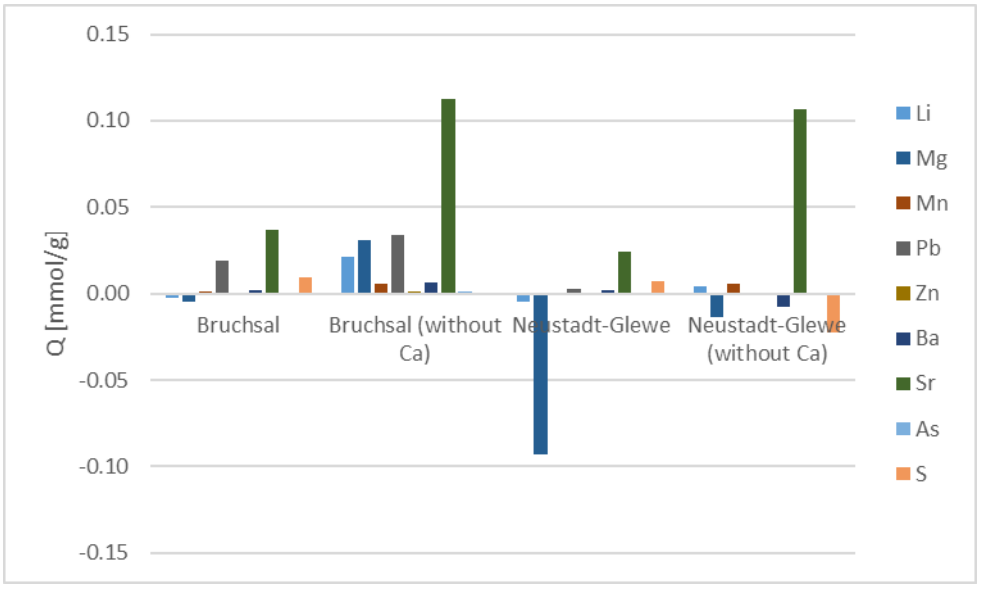
0.15
0.10
0.05
0.00
-0.05
-0.10
-0.15
Q [mmol/g]
Bruchsal
Bruchsal (without Ca)
Neustadt-Glewe
Neustadt-Glewe (without Ca)
Li
Mg
Mn
Pb
Zn
Ba
Sr
As
S

A.4 Study III – Electronic supplement

sample No.						C0		C1		
	T [°C]	volume [mL]	time [min]	LFP [g]	solution	pH	T [°C]	pH	T [°C]	digested mass [g]
max LOD										
max LOQ										
uncertainty [%]										
content [mg/g]										
mean LFP400 [mg/g] at 100% elution				LFP400 equ to 100%						
RR-LFP-D01	25	200	45	1.0244	millipore water	-	-	10.7	20.3	0.099
RR-LFP03-D01	25	200	1440	1.0169	millipore water	-	-	9.25	26.6	0.100
RR-LFP-D02	25	200	45	0.9913	1% H2O2 + 3% CH3COOH	-	-	3.40	21.4	0.101
RR-LFP-D03	25	200	45	0.9935	2.4% H2O2 + 0.1% CH3COOH	-	-	9.31	21.5	0.101
RR-LFP-D04	25	200	45	1.0156	0.1% H2O2 + 1% CH3COOH	-	-	3.85	22.7	0.100
RR-LFP-D10	25	200	45	0.9895	0.1M Na2S2O8	-	-	7.35	21.6	0.102
RR-LFP-D11	25	200	45	1.0228	0.5M Na2S2O8	-	-	4.62	22.1	0.101
RR-LFP-D12	25	200	45	0.9769	1M Na2S2O8	-	-	2.76	21.5	0.100
RR-LFP-D05	25	200	45	0.9998	0.1M NaCl	-	-	10.3	21.6	0.099
RR-LFP-D06	25	200	45	0.9938	0.5M NaCl	-	-	10.2	21.8	0.101
RR-LFP-D07	25	200	45	0.9972	1M NaCl	-	-	10.2	22.0	0.101
RR-LFP-D08	25	200	45	1.0569	2M NaCl	-	-	9.90	21.9	0.100
RR-LFP-D09	25	200	45	0.9926	3M NaCl	-	-	9.57	21.7	0.100
RR-LFP03-D02	25	200	1440	1.0033	0.01M HCl	-	-	5.66	27.3	0.101
RR-LFP03-D03	25	200	1440	0.9929	0.05M HCl	-	-	3.03	27.2	0.100
RR-LFP03-D04	25	200	1440	1.0070	0.1M HCl	-	-	1.66	27.0	0.100
RR-LFP03-D05	25	200	1440	1.0089	0.15M HCl	-	-	1.22	27.0	0.044
RR-LFP03-D06	25	200	1440	0.9958	0.2M HCl	-	-	1.01	26.0	0.042
RR-LFP03-D07	25	200	1440	1.0008	0.3M HCl	-	-	0.76	25.3	0.043
RR-LFP03-D08	25	200	1440	1.0178	0.5M HCl	-	-	0.60	26.6	0.044
content [mmol/g]										
mean LFP400 [mg/g] at 100% elution				LFP400 equ to 100%						
RR-LFP-D01	25	200	45	1.0244	millipore water	-	-	10.7	20.3	0.099
RR-LFP03-D01	25	200	1440	1.0169	millipore water	-	-	9.25	26.6	0.100
RR-LFP-D02	25	200	45	0.9913	1% H2O2 + 3% CH3COOH	-	-	3.40	21.4	0.101
RR-LFP-D03	25	200	45	0.9935	2.4% H2O2 + 0.1% CH3COOH	-	-	9.31	21.5	0.101
RR-LFP-D04	25	200	45	1.0156	0.1% H2O2 + 1% CH3COOH	-	-	3.85	22.7	0.100
RR-LFP-D10	25	200	45	0.9895	0.1M Na2S2O8	-	-	7.35	21.6	0.102
RR-LFP-D11	25	200	45	1.0228	0.5M Na2S2O8	-	-	4.62	22.1	0.101
RR-LFP-D12	25	200	45	0.9769	1M Na2S2O8	-	-	2.76	21.5	0.100
RR-LFP-D05	25	200	45	0.9998	0.1M NaCl	-	-	10.3	21.6	0.099
RR-LFP-D06	25	200	45	0.9938	0.5M NaCl	-	-	10.2	21.8	0.101
RR-LFP-D07	25	200	45	0.9972	1M NaCl	-	-	10.2	22.0	0.101
RR-LFP-D08	25	200	45	1.0569	2M NaCl	-	-	9.90	21.9	0.100
RR-LFP-D09	25	200	45	0.9926	3M NaCl	-	-	9.57	21.7	0.100
RR-LFP03-D02	25	200	1440	1.0033	0.01M HCl	-	-	5.66	27.3	0.101
RR-LFP03-D03	25	200	1440	0.9929	0.05M HCl	-	-	3.03	27.2	0.100
RR-LFP03-D04	25	200	1440	1.0070	0.1M HCl	-	-	1.66	27.0	0.100
RR-LFP03-D05	25	200	1440	1.0089	0.15M HCl	-	-	1.22	27.0	0.044
RR-LFP03-D06	25	200	1440	0.9958	0.2M HCl	-	-	1.01	26.0	0.042
RR-LFP03-D07	25	200	1440	1.0008	0.3M HCl	-	-	0.76	25.3	0.043
RR-LFP03-D08	25	200	1440	1.0178	0.5M HCl	-	-	0.60	26.6	0.044

sample No.	Li	Na	K	Mg	Ca	Sr	Ba	Al	Si	P	As	S	Ti	V	Cr	Mn	Fe	Co	Ni	Cu	Zn	Cd
	mg/L	mg/L	mg/L	mg/L	mg/L	mg/L	mg/L	mg/L	mg/L	mg/L	mg/L	mg/L	mg/L	mg/L	mg/L	mg/L	mg/L	mg/L	mg/L	mg/L	mg/L	mg/L
max LOD	0.0027	0.0339	0.0554	0.0000	0.0080	0.0002	0.0003	0.0178	0.0032	0.0174	0.0100	0.0260	0.0009	0.0031	0.0062	0.0006	0.0018	0.0024	0.0061	0.0056	0.0008	0.0010
max LOQ	0.0090	0.1128	0.1846	0.0001	0.0267	0.0006	0.0011	0.0592	0.0266	0.0581	0.0332	0.0867	0.0056	0.0103	0.0205	0.0021	0.0061	0.0080	0.0204	0.0186	0.0025	0.0034
uncertainty [%]	10.0	10.8	17.3	7.3	8.1	7.0	11.1	15.0	4.9	3.0	5.0	3.3	2.0	2.5	6.5	5.0	4.4	6.7	9.1	5.5	8.8	4.7
content [mg/g]																						
mean LFP400 [mg/g]																						
at 100% elution	-43	<0.3	-0.1	-0.1	<0.1	<0.0002	<0.0003	-0.1	-0.1	-160.5	<0.01	-0.9	0.0	<0.003	<0.006	-0.5	-266.4	0.0	-0.1	-0.1	-0.1	<0.0009
RR-LFP-D01	-1.2	<LOD	<LOD	0.0	0.0	<LOD	<LOD	<LOD	<LOD	-5.1	<LOD	<LOQ	<LOQ	<LOD	<LOQ	1.6	-0.1	<LOQ	0.0	<LOQ	0.0	<LOD
RR-LFP03-D01	-3.0	<LOQ	<LOD	0.0	0.0	<LOQ	<LOD	0.0	0.0	-7.1	<LOD	<LOQ	0.0	<LOQ	<LOD	0.1	-0.2	<LOQ	0.0	0.0	0.0	<LOQ
RR-LFP-D02	-43	<LOD	<LOD	0.0	<LOQ	<LOQ	<LOQ	0.0	<LOQ	-8.7	<LOQ	<LOQ	<LOQ	<LOQ	<LOQ	1.7	-1.8	<LOQ	<LOQ	<LOQ	<LOQ	<LOQ
RR-LFP-D03	-37	<LOD	<LOD	0.0	<LOQ	<LOQ	<LOQ	<LOD	<LOQ	-6.9	<LOQ	<LOQ	<LOQ	<LOQ	<LOQ	1.7	-0.2	<LOQ	<LOQ	<LOQ	<LOQ	<LOQ
RR-LFP-D04	-35	<LOD	<LOD	0.0	0.0	<LOD	<LOD	<LOD	<LOD	-8.3	<LOD	<LOQ	<LOQ	<LOD	<LOQ	1.5	-1.0	<LOQ	0.0	<LOQ	0.0	<LOD
RR-LFP-D10	-41	0.6	<LOD	0.0	<LOQ	<LOQ	<LOQ	<LOD	<LOQ	-6.9	<LOQ	<LOQ	<LOQ	<LOQ	<LOQ	1.7	-0.3	<LOQ	<LOQ	<LOQ	<LOQ	<LOQ
RR-LFP-D11	-42	0.9	<LOD	0.0	0.0	<LOD	<LOD	<LOD	<LOD	-6.7	<LOD	0.2	<LOQ	<LOD	<LOQ	1.7	-0.4	<LOQ	0.0	<LOQ	0.0	<LOD
RR-LFP-D12	-43	3.7	<LOD	0.0	0.0	<LOD	<LOD	<LOD	<LOQ	-6.0	<LOD	3.4	<LOQ	<LOD	<LOQ	1.6	<LOD	<LOQ	0.0	<LOQ	0.0	<LOD
RR-LFP-D05	-1.7	<LOQ	<LOD	0.0	0.0	<LOD	<LOD	<LOD	<LOD	-5.6	<LOD	<LOQ	<LOQ	<LOD	<LOQ	1.6	-0.1	<LOQ	0.0	<LOQ	0.0	<LOD
RR-LFP-D06	-1.0	<LOQ	<LOD	0.0	0.0	<LOD	<LOD	<LOD	<LOQ	-5.4	<LOD	<LOQ	<LOD	<LOD	<LOQ	1.5	<LOD	<LOQ	0.0	<LOQ	0.0	<LOD
RR-LFP-D07	-1.1	0.9	<LOD	0.0	0.0	<LOD	<LOD	<LOD	<LOD	-5.5	<LOD	<LOQ	<LOD	<LOD	<LOQ	1.6	<LOD	<LOQ	0.0	<LOQ	0.0	<LOD
RR-LFP-D08	-1.5	0.8	<LOD	0.0	<LOQ	<LOQ	<LOQ	<LOD	<LOQ	-3.6	<LOQ	<LOQ	<LOQ	<LOQ	<LOQ	1.6	<LOD	<LOQ	<LOQ	<LOQ	<LOQ	<LOQ
RR-LFP-D09	-1.0	1.6	-1.1	0.0	0.0	<LOD	<LOD	<LOD	<LOD	-3.0	<LOD	<LOQ	<LOD	<LOD	<LOQ	1.5	<LOD	<LOQ	0.0	<LOQ	0.0	<LOD
RR-LFP03-D02	-15	<LOQ	<LOD	0.0	0.0	<LOD	<LOD	0.0	-0.1	-9.1	<LOD	<LOQ	0.0	<LOD	<LOD	0.1	0.0	<LOQ	0.0	0.0	0.0	<LOQ
RR-LFP03-D03	-41	<LOD	<LOD	<LOQ	0.0	<LOD	<LOD	0.1	0.0	-110	<LOD	<LOQ	0.3	<LOD	<LOD	0.0	-174	<LOQ	<LOQ	0.0	-0.1	<LOQ
RR-LFP03-D04	-42	<LOQ	<LOD	<LOQ	0.0	<LOD	<LOD	0.0	0.3	-180	<LOD	<LOQ	0.2	<LOD	<LOD	-0.3	-287	<LOD	<LOD	0.1	-0.1	<LOQ
RR-LFP03-D05	-42	<LOD	<LOD	<LOQ	0.0	<LOD	<LOD	0.1	0.9	-192	<LOD	<LOQ	0.3	<LOD	<LOD	-0.5	-304	<LOD	<LOD	0.3	-0.1	<LOD
RR-LFP03-D06	-42	<LOD	<LOD	<LOQ	0.0	<LOD	<LOD	0.2	0.9	-192	<LOD	<LOQ	0.3	<LOD	<LOD	-0.5	-304	<LOD	<LOD	0.4	-0.1	<LOD
RR-LFP03-D07	-42	<LOD	<LOD	<LOQ	<LOQ	<LOD	<LOD	-0.1	0.7	-190	<LOD	<LOQ	0.2	<LOD	<LOQ	-0.5	-303	<LOD	<LOD	-0.1	-0.1	<LOD
RR-LFP03-D08	-42	<LOD	<LOD	<LOQ	<LOQ	<LOD	<LOD	-0.1	0.7	-193	<LOD	<LOQ	0.2	<LOD	<LOD	-0.5	-302	<LOD	<LOD	-0.1	-0.1	<LOD
content [mmol/g]																						
mean LFP400 [mg/g]						<0.0000	<0.0000				<0.000											<0.0000
at 100% elution	-6.20	<0.01	0.00	0.00	<0.002	02	02	0.00	0.00	-5.18	1	-0.03	0.00	<0.00006	<0.0001	-0.01	-4.77	0.00	0.00	0.00	0.00	08
RR-LFP-D01	-0.17	<LOD	<LOD	0.00	0.00	<LOD	<LOD	<LOD	<LOD	-0.17	<LOD	<LOQ	<LOQ	<LOD	<LOQ	0.03	0.00	<LOQ	0.00	<LOQ	0.00	<LOD
RR-LFP03-D01	-0.44	<LOQ	<LOD	0.00	0.00	<LOQ	<LOD	0.00	0.00	-0.23	<LOD	<LOQ	0.00	<LOQ	<LOD	0.00	0.00	<LOQ	0.00	0.00	0.00	<LOQ
RR-LFP-D02	-6.14	<LOD	<LOD	0.00	<LOQ	<LOQ	<LOQ	0.00	<LOQ	-0.28	<LOQ	<LOQ	<LOQ	<LOQ	<LOQ	0.03	-0.03	<LOQ	<LOQ	<LOQ	<LOQ	<LOQ
RR-LFP-D03	-5.29	<LOD	<LOD	0.00	<LOQ	<LOQ	<LOQ	<LOD	<LOQ	-0.22	<LOQ	<LOQ	<LOQ	<LOQ	<LOQ	0.03	0.00	<LOQ	<LOQ	<LOQ	<LOQ	<LOQ
RR-LFP-D04	-5.02	<LOD	<LOD	0.00	0.00	<LOD	<LOD	<LOD	<LOD	-0.27	<LOD	<LOQ	<LOQ	<LOD	<LOQ	0.03	-0.02	<LOQ	0.00	<LOQ	0.00	<LOD
RR-LFP-D10	-5.98	0.02	<LOD	0.00	<LOQ	<LOQ	<LOQ	<LOD	<LOQ	-0.22	<LOQ	<LOQ	<LOQ	<LOQ	<LOQ	0.03	0.00	<LOQ	<LOQ	<LOQ	<LOQ	<LOQ
RR-LFP-D11	-6.07	0.04	<LOD	0.00	0.00	<LOD	<LOD	<LOD	<LOD	-0.22	<LOD	0.01	<LOQ	<LOD	<LOQ	0.03	-0.01	<LOQ	0.00	<LOQ	0.00	<LOD
RR-LFP-D12	-6.14	0.16	<LOD	0.00	0.00	<LOD	<LOD	<LOD	<LOQ	-0.19	<LOD	0.11	<LOQ	<LOD	<LOQ	0.03	<LOD	<LOQ	0.00	<LOQ	0.00	<LOD
RR-LFP-D05	-0.25	<LOQ	<LOD	0.00	0.00	<LOD	<LOD	<LOD	<LOD	-0.18	<LOD	<LOQ	<LOQ	<LOD	<LOQ	0.03	0.00	<LOQ	0.00	<LOQ	0.00	<LOD
RR-LFP-D06	-0.14	<LOQ	<LOD	0.00	0.00	<LOD	<LOD	<LOD	<LOQ	-0.18	<LOD	<LOQ	<LOD	<LOD	<LOQ	0.03	<LOD	<LOQ	0.00	<LOQ	0.00	<LOD
RR-LFP-D07	-0.16	0.04	<LOD	0.00	0.00	<LOD	<LOD	<LOD	<LOD	-0.18	<LOD	<LOQ	<LOD	<LOD	<LOQ	0.03	<LOD	<LOQ	0.00	<LOQ	0.00	<LOD
RR-LFP-D08	-0.22	0.04	<LOD	0.00	<LOQ	<LOQ	<LOQ	<LOD	<LOQ	-0.12	<LOQ	<LOQ	<LOQ	<LOQ	<LOQ	0.03	<LOD	<LOQ	<LOQ	<LOQ	<LOQ	<LOQ
RR-LFP-D09	-0.14	0.07	-0.03	0.00	0.00	<LOD	<LOD	<LOD	<LOD	-0.10	<LOD	<LOQ	<LOD	<LOD	<LOQ	0.03	<LOD	<LOQ	0.00	<LOQ	0.00	<LOD
RR-LFP03-D02	-2.23	<LOQ	<LOD	0.00	0.00	<LOD	<LOD	0.00	0.00	-0.29	<LOD	<LOQ	0.00	<LOD	<LOD	0.00	0.00	<LOQ	0.00	0.00	0.00	<LOQ
RR-LFP03-D03	-5.92	<LOD	<LOD	<LOQ	0.00	<LOD	<LOD	0.01	0.00	-3.56	<LOD	<LOQ	0.01	<LOD	<LOD	0.00	-3.12	<LOQ	<LOQ	0.00	0.00	<LOQ
RR-LFP03-D04	-6.04	<LOQ	<LOD	<LOQ	0.00	<LOD	<LOD	0.00	0.01	-5.80	<LOD	<LOQ	0.00	<LOD	<LOD	-0.01	-5.13	<LOD	<LOD	0.00	0.00	<LOQ
RR-LFP03-D05	-6.03	<LOD	<LOD	<LOQ	0.00	<LOD	<LOD	0.00	0.03	-6.21	<LOD	<LOQ	0.01	<LOD	<LOD	-0.01	-5.44	<LOD	<LOD	0.01	0.00	<LOD
RR-LFP03-D06	-6.03	<LOD	<LOD	<LOQ	0.00	<LOD	<LOD	0.01	0.03	-6.19	<LOD	<LOQ	0.01	<LOD	<LOD	-0.01	-5.43	<LOD	<LOD	0.01	0.00	<LOD
RR-LFP03-D07	-6.03	<LOD	<LOD	<LOQ	<LOQ	<LOD	<LOD	0.00	0.02	-6.13	<LOD	<LOQ	0.00	<LOD	<LOQ	-0.01	-5.43	<LOD	<LOD	0.00	0.00	<LOD
RR-LFP03-D08	-6.05	<LOD	<LOD	<LOQ	<LOQ	<LOD	<LOD	0.00	0.02	-6.22	<LOD	<LOQ	0.00	<LOD	<LOD	-0.01	-5.42	<LOD	<LOD	0.00	0.00	<LOD

sample No.						c0		c1	
	T [°C]	solution	time [min]	LFP [g]	digested mass [g]	pH	T [°C]	pH	T [°C]
method									
LOD									
LOQ									
uncertainty [%]									
load [mg/g]									
RR-LFP05-0001	25	0.1M Na2S2O8	1	1.020	0.102			4.80	20.6
RR-LFP05-0005	25	0.1M Na2S2O8	5	0.996	0.101			5.31	20.3
RR-LFP05-0015	25	0.1M Na2S2O8	15	0.996	0.101			4.31	20.5
RR-LFP05-0030	25	0.1M Na2S2O8	30	1.003	0.101			3.56	20.8
RR-LFP05-0045	25	0.1M Na2S2O8	45	0.994	0.100			3.77	20.8
RR-LFP05-0060	25	0.1M Na2S2O8	60	1.007	0.100			3.42	21.0
RR-LFP05-0120	25	0.1M Na2S2O8	120	0.997	0.102			3.42	21.5
RR-LFP05-0180	25	0.1M Na2S2O8	180	0.995	0.101			3.18	22.6
RR-LFP05-0240	25	0.1M Na2S2O8	240	0.998	0.100			3.21	22.0
RR-LFP05-1440	25	0.1M Na2S2O8	1440	1.007	0.099			2.74	22.4
RR-LFP05-1Wo	25	0.1M Na2S2O8	10080	1.010	0.102			2.37	21.5
RR-LFP05-2Wo	25	0.1M Na2S2O8	20160	1.000	0.102			2.25	22.1
RR-LFP05-Blank1	25	0.1M Na2S2O8	15					3.15	20.3
RR-LFP05-Blank2	25	0.1M Na2S2O8	1440			3.10	20.7	2.85	21.8
RR-LFP05-Blank3	25	0.1M Na2S2O8	10080					2.46	22.1
load [mmol/g]									
RR-LFP05-0001	25	0.1M Na2S2O8	1	1.020	0.102			4.80	20.6
RR-LFP05-0005	25	0.1M Na2S2O8	5	0.996	0.101			5.31	20.3
RR-LFP05-0015	25	0.1M Na2S2O8	15	0.996	0.101			4.31	20.5
RR-LFP05-0030	25	0.1M Na2S2O8	30	1.003	0.101			3.56	20.8
RR-LFP05-0045	25	0.1M Na2S2O8	45	0.994	0.100			3.77	20.8
RR-LFP05-0060	25	0.1M Na2S2O8	60	1.007	0.100			3.42	21.0
RR-LFP05-0120	25	0.1M Na2S2O8	120	0.997	0.102			3.42	21.5
RR-LFP05-0180	25	0.1M Na2S2O8	180	0.995	0.101			3.18	22.6
RR-LFP05-0240	25	0.1M Na2S2O8	240	0.998	0.100			3.21	22.0
RR-LFP05-1440	25	0.1M Na2S2O8	1440	1.007	0.099			2.74	22.4
RR-LFP05-1Wo	25	0.1M Na2S2O8	10080	1.010	0.102			2.37	21.5
RR-LFP05-2Wo	25	0.1M Na2S2O8	20160	1.000	0.102			2.25	22.1
RR-LFP05-Blank1	25	0.1M Na2S2O8	15					3.15	20.3
RR-LFP05-Blank2	25	0.1M Na2S2O8	1440			3.10	20.7	2.85	21.8
RR-LFP05-Blank3	25	0.1M Na2S2O8	10080					2.46	22.1

sample No.	Li	Na	K	Mg	Ca	Sr	Ba	Al	Si	P	As	S	Ti	V	Cr	Mn	Fe	Co	Ni	Cu	Zn	Cd
	mg/L	mg/L	mg/L	mg/L	mg/L	mg/L	mg/L	mg/L	mg/L	mg/L	mg/L	mg/L	mg/L	mg/L	mg/L	mg/L	mg/L	mg/L	mg/L	mg/L	mg/L	mg/L
	dig_	dig_	dig_	dig_	dig_	dig_	dig_	dig_	dig_	fluid	dig_	dig_	dig_	dig_	dig_	dig_	fluid	dig_	dig_	dig_	dig_	dig_
method	OES	OES	OES	OES	OES	OES	OES	OES	OES	OES	OES	OES	OES	OES	OES	OES	OES	OES	OES	OES	OES	OES
LOD	0.0015	0.0339	0.0470	0.0000	0.0080	0.0002	0.0003	0.0109	0.0326	0.0051	0.0071	0.0229	0.0017	0.0036	0.0031	0.0006	0.0016	0.0024	0.0020	0.0037	0.0007	0.0009
LOQ	0.0051	0.1128	0.1568	0.0000	0.0267	0.0006	0.0011	0.0362	0.1087	0.0172	0.0235	0.0763	0.0056	0.0121	0.0102	0.0021	0.0053	0.0080	0.0068	0.0122	0.0023	0.0030
uncertainty [%]	4.7	4.9	6.8	2.9	8.1	3.5	11.1	15.0	1.7	1.6	0.8	3.2	2.0	2.0	5.0	5.0	9.4	5.4	3.6	5.5	2.9	3.3
load [mg/g]																						
RR-LFP05-0001	-42	<LOQ	<LOD	<LOQ	<LOQ	<LOD	<LOD	<LOQ	<LOD	-5.9	<LOD	0.1	<LOQ	<LOD	<LOQ	0.2	-1.1	<LOQ	0.0	<LOD	0.0	<LOQ
RR-LFP05-0005	-42	<LOQ	<LOD	<LOQ	<LOQ	<LOD	<LOD	<LOQ	<LOD	-6.0	<LOD	0.1	<LOD	<LOD	<LOQ	0.1	-0.9	<LOQ	0.0	<LOD	0.0	<LOQ
RR-LFP05-0015	-42	<LOQ	<LOD	<LOQ	<LOQ	<LOD	<LOD	<LOQ	<LOD	-6.2	<LOD	0.1	<LOQ	<LOD	<LOQ	0.2	-1.2	<LOQ	0.0	<LOD	0.0	<LOQ
RR-LFP05-0030	-43	<LOQ	<LOD	<LOQ	<LOQ	<LOD	<LOD	<LOQ	<LOD	-6.6	<LOD	0.1	<LOQ	<LOD	<LOQ	0.2	-1.8	<LOQ	0.0	<LOD	0.0	<LOQ
RR-LFP05-0045	-43	<LOQ	<LOD	<LOQ	<LOQ	<LOD	<LOD	<LOQ	<LOD	-6.3	<LOD	-0.1	<LOD	<LOD	<LOQ	0.0	-1.4	<LOQ	0.0	<LOQ	0.0	<LOQ
RR-LFP05-0060	-43	<LOD	<LOD	<LOQ	<LOQ	<LOD	<LOD	<LOQ	<LOD	-6.6	<LOD	0.1	<LOQ	<LOD	<LOQ	0.2	-2.0	<LOQ	0.0	<LOD	0.0	<LOQ
RR-LFP05-0120	-43	<LOQ	<LOD	<LOQ	<LOQ	<LOD	<LOD	<LOQ	<LOD	-6.5	<LOD	0.1	<LOD	<LOD	<LOQ	0.1	-1.6	<LOQ	0.0	<LOD	0.0	<LOQ
RR-LFP05-0180	-43	<LOQ	<LOD	<LOQ	<LOQ	<LOD	<LOD	<LOQ	<LOD	-6.4	<LOD	0.1	<LOQ	<LOD	<LOQ	0.1	-1.5	<LOQ	0.0	<LOD	0.0	<LOQ
RR-LFP05-0240	-43	<LOQ	<LOD	<LOQ	<LOQ	<LOD	<LOD	<LOQ	<LOD	-6.2	<LOD	0.0	<LOD	<LOD	<LOD	0.1	-1.4	<LOQ	0.0	<LOD	0.0	<LOQ
RR-LFP05-1440	-43	<LOQ	<LOD	<LOQ	<LOQ	<LOD	<LOD	<LOQ	<LOD	-5.5	<LOD	0.2	<LOQ	<LOD	<LOD	0.2	-0.8	<LOQ	0.0	<LOD	0.0	<LOQ
RR-LFP05-1Wo	-43	<LOQ	<LOD	<LOQ	<LOQ	<LOD	<LOD	<LOQ	<LOD	-5.2	<LOD	0.0	<LOQ	<LOD	<LOQ	0.2	-0.7	<LOQ	0.0	<LOD	0.0	<LOQ
RR-LFP05-2Wo	-43	<LOQ	<LOD	<LOQ	<LOQ	<LOD	<LOD	<LOQ	<LOD	-5.6	<LOD	-0.1	<LOD	<LOD	<LOD	0.0	-1.0	<LOQ	0.0	<LOQ	<LOQ	<LOQ
RR-LFP05-Blank1										<LOQ							0.0					
RR-LFP05-Blank2										<LOQ							<LOQ					
RR-LFP05-Blank3										<LOQ							<LOQ					
load [mmol/g]																						
RR-LFP05-0001	-6.07	<LOQ	<LOD	<LOQ	<LOQ	<LOD	<LOD	<LOQ	<LOD	-0.19	<LOD	0.00	<LOQ	<LOD	<LOQ	0.00	-0.02	<LOQ	0.00	<LOD	0.00	<LOQ
RR-LFP05-0005	-6.08	<LOQ	<LOD	<LOQ	<LOQ	<LOD	<LOD	<LOQ	<LOD	-0.19	<LOD	0.00	<LOD	<LOD	<LOQ	0.00	-0.02	<LOQ	0.00	<LOD	0.00	<LOQ
RR-LFP05-0015	-6.12	<LOQ	<LOD	<LOQ	<LOQ	<LOD	<LOD	<LOQ	<LOD	-0.20	<LOD	0.00	<LOQ	<LOD	<LOQ	0.00	-0.02	<LOQ	0.00	<LOD	0.00	<LOQ
RR-LFP05-0030	-6.14	<LOQ	<LOD	<LOQ	<LOQ	<LOD	<LOD	<LOQ	<LOD	-0.21	<LOD	0.00	<LOQ	<LOD	<LOQ	0.00	-0.03	<LOQ	0.00	<LOD	0.00	<LOQ
RR-LFP05-0045	-6.13	<LOQ	<LOD	<LOQ	<LOQ	<LOD	<LOD	<LOQ	<LOD	-0.20	<LOD	0.00	<LOD	<LOD	<LOQ	0.00	-0.02	<LOQ	0.00	<LOQ	0.00	<LOQ
RR-LFP05-0060	-6.14	<LOD	<LOD	<LOQ	<LOQ	<LOD	<LOD	<LOQ	<LOD	-0.21	<LOD	0.00	<LOQ	<LOD	<LOQ	0.00	-0.03	<LOQ	0.00	<LOD	0.00	<LOQ
RR-LFP05-0120	-6.14	<LOQ	<LOD	<LOQ	<LOQ	<LOD	<LOD	<LOQ	<LOD	-0.21	<LOD	0.00	<LOD	<LOD	<LOQ	0.00	-0.03	<LOQ	0.00	<LOD	0.00	<LOQ
RR-LFP05-0180	-6.15	<LOQ	<LOD	<LOQ	<LOQ	<LOD	<LOD	<LOQ	<LOD	-0.21	<LOD	0.00	<LOQ	<LOD	<LOQ	0.00	-0.03	<LOQ	0.00	<LOD	0.00	<LOQ
RR-LFP05-0240	-6.14	<LOQ	<LOD	<LOQ	<LOQ	<LOD	<LOD	<LOQ	<LOD	-0.20	<LOD	0.00	<LOD	<LOD	<LOD	0.00	-0.02	<LOQ	0.00	<LOD	0.00	<LOQ
RR-LFP05-1440	-6.15	<LOQ	<LOD	<LOQ	<LOQ	<LOD	<LOD	<LOQ	<LOD	-0.18	<LOD	0.00	<LOQ	<LOD	<LOD	0.00	-0.01	<LOQ	0.00	<LOD	0.00	<LOQ
RR-LFP05-1Wo	-6.17	<LOQ	<LOD	<LOQ	<LOQ	<LOD	<LOD	<LOQ	<LOD	-0.17	<LOD	0.00	<LOQ	<LOD	<LOQ	0.00	-0.01	<LOQ	0.00	<LOD	0.00	<LOQ
RR-LFP05-2Wo	-6.17	<LOQ	<LOD	<LOQ	<LOQ	<LOD	<LOD	<LOQ	<LOD	-0.18	<LOD	0.00	<LOD	<LOD	<LOD	0.00	-0.02	<LOQ	0.00	<LOQ	<LOQ	<LOQ
RR-LFP05-Blank1										<LOQ							0.00					
RR-LFP05-Blank2										<LOQ							<LOQ					
RR-LFP05-Blank3										<LOQ							<LOQ					

dig_ digestion

sample No. method LOD LOQ uncertainty [%]	T[°C]	solution	time [min]	Cequ,Li [mg/L]	LFP [g]	digested mass [g]	C0 pH	C0 T [°C]	C1 pH	C1 T [°C]
load [mg/g]										
RR-LFP06-D0.05	25	0.1M Na2S2O8	60	11	0.052	0.039			3.20	20.9
RR-LFP06-D0.1	25	0.1M Na2S2O8	60	22	0.103	0.084	3.08	21.1	3.15	20.8
RR-LFP06-D0.5	25	0.1M Na2S2O8	60	106	0.495	0.098			3.44	21.3
RR-LFP06-D1.0	25	0.1M Na2S2O8	60	217	0.993	0.099			3.64	20.8
RR-LFP06-D1.5	25	0.1M Na2S2O8	60	323	1.505	0.100			3.93	21.8
RR-LFP06-D2.0	25	0.1M Na2S2O8	60	429	2.004	0.101			3.74	21.9
RR-LFP06-D3.0	25	0.1M Na2S2O8	60	628	2.998	0.102			3.77	21.9
RR-LFP06-D5.0	25	0.1M Na2S2O8	60	1033	4.996	0.099			3.88	22.4
RR-LFP06-D7.0	25	0.1M Na2S2O8	60	1457	7.016	0.100	3.52	22.3	5.94	23.4
RR-LFP06-D10.0	25	0.1M Na2S2O8	60	1515	9.992	0.099			7.72	22.8
RR-LFP06-D12.0	25	0.1M Na2S2O8	60	1488	11.979	0.099	3.52	22.0	7.47	23.1
RR-LFP06-D15.0	25	0.1M Na2S2O8	60	1511	14.958	0.101	3.58	21.5	7.60	23.8
RR-LFP06-D17.0	25	0.1M Na2S2O8	60	1546	17.085	0.101	3.60	21.7	7.60	23.5
RR-LFP06-D20.0	25	0.1M Na2S2O8	60	1539	20.062	0.099	3.60	21.9	7.90	22.9
RR-LFP06-D25.0	25	0.1M Na2S2O8	60	1557	25.035	0.099	3.59	21.4	8.02	22.8
RR-LFP06-DBlank1 (0.5 g)	25	0.1M Na2S2O8	60	6	0.501	0.101			9.57	20.5
RR-LFP06-DBlank2 (3 g)	25	0.1M Na2S2O8	60	30	3.013	0.101			9.78	21.0
RR-LFP06-DBlank3 (18 g)	25	0.1M Na2S2O8	60	12	17.949	0.101	5.43	21.6	9.86	22.5
load [mmol/g]										
RR-LFP06-D0.05	25	0.1M Na2S2O8	60	11	0.052	0.039			3.20	20.9
RR-LFP06-D0.1	25	0.1M Na2S2O8	60	22	0.103	0.084	3.08	21.1	3.15	20.8
RR-LFP06-D0.5	25	0.1M Na2S2O8	60	106	0.495	0.098			3.44	21.3
RR-LFP06-D1.0	25	0.1M Na2S2O8	60	217	0.993	0.099			3.64	20.8
RR-LFP06-D1.5	25	0.1M Na2S2O8	60	323	1.505	0.100			3.93	21.8
RR-LFP06-D2.0	25	0.1M Na2S2O8	60	429	2.004	0.101			3.74	21.9
RR-LFP06-D3.0	25	0.1M Na2S2O8	60	628	2.998	0.102			3.77	21.9
RR-LFP06-D5.0	25	0.1M Na2S2O8	60	1033	4.996	0.099			3.88	22.4
RR-LFP06-D7.0	25	0.1M Na2S2O8	60	1457	7.016	0.100	3.52	22.3	5.94	23.4
RR-LFP06-D10.0	25	0.1M Na2S2O8	60	1515	9.992	0.099			7.72	22.8
RR-LFP06-D12.0	25	0.1M Na2S2O8	60	1488	11.979	0.099	3.52	22.0	7.47	23.1
RR-LFP06-D15.0	25	0.1M Na2S2O8	60	1511	14.958	0.101	3.58	21.5	7.60	23.8
RR-LFP06-D17.0	25	0.1M Na2S2O8	60	1546	17.085	0.101	3.60	21.7	7.60	23.5
RR-LFP06-D20.0	25	0.1M Na2S2O8	60	1539	20.062	0.099	3.60	21.9	7.90	22.9
RR-LFP06-D25.0	25	0.1M Na2S2O8	60	1557	25.035	0.099	3.59	21.4	8.02	22.8
RR-LFP06-DBlank1 (0.5 g)	25	0.1M Na2S2O8	60	6	0.501	0.101			9.57	20.5
RR-LFP06-DBlank2 (3 g)	25	0.1M Na2S2O8	60	30	3.013	0.101			9.78	21.0
RR-LFP06-DBlank3 (18 g)	25	0.1M Na2S2O8	60	12	17.949	0.101	5.43	21.6	9.86	22.5

sample No.	Li	Na	K	Mg	Ca	Sr	Ba	Al	Si	P	As	S	Ti	V	Cr	Mn	Fe	Co	Ni	Cu	Zn	Cd
	mg/L	mg/L	mg/L	mg/L	mg/L	mg/L	mg/L	mg/L	mg/L	mg/L	mg/L	mg/L	mg/L	mg/L	mg/L	mg/L	mg/L	mg/L	mg/L	mg/L	mg/L	mg/L
	dig_	dig_	dig_	dig_	dig_	dig_	dig_	dig_	dig_	fluid	dig_	dig_	dig_	dig_	dig_	dig_	fluid	dig_	dig_	dig_	dig_	dig_
method	OES	OES	OES	OES	OES	OES	OES	OES	OES	OES	OES	OES	OES	OES	OES	OES	OES	OES	OES	OES	OES	OES
LOD	0.0020	0.0339	0.0470	0.0000	0.0080	0.0002	0.0003	0.0204	0.0326	0.0235	0.0071	0.0229	0.0017	0.0036	0.0031	0.0006	0.0019	0.0024	0.0060	0.0064	0.0007	0.0009
LOQ	0.0065	0.1128	0.1568	0.0000	0.0267	0.0006	0.0011	0.0679	0.1087	0.0784	0.0235	0.0763	0.0056	0.0121	0.0102	0.0021	0.0063	0.0080	0.0199	0.0213	0.0024	0.0030
uncertainty [%]	4.9	11.6	6.8	2.9	8.1	3.5	11.1	15.0	1.7	1.9	0.8	19.9	2.0	2.0	5.0	5.0	8.5	5.4	3.6	5.5	2.9	3.3
load [mg/g]																						
RR-LFP06-D0.05	-43	2.4	<LOQ	<LOQ	<LOQ	<LOQ	<LOQ	<LOD	<LOQ	-8.2	<LOQ	2.6	<LOQ	<LOQ	<LOQ	0.1	-5.1	<LOQ	<LOQ	0.3	<LOQ	<LOQ
RR-LFP06-D0.1	-43	0.6	<LOQ	<LOQ	<LOQ	<LOQ	<LOQ	<LOD	<LOQ	-7.2	<LOQ	0.2	<LOQ	<LOQ	<LOQ	0.1	-3.7	<LOQ	0.0	0.1	0.0	<LOQ
RR-LFP06-D0.5	-43	<LOQ	<LOQ	<LOQ	<LOQ	<LOQ	<LOQ	<LOD	<LOQ	-6.6	<LOQ	<LOQ	<LOQ	<LOQ	<LOQ	0.2	-2.2	<LOQ	0.0	0.0	0.0	<LOQ
RR-LFP06-D1.0	-43	<LOQ	<LOQ	<LOQ	<LOQ	<LOQ	<LOQ	<LOD	<LOQ	-6.6	<LOQ	<LOQ	<LOQ	<LOQ	<LOQ	0.2	-1.6	<LOQ	0.0	0.0	0.0	<LOQ
RR-LFP06-D1.5	-43	<LOQ	<LOQ	<LOQ	<LOQ	<LOQ	<LOQ	<LOD	<LOQ	-6.6	<LOQ	<LOQ	<LOQ	<LOQ	<LOQ	0.2	-1.8	<LOQ	0.0	0.0	0.0	<LOQ
RR-LFP06-D2.0	-43	0.3	<LOQ	<LOQ	<LOQ	<LOQ	<LOQ	0.0	<LOQ	-6.4	<LOQ	<LOQ	<LOQ	<LOQ	<LOQ	0.2	-1.4	<LOQ	0.0	0.0	0.0	<LOQ
RR-LFP06-D3.0	-42	0.3	<LOQ	<LOQ	<LOQ	<LOQ	<LOQ	<LOD	<LOQ	-6.3	<LOQ	<LOQ	<LOQ	<LOQ	<LOQ	0.2	-1.4	<LOQ	0.0	0.0	0.0	<LOQ
RR-LFP06-D5.0	-42	0.4	<LOQ	<LOQ	<LOQ	<LOQ	<LOQ	<LOD	<LOQ	-6.1	<LOQ	<LOQ	<LOQ	<LOQ	<LOQ	0.2	-1.2	<LOQ	0.0	0.0	0.0	<LOQ
RR-LFP06-D7.0	-40	0.8	<LOQ	<LOQ	<LOQ	<LOQ	<LOQ	<LOD	<LOQ	-5.8	<LOQ	<LOQ	<LOQ	<LOQ	<LOQ	0.2	-1.4	<LOQ	0.0	0.0	0.0	<LOQ
RR-LFP06-D10.0	-29	0.5	<LOQ	<LOQ	<LOQ	<LOQ	<LOQ	<LOD	<LOQ	-4.7	<LOQ	<LOQ	<LOQ	<LOQ	<LOQ	0.2	-1.2	<LOQ	0.0	0.0	0.0	<LOQ
RR-LFP06-D12.0	-24	0.6	<LOQ	<LOQ	<LOQ	<LOQ	<LOQ	<LOD	<LOQ	-3.8	<LOQ	<LOQ	<LOQ	<LOQ	<LOQ	0.2	-1.1	<LOQ	0.0	0.0	0.0	<LOQ
RR-LFP06-D15.0	-20	0.5	<LOQ	<LOQ	<LOQ	<LOQ	<LOQ	<LOD	<LOQ	-3.2	<LOQ	<LOQ	<LOQ	<LOQ	<LOQ	0.2	-0.9	<LOQ	0.0	0.0	0.0	<LOQ
RR-LFP06-D17.0	-17	0.4	<LOQ	<LOQ	<LOQ	<LOQ	<LOQ	<LOD	<LOQ	-3.2	<LOQ	<LOQ	<LOQ	<LOQ	<LOQ	0.2	-0.9	<LOQ	0.0	0.0	0.0	<LOQ
RR-LFP06-D20.0	-15	0.5	<LOQ	<LOQ	<LOQ	<LOQ	<LOQ	<LOD	<LOQ	-2.5	<LOQ	<LOQ	<LOQ	<LOQ	<LOQ	0.2	-0.6	<LOQ	0.0	0.0	0.0	<LOQ
RR-LFP06-D25.0	-11	0.4	<LOQ	<LOQ	<LOQ	<LOQ	<LOQ	<LOD	<LOQ	-2.2	<LOQ	<LOQ	<LOQ	<LOQ	<LOQ	0.2	-0.6	<LOQ	0.0	0.0	0.0	<LOQ
RR-LFP06-DBlank1 (0.5 g)	-3.1	<LOD	<LOD	<LOQ	<LOQ	<LOQ	<LOD	<LOQ	<LOD	-5.2	<LOD	-0.1	<LOD	<LOD	<LOQ	0.1	-0.1	<LOQ	0.0	<LOD	0.0	<LOQ
RR-LFP06-DBlank2 (3 g)	-2.3	<LOD	<LOD	<LOQ	<LOQ	<LOQ	<LOD	<LOQ	<LOD	-4.6	<LOD	-0.1	<LOD	<LOD	<LOQ	0.0	-0.1	<LOQ	0.0	<LOQ	<LOQ	<LOQ
RR-LFP06-DBlank3 (18 g)	-0.2	<LOQ	<LOQ	<LOQ	<LOQ	<LOQ	<LOQ	<LOD	<LOQ	-0.3	<LOQ	<LOQ	<LOQ	<LOQ	<LOQ	0.2	0.0	<LOQ	0.0	0.0	0.0	<LOQ
load [mmol/g]																						
RR-LFP06-D0.05	-6.13	0.10	<LOQ	<LOQ	<LOQ	<LOQ	<LOQ	<LOD	<LOQ	-0.26	<LOQ	0.08	<LOQ	<LOQ	<LOQ	0.00	-0.09	<LOQ	<LOQ	0.00	<LOQ	<LOQ
RR-LFP06-D0.1	-6.14	0.03	<LOQ	<LOQ	<LOQ	<LOQ	<LOQ	<LOD	<LOQ	-0.23	<LOQ	0.01	<LOQ	<LOQ	<LOQ	0.00	-0.07	<LOQ	0.00	0.00	0.00	<LOQ
RR-LFP06-D0.5	-6.15	<LOQ	<LOQ	<LOQ	<LOQ	<LOQ	<LOQ	<LOD	<LOQ	-0.21	<LOQ	<LOQ	<LOQ	<LOQ	<LOQ	0.00	-0.04	<LOQ	0.00	0.00	0.00	<LOQ
RR-LFP06-D1.0	-6.14	<LOQ	<LOQ	<LOQ	<LOQ	<LOQ	<LOQ	<LOD	<LOQ	-0.21	<LOQ	<LOQ	<LOQ	<LOQ	<LOQ	0.00	-0.03	<LOQ	0.00	0.00	0.00	<LOQ
RR-LFP06-D1.5	-6.13	<LOQ	<LOQ	<LOQ	<LOQ	<LOQ	<LOQ	<LOD	<LOQ	-0.21	<LOQ	<LOQ	<LOQ	<LOQ	<LOQ	0.00	-0.03	<LOQ	0.00	0.00	0.00	<LOQ
RR-LFP06-D2.0	-6.13	0.01	<LOQ	<LOQ	<LOQ	<LOQ	<LOQ	0.00	<LOQ	-0.21	<LOQ	<LOQ	<LOQ	<LOQ	<LOQ	0.00	-0.03	<LOQ	0.00	0.00	0.00	<LOQ
RR-LFP06-D3.0	-6.12	0.01	<LOQ	<LOQ	<LOQ	<LOQ	<LOQ	<LOD	<LOQ	-0.20	<LOQ	<LOQ	<LOQ	<LOQ	<LOQ	0.00	-0.03	<LOQ	0.00	0.00	0.00	<LOQ
RR-LFP06-D5.0	-6.11	0.02	<LOQ	<LOQ	<LOQ	<LOQ	<LOQ	<LOD	<LOQ	-0.20	<LOQ	<LOQ	<LOQ	<LOQ	<LOQ	0.00	-0.02	<LOQ	0.00	0.00	0.00	<LOQ
RR-LFP06-D7.0	-5.83	0.03	<LOQ	<LOQ	<LOQ	<LOQ	<LOQ	<LOD	<LOQ	-0.19	<LOQ	<LOQ	<LOQ	<LOQ	<LOQ	0.00	-0.02	<LOQ	0.00	0.00	0.00	<LOQ
RR-LFP06-D10.0	-4.13	0.02	<LOQ	<LOQ	<LOQ	<LOQ	<LOQ	<LOD	<LOQ	-0.15	<LOQ	<LOQ	<LOQ	<LOQ	<LOQ	0.00	-0.02	<LOQ	0.00	0.00	0.00	<LOQ
RR-LFP06-D12.0	-3.42	0.02	<LOQ	<LOQ	<LOQ	<LOQ	<LOQ	<LOD	<LOQ	-0.12	<LOQ	<LOQ	<LOQ	<LOQ	<LOQ	0.00	-0.02	<LOQ	0.00	0.00	0.00	<LOQ
RR-LFP06-D15.0	-2.83	0.02	<LOQ	<LOQ	<LOQ	<LOQ	<LOQ	<LOD	<LOQ	-0.10	<LOQ	<LOQ	<LOQ	<LOQ	<LOQ	0.00	-0.02	<LOQ	0.00	0.00	0.00	<LOQ
RR-LFP06-D17.0	-2.49	0.02	<LOQ	<LOQ	<LOQ	<LOQ	<LOQ	<LOD	<LOQ	-0.10	<LOQ	<LOQ	<LOQ	<LOQ	<LOQ	0.00	-0.02	<LOQ	0.00	0.00	0.00	<LOQ
RR-LFP06-D20.0	-2.12	0.02	<LOQ	<LOQ	<LOQ	<LOQ	<LOQ	<LOD	<LOQ	-0.08	<LOQ	<LOQ	<LOQ	<LOQ	<LOQ	0.00	-0.01	<LOQ	0.00	0.00	0.00	<LOQ
RR-LFP06-D25.0	-1.63	0.02	<LOQ	<LOQ	<LOQ	<LOQ	<LOQ	<LOD	<LOQ	-0.07	<LOQ	<LOQ	<LOQ	<LOQ	<LOQ	0.00	-0.01	<LOQ	0.00	0.00	0.00	<LOQ
RR-LFP06-DBlank1 (0.5 g)	-0.44	<LOD	<LOD	<LOQ	<LOQ	<LOQ	<LOD	<LOQ	<LOD	-0.17	<LOD	0.00	<LOD	<LOD	<LOQ	0.00	0.00	<LOQ	0.00	<LOD	0.00	<LOQ
RR-LFP06-DBlank2 (3 g)	-0.34	<LOD	<LOD	<LOQ	<LOQ	<LOQ	<LOD	<LOQ	<LOD	-0.15	<LOD	0.00	<LOD	<LOD	<LOQ	0.00	0.00	<LOQ	0.00	<LOQ	<LOQ	<LOQ
RR-LFP06-DBlank3 (18 g)	-0.03	<LOQ	<LOQ	<LOQ	<LOQ	<LOQ	<LOQ	<LOD	<LOQ	-0.01	<LOQ	<LOQ	<LOQ	<LOQ	<LOQ	0.00	0.00	<LOQ	0.00	0.00	0.00	<LOQ

dig_ digestion

sample No.	T [°C]	stirring time [min]	LFP mass [g]	digested mass [g]	c0		c1		c(Na2S2O3) [mol/L]	cEqu,Li [mg/L]	Li mg/L	Na mg/L	K mg/L	Mg mg/L	Ca mg/L	Al mg/L	Si mg/L	P mg/L	S mg/L	Mn mg/L	Fe mg/L	Ni mg/L	Cu mg/L	Zn mg/L
					pH	T [°C]	pH	T [°C]																
method											dig_ OES	dig_ OES	fluid OES	fluid OES	fluid OES	fluid OES	fluid OES	fluid OES	dig_ OES	fluid OES	fluid OES	dig_ OES	dig_ OES	dig_ OES
LOD											0.0002	0.0171	0.0660	0.0005	0.0023	0.0005	0.0185	0.0203	0.0130	0.0001	0.0029	0.0060	0.0064	0.0005
LOQ											0.0006	0.0569	0.2199	0.0017	0.0077	0.0016	0.0616	0.0678	0.0434	0.0004	0.0097	0.0199	0.0213	0.0017
uncertainty [%]											4.9	3.9	21.4	4.6	9.9	8.1	2.1	5.3	19.9	5.0	10.3	2.9	1.6	2.2
load [mg/g]																								
RR-LFP02-01	25	1440	0.963	0.100	-	-	7.30	24.2	0.1	206	0.3	0.2	<LOD	<LOD	0.0	<LOD	<LOD	<LOD	-1.0	<LOD	<LOD	0.0	0.0	0.0
RR-LFP02-02	25	1440	1.037	0.099	-	-	7.10	25.0	0.3	178	3.3	0.6	<LOD	<LOD	-0.1	<LOD	<LOD	<LOD	-1.0	<LOD	<LOD	0.0	0.0	0.0
RR-LFP02-03	25	1440	0.973	0.099	-	-	6.99	25.3	0.5	159	7.7	1.2	<LOD	<LOD	-1.1	<LOD	<LOD	<LOD	2.5	<LOD	<LOD	0.0	0.0	0.0
RR-LFP02-04	25	1440	0.988	0.101	-	-	6.95	24.9	1.0	114	16	8.2	<LOD	<LOD	0.0	<LOD	<LOD	<LOD	12	<LOD	<LOD	0.0	0.0	0.0
RR-LFP02-05	25	1440	1.026	0.100	-	-	7.05	24.6	1.5	73	21	20	<LOD	<LOD	1.8	<LOD	<LOD	<LOD	26	<LOD	<LOD	0.0	0.0	0.0
RR-LFP02-Blank	25	1440	0.000	0.000	-	-	8.79	25.5	0.5	204			<LOD	<LOD	-0.2	<LOD	<LOD	<LOD		<LOD	<LOD			
load [mmol/g]																								
RR-LFP02-01	25	1440	0.963	0.100	-	-	7.30	24.2	0.1	206	0.04	0.01	<LOD	<LOD	0.00	<LOD	<LOD	<LOD	-0.03	<LOD	<LOD	0.00	0.00	0.00
RR-LFP02-02	25	1440	1.037	0.099	-	-	7.10	25.0	0.3	178	0.47	0.03	<LOD	<LOD	0.00	<LOD	<LOD	<LOD	-0.03	<LOD	<LOD	0.00	0.00	0.00
RR-LFP02-03	25	1440	0.973	0.099	-	-	6.99	25.3	0.5	159	1.11	0.05	<LOD	<LOD	-0.03	<LOD	<LOD	<LOD	0.08	<LOD	<LOD	0.00	0.00	0.00
RR-LFP02-04	25	1440	0.988	0.101	-	-	6.95	24.9	1.0	114	2.32	0.36	<LOD	<LOD	0.00	<LOD	<LOD	<LOD	0.37	<LOD	<LOD	0.00	0.00	0.00
RR-LFP02-05	25	1440	1.026	0.100	-	-	7.05	24.6	1.5	73	3.01	0.89	<LOD	<LOD	0.04	<LOD	<LOD	<LOD	0.81	<LOD	<LOD	0.00	0.00	0.00
RR-LFP02-Blank	25	1440	0.000	0.000	-	-	8.79	25.5	0.5	204			<LOD	<LOD	0.00	<LOD	<LOD	<LOD		<LOD	<LOD			

dig_ digestion

sample No.	time			digested	C0		C1			Li	Na	Al	P	S	Mn	Fe	Ni	Cu	Zn
	[min]	T [°C]	LFP [g]	mass [g]	pH	T [°C]	pH	T [°C]	c(Na2S2O3)	mg/L	mg/L	mg/L	mg/L	mg/L	mg/L	mg/L	mg/L	mg/L	mg/L
method										fluid OES	dig_OES	dig_OES	fluid OES	dig_OES	dig_OES	fluid OES	dig_OES	dig_OES	dig_OES
LOD										0.0028	0.0113	0.0071	0.0232	0.0108	0.0001	0.0036	0.0029	0.0017	0.0012
LOQ										0.0093	0.0378	0.0237	0.0774	0.0359	0.0003	0.0120	0.0097	0.0058	0.0040
uncertainty [%]										12.2	2.2	1.4	6.2	0.3	1.6	6.1	2.6	2.6	2.3
load [mg/g]																			
RR-LFP07-0001	1	25	0.995	0.102	9.39	21.4	7.38	21.0	0.5M	-0.1	<LOQ	<LOQ	<LOD	-0.2	0.0	<LOD	0.0	0.0	0.0
RR-LFP07-0005	5	25	1.047	0.099	9.30	21.2	7.19	21.1	0.5M	5.2	<LOQ	<LOD	<LOD	0.1	0.1	<LOD	0.0	0.0	0.0
RR-LFP07-0015	15	25	0.992	0.101	9.33	21.3	7.22	21.3	0.5M	4.9	<LOQ	<LOD	<LOD	-0.4	0.0	<LOD	0.0	0.0	0.0
RR-LFP07-0030	30	25	1.000	0.101	9.27	21.2	7.03	21.2	0.5M	6.9	<LOQ	<LOD	<LOD	0.1	0.2	<LOD	0.0	0.0	0.0
RR-LFP07-0045	45	25	1.024	0.102	9.29	21.4	6.97	21.4	0.5M	5.8	<LOQ	<LOD	<LOD	-0.3	0.0	<LOD	0.0	0.0	0.0
RR-LFP07-0060	60	25	1.040	0.102	9.21	21.3	6.98	20.9	0.5M	5.9	<LOQ	<LOD	<LOD	0.1	0.2	<LOD	0.0	0.0	0.0
RR-LFP07-0120	120	25	1.001	0.100	9.25	21.1	6.86	23.0	0.5M	6.4	<LOQ	<LOQ	<LOD	0.1	0.2	<LOD	0.0	0.0	0.0
RR-LFP07-0180	180	25	0.999	0.101	9.23	21.3	6.87	21.8	0.5M	7.1	<LOQ	<LOQ	<LOD	0.2	0.3	<LOD	0.0	0.0	0.0
RR-LFP07-0240	240	25	1.002	0.101	9.25	21.5	6.84	23.1	0.5M	8.0	<LOQ	<LOD	<LOD	0.3	0.3	<LOD	0.0	0.0	0.0
RR-LFP07-1440	1440	25	1.001	0.099	9.28	21.4	7.14	22.7	0.5M	23	<LOQ	<LOD	-0.8	6.8	0.3	<LOD	0.0	0.0	0.0
RR-LFP07-2T	2880	25	1.055	0.099	9.16	21.2	7.40	22.4	0.5M	31	<LOQ	<LOQ	-1.1	28	0.2	<LOD	0.0	0.0	0.0
RR-LFP07-4T	5760	25	1.007	0.100	9.03	21.4	7.54	21.1	0.5M	32	5.8	<LOD	-1.2	26	0.1	<LOD	0.0	0.0	0.0
RR-LFP07-5T	7200	25	1.037	0.101	8.98	21.7	7.67	22.1	0.5M	38	5.7	<LOD	-1.6	40	0.2	<LOD	0.0	0.0	0.0
RR-LFP07-1Wo	10080	25	1.005	0.099	9.22	21.2	6.74	22.9	0.5M	44	6.8	<LOD	-1.9	47	0.2	<LOQ	0.0	0.0	0.0
RR-LFP07-10T	14400	25	1.003	0.098	9.05	21.3	6.93	22.1	0.5M	37	6.2	<LOQ	-2.0	48	0.2	<LOQ	0.0	0.0	0.0
RR-LFP07-2Wo	21570	25	1.023	0.101	9.15	21.6	5.49	22.3	0.5M	39	7.9	<LOD	-22	83	0.2	-35.0	0.0	0.0	0.0
RR-LFP07-Blank1	15	25	0.000	0.000	9.34	20.9	9.09	21.7	0.5M	7.3			<LOD			<LOD			
RR-LFP07-Blank2	1440	25	0.000	0.000	9.10	21.4	8.91	23.5	0.5M	7.6			<LOD			<LOD			
RR-LFP07-Blank3	10080	25	0.000	0.000	9.24	21.5	9.10	23.9	0.5M	8.8			<LOD			<LOD			
RR-LFP07-Blank4	5770	25	0.000	0.000	8.97	21.3	8.80	22.6	0.5M	-0.3			<LOD			<LOD			
load [mmol/g]																			
RR-LFP07-0001	1	25	0.995	0.102	9.39	21.4	7.38	21.0	0.5M	-0.01	<LOQ		<LOD	-0.01		<LOD			
RR-LFP07-0005	5	25	1.047	0.099	9.30	21.2	7.19	21.1	0.5M	0.76	<LOQ		<LOD	0.00		<LOD			
RR-LFP07-0015	15	25	0.992	0.101	9.33	21.3	7.22	21.3	0.5M	0.70	<LOQ		<LOD	-0.01		<LOD			
RR-LFP07-0030	30	25	1.000	0.101	9.27	21.2	7.03	21.2	0.5M	0.99	<LOQ		<LOD	0.00		<LOD			
RR-LFP07-0045	45	25	1.024	0.102	9.29	21.4	6.97	21.4	0.5M	0.83	<LOQ		<LOD	-0.01		<LOD			
RR-LFP07-0060	60	25	1.040	0.102	9.21	21.3	6.98	20.9	0.5M	0.85	<LOQ		<LOD	0.00		<LOD			
RR-LFP07-0120	120	25	1.001	0.100	9.25	21.1	6.86	23.0	0.5M	0.93	<LOQ		<LOD	0.00		<LOD			
RR-LFP07-0180	180	25	0.999	0.101	9.23	21.3	6.87	21.8	0.5M	1.02	<LOQ		<LOD	0.01		<LOD			
RR-LFP07-0240	240	25	1.002	0.101	9.25	21.5	6.84	23.1	0.5M	1.15	<LOQ		<LOD	0.01		<LOD			
RR-LFP07-1440	1440	25	1.001	0.099	9.28	21.4	7.14	22.7	0.5M	3.25	<LOQ		-0.03	0.21		<LOD			
RR-LFP07-2T	2880	25	1.055	0.099	9.16	21.2	7.40	22.4	0.5M	4.47	<LOQ		-0.03	0.87		<LOD			
RR-LFP07-4T	5760	25	1.007	0.100	9.03	21.4	7.54	21.1	0.5M	4.60	0.25		-0.04	0.80		<LOD			
RR-LFP07-5T	7200	25	1.037	0.101	8.98	21.7	7.67	22.1	0.5M	5.51	0.25		-0.05	1.24		<LOD			
RR-LFP07-1Wo	10080	25	1.005	0.099	9.22	21.2	6.74	22.9	0.5M	6.35	0.30		-0.06	1.48		-			
RR-LFP07-10T	14400	25	1.003	0.098	9.05	21.3	6.93	22.1	0.5M	5.28	0.27		-0.07	1.51		<LOQ			
RR-LFP07-2Wo	21570	25	1.023	0.101	9.15	21.6	5.49	22.3	0.5M	5.58	0.34		-0.71	2.58		-0.63			
RR-LFP07-Blank1	15	25	0.000	0.000	9.34	20.9	9.09	21.7	0.5M	1.06			<LOD			<LOD			
RR-LFP07-Blank2	1440	25	0.000	0.000	9.10	21.4	8.91	23.5	0.5M	1.09			<LOD			<LOD			
RR-LFP07-Blank3	10080	25	0.000	0.000	9.24	21.5	9.10	23.9	0.5M	1.27			<LOD			<LOD			
RR-LFP07-Blank4	5770	25	0.000	0.000	8.97	21.3	8.80	22.6	0.5M	-0.05			<LOD			<LOD			

dig_ digestion

sample No.	c0		c1							c0, Li	cEqu,Li
	T [°C]	pH	T [°C]	pH	T [°C]	LFP [g]	digested mass [g]	time [min]	c(Na2S2O3) [mol/L]	[mg/L]	[mg/L]
max LOD											
max LOQ											
uncertainty [%]											
max LOD											
max LOQ											
uncertainty [%]											
max LOD											
max LOQ											
uncertainty [%]											
max LOD											
max LOQ											
uncertainty [%]											
25°C											0
RR-LFP08-0010	25	9.09	20.6	8.04	22.8	1.008	0.100	10080	0.5	15	1
RR-LFP08-0050	25	8.96	20.6	6.88	22.1	1.081	0.100	10080	0.5	53	0
RR-LFP08-0100	25	9.03	20.7	7.28	21.8	1.011	0.100	10080	0.5	96	0
RR-LFP08-0150	25	9.10	20.8	7.54	23.1	1.080	0.099	10080	0.5	146	3
RR-LFP08-0200	25	9.14	20.8	6.42	23.4	1.053	0.098	10080	0.5	200	8
RR-LFP08-0300	25	9.20	20.9	7.45	24.5	1.008	0.098	10080	0.5	288	116
RR-LFP08-0500	25	9.09	20.8	7.27	22.9	1.005	0.098	10080	0.5	490	297
RR-LFP08-1000	25	9.10	20.7	6.99	23.7	1.001	0.101	10080	0.5	969	775
RR-LFP08-Blank1	25	9.02	20.7	8.76	23.3	0.000	0.000	10080	0.5	100	99
RR-LFP08-Blank2	25	9.11	20.9	8.96	24.7	0.000	0.000	10080	0.5	295	289
40°C											0
RR-LFP09-0010	40	8.77	27.5	5.04	28.1	1.025	0.099	10080	0.5	10	22
RR-LFP09-0050	40	8.90	27.4	5.07	28.4	1.013	0.099	10080	0.5	52	33
RR-LFP09-0100	40	8.90	23.9	4.96	28.7	1.003	0.100	10080	0.5	102	51
RR-LFP09-0150	40	8.90	31.4	4.89	29.0	0.993	0.099	10080	0.5	151	65
RR-LFP09-0200	40	8.54	25.4	4.75	25.9	1.006	0.099	10080	0.5	194	108
RR-LFP09-0300	40	9.04	26.1	4.58	28.7	1.003	0.100	10080	0.5	268	196
RR-LFP09-0500	40	8.92	26.3	4.41	27.8	1.006	0.100	10080	0.5	381	284
RR-LFP09-1000	40	8.78	28.1	4.15	26.3	1.023	0.099	10080	0.5	824	647
RR-LFP09-Blank1	40	8.90	26.8	8.28	28.0	0.000	0.000	10080	0.5	102	119
RR-LFP09-Blank2	40	8.80	25.3	7.78	30.8	0.000	0.000	10080	0.5	227	244
60°C											
RR-LFP10-0010	60	5.20	33.1	4.07	34.2	1.073	0.099	10080	0.5	11	19
RR-LFP10-0050	60	5.19	27.4	4.35	37.3	1.011	0.098	10080	0.5	50	55
RR-LFP10-0100	60	5.29	28.0	4.06	32.7	1.015	0.101	10080	0.5	99	103
RR-LFP10-0150	60	5.06	36.6	4.11	33.9	1.026	0.098	10080	0.5	148	156
RR-LFP10-0200	60	5.16	30.6	4.12	32.1	1.013	0.099	10080	0.5	194	210
RR-LFP10-0300	60	5.40	32.9	4.08	31.6	1.016	0.100	10080	0.5	272	293
RR-LFP10-0500	60	5.05	35.0	4.14	29.8	1.020	0.101	10080	0.5	393	383
RR-LFP10-1000	60	5.12	26.4	4.12	35.7	1.019	0.100	10080	0.5	860	770
RR-LFP10-Blank1	60	4.97	30.2	4.66	39.2	0.000	0.000	10080	0.5	93	93
RR-LFP10-Blank2	60	5.15	32.9	4.59	38.1	0.000	0.000	10080	0.5	231	261
80°C											
RR-LFP11-0010	80	5.34	38.0	4.96	38.0	1.033	0.100	10080	0.5	10	19
RR-LFP11-0050	80	5.35	35.2	4.97	36.3	1.021	0.100	10080	0.5	51	61
RR-LFP11-0100	80	5.47	36.8	4.99	36.0	1.030	0.101	10080	0.5	103	114
RR-LFP11-0150	80	5.23	38.0	5.00	39.1	1.001	0.100	10080	0.5	159	159
RR-LFP11-0200	80	5.11	37.8	5.07	37.1	1.006	0.100	10080	0.5	211	211
RR-LFP11-0300	80	5.06	37.4	4.98	36.0	1.018	0.100	10080	0.5	292	292
RR-LFP11-0500	80	5.13	37.6	5.02	38.1	1.019	0.100	10080	0.5	500	500
RR-LFP11-1000	80	5.16	38.0	5.00	38.6	1.007	0.103	10080	0.5	937	937
RR-LFP11-Blank1	80	5.07	38.0	4.62	36.9	0.000	0.000	10080	0.5	102	102
RR-LFP11-Blank2	80	5.06	38.0	4.63	36.7	0.000	0.000	10080	0.5	292	292

sample No.	Q,Li [mg/L]		Q,Na [mg/L]		Q,Al [mg/L]	Q,P [mg/L]		Q,S [mg/L]		Q,Mn [mg/L]	Q,Fe [mg/L]		Q,Ni [mg/L]	Q,Cu [mg/L]	Q,Zn [mg/L]
max LOD	0.0013		0.0248		0.0204	0.0079		0.0131		0.0005	0.0027		0.0034	0.0036	0.0012
max LOQ	0.0042		0.0825		0.0679	0.0263		0.0438		0.0018	0.0090		0.0114	0.0120	0.0040
uncertainty [%]	5.3		11.6		1.4	2.8		11.0		2.5	29.5		2.8	2.6	2.3
max LOD	0.0020		0.0248		0.0204	0.0122		0.0131		0.0005	0.0036		0.0034	0.0036	0.0007
max LOQ	0.0065		0.0825		0.0679	0.0406		0.0438		0.0018	0.0120		0.0114	0.0120	0.0024
uncertainty [%]	3.5		11.6		1.4	6.2		11.0		2.5	6.1		2.8	1.4	1.6
max LOD	0.0020		0.0248		0.0204	0.0215		0.0131		0.0005	0.0036		0.0034	0.0036	0.0007
max LOQ	0.0065		0.0825		0.0679	0.0718		0.0438		0.0018	0.0120		0.0114	0.0120	0.0024
uncertainty [%]	3.5		11.6		1.4	2.9		11.0		2.5	6.1		2.8	1.4	1.6
max LOD	0.0020		0.0339		0.0204	0.0215		0.0229		0.0006	0.0035		0.0034	0.0037	0.0007
max LOQ	0.0065		0.1128		0.0679	0.0718		0.0763		0.0021	0.0117		0.0114	0.0122	0.0024
uncertainty [%]	4.7		11.6		15.0	6.4		11.0		5.0	2.8		3.6	5.5	2.9
	[mg/g]	[mmol/g]	[mg/g]	[mmol/g]	[mg/g]	[mg/g]	[mmol/g]	[mg/g]	[mmol/g]	[mg/g]	[mg/g]	[mmol/g]	[mg/g]	[mg/g]	[mg/g]
25°C	fluid OES	fluid OES	dig_ OES	dig_ OES	dig_ OES	fluid OES	fluid OES	dig_ OES	dig_ OES	dig_ OES	fluid OES	fluid OES	dig_ OES	dig_ OES	dig_ OES
RR-LFP08-0010	2.8	0.40	25	1.08	<LOD	-2.9	-0.10	4.1	0.13	0.2	<LOD	<LOD	0.0	0.0	0.0
RR-LFP08-0050	9.7	1.39	27	1.18	<LOD	-2.4	-0.08	12	0.38	0.2	-0.1	0.00	0.0	0.0	0.0
RR-LFP08-0100	19	2.72	18	0.80	<LOD	-2.3	-0.07	22	0.68	0.2	<LOD	<LOD	0.0	0.0	0.0
RR-LFP08-0150	26	3.80	24	1.03	<LOQ	-2.0	-0.06	39	1.23	0.2	<LOD	<LOD	0.0	0.0	0.0
RR-LFP08-0200	37	5.26	8.6	0.38	<LOQ	-2.8	-0.09	56	1.74	0.2	-1.4	-0.03	0.0	0.0	0.0
RR-LFP08-0300	34	4.94	14	0.60	<LOQ	-2.4	-0.08	49	1.52	0.2	<LOD	<LOD	0.0	0.0	0.0
RR-LFP08-0500	38	5.53	4.7	0.20	<LOD	-2.1	-0.07	48	1.51	0.1	<LOD	<LOD	0.0	0.1	0.0
RR-LFP08-1000	39	5.59	4.3	0.19	<LOD	-2.3	-0.07	51	1.58	0.0	<LOD	<LOD	0.0	0.1	0.0
RR-LFP08-Blank1	0.2	0.03				<LOD	<LOD				<LOD	<LOD			
RR-LFP08-Blank2	1.1	0.16				<LOD	<LOD				<LOD	<LOD			
40°C	dig_ OES	dig_ OES	dig_ OES	dig_ OES	dig_ OES	fluid OES	fluid OES	dig_ OES	dig_ OES	dig_ OES	fluid OES	fluid OES	dig_ OES	dig_ OES	dig_ OES
RR-LFP09-0010	1.2	0.17	84	3.67	<LOD	-56	-1.80	115	3.59	0.1	-92	-1.65	<LOQ	0.1	0.0
RR-LFP09-0050	7.7	1.11	68	2.94	<LOD	-50	-1.61	88	2.75	0.0	-81	-1.45	0.0	0.1	<LOQ
RR-LFP09-0100	16	2.26	45	1.95	<LOD	-53	-1.72	89	2.77	0.1	-86	-1.54	0.0	0.0	0.0
RR-LFP09-0150	25	3.60	13	0.57	<LOD	-70	-2.27	134	4.17	0.1	-117	-2.10	0.0	0.1	<LOQ
RR-LFP09-0200	27	3.87	7.0	0.30	<LOD	-72	-2.33	138	4.30	0.1	-121	-2.17	<LOQ	0.1	0.0
RR-LFP09-0300	31	4.42	0.7	0.03	<LOD	-71	-2.29	125	3.89	-0.1	-117	-2.09	<LOQ	0.1	<LOQ
RR-LFP09-0500	31	4.50	0.1	0.01	<LOD	-59	-1.92	128	3.99	0.1	-94	-1.69	0.0	0.1	0.0
RR-LFP09-1000	30	4.33	-0.1	0.00	<LOD	-59	-1.91	122	3.80	-0.2	-91	-1.63	0.0	0.1	<LOQ
RR-LFP09-Blank1						<LOD	<LOD				<LOD	<LOD			
RR-LFP09-Blank2						<LOD	<LOD				<LOD	<LOD			

dig_ digestion

sample No.	Q,Li [mg/L]		Q,Na [mg/L]		Q,Al [mg/L]	Q,P [mg/L]		Q,S [mg/L]		Q,Mn [mg/L]	Q,Fe [mg/L]		Q,Ni [mg/L]	Q,Cu [mg/L]	Q,Zn [mg/L]
max LOD	0.0013		0.0248		0.0204	0.0079		0.0131		0.0005	0.0027		0.0034	0.0036	0.0012
max LOQ	0.0042		0.0825		0.0679	0.0263		0.0438		0.0018	0.0090		0.0114	0.0120	0.0040
uncertainty [%]	5.3		11.6		1.4	2.8		11.0		2.5	29.5		2.8	2.6	2.3
max LOD	0.0020		0.0248		0.0204	0.0122		0.0131		0.0005	0.0036		0.0034	0.0036	0.0007
max LOQ	0.0065		0.0825		0.0679	0.0406		0.0438		0.0018	0.0120		0.0114	0.0120	0.0024
uncertainty [%]	3.5		11.6		1.4	6.2		11.0		2.5	6.1		2.8	1.4	1.6
max LOD	0.0020		0.0248		0.0204	0.0215		0.0131		0.0005	0.0036		0.0034	0.0036	0.0007
max LOQ	0.0065		0.0825		0.0679	0.0718		0.0438		0.0018	0.0120		0.0114	0.0120	0.0024
uncertainty [%]	3.5		11.6		1.4	2.9		11.0		2.5	6.1		2.8	1.4	1.6
max LOD	0.0020		0.0339		0.0204	0.0215		0.0229		0.0006	0.0035		0.0034	0.0037	0.0007
max LOQ	0.0065		0.1128		0.0679	0.0718		0.0763		0.0021	0.0117		0.0114	0.0122	0.0024
uncertainty [%]	4.7		11.6		15.0	6.4		11.0		5.0	2.8		3.6	5.5	2.9
	[mg/g]	[mmol/g]	[mg/g]	[mmol/g]	[mg/g]	[mg/g]	[mmol/g]	[mg/g]	[mmol/g]	[mg/g]	[mg/g]	[mmol/g]	[mg/g]	[mg/g]	[mg/g]
60°C	dig_ OES	dig_ OES	dig_ OES	dig_ OES	dig_ OES	dig_ OES	dig_ OES	dig_ OES	dig_ OES	dig_ OES	fluid OES	fluid OES	dig_ OES	dig_ OES	dig_ OES
RR-LFP10-0010	-1.6	-0.23	2.0	0.09	<LOD	-98	-3.17	379	11.81	0.1	-6.2	-0.11	0.0	0.0	<LOQ
RR-LFP10-0050	-1.2	-0.17	0.6	0.03	<LOD	-129	-4.15	497	15.49	0.0	<LOQ	<LOQ	0.0	0.1	<LOQ
RR-LFP10-0100	-1.1	-0.16	0.8	0.03	<LOD	-121	-3.90	473	14.75	0.0	-4.8	-0.09	0.0	0.1	<LOQ
RR-LFP10-0150	<LOD	<LOD	-0.7	-0.03	<LOD	-145	-4.67	564	17.59	0.0	<LOQ	<LOQ	0.0	0.1	<LOQ
RR-LFP10-0200	<LOD	<LOD	-0.6	-0.03	<LOD	-145	-4.67	567	17.68	0.0	<LOD	<LOD	0.0	0.1	<LOQ
RR-LFP10-0300	<LOQ	<LOQ	-0.7	-0.03	<LOD	-145	-4.67	558	17.40	0.0	<LOQ	<LOQ	0.0	0.1	<LOQ
RR-LFP10-0500	<LOQ	<LOQ	-0.6	-0.03	<LOD	-145	-4.67	566	17.66	0.0	<LOQ	<LOQ	0.0	0.1	<LOQ
RR-LFP10-1000	<LOQ	<LOQ	-0.7	-0.03	<LOD	-145	-4.67	561	17.49	0.0	<LOQ	<LOQ	0.0	0.1	<LOQ
RR-LFP10-Blank1						<LOD	<LOD				<LOQ	<LOQ			
RR-LFP10-Blank2						<LOD	<LOD				<LOQ	<LOQ			
80°C	dig_ OES	dig_ OES	dig_ OES	dig_ OES	dig_ OES	dig_ OES	dig_ OES	dig_ OES	dig_ OES	dig_ OES	fluid OES	fluid OES	dig_ OES	dig_ OES	dig_ OES
RR-LFP11-0010	<LOD	<LOD	0.5	0.02	<LOD	-133	-4.30	489	15.25	0.0	<LOD	<LOD	0.0	0.0	0.0
RR-LFP11-0050	<LOQ	<LOQ	0.1	0.00	<LOD	-134	-4.32	480	14.97	0.0	<LOD	<LOD	0.0	0.1	<LOQ
RR-LFP11-0100	<LOD	<LOD	-0.4	-0.02	0.3	-144	-4.64	533	16.63	0.0	<LOD	<LOD	0.8	0.2	0.0
RR-LFP11-0150	<LOD	<LOD	-0.6	-0.02	0.1	-144	-4.66	528	16.47	0.0	<LOD	<LOD	0.5	0.2	<LOQ
RR-LFP11-0200	<LOD	<LOD	-0.4	-0.02	0.7	-144	-4.64	537	16.74	0.0	<LOD	<LOD	1.8	0.4	0.0
RR-LFP11-0300	<LOQ	<LOQ	-0.5	-0.02	0.2	-140	-4.53	523	16.30	0.0	<LOD	<LOD	0.7	0.2	0.0
RR-LFP11-0500	<LOQ	<LOQ	-0.6	-0.03	<LOD	-145	-4.67	561	17.50	0.0	<LOD	<LOD	0.0	0.1	<LOQ
RR-LFP11-1000	<LOQ	<LOQ	<LOD	<LOD	<LOQ	-145	-4.67	>cal	>cal	0.0	<LOD	<LOD	0.0	<LOD	<LOQ
RR-LFP11-Blank1											<LOD	<LOD			
RR-LFP11-Blank2											<LOD	<LOD			

dig_ digestion

sample No. (Bruchsal kinetics) method LOD LOQ uncertainty [%]	T [°C]	volume [mL]	time [min]	LFP [g]	c0 pH	c0 T [°C]	c1 pH	c1 T [°C]	digested mass [g]
load [mg/g]									
RR-LFP-TW1-0001	60	200	1	1.089	7.24	36.9	6.68	31.4	0.101
RR-LFP-TW1-0015	60	200	15	1.051	7.25	30.9	6.56	33.9	0.099
RR-LFP-TW1-0030	60	200	30	1.056	7.20	30.6	6.34	34.7	0.101
RR-LFP-TW1-0060	60	200	60	1.099	7.16	30.9	5.53	35.0	0.101
RR-LFP-TW1-0120	60	200	120	1.072	7.18	30.5	4.74	33.0	0.099
RR-LFP-TW1-0180	60	200	180	1.027	7.15	37.6	4.63	30.0	0.100
RR-LFP-TW1-0240	60	200	240	1.071	7.20	31.2	4.49	34.1	0.100
RR-LFP-TW1-1440	60	200	1440	1.010	7.19	34.4	4.08	31.0	0.099
RR-LFP-TW1-3T	60	200	4320	1.015	7.34	27.1	4.29	33.9	0.100
RR-LFP-TW1-5T	60	200	7200	1.025	7.15	35.9	3.77	34.3	0.101
RR-LFP-TW1-1Wo	60	200	10080	1.038	7.25	27.7	3.67	32.3	0.100
RR-LFP-TW1-2Wo	60	200	20160	1.007	7.14	33.0	4.23	33.9	0.100
RR-LFP-TW1-Blank1	60	200	15	0.000	7.12	36.8	7.14	36.7	0.000
RR-LFP-TW1-Blank2	60	200	1440	0.000	7.14	36.6	7.06	31.3	0.000
RR-LFP-TW1-Blank3	60	200	10080	0.000	7.11	38.8	5.67	33.6	0.000
load [mmol/g]									
RR-LFP-TW1-0001	60	200	1	1.089	7.24	36.9	6.68	31.4	0.101
RR-LFP-TW1-0015	60	200	15	1.051	7.25	30.9	6.56	33.9	0.099
RR-LFP-TW1-0030	60	200	30	1.056	7.20	30.6	6.34	34.7	0.101
RR-LFP-TW1-0060	60	200	60	1.099	7.16	30.9	5.53	35.0	0.101
RR-LFP-TW1-0120	60	200	120	1.072	7.18	30.5	4.74	33.0	0.099
RR-LFP-TW1-0180	60	200	180	1.027	7.15	37.6	4.63	30.0	0.100
RR-LFP-TW1-0240	60	200	240	1.071	7.20	31.2	4.49	34.1	0.100
RR-LFP-TW1-1440	60	200	1440	1.010	7.19	34.4	4.08	31.0	0.099
RR-LFP-TW1-3T	60	200	4320	1.015	7.34	27.1	4.29	33.9	0.100
RR-LFP-TW1-5T	60	200	7200	1.025	7.15	35.9	3.77	34.3	0.101
RR-LFP-TW1-1Wo	60	200	10080	1.038	7.25	27.7	3.67	32.3	0.100
RR-LFP-TW1-2Wo	60	200	20160	1.007	7.14	33.0	4.23	33.9	0.100
RR-LFP-TW1-Blank1	60	200	15	0.000	7.12	36.8	7.14	36.7	0.000
RR-LFP-TW1-Blank2	60	200	1440	0.000	7.14	36.6	7.06	31.3	0.000
RR-LFP-TW1-Blank3	60	200	10080	0.000	7.11	38.8	5.67	33.6	0.000

sample No.	Li	Na	K	Rb	Cs	Mg	Ca	Sr	Ba	B	Al	Si	Pb	P	As	Sb	S	Ti	V	Cr	Mn	Fe	Co	Ni	Cu	Zn	Cd
(Bruchsal kinetics)	mg/L	mg/L	mg/L	mg/L	mg/L	mg/L	mg/L	mg/L	mg/L	mg/L	mg/L	mg/L	mg/L	mg/L	mg/L	mg/L	mg/L	mg/L	mg/L	mg/L	mg/L	mg/L	mg/L	mg/L	mg/L	mg/L	mg/L
	fluid	dig_	dig_	dig_	dig_	dig_	dig_	dig_	dig_	dig_	dig_	dig_	dig_	fluid	dig_	dig_	dig_	dig_	dig_	dig_	dig_	fluid	dig_	dig_	dig_	dig_	dig_
method	OES	OES	MS	MS	MS	MS	OES	MS	MS	MS	MS	OES	MS	OES	MS	MS	OES	MS	MS	MS	MS	OES	MS	MS	MS	MS	MS
LOD	0.0035	0.1582	0.0003	0.000	0.000	0.0002	0.0052	0.000	0.000	0.0001	0.0001	0.0032	0.000	0.0033	0.000	0.000	0.0260	0.0000	0.000	0.000	0.000	0.0001	0.000	0.000	0.000	0.000	0.000
LOQ	0.0117	0.5273	0.0009	0.000	0.000	0.0007	0.0173	0.000	0.000	0.0004	0.0002	0.0106	0.000	0.0108	0.000	0.000	0.0867	0.0001	0.000	0.000	0.000	0.0004	0.000	0.000	0.000	0.000	0.000
uncertainty [%]	8.8	1.6	11.9	0.3	1.2	8.0	7.8	3.5	6.6	3.0	5.4	4.9	3.8	2.7	6.8	5.1	3.3	4.1	3.3	4.7	2.6	2.5	5.1	4.3	3.8	5.9	3.6
load [mg/g]																											
RR-LFP-TW1-0001	0.8	1.1	0.3	<LOQ	<LOQ	0.0	2.6	0.2	0.1	<LOQ	0.0	0.0	<LOQ	<LOQ	0.0	<LOQ	0.2	0.0	<LOQ	0.0	0.0	<LOD	0.0	0.0	-0.1	0.3	<LOQ
RR-LFP-TW1-0015	3.5	1.4	0.4	<LOQ	<LOQ	0.1	2.7	0.3	0.1	<LOQ	0.0	0.0	<LOQ	<LOD	0.1	<LOQ	1.4	0.0	<LOQ	0.0	0.0	<LOD	0.0	0.0	-0.1	0.3	<LOQ
RR-LFP-TW1-0030	7.5	1.2	0.3	<LOQ	<LOQ	0.1	2.7	0.3	0.1	<LOQ	0.0	0.0	<LOQ	<LOQ	0.0	<LOQ	3.3	0.0	<LOQ	0.0	0.1	<LOQ	0.0	0.0	-0.1	0.3	<LOQ
RR-LFP-TW1-0060	18	3.3	0.3	<LOQ	<LOQ	0.1	3.1	0.3	0.1	<LOQ	0.0	0.0	<LOQ	-0.5	0.0	<LOQ	16	0.0	<LOQ	0.0	0.0	<LOQ	0.0	0.0	-0.1	0.2	<LOQ
RR-LFP-TW1-0120	19	12	0.3	<LOQ	<LOQ	0.0	3.7	0.4	0.1	<LOQ	0.0	0.0	<LOQ	-2.4	0.0	<LOQ	27	0.1	<LOQ	0.0	0.0	-4.1	0.0	0.0	-0.1	0.1	<LOQ
RR-LFP-TW1-0180	23	16	0.4	<LOQ	<LOQ	0.1	5.4	0.6	0.1	<LOQ	0.0	0.0	<LOQ	-9.2	0.0	<LOQ	47	0.0	<LOQ	0.0	0.0	-17	0.0	0.0	-0.1	0.1	<LOQ
RR-LFP-TW1-0240	22	21	0.4	<LOQ	<LOQ	0.1	6.0	0.6	0.1	<LOQ	0.0	0.0	<LOQ	-15	0.0	<LOQ	58	0.0	<LOQ	0.0	0.0	-29	0.0	0.0	-0.1	0.1	<LOQ
RR-LFP-TW1-1440	11	46	0.6	<LOQ	<LOQ	0.1	8.6	1.0	0.2	<LOQ	0.0	0.0	<LOQ	-57	0.0	<LOQ	119	0.0	<LOQ	0.0	0.0	-106	0.0	0.0	-0.1	0.1	<LOQ
RR-LFP-TW1-3T	10	35	0.6	<LOQ	<LOQ	0.1	13	1.3	0.3	<LOQ	0.0	0.0	0.0	-65	0.0	0.0	190	0.2	<LOQ	0.0	0.0	-123	0.0	0.0	-0.1	0.1	<LOQ
RR-LFP-TW1-5T	2.8	16	0.3	0.0	0.1	0.0	91	1.1	0.1	<LOQ	0.0	-0.1	0.0	-104	0.3	0.0	267	0.1	<LOQ	0.0	-0.2	-30	0.0	0.0	-0.1	0.0	<LOQ
RR-LFP-TW1-1Wo	1.4	6.2	0.2	0.0	0.1	-0.1	122	0.9	0.1	<LOQ	-0.1	-0.1	0.0	-114	0.3	0.0	318	0.0	<LOQ	0.0	-0.3	-8.2	0.0	0.0	-0.1	0.0	<LOQ
RR-LFP-TW1-2Wo	-0.8	0.4	0.1	0.0	0.1	-0.1	154	1.4	0.2	<LOQ	-0.1	-0.1	0.0	-100	0.2	<LOQ	344	0.0	<LOQ	0.0	-0.3	<LOD	0.0	-0.1	-0.1	0.0	<LOQ
RR-LFP-TW1-Blank1	0.2													<LOD								<LOQ					
RR-LFP-TW1-Blank2	0.1													<LOD								<LOQ					
RR-LFP-TW1-Blank3	-0.2													<LOQ								<LOQ					
load [mmol/g]																											
RR-LFP-TW1-0001	0.11	0.05	0.01	<LOQ	<LOQ	0.00	0.06	0.00	0.00	<LOQ	0.00	0.00	<LOQ	<LOQ	0.00	<LOQ	0.01	0.00	<LOQ	0.00	0.00	<LOD	0.00	0.00	0.00	0.01	<LOQ
RR-LFP-TW1-0015	0.50	0.06	0.01	<LOQ	<LOQ	0.00	0.07	0.00	0.00	<LOQ	0.00	0.00	<LOQ	<LOD	0.00	<LOQ	0.04	0.00	<LOQ	0.00	0.00	<LOD	0.00	0.00	0.00	0.00	<LOQ
RR-LFP-TW1-0030	1.08	0.05	0.01	<LOQ	<LOQ	0.00	0.07	0.00	0.00	<LOQ	0.00	0.00	<LOQ	<LOQ	0.00	<LOQ	0.10	0.00	<LOQ	0.00	0.00	<LOQ	0.00	0.00	0.00	0.00	<LOQ
RR-LFP-TW1-0060	2.53	0.14	0.01	<LOQ	<LOQ	0.00	0.08	0.00	0.00	<LOQ	0.00	0.00	<LOQ	-0.02	0.00	<LOQ	0.50	0.00	<LOQ	0.00	0.00	<LOQ	0.00	0.00	0.00	0.00	<LOQ
RR-LFP-TW1-0120	2.75	0.53	0.01	<LOQ	<LOQ	0.00	0.09	0.00	0.00	<LOQ	0.00	0.00	<LOQ	-0.08	0.00	<LOQ	0.83	0.00	<LOQ	0.00	0.00	-0.07	0.00	0.00	0.00	0.00	<LOQ
RR-LFP-TW1-0180	3.37	0.68	0.01	<LOQ	<LOQ	0.00	0.13	0.01	0.00	<LOQ	0.00	0.00	<LOQ	-0.30	0.00	<LOQ	1.46	0.00	<LOQ	0.00	0.00	-0.31	0.00	0.00	0.00	0.00	<LOQ
RR-LFP-TW1-0240	3.10	0.91	0.01	<LOQ	<LOQ	0.00	0.15	0.01	0.00	<LOQ	0.00	0.00	<LOQ	-0.49	0.00	<LOQ	1.80	0.00	<LOQ	0.00	0.00	-0.51	0.00	0.00	0.00	0.00	<LOQ
RR-LFP-TW1-1440	1.61	2.00	0.01	<LOQ	<LOQ	0.00	0.22	0.01	0.00	<LOQ	0.00	0.00	<LOQ	-1.85	0.00	<LOQ	3.70	0.00	<LOQ	0.00	0.00	-1.89	0.00	0.00	0.00	0.00	<LOQ
RR-LFP-TW1-3T	1.51	1.54	0.01	<LOQ	<LOQ	0.00	0.32	0.01	0.00	<LOQ	0.00	0.00	0.00	-2.09	0.00	0.00	5.94	0.00	<LOQ	0.00	0.00	-2.20	0.00	0.00	0.00	0.00	<LOQ
RR-LFP-TW1-5T	0.40	0.69	0.01	0.00	0.00	0.00	2.26	0.01	0.00	<LOQ	0.00	0.00	0.00	-3.35	0.00	0.00	8.34	0.00	<LOQ	0.00	0.00	-0.53	0.00	0.00	0.00	0.00	<LOQ
RR-LFP-TW1-1Wo	0.21	0.27	0.00	0.00	0.00	0.00	3.05	0.01	0.00	<LOQ	0.00	0.00	0.00	-3.68	0.00	0.00	9.91	0.00	<LOQ	0.00	-0.01	-0.15	0.00	0.00	0.00	0.00	<LOQ
RR-LFP-TW1-2Wo	-0.11	0.02	0.00	0.00	0.00	0.00	3.83	0.02	0.00	<LOQ	0.00	0.00	0.00	-3.22	0.00	<LOQ	10.71	0.00	<LOQ	0.00	-0.01	<LOD	0.00	0.00	0.00	0.00	<LOQ
RR-LFP-TW1-Blank1	0.04													<LOD								<LOQ					
RR-LFP-TW1-Blank2	0.01													<LOD								<LOQ					
RR-LFP-TW1-Blank3	-0.03													<LOQ								<LOQ					

dig_ digestion

sample No. (Neustadt-Glewe kinetics) method LOD LOQ uncertainty [%]	T [°C]	c(Na2S2O3)	time [min]	LFP [g]	digested mass [g]	pH	c0 T [°C]	pH	c1 T [°C]
load [mg/g]									
RR-LFP400-des (NDB)									
RR-LFP-NDB1-0001	60	0.5M	1	0.999	0.100	7.34	30.0	5.87	37.1
RR-LFP-NDB1-0015	60	0.5M	15	1.000	0.102	7.28	28.5	5.62	37.5
RR-LFP-NDB1-0030	60	0.5M	30	1.000	0.099	7.16	29.9	5.57	37.5
RR-LFP-NDB1-0060	60	0.5M	60	1.000	0.100	7.04	30.0	5.35	37.1
RR-LFP-NDB1-0120	60	0.5M	120	1.001	0.100	7.20	29.0	5.34	40.8
RR-LFP-NDB1-0180	60	0.5M	180	1.000	0.101	7.15	31.2	4.54	40.9
RR-LFP-NDB1-0240	60	0.5M	240	1.000	0.101	7.26	28.6	4.24	40.4
RR-LFP-NDB1-1440	60	0.5M	1440	1.001	0.102	7.30	28.8	3.78	39.6
RR-LFP-NDB1-3T	60	0.5M	4320	1.000	0.102	7.62	34.0	3.76	41.1
RR-LFP-NDB1-5T	60	0.5M	7200	1.000	0.101	7.66	28.9	3.59	38.6
RR-LFP-NDB1-1Wo	60	0.5M	10109	1.000	0.100	7.65	28.7	3.97	35.1
RR-LFP-NDB1-Blank1	60	0.5M	15	0.000		7.34	29.4	7.25	35.0
RR-LFP-NDB1-Blank2	60	0.5M	1440	0.000		7.42	28.6	5.65	40.8
RR-LFP-NDB1-Blank3	60	0.5M	10080	0.000		7.66	29.7	4.91	41.6
load [mmol/g]									
RR-LFP-NDB1-0001	60	0.5M	1	0.999	0.100	7.34	30.0	5.87	37.1
RR-LFP-NDB1-0015	60	0.5M	15	1.000	0.102	7.28	28.5	5.62	37.5
RR-LFP-NDB1-0030	60	0.5M	30	1.000	0.099	7.16	29.9	5.57	37.5
RR-LFP-NDB1-0060	60	0.5M	60	1.000	0.100	7.04	30.0	5.35	37.1
RR-LFP-NDB1-0120	60	0.5M	120	1.001	0.100	7.20	29.0	5.34	40.8
RR-LFP-NDB1-0180	60	0.5M	180	1.000	0.101	7.15	31.2	4.54	40.9
RR-LFP-NDB1-0240	60	0.5M	240	1.000	0.101	7.26	28.6	4.24	40.4
RR-LFP-NDB1-1440	60	0.5M	1440	1.001	0.102	7.30	28.8	3.78	39.6
RR-LFP-NDB1-3T	60	0.5M	4320	1.000	0.102	7.62	34.0	3.76	41.1
RR-LFP-NDB1-5T	60	0.5M	7200	1.000	0.101	7.66	28.9	3.59	38.6
RR-LFP-NDB1-1Wo	60	0.5M	10109	1.000	0.100	7.65	28.7	3.97	35.1

sample No. (Neustadt-Glewe kinetics)	Li	Na	K	Rb	Cs	Mg	Ca	Sr	Ba	B	Al	Si	Pb	P	As	Sb	S	Ti	V	Cr	Mn	Fe	Co	Ni	Cu	Zn	Cd
	mg/L	mg/L	mg/L	mg/L	mg/L	mg/L	mg/L	mg/L	mg/L	mg/L	mg/L	mg/L	mg/L	mg/L	mg/L	mg/L	mg/L	mg/L	mg/L	mg/L	mg/L	mg/L	mg/L	mg/L	mg/L	mg/L	mg/L
	fluid	dig_	dig_	dig_	dig_	dig_	dig_	dig_	dig_	fluid	dig_	dig_	dig_	fluid	dig_	dig_	dig_	dig_	dig_	dig_	dig_	fluid	dig_	dig_	dig_	dig_	dig_
method	OES	OES	MS	MS	MS	OES	OES	OES	MS	OES	MS	OES	MS	OES	OES	MS	OES	MS	MS	MS	MS	OES	MS	MS	OES	OES	MS
LOD	0.0022	0.0064	0.0010	0.000	0.000	0.0001	0.0091	0.0002	0.000	0.0080	0.0001	0.0425	0.000	0.0153	0.0078	0.000	0.0169	0.0000	0.000	0.000	0.000	0.0059	0.000	0.000	0.0040	0.0006	0.000
LOQ	0.0072	0.0213	0.0032	0.000	0.000	0.0003	0.0302	0.0006	0.000	0.0265	0.0002	0.1417	0.000	0.0511	0.0260	0.000	0.0562	0.0001	0.000	0.000	0.000	0.0196	0.000	0.000	0.0134	0.0019	0.000
uncertainty [%]	3.6	7.5	51.0	0.4	0.1	2.8	1.1	5.9	1.2	5.6	1.8	0.0	1.5	9.0	1.4	21.8	1.2	1.5	3.4	2.5	4.5	3.9	3.9	2.4	1.2	1.1	2.0
load [mg/g]																											
RR-LFP400-des (NDB)		1.1	0.0	<LOQ	<LOQ	0.1	<LOQ	<LOD	<LOQ		0.1	<LOD	<LOQ		<LOD	<LOQ	1.5	0.0	<LOQ	<LOQ	0.2		0.0	0.0	<LOD	0.1	<LOQ
RR-LFP-NDB1-0001	-0.4	1.3	0.1	<LOQ	<LOQ	0.1	2.1	0.2	0.0	<LOD	0.0	<LOD	0.1	<LOD	<LOD	<LOQ	0.1	0.0	<LOQ	<LOQ	0.0	<LOQ	0.0	0.0	<LOD	0.1	<LOQ
RR-LFP-NDB1-0015	-0.4	2.6	0.1	<LOQ	<LOQ	0.2	2.7	0.3	0.0	<LOQ	0.0	<LOD	0.1	<LOD	<LOD	<LOQ	0.6	0.0	<LOQ	<LOQ	0.0	<LOQ	0.0	0.0	<LOD	0.1	<LOQ
RR-LFP-NDB1-0030	-0.4	3.1	0.1	<LOQ	<LOQ	0.2	2.8	0.3	0.0	<LOD	0.0	<LOD	0.1	<LOD	<LOD	<LOQ	0.7	0.0	<LOQ	<LOQ	0.0	<LOQ	0.0	0.0	<LOD	0.1	<LOQ
RR-LFP-NDB1-0060	-0.2	6.6	0.1	<LOQ	<LOQ	0.2	3.2	0.4	0.0	<LOD	0.0	<LOD	0.1	-0.3	<LOD	<LOQ	1.8	0.0	<LOQ	<LOQ	0.0	<LOQ	0.0	0.0	<LOD	0.0	<LOQ
RR-LFP-NDB1-0120	0.3	15	0.1	<LOQ	<LOQ	0.2	3.7	0.4	0.1	<LOD	0.0	<LOD	0.1	-0.2	<LOD	<LOQ	5.6	0.0	<LOQ	<LOQ	0.0	-0.6	0.0	0.0	<LOD	0.0	<LOQ
RR-LFP-NDB1-0180	0.6	26	0.1	<LOQ	<LOQ	0.2	3.8	0.4	0.1	<LOD	0.0	<LOD	0.1	-0.9	<LOD	<LOQ	12	0.0	<LOQ	<LOQ	0.0	-1.7	0.0	0.0	<LOD	0.0	<LOQ
RR-LFP-NDB1-0240	1.0	37	0.1	<LOQ	<LOQ	0.2	4.1	0.5	0.1	<LOD	0.0	<LOD	0.0	-1.9	<LOD	<LOQ	19	0.0	<LOQ	<LOQ	0.0	-3.7	0.0	0.0	<LOD	0.0	<LOQ
RR-LFP-NDB1-1440	0.2	88	0.1	<LOQ	<LOQ	0.2	6.6	0.8	0.1	<LOD	0.0	<LOD	<LOQ	-42	<LOD	<LOQ	105	0.1	<LOQ	0.0	0.0	-92	0.0	0.0	<LOD	0.0	<LOQ
RR-LFP-NDB1-3T	-0.4	50	0.1	<LOQ	<LOQ	0.3	69	1.2	0.1	<LOD	0.0	<LOD	0.1	-48	<LOD	<LOQ	180	0.0	<LOQ	<LOQ	-0.1	-98	0.0	0.0	<LOD	<LOQ	<LOQ
RR-LFP-NDB1-5T	-1.0	13	0.0	<LOQ	<LOQ	0.0	139	1.2	0.0	<LOD	0.0	<LOD	0.0	-65	<LOD	<LOQ	249	0.0	<LOQ	<LOQ	-0.2	-41	0.0	0.0	<LOD	<LOQ	<LOQ
RR-LFP-NDB1-1Wo	-1.1	14	0.0	<LOQ	<LOQ	0.0	136	1.2	0.0	<LOD	0.0	<LOD	0.0	-51	<LOD	<LOQ	265	0.0	<LOQ	<LOQ	-0.1	-10	0.0	0.0	<LOD	-0.1	<LOQ
RR-LFP-NDB1-Blank1	0.0									<LOD				<LOD								<LOD					
RR-LFP-NDB1-Blank2	0.0									<LOD				<LOD								<LOD					
RR-LFP-NDB1-Blank3	0.0									<LOD				<LOD								<LOD					
load [mmol/g]																											
RR-LFP-NDB1-0001	-0.06	0.06	0.00	<LOQ	<LOQ	0.01	0.05	0.00	0.00	<LOD	0.00	<LOD	0.00	<LOD	<LOD	<LOQ	0.00	0.00	<LOQ	<LOQ	0.00	<LOQ	0.00	0.00	<LOD	0.00	<LOQ
RR-LFP-NDB1-0015	-0.06	0.11	0.00	<LOQ	<LOQ	0.01	0.07	0.00	0.00	<LOQ	0.00	<LOD	0.00	<LOD	<LOD	<LOQ	0.02	0.00	<LOQ	<LOQ	0.00	<LOQ	0.00	0.00	<LOD	0.00	<LOQ
RR-LFP-NDB1-0030	-0.05	0.13	0.00	<LOQ	<LOQ	0.01	0.07	0.00	0.00	<LOD	0.00	<LOD	0.00	<LOD	<LOD	<LOQ	0.02	0.00	<LOQ	<LOQ	0.00	<LOQ	0.00	0.00	<LOD	0.00	<LOQ
RR-LFP-NDB1-0060	-0.03	0.29	0.00	<LOQ	<LOQ	0.01	0.08	0.00	0.00	<LOD	0.00	<LOD	0.00	-0.01	<LOD	<LOQ	0.06	0.00	<LOQ	<LOQ	0.00	<LOQ	0.00	0.00	<LOD	0.00	<LOQ
RR-LFP-NDB1-0120	0.05	0.67	0.00	<LOQ	<LOQ	0.01	0.09	0.00	0.00	<LOD	0.00	<LOD	0.00	-0.01	<LOD	<LOQ	0.17	0.00	<LOQ	<LOQ	0.00	-0.01	0.00	0.00	<LOD	0.00	<LOQ
RR-LFP-NDB1-0180	0.08	1.15	0.00	<LOQ	<LOQ	0.01	0.10	0.00	0.00	<LOD	0.00	<LOD	0.00	-0.03	<LOD	<LOQ	0.38	0.00	<LOQ	<LOQ	0.00	-0.03	0.00	0.00	<LOD	0.00	<LOQ
RR-LFP-NDB1-0240	0.14	1.62	0.00	<LOQ	<LOQ	0.01	0.10	0.01	0.00	<LOD	0.00	<LOD	0.00	-0.06	<LOD	<LOQ	0.58	0.00	<LOQ	<LOQ	0.00	-0.07	0.00	0.00	<LOD	0.00	<LOQ
RR-LFP-NDB1-1440	0.02	3.82	0.00	<LOQ	<LOQ	0.01	0.17	0.01	0.00	<LOD	0.00	<LOD	<LOQ	-1.37	<LOD	<LOQ	3.29	0.00	<LOQ	0.00	0.00	-1.65	0.00	0.00	<LOD	0.00	<LOQ
RR-LFP-NDB1-3T	-0.06	2.18	0.00	<LOQ	<LOQ	0.01	1.71	0.01	0.00	<LOD	0.00	<LOD	0.00	-1.54	<LOD	<LOQ	5.60	0.00	<LOQ	<LOQ	0.00	-1.75	0.00	0.00	<LOD	<LOQ	<LOQ
RR-LFP-NDB1-5T	-0.14	0.55	0.00	<LOQ	<LOQ	0.00	3.47	0.01	0.00	<LOD	0.00	<LOD	0.00	-2.09	<LOD	<LOQ	7.76	0.00	<LOQ	<LOQ	0.00	-0.74	0.00	0.00	<LOD	<LOQ	<LOQ
RR-LFP-NDB1-1Wo	-0.16	0.63	0.00	<LOQ	<LOQ	0.00	3.40	0.01	0.00	<LOD	0.00	<LOD	0.00	-1.66	<LOD	<LOQ	8.25	0.00	<LOQ	<LOQ	0.00	-0.19	0.00	0.00	<LOD	0.00	<LOQ

dig_ digestion

sample No. (Bruchsal isotherm) method LOD LOQ uncertainty [%]	T [°C]	time [min]	pH	c0 T [°C]	pH	c1 T [°C]	LFP [g]	digested mass [g]	C,Equ,Li [mg/L]
load [mg/g]									
RR-LFP-TW2-0.05c	60	180	7.10	28.2	6.92	33.4	0.057	0.068	150
RR-LFP-TW2-0.5c	60	180	7.11	33.5	4.96	31.2	0.509	0.099	81
RR-LFP-TW2-1c	60	180	7.06	33.5	4.58	34.5	0.981	0.099	30
RR-LFP-TW2-2c	60	180	6.93	33.5	4.23	33.0	2.026	0.100	9
RR-LFP-TW2-3c	60	180	7.14	29.8	4.07	31.0	2.959	0.098	4
RR-LFP-TW2-4c	60	180	7.01	33.0	4.00	33.8	4.004	0.100	13
RR-LFP-TW2-5c	60	180	6.94	31.5	3.85	30.6	5.008	0.102	0
RR-LFP-TW2-6c	60	180	7.15	27.8	3.85	34.5	5.989	0.100	0
RR-LFP-TW2-7c	60	180	7.03	29.5	3.76	32.3	6.999	0.101	0
RR-LFP-TW2-10c	60	180	6.89	34.9	3.63	31.1	9.971	0.100	0
RR-LFP-TW2-15c	60	180	7.10	31.7	3.71	33.8	15.049	0.099	0
load [mmol/g]									
RR-LFP-TW2-0.05c	60	180	7.10	28.2	6.92	33.4	0.057	0.068	150
RR-LFP-TW2-0.5c	60	180	7.11	33.5	4.96	31.2	0.509	0.099	81
RR-LFP-TW2-1c	60	180	7.06	33.5	4.58	34.5	0.981	0.099	30
RR-LFP-TW2-2c	60	180	6.93	33.5	4.23	33.0	2.026	0.100	9
RR-LFP-TW2-3c	60	180	7.14	29.8	4.07	31.0	2.959	0.098	4
RR-LFP-TW2-4c	60	180	7.01	33.0	4.00	33.8	4.004	0.100	13
RR-LFP-TW2-5c	60	180	6.94	31.5	3.85	30.6	5.008	0.102	0
RR-LFP-TW2-6c	60	180	7.15	27.8	3.85	34.5	5.989	0.100	0
RR-LFP-TW2-7c	60	180	7.03	29.5	3.76	32.3	6.999	0.101	0
RR-LFP-TW2-10c	60	180	6.89	34.9	3.63	31.1	9.971	0.100	0
RR-LFP-TW2-15c	60	180	7.10	31.7	3.71	33.8	15.049	0.099	0

sample No. (Bruchsal isotherm)	Li mg/L dig_	Na mg/L dig_	K mg/L dig_	Rb mg/L dig_	Cs mg/L dig_	Mg mg/L dig_	Ca mg/L dig_	Sr mg/L dig_	Ba mg/L dig_	B mg/L fluid	Al mg/L dig_	Si mg/L fluid	Pb mg/L dig_	P mg/L fluid	As mg/L dig_	Sb mg/L dig_	S mg/L dig_	Ti mg/L dig_	V mg/L dig_	Cr mg/L dig_	Mn mg/L dig_	Fe mg/L fluid	Co mg/L dig_	Ni mg/L dig_	Cu mg/L dig_	Zn mg/L dig_	Cd mg/L dig_
method	OES	OES	MS	MS	MS	OES	OES	OES	OES	OES	MS	OES	MS	OES	MS	MS	OES	MS	MS	MS	OES	OES	MS	MS	MS	OES	MS
LOD	0.0015	0.3091	0.0008	0.000	0.000	0.000	0.0080	0.0002	0.0003	0.0032	0.0003	0.0141	0.000	0.0220	0.000	0.000	0.0229	0.0000	0.000	0.000	0.0002	0.0023	0.000	0.000	0.000	0.0007	0.000
LOQ	0.0051	1.0304	0.0027	0.000	0.000	0.000	0.0267	0.0006	0.0011	0.0105	0.0009	0.0472	0.000	0.0733	0.000	0.000	0.0763	0.0002	0.000	0.000	0.0008	0.0077	0.000	0.000	0.000	0.0023	0.000
uncertainty [%]	4.7	6.7	8.2	1.0	0.5	2.9	8.1	3.5	11.1	2.6	3.9	1.6	1.4	17.4	5.6	3.4	3.2	3.4	2.5	3.2	2.9	8.1	2.6	3.7	3.2	2.9	2.6
load [mg/g]																											
RR-LFP-TW2-0.05c	10	107	n. v.	0.0	0.0	0.6	14	0.8	0.0	0.5	0.0	0.3	<LOQ	n. v.	0.3	<LOQ	58	0.1	<LOQ	<LOQ	0.1	n. v.	0.0	0.0	<LOQ	1.4	<LOQ
RR-LFP-TW2-0.5c	27	11.4	0.2	<LOQ	<LOQ	0.1	3.7	0.4	0.1	0.1	0.0	0.0	<LOQ	n. v.	0.1	<LOQ	44	0.0	<LOQ	0.0	0.1	-0.9	0.0	0.0	-0.1	0.1	<LOQ
RR-LFP-TW2-1c	24	17.4	0.4	<LOQ	<LOQ	0.1	5.0	0.6	0.2	0.0	0.0	0.0	<LOQ	-1.0	<LOQ	<LOQ	50	0.0	<LOQ	<LOQ	0.0	-2.0	0.0	0.0	<LOQ	0.0	<LOQ
RR-LFP-TW2-2c	14	32.5	0.3	<LOQ	<LOQ	0.0	4.7	0.5	0.2	0.0	0.0	0.0	<LOQ	-0.9	<LOQ	<LOQ	42	0.0	<LOQ	0.0	0.0	-1.8	0.0	0.0	-0.1	0.0	<LOQ
RR-LFP-TW2-3c	10	40.0	0.3	<LOQ	<LOQ	0.0	4.3	0.5	0.1	0.0	0.0	0.0	<LOQ	-0.8	<LOQ	<LOQ	40	0.0	<LOQ	<LOQ	0.0	-1.5	0.0	0.0	<LOQ	0.0	<LOQ
RR-LFP-TW2-4c	6.5	21.5	0.4	<LOQ	<LOQ	0.0	3.5	0.4	0.1	0.0	0.0	0.0	<LOQ	-0.4	<LOQ	<LOQ	19	<LOQ	<LOQ	0.0	-0.1	-0.8	0.0	0.0	-0.1	0.0	<LOQ
RR-LFP-TW2-5c	5.8	41.0	0.4	<LOQ	<LOQ	0.0	3.9	0.5	0.1	0.0	0.0	0.0	<LOQ	-0.6	<LOQ	<LOQ	34	0.0	<LOQ	0.0	-0.1	-1.2	0.0	0.0	-0.1	0.0	<LOQ
RR-LFP-TW2-6c	4.6	40.4	0.4	<LOQ	<LOQ	0.0	3.9	0.5	0.1	0.0	0.0	0.0	<LOQ	-0.6	<LOQ	<LOQ	24	<LOQ	<LOQ	<LOQ	-0.1	-1.2	0.0	0.0	<LOQ	0.0	<LOQ
RR-LFP-TW2-7c	4.1	41.1	0.4	<LOQ	<LOQ	0.0	4.0	0.5	0.1	0.0	0.0	0.0	<LOQ	-0.5	<LOQ	<LOQ	31	0.0	<LOQ	0.0	-0.1	-1.0	0.0	0.0	-0.1	0.0	<LOQ
RR-LFP-TW2-10c	2.8	38.5	0.5	<LOQ	<LOQ	0.0	3.9	0.5	0.1	0.0	0.0	0.0	<LOQ	-0.5	<LOQ	<LOQ	25	<LOQ	<LOQ	<LOQ	-0.1	-1.0	0.0	0.0	<LOQ	0.0	<LOQ
RR-LFP-TW2-15c	1.8	31.8	0.5	<LOQ	<LOQ	0.0	3.7	0.5	0.1	0.0	0.0	0.0	<LOQ	-0.3	<LOQ	<LOQ	22	0.0	<LOQ	0.0	-0.1	-0.7	0.0	0.0	-0.1	0.0	<LOQ
load [mmol/g]																											
RR-LFP-TW2-0.05c	1.47	4.67	n. v.	0.00	0.00	0.03	0.34	0.01	0.00	0.04	0.00	0.01	<LOQ	n. v.	0.00	<LOQ	1.80	0.00	<LOQ	<LOQ	0.00	n. v.	0.00	0.00	<LOQ	0.02	<LOQ
RR-LFP-TW2-0.5c	3.85	0.49	0.01	<LOQ	<LOQ	0.00	0.09	0.00	0.00	0.00	0.00	0.00	<LOQ	n. v.	0.00	<LOQ	1.37	0.00	<LOQ	0.00	0.00	-0.02	0.00	0.00	0.00	0.00	<LOQ
RR-LFP-TW2-1c	3.41	0.76	0.01	<LOQ	<LOQ	0.00	0.12	0.01	0.00	0.00	0.00	0.00	<LOQ	-0.03	<LOQ	<LOQ	1.57	0.00	<LOQ	<LOQ	0.00	-0.04	0.00	0.00	<LOQ	0.00	<LOQ
RR-LFP-TW2-2c	1.97	1.42	0.01	<LOQ	<LOQ	0.00	0.12	0.01	0.00	0.00	0.00	0.00	<LOQ	-0.03	<LOQ	<LOQ	1.31	0.00	<LOQ	0.00	0.00	-0.03	0.00	0.00	0.00	0.00	<LOQ
RR-LFP-TW2-3c	1.45	1.74	0.01	<LOQ	<LOQ	0.00	0.11	0.01	0.00	0.00	0.00	0.00	<LOQ	-0.02	<LOQ	<LOQ	1.25	0.00	<LOQ	<LOQ	0.00	-0.03	0.00	0.00	<LOQ	0.00	<LOQ
RR-LFP-TW2-4c	0.94	0.94	0.01	<LOQ	<LOQ	0.00	0.09	0.00	0.00	0.00	0.00	0.00	<LOQ	-0.01	<LOQ	<LOQ	0.60	<LOQ	<LOQ	0.00	0.00	-0.01	0.00	0.00	0.00	0.00	<LOQ
RR-LFP-TW2-5c	0.84	1.78	0.01	<LOQ	<LOQ	0.00	0.10	0.01	0.00	0.00	0.00	0.00	<LOQ	-0.02	<LOQ	<LOQ	1.05	0.00	<LOQ	0.00	0.00	-0.02	0.00	0.00	0.00	0.00	<LOQ
RR-LFP-TW2-6c	0.66	1.76	0.01	<LOQ	<LOQ	0.00	0.10	0.01	0.00	0.00	0.00	0.00	<LOQ	-0.02	<LOQ	<LOQ	0.74	<LOQ	<LOQ	<LOQ	0.00	-0.02	0.00	0.00	<LOQ	0.00	<LOQ
RR-LFP-TW2-7c	0.59	1.79	0.01	<LOQ	<LOQ	0.00	0.10	0.01	0.00	0.00	0.00	0.00	<LOQ	-0.02	<LOQ	<LOQ	0.97	0.00	<LOQ	0.00	0.00	-0.02	0.00	0.00	0.00	0.00	<LOQ
RR-LFP-TW2-10c	0.40	1.68	0.01	<LOQ	<LOQ	0.00	0.10	0.01	0.00	0.00	0.00	0.00	<LOQ	-0.01	<LOQ	<LOQ	0.77	<LOQ	<LOQ	<LOQ	0.00	-0.02	0.00	0.00	<LOQ	0.00	<LOQ
RR-LFP-TW2-15c	0.27	1.38	0.01	<LOQ	<LOQ	0.00	0.09	0.01	0.00	0.00	0.00	0.00	<LOQ	-0.01	<LOQ	<LOQ	0.68	0.00	<LOQ	0.00	0.00	-0.01	0.00	0.00	0.00	0.00	<LOQ

dig_ digestion

n. v. no value

sample No. (Neustadt-Glewe isotherm) method LOD LOQ uncertainty [%]	T [°C]	volume [mL]	time [min]	LFP [g]	digested mass [g]	c0 pH	c0 T [°C]	c1 pH	c1 T [°C]	mass/volume ratio, experiment [g/L]	cEqu, Li [mg/L]
load [mg/g]											
RR-LFP-NDB2-0.05	60	250	240	0.050		-	-	6.04	39.6	0.2	11.5
RR-LFP-NDB2-0.1	60	250	240	0.100		-	-	6.09	39.7	0.4	11.3
RR-LFP-NDB2-0.3	60	250	240	0.300		-	-	4.89	39.9	1.2	10.8
RR-LFP-NDB2-0.5	60	250	240	0.500		-	-	5.27	39.5	2.0	8.1
RR-LFP-NDB2-1	60	250	240	1.000		-	-	4.48	40.3	4.0	7.1
RR-LFP-NDB2-2	60	250	240	2.000		-	-	3.99	40.2	8.0	2.4
RR-LFP-NDB2-3	60	250	240	3.000		-	-	4.82	40.4	12.0	2.9
RR-LFP-NDB2-4	60	250	240	4.000		-	-	3.94	38.6	16.0	<LOQ
RR-LFP-NDB2-5	60	250	240	5.000		-	-	3.83	37.6	20.0	<LOQ
RR-LFP-NDB2-7	60	250	240	7.001		-	-	3.78	35.4	28.0	<LOQ
RR-LFP-NDB2-10	60	250	240	10.000		-	-	3.77	40.9	40.0	<LOQ
RR-LFP-NDB2-12	60	250	240	12.001		-	-	3.69	40.7	48.0	<LOQ
RR-LFP-NDB2-15	60	250	240	15.000		-	-	3.63	42.0	60.0	<LOQ
RR-LFP-NDB2-Blank1	60	200	240	0.000		7.05	34.6	7.82	35.5	0	
RR-LFP-NDB2-Blank2	60	250	240	0.000		-	-	7.23	38.5	0	
RR-LFP-NDB2-Blank3	60	200	240	0.000		7.16	35.9	7.08	37.0	0	
load [mmol/g]											
RR-LFP-NDB2-0.05	60	250	240	0.050		-	-	6.04	39.6	0.2	11.5
RR-LFP-NDB2-0.1	60	250	240	0.100		-	-	6.09	39.7	0.4	11.3
RR-LFP-NDB2-0.3	60	250	240	0.300		-	-	4.89	39.9	1.2	10.8
RR-LFP-NDB2-0.5	60	250	240	0.500		-	-	5.27	39.5	2.0	8.1
RR-LFP-NDB2-1	60	250	240	1.000		-	-	4.48	40.3	4.0	7.1
RR-LFP-NDB2-2	60	250	240	2.000		-	-	3.99	40.2	8.0	2.4
RR-LFP-NDB2-3	60	250	240	3.000		-	-	4.82	40.4	12.0	2.9
RR-LFP-NDB2-4	60	250	240	4.000		-	-	3.94	38.6	16.0	<LOQ
RR-LFP-NDB2-5	60	250	240	5.000		-	-	3.83	37.6	20.0	<LOQ
RR-LFP-NDB2-7	60	250	240	7.001		-	-	3.78	35.4	28.0	<LOQ
RR-LFP-NDB2-10	60	250	240	10.000		-	-	3.77	40.9	40.0	<LOQ
RR-LFP-NDB2-12	60	250	240	12.001		-	-	3.69	40.7	48.0	<LOQ
RR-LFP-NDB2-15	60	250	240	15.000		-	-	3.63	42.0	60.0	<LOQ

sample No. (Neustadt-Glewe isotherm)	Li	Na	K	Rb	Cs	Mg	Ca	Sr	Ba	B	Al	Si	Pb	P	As	Sb	S	Ti	V	Cr	Mn	Fe	Co	Ni	Cu	Zn	Cd
	mg/L	mg/L	mg/L	mg/L	mg/L	mg/L	mg/L	mg/L	mg/L	mg/L	mg/L	mg/L	mg/L	mg/L	mg/L	mg/L	mg/L	mg/L	mg/L	mg/L	mg/L	mg/L	mg/L	mg/L	mg/L	mg/L	mg/L
	dig_	dig_	dig_	dig_	dig_	dig_	dig_	dig_	dig_	dig_	dig_	dig_	dig_	fluid	dig_	dig_	dig_	dig_	dig_	dig_	dig_	fluid	dig_	dig_	dig_	dig_	dig_
method	OES	OES	MS	MS	MS	OES	OES	MS	MS	MS	MS	OES	MS	OES	MS	MS	OES	MS	MS	MS	MS	OES	MS	OES	MS	MS	MS
LOD	0.0020	0.0143	0.0010	0.000	0.000	0.0023	0.0085	0.000	0.000	0.000	0.0001	0.0224	0.000	0.0353	0.000	0.000	0.0199	0.0000	0.000	0.000	0.000	0.0007	0.000	0.0030	0.000	0.000	0.000
LOQ	0.0066	0.0476	0.0032	0.000	0.000	0.0076	0.0283	0.000	0.000	0.000	0.0002	0.0747	0.000	0.1176	0.000	0.000	0.0664	0.0001	0.000	0.000	0.000	0.0022	0.000	0.0101	0.000	0.000	0.000
uncertainty [%]	2.7	7.4	51.0	0.4	0.1	4.2	3.4	1.2	1.2	0.6	1.8	5.3	1.5	2.3	1.1	21.8	2.0	1.5	3.4	2.5	4.5	4.1	3.9	4.5	3.0	1.4	2.0
load [mg/g]																											
RR-LFP-NDB2-0.05	0.2	24	0.1	<LOQ	<LOQ	0.4	4.4	0.4	0.0	<LOQ	0.0	<LOD	1.7	n. v.	<LOQ	<LOQ	3.7	0.0	<LOQ	<LOQ	0.2	n. v.	0.0	<LOQ	<LOQ	0.9	<LOQ
RR-LFP-NDB2-0.1	0.5	23	0.1	<LOQ	<LOQ	0.3	4.4	0.4	0.0	<LOQ	0.0	<LOD	1.2	n. v.	<LOQ	<LOQ	2.3	0.0	<LOQ	<LOQ	0.2	n. v.	0.0	<LOQ	<LOQ	0.5	<LOQ
RR-LFP-NDB2-0.3	0.5	29	0.1	<LOQ	<LOQ	0.2	4.1	0.4	0.0	<LOQ	0.0	<LOD	0.3	n. v.	<LOQ	<LOQ	3.3	<LOQ	<LOQ	0.0	0.1	n. v.	0.0	<LOQ	<LOQ	0.1	<LOQ
RR-LFP-NDB2-0.5	1.3	27	0.1	<LOQ	<LOQ	0.2	4.2	0.4	0.0	<LOQ	0.0	<LOD	0.2	n. v.	<LOQ	<LOQ	6.9	0.0	<LOQ	<LOQ	0.1	n. v.	0.0	<LOQ	<LOQ	0.1	<LOQ
RR-LFP-NDB2-1	0.7	30	0.1	<LOQ	<LOQ	0.2	3.9	0.4	0.0	<LOQ	0.0	<LOD	0.0	n. v.	<LOQ	<LOQ	9.6	<LOQ	<LOQ	<LOQ	0.1	n. v.	0.0	0.1	<LOQ	<LOQ	<LOQ
RR-LFP-NDB2-2	0.9	38	0.1	<LOQ	<LOQ	0.2	3.9	0.4	0.0	<LOQ	0.0	<LOD	0.0	-2.2	<LOQ	<LOQ	18	0.0	<LOQ	<LOQ	0.0	-4.8	0.0	<LOQ	<LOQ	<LOQ	<LOQ
RR-LFP-NDB2-3	0.5	28	0.1	<LOQ	<LOQ	0.2	3.7	0.4	0.0	<LOQ	0.0	<LOD	0.0	-1.4	<LOQ	<LOQ	13	<LOQ	<LOQ	<LOQ	0.0	-3.3	0.0	<LOQ	<LOQ	<LOQ	<LOQ
RR-LFP-NDB2-4	0.4	29	0.1	<LOQ	<LOQ	0.2	3.7	0.4	0.0	<LOQ	0.0	<LOD	<LOQ	-2.2	<LOQ	<LOQ	16	0.0	<LOQ	<LOQ	0.0	-4.9	0.0	<LOQ	<LOQ	<LOQ	<LOQ
RR-LFP-NDB2-5	0.3	29	0.1	<LOQ	<LOQ	0.1	3.6	0.4	0.0	<LOQ	0.0	<LOD	<LOQ	-2.2	<LOQ	<LOQ	14	<LOQ	<LOQ	<LOQ	0.0	-5.0	0.0	<LOQ	<LOQ	<LOQ	<LOQ
RR-LFP-NDB2-7	0.1	26	0.1	<LOQ	<LOQ	0.1	3.8	0.4	0.0	<LOQ	0.0	<LOD	<LOQ	-2.6	<LOQ	<LOQ	15	0.0	<LOQ	<LOQ	0.0	-5.9	0.0	<LOQ	<LOQ	<LOQ	<LOQ
RR-LFP-NDB2-10	0.2	23	0.1	<LOQ	<LOQ	0.1	3.5	0.4	0.0	<LOQ	0.0	<LOD	<LOQ	-2.4	<LOQ	<LOQ	12	<LOQ	<LOQ	<LOQ	0.0	-5.6	0.0	<LOQ	<LOQ	<LOQ	<LOQ
RR-LFP-NDB2-12	0.0	22	0.1	<LOQ	<LOQ	0.1	3.5	0.4	0.0	<LOQ	0.0	<LOD	<LOQ	-2.4	<LOQ	<LOQ	12	<LOQ	<LOQ	<LOQ	0.0	-5.7	0.0	<LOQ	<LOQ	<LOQ	<LOQ
RR-LFP-NDB2-15	-0.1	21	0.2	<LOQ	<LOQ	0.1	3.4	0.4	0.0	<LOQ	0.0	<LOD	<LOQ	-2.5	<LOQ	<LOQ	13	0.0	<LOQ	<LOQ	0.0	-6.1	0.0	<LOQ	<LOQ	<LOQ	<LOQ
RR-LFP-NDB2-Blank1														n. v.								n. v.					
RR-LFP-NDB2-Blank2														n. v.								n. v.					
RR-LFP-NDB2-Blank3														n. v.								n. v.					
load [mmol/g]																											
RR-LFP-NDB2-0.05	0.03	1.04	0.00	<LOQ	<LOQ	0.02	0.11	0.00	0.00	<LOQ	0.00	<LOD	0.01	n. v.	<LOQ	<LOQ	0.12	0.00	<LOQ	<LOQ	0.00	n. v.	0.00	<LOQ	<LOQ	0.01	<LOQ
RR-LFP-NDB2-0.1	0.07	1.01	0.00	<LOQ	<LOQ	0.01	0.11	0.00	0.00	<LOQ	0.00	<LOD	0.01	n. v.	<LOQ	<LOQ	0.07	0.00	<LOQ	<LOQ	0.00	n. v.	0.00	<LOQ	<LOQ	0.01	<LOQ
RR-LFP-NDB2-0.3	0.07	1.26	0.00	<LOQ	<LOQ	0.01	0.10	0.00	0.00	<LOQ	0.00	<LOD	0.00	n. v.	<LOQ	<LOQ	0.10	<LOQ	<LOQ	0.00	0.00	n. v.	0.00	<LOQ	<LOQ	0.00	<LOQ
RR-LFP-NDB2-0.5	0.19	1.18	0.00	<LOQ	<LOQ	0.01	0.10	0.00	0.00	<LOQ	0.00	<LOD	0.00	n. v.	<LOQ	<LOQ	0.22	0.00	<LOQ	<LOQ	0.00	n. v.	0.00	<LOQ	<LOQ	0.00	<LOQ
RR-LFP-NDB2-1	0.11	1.32	0.00	<LOQ	<LOQ	0.01	0.10	0.00	0.00	<LOQ	0.00	<LOD	0.00	n. v.	<LOQ	<LOQ	0.30	<LOQ	<LOQ	<LOQ	0.00	n. v.	0.00	0.00	<LOQ	<LOQ	<LOQ
RR-LFP-NDB2-2	0.12	1.66	0.00	<LOQ	<LOQ	0.01	0.10	0.00	0.00	<LOQ	0.00	<LOD	0.00	-0.07	<LOQ	<LOQ	0.56	0.00	<LOQ	<LOQ	0.00	-0.09	0.00	<LOQ	<LOQ	<LOQ	<LOQ
RR-LFP-NDB2-3	0.07	1.23	0.00	<LOQ	<LOQ	0.01	0.09	0.00	0.00	<LOQ	0.00	<LOD	0.00	-0.05	<LOQ	<LOQ	0.40	<LOQ	<LOQ	<LOQ	0.00	-0.06	0.00	<LOQ	<LOQ	<LOQ	<LOQ
RR-LFP-NDB2-4	0.06	1.28	0.00	<LOQ	<LOQ	0.01	0.09	0.00	0.00	<LOQ	0.00	<LOD	<LOQ	-0.07	<LOQ	<LOQ	0.49	0.00	<LOQ	<LOQ	0.00	-0.09	0.00	<LOQ	<LOQ	<LOQ	<LOQ
RR-LFP-NDB2-5	0.04	1.25	0.00	<LOQ	<LOQ	0.01	0.09	0.00	0.00	<LOQ	0.00	<LOD	<LOQ	-0.07	<LOQ	<LOQ	0.42	<LOQ	<LOQ	<LOQ	0.00	-0.09	0.00	<LOQ	<LOQ	<LOQ	<LOQ
RR-LFP-NDB2-7	0.01	1.14	0.00	<LOQ	<LOQ	0.01	0.09	0.00	0.00	<LOQ	0.00	<LOD	<LOQ	-0.08	<LOQ	<LOQ	0.48	0.00	<LOQ	<LOQ	0.00	-0.11	0.00	<LOQ	<LOQ	<LOQ	<LOQ
RR-LFP-NDB2-10	0.03	0.99	0.00	<LOQ	<LOQ	0.00	0.09	0.00	0.00	<LOQ	0.00	<LOD	<LOQ	-0.08	<LOQ	<LOQ	0.37	<LOQ	<LOQ	<LOQ	0.00	-0.10	0.00	<LOQ	<LOQ	<LOQ	<LOQ
RR-LFP-NDB2-12	0.00	0.95	0.00	<LOQ	<LOQ	0.00	0.09	0.00	0.00	<LOQ	0.00	<LOD	<LOQ	-0.08	<LOQ	<LOQ	0.37	<LOQ	<LOQ	<LOQ	0.00	-0.10	0.00	<LOQ	<LOQ	<LOQ	<LOQ
RR-LFP-NDB2-15	-0.01	0.89	0.00	<LOQ	<LOQ	0.00	0.08	0.00	0.00	<LOQ	0.00	<LOD	<LOQ	-0.08	<LOQ	<LOQ	0.41	0.00	<LOQ	<LOQ	0.00	-0.11	0.00	<LOQ	<LOQ	<LOQ	<LOQ

dig_ digestion
n. v. no value

sample No. (Bruchsal kinetics)	Li	Na	K	Mg	Ca	Sr	Ba	B	Al	Si	Pb	P	As	S	Mn	Fe	Ni	Cu	Zn	Cd
	mg/L	mg/L	mg/L	mg/L	mg/L	mg/L	mg/L	mg/L	mg/L	mg/L	mg/L	mg/L	mg/L	mg/L	mg/L	mg/L	mg/L	mg/L	mg/L	mg/L
LOD	0.0035	0.1582	0.0003	0.0002	0.0052	0.0000	0.0000	0.0001	0.0001	0.0032	0.0000	0.0033	0.0000	0.0260	0.0000	0.0001	0.0000	0.0000	0.0000	0.0000
LOQ	0.0117	0.5273	0.0009	0.0007	0.0173	0.0000	0.0000	0.0004	0.0002	0.0106	0.0000	0.0108	0.0000	0.0867	0.0000	0.0004	0.0000	0.0000	0.0000	0.0000
uncertainty [%]	8.8	1.6	11.9	8.0	7.8	3.5	6.6	3.0	5.4	4.9	3.8	2.7	6.8	3.3	2.6	2.5	4.3	3.8	5.9	3.6
cEqu [mg/L]																				
RR-LFP-TW1-0001a	157	59949	3301	338	7558	369	5.2	37	<LOD	23		<LOQ	2.7	33462	21	<LOQ	<LOD	<LOD	8.0	<LOQ
RR-LFP-TW1-0015a	142	58973	3239	331	7420	361	5.2	36	<LOD	22		<LOQ	2.9	33100	21	<LOQ	<LOD	<LOD	7.9	<LOQ
RR-LFP-TW1-0030a	124	59417	3300	337	7497	366	5.2	36	<LOD	22		<LOQ	2.7	33238	21	<LOQ	<LOD	<LOD	8.1	<LOQ
RR-LFP-TW1-0060a	63	59179	3288	334	7474	363	5.1	36	<LOD	22		2.6	2.4	32764	21	<LOQ	<LOD	<LOD	8.5	<LOQ
RR-LFP-TW1-0120a	57	59434	3282	331	7493	364	5.0	36	<LOD	23		13	2.7	32832	21	22	<LOD	<LOD	9.4	<LOQ
RR-LFP-TW1-0180a	41	58635	3244	329	7391	357	4.7	36	<LOD	22		47	3.0	32529	21	90	<LOD	<LOD	9.3	<LOQ
RR-LFP-TW1-0240a	44	58893	3262	329	7409	357	4.5	35	<LOD	22		82	2.9	32433	21	153	<LOD	<LOD	9.4	<LOQ
RR-LFP-TW1-1440a	101	58589	3225	327	7378	356	3.6	36	<LOD	23		289	3.1	32162	22	534	<LOD	<LOD	9.5	<LOQ
RR-LFP-TW1-3Ta	104	58730	3237	329	7372	358	2.9	36	<LOD	23		329	2.8	32112	22	625	<LOD	<LOD	9.5	<LOQ
RR-LFP-TW1-5Ta	141	59241	3276	332	6492	355	4.2	36	<LOD	22		531	<LOD	30272	22	152	<LOD	<LOD	9.4	<LOQ
RR-LFP-TW1-1Woa	150	59262	3278	331	5848	353	4.5	36	<LOD	23		591	<LOD	28958	22	43	<LOD	<LOD	9.3	<LOQ
RR-LFP-TW1-2Woa	159	59239	3279	332	4568	335	<LOQ	36	<LOD	23		503	<LOD	26716	20	<LOQ	<LOD	<LOD	8.0	<LOQ
load [mg/g]																				
RR-LFP-TW1-0001	0.8	1.1	0.3	0.0	2.6	0.2	0.1	<LOQ	0.0	0.0	<LOQ	<LOQ	0.0	0.2	0.0	<LOD	0.0	-0.1	0.3	<LOQ
RR-LFP-TW1-0015	3.5	1.4	0.4	0.1	2.7	0.3	0.1	<LOQ	0.0	0.0	<LOQ	<LOD	0.1	1.4	0.0	<LOD	0.0	-0.1	0.3	<LOQ
RR-LFP-TW1-0030	7.5	1.2	0.3	0.1	2.7	0.3	0.1	<LOQ	0.0	0.0	<LOQ	<LOQ	0.0	3.3	0.1	<LOQ	0.0	-0.1	0.3	<LOQ
RR-LFP-TW1-0060	18	3.3	0.3	0.1	3.1	0.3	0.1	<LOQ	0.0	0.0	<LOQ	-0.5	0.0	16	0.0	<LOQ	0.0	-0.1	0.2	<LOQ
RR-LFP-TW1-0120	19	12	0.3	0.0	3.7	0.4	0.1	<LOQ	0.0	0.0	<LOQ	-2.4	0.0	27	0.0	-4.1	0.0	-0.1	0.1	<LOQ
RR-LFP-TW1-0180	23	16	0.4	0.1	5.4	0.6	0.1	<LOQ	0.0	0.0	<LOQ	-9.2	0.0	47	0.0	-17	0.0	-0.1	0.1	<LOQ
RR-LFP-TW1-0240	22	21	0.4	0.1	6.0	0.6	0.1	<LOQ	0.0	0.0	<LOQ	-15	0.0	58	0.0	-29	0.0	-0.1	0.1	<LOQ
RR-LFP-TW1-1440	11	46	0.6	0.1	8.6	1.0	0.2	<LOQ	0.0	0.0	<LOQ	-57	0.0	119	0.0	-106	0.0	-0.1	0.1	<LOQ
RR-LFP-TW1-3T	10	35	0.6	0.1	13	1.3	0.3	<LOQ	0.0	0.0	0.0	-65	0.0	190	0.0	-123	0.0	-0.1	0.1	<LOQ
RR-LFP-TW1-5T	2.8	16	0.3	0.0	91	1.1	0.1	<LOQ	0.0	-0.1	0.0	-104	0.3	267	-0.2	-30	0.0	-0.1	0.0	<LOQ
RR-LFP-TW1-1Wo	1.4	6.2	0.2	-0.1	122	0.9	0.1	<LOQ	-0.1	-0.1	0.0	-114	0.3	318	-0.3	-8.2	0.0	-0.1	0.0	<LOQ
RR-LFP-TW1-2Wo	-0.8	0.4	0.1	-0.1	154	1.4	0.2	<LOQ	-0.1	-0.1	0.0	-100	0.2	344	-0.3	<LOD	-0.1	-0.1	0.0	<LOQ
load [mmol/g]																				
RR-LFP-TW1-0001	0.11	0.05	0.01	0.00	0.06	0.00	0.00	<LOQ	0.00	0.00	<LOQ	<LOQ	0.00	0.01	0.00	<LOD	0.00	0.00	0.01	<LOQ
RR-LFP-TW1-0015	0.50	0.06	0.01	0.00	0.07	0.00	0.00	<LOQ	0.00	0.00	<LOQ	<LOD	0.00	0.04	0.00	<LOD	0.00	0.00	0.00	<LOQ
RR-LFP-TW1-0030	1.08	0.05	0.01	0.00	0.07	0.00	0.00	<LOQ	0.00	0.00	<LOQ	<LOQ	0.00	0.10	0.00	<LOQ	0.00	0.00	0.00	<LOQ
RR-LFP-TW1-0060	2.53	0.14	0.01	0.00	0.08	0.00	0.00	<LOQ	0.00	0.00	<LOQ	-0.02	0.00	0.50	0.00	<LOQ	0.00	0.00	0.00	<LOQ
RR-LFP-TW1-0120	2.75	0.53	0.01	0.00	0.09	0.00	0.00	<LOQ	0.00	0.00	<LOQ	-0.08	0.00	0.83	0.00	-0.07	0.00	0.00	0.00	<LOQ
RR-LFP-TW1-0180	3.37	0.68	0.01	0.00	0.13	0.01	0.00	<LOQ	0.00	0.00	<LOQ	-0.30	0.00	1.46	0.00	-0.31	0.00	0.00	0.00	<LOQ
RR-LFP-TW1-0240	3.10	0.91	0.01	0.00	0.15	0.01	0.00	<LOQ	0.00	0.00	<LOQ	-0.49	0.00	1.80	0.00	-0.51	0.00	0.00	0.00	<LOQ
RR-LFP-TW1-1440	1.61	2.00	0.01	0.00	0.22	0.01	0.00	<LOQ	0.00	0.00	<LOQ	-1.85	0.00	3.70	0.00	-1.89	0.00	0.00	0.00	<LOQ
RR-LFP-TW1-3T	1.51	1.54	0.01	0.00	0.32	0.01	0.00	<LOQ	0.00	0.00	0.00	-2.09	0.00	5.94	0.00	-2.20	0.00	0.00	0.00	<LOQ
RR-LFP-TW1-5T	0.40	0.69	0.01	0.00	2.26	0.01	0.00	<LOQ	0.00	0.00	0.00	-3.35	0.00	8.34	0.00	-0.53	0.00	0.00	0.00	<LOQ
RR-LFP-TW1-1Wo	0.21	0.27	0.00	0.00	3.05	0.01	0.00	<LOQ	0.00	0.00	0.00	-3.68	0.00	9.91	-0.01	-0.15	0.00	0.00	0.00	<LOQ
RR-LFP-TW1-2Wo	-0.11	0.02	0.00	0.00	3.83	0.02	0.00	<LOQ	0.00	0.00	0.00	-3.22	0.00	10.71	-0.01	no value	0.00	0.00	0.00	<LOQ

sample No. (Bruchsal kinetics)	Li	Na	K	Mg	Ca	Sr	Ba	B	Al	Si	Pb	P	As	S	Mn	Fe	Ni	Cu	Zn	Cd
	mg/L	mg/L	mg/L	mg/L	mg/L	mg/L	mg/L	mg/L	mg/L	mg/L	mg/L	mg/L	mg/L	mg/L	mg/L	mg/L	mg/L	mg/L	mg/L	mg/L
LOD	0.0035	0.1582	0.0003	0.0002	0.0052	0.0000	0.0000	0.0001	0.0001	0.0032	0.0000	0.0033	0.0000	0.0260	0.0000	0.0001	0.0000	0.0000	0.0000	0.0000
LOQ	0.0117	0.5273	0.0009	0.0007	0.0173	0.0000	0.0000	0.0004	0.0002	0.0106	0.0000	0.0108	0.0000	0.0867	0.0000	0.0004	0.0000	0.0000	0.0000	0.0000
uncertainty [%]	8.8	1.6	11.9	8.0	7.8	3.5	6.6	3.0	5.4	4.9	3.8	2.7	6.8	3.3	2.6	2.5	4.3	3.8	5.9	3.6
Kd value [L/g]																				
RR-LFP-TW1-0001	0.0050	0.0000	0.0001	0.0001	0.0003	0.0006	0.0103			-0.0004			0.0176	0.0000	0.0013				0.0426	
RR-LFP-TW1-0015	0.0246	0.0000	0.0001	0.0002	0.0004	0.0007	0.0104			0.0006			0.0238	0.0000	0.0011				0.0394	
RR-LFP-TW1-0030	0.0608	0.0000	0.0001	0.0002	0.0004	0.0007	0.0119			-0.0004			-0.0037	0.0001	0.0026				0.0362	
RR-LFP-TW1-0060	0.2783	0.0001	0.0001	0.0002	0.0004	0.0008	0.0127			-0.0004		-0.1820	-0.0041	0.0005	0.0019				0.0232	
RR-LFP-TW1-0120	0.3324	0.0002	0.0001	0.0001	0.0005	0.0010	0.0151			-0.0011		-0.1865	0.0163	0.0008	0.0017	-0.1865			0.0058	
RR-LFP-TW1-0180	0.5729	0.0003	0.0001	0.0002	0.0007	0.0016	0.0267			-0.0005		-0.1947	0.0157	0.0014	0.0023	-0.1947			0.0059	
RR-LFP-TW1-0240	0.4882	0.0004	0.0001	0.0002	0.0008	0.0018	0.0316			-0.0005		-0.1868	-0.0034	0.0018	0.0016	-0.1868			0.0059	
RR-LFP-TW1-1440	0.1104	0.0008	0.0002	0.0002	0.0012	0.0028	0.0599			-0.0008		-0.1981	-0.0033	0.0037	-0.0003	-0.1981			0.0054	
RR-LFP-TW1-3T	0.1001	0.0006	0.0002	0.0002	0.0017	0.0035	0.1052			-0.0014		-0.1970	-0.0036	0.0059	0.0006	-0.1970			0.0057	
RR-LFP-TW1-5T	0.0198	0.0003	0.0001	-0.0001	0.0140	0.0032	0.0332			-0.0035		-0.1952		0.0088	-0.0074	-0.1952			0.0023	
RR-LFP-TW1-1Wo	0.0095	0.0001	0.0000	-0.0004	0.0209	0.0027	0.0136			-0.0035		-0.1927		0.0110	-0.0130	-0.1927			0.0007	
RR-LFP-TW1-2Wo	-0.0048	0.0000	0.0000	-0.0003	0.0336	0.0041				-0.0035		-0.1985		0.0129	-0.0152				0.0046	
selectivity order	1	9	11	10	8	6	2			12		14	3	7	5	13			4	

sample No. (Bruchsal isotherm)	Li mg/L	Na mg/L	K mg/L	Mg mg/L	Ca mg/L	Sr mg/L	Ba mg/L	B mg/L	Si mg/L	Pb mg/L	P mg/L	As mg/L	S mg/L	Mn mg/L	Fe mg/L	Zn mg/L
LOD	0.0015	0.3091	0.0008	0.0000	0.0080	0.0002	0.0003	0.0032	0.0141	0.0000	0.0220	0.0000	0.0229	0.0002	0.0023	0.0007
LOQ	0.0051	1.0304	0.0027	0.0000	0.0267	0.0006	0.0011	0.0105	0.0472	0.0000	0.0733	0.0000	0.0763	0.0008	0.0077	0.0023
uncertainty [%]	4.7	6.7	8.2	2.9	8.1	3.5	11.1	2.6	1.6	1.4	17.4	5.6	3.2	2.9	8.1	2.9
Cequ [mg/L]																
RR-LFP-TW2-0.05a	150	56775	3161	332	7140	358	6.2	37	19		<LOQ	<LOQ	32581	20	<LOQ	5.1
RR-LFP-TW2-0.5a	81	55025	3101	326	6940	348	5.8	37	19		<LOQ	<LOQ	33134	19	23	6.1
RR-LFP-TW2-1a	30	54892	3100	326	6912	349	5.3	36	20		48	<LOQ	32914	19	97	6.0
RR-LFP-TW2-2a	8.8	55839	3095	325	7018	345	4.7	36	19		89	<LOQ	31893	19	183	6.0
RR-LFP-TW2-3a	3.6	54664	3047	321	6917	341	4.3	35	19		111	<LOQ	31731	18	221	5.9
RR-LFP-TW2-4a	13	58387	3149	330	7317	349	4.6	37	19		76	<LOQ	31988	18	158	5.7
RR-LFP-TW2-5a	<LOQ	55723	3065	323	7047	338	3.4	36	19		148	<LOQ	31286	17	308	5.8
RR-LFP-TW2-6a	<LOQ	54699	3084	324	6931	335	3.2	36	20		166	<LOQ	31263	17	347	5.6
RR-LFP-TW2-7a	<LOQ	51600	2975	314	6552	325	2.7	35	19		175	<LOQ	30778	16	367	5.5
RR-LFP-TW2-10a	<LOQ	53635	3051	324	6803	326	<LOQ	35	20		225	<LOQ	31572	16	479	5.8
RR-LFP-TW2-15a	<LOQ	52388	3015	322	6645	314	<LOQ	35	20		245	<LOQ	30612	15	549	5.1
load [mg/g]																
RR-LFP-TW2-0.05c	10	107	no value	0.6	14	0.8	0.0	0.5	0.3	<LOQ	<LOQ	0.3	57.6	0.1	<LOQ	1.4
RR-LFP-TW2-0.5c	27	11	0.2	0.1	3.7	0.4	0.1	0.1	0.0	<LOQ	<LOQ	0.1	44.1	0.1	-0.9	0.1
RR-LFP-TW2-1c	24	17	0.4	0.1	5.0	0.6	0.2	0.0	0.0	<LOQ	-1.0	<LOQ	50.4	0.0	-2.0	0.0
RR-LFP-TW2-2c	14	33	0.3	0.0	4.7	0.5	0.2	0.0	0.0	<LOQ	-0.9	<LOQ	42.1	0.0	-1.8	0.0
RR-LFP-TW2-3c	10	40	0.3	0.0	4.3	0.5	0.1	0.0	0.0	<LOQ	-0.8	<LOQ	40.2	0.0	-1.5	0.0
RR-LFP-TW2-4c	6.5	22	0.4	0.0	3.5	0.4	0.1	0.0	0.0	<LOQ	-0.4	<LOQ	19.1	-0.1	-0.8	0.0
RR-LFP-TW2-5c	5.8	41	0.4	0.0	3.9	0.5	0.1	0.0	0.0	<LOQ	-0.6	<LOQ	33.5	-0.1	-1.2	0.0
RR-LFP-TW2-6c	4.6	40	0.4	0.0	3.9	0.5	0.1	0.0	0.0	<LOQ	-0.6	<LOQ	23.8	-0.1	-1.2	0.0
RR-LFP-TW2-7c	4.1	41	0.4	0.0	4.0	0.5	0.1	0.0	0.0	<LOQ	-0.5	<LOQ	31.0	-0.1	-1.0	0.0
RR-LFP-TW2-10c	2.8	39	0.5	0.0	3.9	0.5	0.1	0.0	0.0	<LOQ	-0.5	<LOQ	24.6	-0.1	-1.0	0.0
RR-LFP-TW2-15c	1.8	32	0.5	0.0	3.7	0.5	0.1	0.0	0.0	<LOQ	-0.3	<LOQ	21.8	-0.1	-0.7	0.0
load [mmol/g]																
RR-LFP-TW2-0.05c	1.47	4.67	no value	0.03	0.34	0.01	0.00	0.04	0.01	<LOQ	no value	0.00	1.80	0.00	<LOQ	0.02
RR-LFP-TW2-0.5c	3.85	0.49	0.01	0.002	0.09	0.004	0.001	0.005	0.001	<LOQ	no value	0.001	1.37	0.001	-0.02	0.001
RR-LFP-TW2-1c	3.41	0.76	0.01	0.002	0.12	0.01	0.001	0.003	0.000	<LOQ	-0.03	<LOQ	1.57	0.000	-0.04	0.001
RR-LFP-TW2-2c	1.97	1.42	0.01	0.00	0.12	0.01	0.00	0.00	0.00	<LOQ	-0.03	<LOQ	1.31	0.00	-0.03	0.00
RR-LFP-TW2-3c	1.45	1.74	0.01	0.00	0.11	0.01	0.00	0.00	0.00	<LOQ	-0.02	<LOQ	1.25	0.00	-0.03	0.00
RR-LFP-TW2-4c	0.94	0.94	0.01	0.00	0.09	0.00	0.00	0.00	0.00	<LOQ	-0.01	<LOQ	0.60	0.00	-0.01	0.00
RR-LFP-TW2-5c	0.84	1.78	0.01	0.00	0.10	0.01	0.00	0.00	0.00	<LOQ	-0.02	<LOQ	1.05	0.00	-0.02	0.00
RR-LFP-TW2-6c	0.66	1.76	0.01	0.00	0.10	0.01	0.00	0.00	0.00	<LOQ	-0.02	<LOQ	0.74	0.00	-0.02	0.00
RR-LFP-TW2-7c	0.59	1.79	0.01	0.00	0.10	0.01	0.00	0.00	0.00	<LOQ	-0.02	<LOQ	0.97	0.00	-0.02	0.00
RR-LFP-TW2-10c	0.40	1.68	0.01	0.00	0.10	0.01	0.00	0.00	0.00	<LOQ	-0.01	<LOQ	0.77	0.00	-0.02	0.00
RR-LFP-TW2-15c	0.27	1.38	0.01	0.00	0.09	0.01	0.00	0.00	0.00	<LOQ	-0.01	<LOQ	0.68	0.00	-0.01	0.00

sample No. (Bruchsal isotherm)	Li mg/L	Na mg/L	K mg/L	Mg mg/L	Ca mg/L	Sr mg/L	Ba mg/L	B mg/L	Si mg/L	Pb mg/L	P mg/L	As mg/L	S mg/L	Mn mg/L	Fe mg/L	Zn mg/L
LOD	0.0015	0.3091	0.0008	0.0000	0.0080	0.0002	0.0003	0.0032	0.0141	0.0000	0.0220	0.0000	0.0229	0.0002	0.0023	0.0007
LOQ	0.0051	1.0304	0.0027	0.0000	0.0267	0.0006	0.0011	0.0105	0.0472	0.0000	0.0733	0.0000	0.0763	0.0008	0.0077	0.0023
uncertainty [%]	4.7	6.7	8.2	2.9	8.1	3.5	11.1	2.6	1.6	1.4	17.4	5.6	3.2	2.9	8.1	2.9
Kd value [L/g]																
RR-LFP-TW2-0.05c	0.0682	0.0019		0.0018	0.0019	0.0023	0.0000	0.0121	0.0162				0.0018	0.0034		0.2769
RR-LFP-TW2-0.5c	0.3313	0.0002	0.0001	0.0002	0.0005	0.0010	0.0183	0.0015	0.0011				0.0013	0.0042	-0.0393	0.0097
RR-LFP-TW2-1c	0.7965	0.0003	0.0001	0.0002	0.0007	0.0016	0.0314	0.0008	0.0003		-0.0204		0.0015	0.0013	-0.0204	0.0067
RR-LFP-TW2-2c	1.5619	0.0006	0.0001	0.0001	0.0007	0.0016	0.0321	0.0003	0.0005		-0.0099		0.0013	-0.0008	-0.0099	0.0056
RR-LFP-TW2-3c	2.7713	0.0007	0.0001	0.0001	0.0006	0.0014	0.0304	0.0004	0.0002		-0.0068		0.0013	-0.0013	-0.0068	0.0054
RR-LFP-TW2-4c	0.5032	0.0004	0.0001	0.0001	0.0005	0.0012	0.0193	0.0001	0.0002		-0.0050		0.0006	-0.0034	-0.0050	0.0045
RR-LFP-TW2-5c		0.0007	0.0001	0.0001	0.0006	0.0013	0.0343	0.0002	0.0001		-0.0040		0.0011	-0.0034	-0.0040	0.0033
RR-LFP-TW2-6c		0.0007	0.0001	0.0001	0.0006	0.0013	0.0333	0.0002	0.0000		-0.0033		0.0008	-0.0038	-0.0033	0.0013
RR-LFP-TW2-7c		0.0008	0.0001	0.0001	0.0006	0.0014	0.0406	0.0001	0.0001		-0.0029		0.0010	-0.0042	-0.0029	0.0030
RR-LFP-TW2-10c		0.0007	0.0002	0.0001	0.0006	0.0015		0.0001	0.0000		-0.0020		0.0008	-0.0052	-0.0020	0.0013
RR-LFP-TW2-15c		0.0006	0.0002	0.0001	0.0006	0.0015		0.0000	0.0000		-0.0013		0.0007	-0.0065	-0.0013	0.0028
selectivity order	1	10	12	11	9	8	2	5	7		14		6	4	13	3

sample No. (Neustadt-Glewe kinetics)	Li	Na	K	Mg	Ca	Sr	Ba	Pb	P	S	Mn	Fe	Zn
	mg/L	mg/L	mg/L	mg/L	mg/L	mg/L	mg/L	mg/L	mg/L	mg/L	mg/L	mg/L	mg/L
LOD	0.0022	0.0064	0.0010	0.0001	0.0091	0.0002	0.0000	0.0000	0.0153	0.0169	0.0000	0.0059	0.0006
LOQ	0.0072	0.0213	0.0032	0.0003	0.0302	0.0006	0.0000	0.0000	0.0511	0.0562	0.0000	0.0196	0.0019
uncertainty [%]	3.6	7.5	51.0	2.8	1.1	5.9	1.2	1.5	9.0	1.2	4.5	3.9	1.1
cEqu [mg/L]													
RR-LFP-NDB1-0001a	13	89876	832	1175	7974	492	4.6		<LOD	31557	11	<LOQ	2.2
RR-LFP-NDB1-0015a	13	99762	887	1301	8391	515	4.8		<LOD	33208	12	<LOQ	2.3
RR-LFP-NDB1-0030a	13	100141	899	1303	8424	517	4.8		<LOD	33327	12	<LOQ	2.3
RR-LFP-NDB1-0060a	12	100210	907	1303	8406	517	4.7		1.4	32930	12	<LOQ	2.3
RR-LFP-NDB1-0120a	9.7	99917	904	1297	8330	514	4.6		1.2	32640	11	3.0	2.5
RR-LFP-NDB1-0180a	8.3	100599	895	1309	8368	505	4.7		4.5	32914	12	8.5	2.6
RR-LFP-NDB1-0240a	6.9	99627	893	1295	8327	511	4.7		9.7	32810	12	18	2.6
RR-LFP-NDB1-1440a	10	100698	877	1310	7833	509	3.6		212	31645	13	462	2.8
RR-LFP-NDB1-3Ta	13	100014	891	1300	7403	503	3.4		238	31240	13	488	2.8
RR-LFP-NDB1-5Ta	16	100122	901	1300	6141	495	4.2		324	28913	13	207	2.9
RR-LFP-NDB1-1Woa	17	100808	907	1311	6028	500	4.3		257	28580	12	52	2.8
load [mg/g]													
RR-LFP-NDB1-0001	-0.4	1.3	0.1	0.1	2.1	0.2	0.0	0.1	<LOD	0.1	0.0	<LOQ	0.1
RR-LFP-NDB1-0015	-0.4	2.6	0.1	0.2	2.7	0.3	0.0	0.1	<LOD	0.6	0.0	<LOQ	0.1
RR-LFP-NDB1-0030	-0.4	3.1	0.1	0.2	2.8	0.3	0.0	0.1	<LOD	0.7	0.0	<LOQ	0.1
RR-LFP-NDB1-0060	-0.2	6.6	0.1	0.2	3.2	0.4	0.0	0.1	-0.3	1.8	0.0	<LOQ	0.0
RR-LFP-NDB1-0120	0.3	15	0.1	0.2	3.7	0.4	0.1	0.1	-0.2	5.6	0.0	-0.6	0.0
RR-LFP-NDB1-0180	0.6	26	0.1	0.2	3.8	0.4	0.1	0.1	-0.9	12	0.0	-1.7	0.0
RR-LFP-NDB1-0240	1.0	37	0.1	0.2	4.1	0.5	0.1	0.0	-1.9	19	0.0	-3.7	0.0
RR-LFP-NDB1-1440	0.2	88	0.1	0.2	6.6	0.8	0.1	<LOQ	-42	105	0.0	-92	0.0
RR-LFP-NDB1-3T	-0.4	50	0.1	0.3	69	1.2	0.1	0.1	-48	180	-0.1	-98	<LOQ
RR-LFP-NDB1-5T	-1.0	13	0.0	0.0	139	1.2	0.0	0.0	-65	249	-0.2	-41	<LOQ
RR-LFP-NDB1-1Wo	-1.1	14	0.0	0.0	136	1.2	0.0	0.0	-51	265	-0.1	-10	-0.1
load [mmol/g]													
RR-LFP-NDB1-0001	-0.06	0.06	0.00	0.01	0.05	0.00	0.00	0.00	<LOD	0.00	0.00	<LOQ	0.00
RR-LFP-NDB1-0015	-0.06	0.11	0.00	0.01	0.07	0.00	0.00	0.00	<LOD	0.02	0.00	<LOQ	0.00
RR-LFP-NDB1-0030	-0.05	0.13	0.00	0.01	0.07	0.00	0.00	0.00	<LOD	0.02	0.00	<LOQ	0.00
RR-LFP-NDB1-0060	-0.03	0.29	0.00	0.01	0.08	0.00	0.00	0.00	-0.01	0.06	0.00	<LOQ	0.00
RR-LFP-NDB1-0120	0.05	0.67	0.00	0.01	0.09	0.00	0.00	0.00	-0.01	0.17	0.00	-0.01	0.00
RR-LFP-NDB1-0180	0.08	1.15	0.00	0.01	0.10	0.00	0.00	0.00	-0.03	0.38	0.00	-0.03	0.00
RR-LFP-NDB1-0240	0.14	1.62	0.003	0.01	0.10	0.01	0.000	0.00	-0.06	0.58	0.001	-0.07	0.00
RR-LFP-NDB1-1440	0.02	3.82	0.00	0.01	0.17	0.01	0.00	<LOQ	-1.37	3.29	0.00	-1.65	0.00
RR-LFP-NDB1-3T	-0.06	2.18	0.00	0.01	1.71	0.01	0.00	0.00	-1.54	5.60	0.00	-1.75	<LOQ
RR-LFP-NDB1-5T	-0.14	0.55	0.00	0.00	3.47	0.01	0.00	0.00	-2.09	7.76	0.00	-0.74	<LOQ
RR-LFP-NDB1-1Wo	-0.16	0.63	0.00	0.00	3.40	0.01	0.00	0.00	-1.66	8.25	0.00	-0.19	0.00
Kd value [L/g]													
RR-LFP-NDB1-0001	-0.0319	0.0000	0.0001	0.0001	0.0003	0.0004	0.0062			0.0000	0.0032		0.0296
RR-LFP-NDB1-0015	-0.0292	0.0000	0.0002	0.0001	0.0003	0.0006	0.0075			0.0000	0.0030		0.0262
RR-LFP-NDB1-0030	-0.0290	0.0000	0.0001	0.0001	0.0003	0.0006	0.0083			0.0000	0.0035		0.0251
RR-LFP-NDB1-0060	-0.0183	0.0001	0.0001	0.0001	0.0004	0.0007	0.0096		-0.2000	0.0001	0.0039		0.0191
RR-LFP-NDB1-0120	0.0356	0.0002	0.0001	0.0001	0.0004	0.0008	0.0112		-0.1999	0.0002	0.0043	-0.1999	0.0069
RR-LFP-NDB1-0180	0.0690	0.0003	0.0001	0.0002	0.0005	0.0008	0.0115		-0.2001	0.0004	0.0038	-0.2001	0.0009
RR-LFP-NDB1-0240	0.1381	0.0004	0.0001	0.0001	0.0005	0.0009	0.0125		-0.2000	0.0006	0.0033	-0.2000	-0.0001
RR-LFP-NDB1-1440	0.0153	0.0009	0.0001	0.0002	0.0008	0.0015	0.0299		-0.1998	0.0033	0.0011	-0.1998	-0.0047
RR-LFP-NDB1-3T	-0.0304	0.0005	0.0001	0.0002	0.0093	0.0024	0.0254		-0.2000	0.0057	-0.0047	-0.2000	
RR-LFP-NDB1-5T	-0.0619	0.0001	0.0000	0.0000	0.0227	0.0025	0.0092		-0.1999	0.0086	-0.0119	-0.1999	
RR-LFP-NDB1-1Wo	-0.0676	0.0001	0.0000	0.0000	0.0226	0.0024	0.0079		-0.2000	0.0093	-0.0117	-0.2000	-0.0193
selectivity order	1	7	9	8	6	4	2		12	5	3	11	10

sample No. (Neustadt-Glewe isotherm)	Li	Na	K	Mg	Ca	Sr	Ba	Pb	P	S	Mn	Fe	Zn
	mg/L	mg/L	mg/L	mg/L	mg/L	mg/L	mg/L	mg/L	mg/L	mg/L	mg/L	mg/L	mg/L
LOD	0.0020	0.0143	0.0010	0.0023	0.0085	0.0000	0.0000	0.0000	0.0353	0.0199	0.0000	0.0007	0.0000
LOQ	0.0066	0.0476	0.0032	0.0076	0.0283	0.0000	0.0000	0.0000	0.1176	0.0664	0.0000	0.0022	0.0000
uncertainty [%]	2.7	7.4	51.0	4.2	3.4	1.2	1.2	1.5	2.3	2.0	4.5	4.1	1.4
Cequ [mg/L]													
RR-LFP-NDB2-0.05a	12	97212	928	1324	8018	459	2.9		<LOD	32354	11	<LOQ	2.2
RR-LFP-NDB2-0.1a	11	97306	936	1325	8049	464	2.9		<LOD	32315	11	<LOQ	2.3
RR-LFP-NDB2-0.3a	11	97580	946	1330	8072	458	2.9		<LOD	32384	11	<LOQ	2.5
RR-LFP-NDB2-0.5a	8.1	97973	951	1331	8051	463	2.9		<LOD	32435	11	<LOQ	2.5
RR-LFP-NDB2-1a	7.1	97201	947	1320	8006	461	2.8		<LOD	32346	11	<LOQ	2.6
RR-LFP-NDB2-2a	2.4	96874	945	1316	7990	460	2.7		18	32191	11	39	2.6
RR-LFP-NDB2-3a	2.9	97199	948	1321	8035	459	2.6		17	32287	11	40	2.6
RR-LFP-NDB2-4a	0.0	96815	917	1328	7955	453	2.4		35	31785	11	78	2.5
RR-LFP-NDB2-5a	0.0	97505	929	1333	8011	459	2.3		43	31947	11	99	2.6
RR-LFP-NDB2-7a	0.0	97043	930	1327	8020	453	2.1		72	31579	11	165	2.6
RR-LFP-NDB2-10a	0.0	97455	938	1333	8053	457	<LOQ		94	31382	11	224	2.6
RR-LFP-NDB2-12a	0.0	96402	929	1322	7926	446	<LOQ		117	31387	11	275	2.6
RR-LFP-NDB2-15a	0.0	96964	945	1330	7810	441	<LOQ		151	31067	11	366	2.7
load [mg/g]													
RR-LFP-NDB2-0.05	0.2	24	0.1	0.4	4.4	0.4	0.0	1.7	no value	3.7	0.2	no value	0.9
RR-LFP-NDB2-0.1	0.5	23	0.1	0.3	4.4	0.4	0.0	1.2	no value	2.3	0.2	no value	0.5
RR-LFP-NDB2-0.3	0.5	29	0.1	0.2	4.1	0.4	0.0	0.3	no value	3.3	0.1	no value	0.1
RR-LFP-NDB2-0.5	1.3	27	0.1	0.2	4.2	0.4	0.0	0.2	no value	6.9	0.1	no value	0.1
RR-LFP-NDB2-1	0.7	30	0.1	0.2	3.9	0.4	0.0	0.0	no value	9.6	0.1	no value	<LOQ
RR-LFP-NDB2-2	0.9	38	0.1	0.2	3.9	0.4	0.0	0.0	-2.2	18	0.0	-4.8	<LOQ
RR-LFP-NDB2-3	0.5	28	0.1	0.2	3.7	0.4	0.0	0.0	-1.4	13	0.0	-3.3	<LOQ
RR-LFP-NDB2-4	0.4	29	0.1	0.2	3.7	0.4	0.0	<LOQ	-2.2	16	0.0	-4.9	<LOQ
RR-LFP-NDB2-5	0.3	29	0.1	0.1	3.6	0.4	0.0	<LOQ	-2.2	14	0.0	-5.0	<LOQ
RR-LFP-NDB2-7	0.1	26	0.1	0.1	3.8	0.4	0.0	<LOQ	-2.6	15	0.0	-5.9	<LOQ
RR-LFP-NDB2-10	0.2	23	0.1	0.1	3.5	0.4	0.0	<LOQ	-2.4	12	0.0	-5.6	<LOQ
RR-LFP-NDB2-12	0.0	22	0.1	0.1	3.5	0.4	0.0	<LOQ	-2.4	12	0.0	-5.7	<LOQ
RR-LFP-NDB2-15	-0.1	21	0.2	0.1	3.4	0.4	0.0	<LOQ	-2.5	13	0.0	-6.1	<LOQ
load [mmol/g]													
RR-LFP-NDB2-0.05	0.03	1.04	0.00	0.02	0.11	0.00	0.00	0.01	no value	0.12	0.00	no value	0.01
RR-LFP-NDB2-0.1	0.07	1.01	0.00	0.01	0.11	0.00	0.00	0.01	no value	0.07	0.00	no value	0.01
RR-LFP-NDB2-0.3	0.07	1.26	0.00	0.01	0.10	0.00	0.00	0.00	no value	0.10	0.00	no value	0.00
RR-LFP-NDB2-0.5	0.19	1.18	0.00	0.01	0.10	0.00	0.00	0.00	no value	0.22	0.00	no value	0.00
RR-LFP-NDB2-1	0.11	1.32	0.00	0.01	0.10	0.00	0.00	0.00	no value	0.30	0.00	no value	<LOQ
RR-LFP-NDB2-2	0.12	1.66	0.00	0.01	0.10	0.00	0.00	0.00	-0.07	0.56	0.00	-0.09	<LOQ
RR-LFP-NDB2-3	0.07	1.23	0.00	0.01	0.09	0.00	0.00	0.00	-0.05	0.40	0.00	-0.06	<LOQ
RR-LFP-NDB2-4	0.06	1.28	0.00	0.01	0.09	0.00	0.00	<LOQ	-0.07	0.49	0.00	-0.09	<LOQ
RR-LFP-NDB2-5	0.04	1.25	0.00	0.01	0.09	0.00	0.00	<LOQ	-0.07	0.42	0.00	-0.09	<LOQ
RR-LFP-NDB2-7	0.01	1.14	0.00	0.01	0.09	0.00	0.00	<LOQ	-0.08	0.48	0.00	-0.11	<LOQ
RR-LFP-NDB2-10	0.03	0.99	0.00	0.00	0.09	0.00	0.00	<LOQ	-0.08	0.37	0.00	-0.10	<LOQ
RR-LFP-NDB2-12	0.00	0.95	0.00	0.00	0.09	0.00	0.00	<LOQ	-0.08	0.37	0.00	-0.10	<LOQ
RR-LFP-NDB2-15	-0.01	0.89	0.00	0.00	0.08	0.00	0.00	<LOQ	-0.08	0.41	0.00	-0.11	<LOQ
Kd value [L/g]													
RR-LFP-NDB2-0.05	0.0185	0.0002	0.0001	0.0003	0.0006	0.0009	0.0133			0.0001	0.0217		0.3977
RR-LFP-NDB2-0.1	0.0425	0.0002	0.0001	0.0002	0.0005	0.0009	0.0130			0.0001	0.0145		0.1957
RR-LFP-NDB2-0.3	0.0421	0.0003	0.0001	0.0002	0.0005	0.0009	0.0128			0.0001	0.0079		0.0279
RR-LFP-NDB2-0.5	0.1636	0.0003	0.0001	0.0002	0.0005	0.0009	0.0138			0.0002	0.0087		0.0227
RR-LFP-NDB2-1	0.1023	0.0003	0.0001	0.0002	0.0005	0.0008	0.0130			0.0003	0.0053		
RR-LFP-NDB2-2	0.3554	0.0004	0.0001	0.0001	0.0005	0.0009	0.0140		-0.1250	0.0006	0.0038	-0.1250	
RR-LFP-NDB2-3	0.1628	0.0003	0.0001	0.0001	0.0005	0.0009	0.0129		-0.0833	0.0004	0.0030	-0.0833	
RR-LFP-NDB2-4		0.0003	0.0001	0.0001	0.0005	0.0009	0.0137		-0.0625	0.0005	0.0024	-0.0625	
RR-LFP-NDB2-5		0.0003	0.0002	0.0001	0.0005	0.0009	0.0136		-0.0500	0.0004	0.0024	-0.0500	
RR-LFP-NDB2-7		0.0003	0.0002	0.0001	0.0005	0.0009	0.0140		-0.0357	0.0005	0.0020	-0.0357	
RR-LFP-NDB2-10		0.0002	0.0002	0.0001	0.0004	0.0009			-0.0250	0.0004	0.0012	-0.0250	
RR-LFP-NDB2-12		0.0002	0.0002	0.0001	0.0004	0.0009			-0.0208	0.0004	0.0007	-0.0208	
RR-LFP-NDB2-15		0.0002	0.0002	0.0001	0.0004	0.0009			-0.0167	0.0004	0.0005	-0.0167	
selectivity order	1	7	10	9	6	5	3			8	4		2